REPUBLIQUE DU CAMEROUN
Paix – Travail – Patrie
****
UNIVERSITE DE YAOUNDE I
FACULTE DES SCIENCES
DEPARTEMENT DE PHYSIQUE
****

REPUBLIC OF CAMEROUN
Peace – Work – Fatherland
****
UNIVERSITY OF YAOUNDE I
FACULTY OF SCIENCE
DEPARTMENT OF PHYSICS
****

Nonlinear excitations in DNA molecule

Thesis Submitted and defended in fulfillment of the requirements for the award of Doctorat/PhD in Physics

Par : **TOKO DONATIEN**
Holder of D.E.A in Physics

Sous la direction de
KOFANE Timoléon Crépin
Professor, University of Yaounde I, Cameroon
MOHAMADOU Alidou
Associate Professor, University of Maroua, Cameroon

Année Académique : 2017

Résumé

Le domaine des mathématiques appliquées est parmis les domaines de recherche qui s'est développé au cours des dernières millénaires et continue à se développer. Les modèles mathématiques permettent aux chercheurs d'analyser une structure simplifiée d'un système biologique et de prédire son comportement. En fait, la recherche interdisciplinaire peut offrir des réponses à plusieurs phénomènes inexpliqués et la biomathématique, en particulier, permet l'analyse des organismes vivants. Une telle analyse pourrait impliquer l'apparition, le développement ou même la mort des organismes, ou tout simplement expliquer les causes et les conditions dans lesquelles un processus a lieu. L'acide désoxyribonucléique (ADN) est d'un pôle majeur pour les biologistes, biomathématiciens, chimistes ainsi que les biologistes. L'ADN est un long polymère constitué de deux chaînes de bases, dans laquelle l'information génétique est stockée. Les bases nucléiques d'un brin d'ADN peuvent interagir avec les bases nucléiques d'un autre brin d'ADN à travers des liaisons hydrogène et selon les règles de la complémentarité des bases pour former des pairs de bases. Notre travail est centré sur la dynamique non linéaire de la molécule d'ADN, en particulier l'étude de sa dénaturation. Nous commençons par la révision de l'un des premiers modèles non linéaires du processus de dénaturation de l'ADN, qui néglige les inhomogénéités dues à la séquence de base et l'asymétrie des deux brins: le modèle Peyrard Bishop (PB). En utilisant la méthode semi-discrète, nous obtenons une équation de Schrödinger non linéaire avec des termes d'ordre supérieur. Par la suite, l'instabilité de modulation (IM) est étudiée par l'analyse de la stabilité linéaire ainsi que l'approche variationnelle. L'effet du couplage entre les paires de bases est examiné. Sachant que le modèle de PB ne prend pas en compte la nature hélicoïdale de la molécule d'ADN, nous considérons le modèle de Peyrard Bishop Dauxois (PBD), qui prend en compte la double hélice de l'ADN. Nous montrons en utilisant la méthode des perturbations réductrices que la dynamique du système peut être décrite par un ensemble d'équations de Schrödinger non linéaires couplés. Les scénarios pertinents de l'instabilité de modulation (IM) sont explorés et nous notons que le système est stable en dessous de la modulation pour certaines valeurs des paramètres du modèle de PBD. Nous rappelons également l'impact de la vitesse de groupe sur la stabilité du système étudié. Le modèle de PBD ne prend pas en compte l'angle de torsion entre les paires de bases adjacentes et l'effet de solvant. Donc, nous avons réexaminé le modèle de PBD améliorée par Marco Zoli. L'équation de Schrödinger non linéaire discrète généralisée est ensuite obtenue pour le modèle de torsion de l'ADN avec

Nonlinear excitations in DNA molecule

Dissertation submitted in partial fulfillment of the requirements for the degree of Doctor of Philosophy in Mechanics.

By
Donatien TOKO

D.E.A. (Master of Philosophy) in Physics, Option Mechanics
Registration N° 02Y085

directed by
MOHAMADOU ALIDOU
M.C. University of Douala

Under the supervision of

Timoléon Crépin KOFANE

Full Professor, U.Y. I

July 20, 2018

Dedication

This work is dedicated to my family:

✠ At my father NDEFO Louis.

✠ My big brothers **TAPTUE André Marie**, **FOTUE Henry Fiacre** and **FOBA Paul Roger**.

✠ To my lovely spouse **Mireille** and my sons **Daniella**, **Shekina** and **Prince EZECHIEL**

Acknowledgments

To Almighty God, who inspired me by his Holy Spirit in this work, that his name be blessed forever.

First of all I would like to express my sincere gratitude to **Professor Timoléon Crépin KOFANE**, my supervisor and head of Mechanics Laboratory, for his high human qualities, guidance and constant support during this research work. He gave me the opportunity to work in the Mechanics Lab and showed me the way to postgraduate study. In spite of huge academic and administrative duties, he always found time to discuss with me and answer my queries.

I am profoundly indebted to **Professor Alidou MOHAMADOU** my thesis director and dean of the **Science Faculty** of **University of Maroua Cameroon**, for motivating discussions and great time we had during my dissertation. From the early years of hesitation and confusion till the completion of this doctoral program, he did not spare his time when helping me. He provided me with the necessary courage to tackle research. He also provided me with many useful references, documents, suggestions, friendly encouragements, fruitful discussions. He has been a good advisor for me.

I am also thankful to the initiator of the present thesis, **TABI CONRAD BERTRAND** Docteur of **University of Yaounde 1**, for his constructive comments, suggestions and his careful review on this thesis.

I am deeply grateful to Professor **BEN-BOLIE**, associate professor at the **University of Yaounde 1** for his academic and administrative contributions; May God always give him wisdom to help students

I owe a lot of gratitude to **Professor Paul WOAFO**,
Professor Clément TCHAWOUA, **Professor David YEMELE**, who are among the brilliant people who gave me one of the greatest gifts of all, knowledge.

Finally, I am missing the words to express my gratitude to my lovely spouse **Mireille**

who suffered a lot from my absence throughout this work. Without her love and support, the completion of this work would have never been possible. Our kids were born during these years, and ever since they have filled our lives with the most indescribable joy.

To my spiritual mother **Metonou Germaines** for her prayers

To my brothers, sisters and relatives of the family who have **Fodouop** spared no effort in the culmination of this work. they find here the expression of my affection and my gratitude.

To all my classmates and all those who have in some way contributed to the development of this work.

To my friends: **Serge NGANKOU Otis**; **TAGNE TEBU Serge**; **Fomekong Charles**; **NANTCHO WILLIAM Maturin**, was to always have with me to support me.

May all those, who has contributed in any manner their efforts to this work, see in these words the expression of my profound gratefulness.

Contents

List of Figures

List of abbreviations

DNA: *deoxyribose nucleic acid*

PB: *Peyrard Bishop*

PBD: *Peyrard Bishop Dauxois*

PBD: *Peyrard Bishop Dauxois*

NLSE: *Nonlinear Schrödinger equation*

MI: *Modulational instability*

ODE: *Ordinary differential equation*

VA: *variational approach*

MI: *Modulational instability*

LS: *Linear stability*

PDE: *Partial differential equation*

CQDNLS: *Cubic-quintic discrete nonlinear Schrödinger*

DNLS: *Discrete nonlinear Schrödinger*

CDNLS: *Coupled discrete nonlinear Schrödinger*

MDNLS: *Modified discrete nonlinear Schrödinger*

RNA: *ribose nucleic acid*

NMR: *Nuclear magnetic resonance*

HPB: *helicoidal Peyrard-Bishop*

ATP: *adenosine triphospliate*

PDE: *partial differential equation*

ITM: *improved tanh method*

LS: *Linear stability*

Résumé

Le domaine des mathématiques appliquées est parmis les domaines de recherche qui s'est développé au cours des dernières millénaires et continue à se développer. Les modèles mathématiques permettent aux chercheurs d'analyser une structure simplifiée d'un système biologique et de prédire son comportement. En fait, la recherche interdisciplinaire peut offrir des réponses à plusieurs phénomènes inexpliqués et la biomathématique, en particulier, permet l'analyse des organismes vivants. Une telle analyse pourrait impliquer l'apparition, le développement ou même la mort des organismes, ou tout simplement expliquer les causes et les conditions dans lesquelles un processus a lieu. L'acide désoxyribonucléique (ADN) est d'un pôle majeur pour les biologistes, biomathématiciens, chimistes ainsi que les biologistes. L'ADN est un long polymère constitué de deux chaînes de bases, dans laquelle l'information génétique est stockée. Les bases nucléiques d'un brin d'ADN peuvent interagir avec les bases nucléiques d'un autre brin d'ADN à travers des liaisons hydrogène et selon les règles de la complémentarité des bases pour former des pairs de bases. Notre travail est centré sur la dynamique non linéaire de la molécule d'ADN, en particulier l'étude de sa dénaturation. Nous commençons par la révision de l'un des premiers modèles non linéaires du processus de dénaturation de l'ADN, qui néglige les inhomogénéités dues à la séquence de base et l'asymétrie des deux brins: le modèle Peyrard Bishop (PB). En utilisant la méthode semi-discrète, nous obtenons une équation de Schrödinger non linéaire avec des termes d'ordre supérieur. Par la suite, l'instabilité de modulation (IM) est étudiée par l'analyse de la stabilité linéaire ainsi que l'approche variationnelle. L'effet du couplage entre les paires de bases est examiné. Sachant que le modèle de PB ne prend pas en compte la nature hélicoïdale de la molécule d'ADN, nous considérons le modèle de Peyrard Bishop Dauxois (PBD), qui prend en compte la double hélice de l'ADN. Nous montrons en utilisant la méthode des perturbations réductrices que la dynamique du système peut être décrite par un ensemble d'équations de Schrödinger non linéaires couplés. Les scénarios pertinents de l'instabilité de modulation (IM) sont explorés et nous notons que le système est stable en dessous de la modulation pour certaines valeurs des paramètres du modèle de PBD. Nous rappelons également l'impact de la vitesse de groupe sur la stabilité du système étudié. Le modèle de PBD ne prend pas en compte l'angle de torsion entre les paires de bases adjacentes et l'effet de solvant. Donc, nous avons réexaminé le modèle de PBD améliorée par Marco Zoli. L'équation de Schrödinger non linéaire discrète généralisée est ensuite obtenue pour le modèle de torsion de l'ADN avec

interaction de solvant. Nous présentons une expression analytique du gain de modulation et nous montrons les effets de l'angle de torsion sur celui-ci ainsi que sur le diagramme de la stabilité. Des simulations numériques sont effectuées pour montrer la validité de l'approche analytique. L'impact de l'angle de torsion est étudié et l'on obtient que l'angle de torsion affecte la dynamique des modes stables générés par la molécule. La localisation de l'énergie dans le cadre du modèle de torsion de l'ADN avec interaction de solvant est également étudiée. Les degrés de liberté de la séquence d'ADN de rotation et de torsion sont considérés comme jouant un rôle important pour la transcription de l'ADN en tant que témoins du modèle rotationnel de Yakushevich. En utilisant la méthode de perturbation, nous tirons de ce modèle l'équation de Schrödinger non linéaire discrète et couplée qui nous a permis d'étudier l'instabilité de modulation (IM) grâce à une simple mode d'excitation d'une part et une double mode d'excitation d'autre part. Nous avons porté notre attention sur l'effet des paramètres de couplage, y compris les coefficients de torsion. Des simulations numériques de l'équation de Schrödinger non linéaire discrète ont été effectuées afin de vérifier la validité de nos résultats analytiques. Nous avons également été intéressés à chercher des solutions analytiques exactes des modèles de PB et de PBD. En ce qui concerne le modèle de PB, l'effet de couplage harmonique est mis en évidence, alors que dans le modèle de PBD, nous avons jeté notre dévolu sur l'impact de l'angle de torsion et le coefficient solvant. La stabilité de ces solutions a été également étudiée.

Mots clés

ADN, ARN, enzymes, réplication, transcription, transport de charges, instabilité modulationnelle, localisation de l'énergie, solitons, excitations non linéaires, Schrödinger, angle de torsion.

Abstract

Applied mathematics is one of the research fields that developed over the last few thousand years and still continues to develop. Mathematical models allow researchers to analyze a simplified structure of a biological system and predict its behavior. In fact, interdisciplinary research can offer answers to several unexplained phenomena and mathematical biology, in particular, allows the analysis of living organisms. Such analysis might involve the appearance, the development or even the death of the organisms, or simply explain the causes and the conditions in which a process takes place. Deoxyribonucleic acid (DNA) is one of a major focus for mathematical biologists, biophysicists, chemists as well as biologists. DNA is a long polymer consisting of two chains of bases, in which the genetic information is stored. A base from one chain has a corresponding base on the other chain which together forms a so-called base-pair. Our starting is focused on the nonlinear dynamics of the DNA molecule, particularly the study of its denaturation. We revisit one of the first nonlinear models of denaturation process of DNA, which neglects the inhomogeneities due to the base sequence and the asymmetry of the two strands: the Peyrard Bishop (PB) model. Using the semi-discrete method, we derive a nonlinear Schrödinger equation with higher-order term. Thereafter, the modulational instability (MI) is investigated through the linear stability analysis as well as the variational approach. The effect of the coupling between the base pairs is examined. Knowing that the PB model does not take into account the helical nature of the DNA molecule, we consider the Peyrard Bishop Dauxois model, which takes into account the double helix of DNA. We show using the reductive perturbation method that the dynamics of the system can be described by a set of coupled nonlinear Schrödinger equations. The relevant MI scenarios are explored and we note that the system is stable under the modulation for certain parameter values of the PBD model. We also point out the impact of the group velocity on the stability of the system understudy. The PBD model does not take into account the angle of torsion between pairs of adjacent bases and the effect of solvent. So, we reconsidered the PBD model improved by Marco Zoli. The generalized discrete nonlinear Schrödinger equation is then derived for the twisted DNA with solvent interaction. We present an analytical expression for the MI gain and show the effects of twist angle on MI gain spectra as well as on stability diagram. Numerical simulations are carried out to show the validity of the analytical approach. The impact of the twist angle is investigated and we obtain that the twist angle affects the dynamics of stable patterns gener-

ated through the molecule. Energy localization in the framework of twisted DNA with solvent interaction is also studied. The rotational and torsional degrees of freedom of the DNA sequence are considered to play an important role for DNA transcription as witnesses rotational model of Yakushevich. Using the perturbation method, we derive from this model a discrete coupled nonlinear Schrödinger equation that allowed us to study the MI through a simple mode excitation as well as through a double mode excitation. We have focused our attention on the effect of the coupling parameters, including the torsion coefficients. Direct numerical simulations of the nonlinear Schrödinger equation have been carried out in order to verify the validity of our analytical results. We have also been interested to look for exact analytical solutions of the PB and PBD models. As regards the model of PB, the effect of harmonic coupling is highlighted, while in the PBD model, we threw our sights on the impact of the angle of torsion and the solvent coefficient. The stability of these solitons has been also investigated.

Keywords: DNA, RNA, enzymes, replication, transcription, carrying loads, modulational instability, localization of the energy, solitons, nonlinear excitations, Schrödinger, torsion angle.

General Introduction

Nature represents a challenge for the scientific community nowadays. Natural processes, such as the wind or the rain, natural resources, for example, coal or oil, and living organisms present interesting phenomena which need further investigations to be explained. Researchers all over the world study these phenomena and create and analyze models of the system, which sometimes reveal hidden features. The goal of mathematical biology is to analyze biological systems, using mathematical tools and techniques. Based on the techniques applied in biology and medicine, mathematical biology can be classified into: biological mathematical modeling, complex systems biology, bioinformatics and biocomputing. The first two fields require analytical mathematical knowledge, while the latter two also require computational resources. However, sometimes these fields overlap and a biological application can be considered part of two or more branches of mathematical biology. Recently, many research projects focus on microscopic modeling. Existing techniques are, in many cases, incapable of providing a full analysis at the microscopic level, which explains the need for the development of mathematical models. An example of such a system is deoxyribonucleic acid (DNA) in which most processes take place at the Ångstrom level and on a timescale smaller then the microsecond timescale, which is inaccessible even for electron microscopes, such as Scanning Tunneling Microscope. DNA is a nucleic acid that contains genetic instructions for the development and functioning of living organisms. Note that viruses contain RNA genomes instead of DNA and are not normally considered living organisms. The main role of DNA is the long-term storage of information. The DNA segments which carry genetic information are called genes. There are also DNA sequences with structural purposes and those involved in regulating the expression of genetic information, as well as many redundant and repetitive unused sequences. From a structural point of view, DNA is a long polymer composed of simple units called nucleotides, which are held together by a backbone of sugars and phosphate groups. The nucleotides composing a DNA sequence differ in their bases, which encode the genetic information copied by cells from DNA into RNA in order to use. These bases are of four types, from two different categories: the purines: Adenine (A) and Guanine (G) having two organic cycles and the pyrimidines: Cytosine (C) and Thymine (T) with only one organic cycle. Note that nucleotides are structural units for both, DNA and RNA, and have several purposes. Nucleotides not only participate in enzymatic reactions, but also in cellular signaling and they can be sources of chemical energy. In the understanding of

the living world, physics often brings a very informative complementary perspective to that, primordial, biology. The description of the static structure of DNA proposed by Watson and Crick in 1953 [1] for example has opened the way for the theoretical study of the dynamics of this molecule and, for 40 years, DNA continues to be the subject of study of theoretical and experimental physics very thorough. Absorption ultraviolet spectroscopy experiments at 260 nm provided very important information on the thermal denaturation of DNA [2]-[3]. Through the recording of the absorption coefficient of a DNA molecule in a heated solvent, these experiments show that at particular temperatures, the finite portions of the sequence opens abruptly, until it reaches the temperature where the double strand is dissociate completely. The representation of the fraction of the open bases pairs versus temperature shows that each local opening appears to be a discontinuous transition of phase [4]. The processes of transcription and replication are of vital importance, but are also much more difficult to model than the thermal denaturation, since they involve both the intrinsic structure of DNA and external elements (enzymes, proteins, etc ...). For little finely understand this intrinsic dynamic structure, so it is wise and prudent to begin to look at the thermal denaturation. The first efforts in this direction favored a system description in terms of discrete states, such as the Ising model or Poland-Scheraga [5]. However, a Hamiltonian approach may be desirable for several reasons. First, a continuous model is more acceptable to the extent that the nature of the configurational states describing the separation of two bases are continuous, so that the discretization of these states is only an approximation, whose rigorous verification limits is often overlooked. In addition, the nonlinearity is an essential property of biological systems. More specifically, DNA is a system whose dynamics is characterized by low-amplitude vibrations at temperatures of about 300 K and large fluctuations when approaching the denaturation at above 350 K. Therefore, only a nonlinear Hamiltonian is able to describe the dynamics of DNA on such a range of temperatures. Finally, the construction of a Hamiltonian model for a particular system is used to study both the temporal dynamics that its thermodynamic properties. This is of major importance, since these two approaches are often complementary. For example, the thermal denaturation of DNA is an equilibrium phase transition. We study it more largely by the tools of statistical physics of equilibrium [4]. But, when the temperature increased for a DNA molecule placed in a solvent, the molecule is carried to this amplification by denaturation of the bubbles which are metastable states, ie dynamic structures of long life. In following, we will see that other phenomena of dynamic nature, result from the nonlinear dynamics of DNA. In other words, a complete understanding of the phenomenon of distortion analysis requires dynamic and thermodynamic time for which a Hamiltonian formulation is undoubtedly the most appropriate. Describing the DNA thermal denaturation, ie the distance between the base pairs, was proposed by GAO and Prohofsky in 1984 [**?**]. This model has been used since 1989 by Peyrard and Bishop [**?**] to study the thermal denaturation more thrust. The Prohofsky model, which assumes a harmonic interaction between adjacent monomers on the same strand (stack-

ing interaction), leads, however, to a too progressive denaturation compared to experimental denaturation curves. This led Dauxois, Peyrard and Bishop in 1993 to provide an improved [7] model. These authors have shown that homogeneous DNA model (PBO), which includes a stacking anharmonic interaction, reproduces a first order transition in very good agreement with experiment. Since the PBD model was the subject of theoretical studies on solitons [8, 9], the charge transport along the DNA [10, 11], bubble dynamics [12] etc ... With some minor modifications, the PBD model has also been used to study the denaturation of heterogeneous sequences in the one-dimensional case [13] and three-dimensional [14]. The use of some of these Hamiltonians leads to several types of non-linear equation such as the NLS equation, discrete (DNLS) equation, cubic-quintic (CQ)-NLS equation... The different solutions of NLS equations obtained have allowed to recover the solitary waves and study the stability of these solutions. An interesting question concerns how such solitary wave structures may arise (i.e., which is the underlying physical mechanism for their manifestation and how they may be generated) in this context of solitary waves in DNA [**?**]. Theoretically, several methods of creating solitary waves have been proposed amongst which modulational instability (MI), which is a universal phenomenon of the nonlinear physics [17]. In fact, on account of the MI a specific range of wave numbers of plane-wave profiles becomes unstable to modulations, leading to an exponential growth of the unstable modes and eventually to delocalization (upon excitation of such wavenumbers) in momentum space [16, 18, 19]. That is equivalent to localization in position space, and hence the formation of localized coherent solitary wave structures [16, 19, 20]. The MI is a general feature of continuum as well as discrete nonlinear matter-wave equations and has been both experimentally and theoretically established as the responsible of not only responsible for the onset of nonlinear excitations but also the location of the energy. In this thesis, we aim to examine analytically and numerically the generation (through the process of MI) as well as propagation of matter waves in DNA molecule using several types of stacking potential.

Chapter 1 presents a brief review of literature on the DNA molecule. We present DNA both as dynamical and biological entity, then, we present the mathematical models used to study the dynamics of DNA.

In chapter 2, we deal with the analytical and numerical methods used in different models studied. Particularly, we present the perturbation method, the Fourier series expansion method, the extended tanh-function method, the linear stability analysis, the variational approach, as well as some numerical method which may be useful to validate our study.

In chapter 3, we present the results obtained in each study with the considered discussions and conclusions. We examine analytically and numerically the possibility of generate soliton-like excitations through the DNA model.

Finally, we end the thesis by giving a general conclusion. We also propose several problems and related lattice models which may be interesting for further studies.

Chapter 1

Generalities on the DNA molecule

1.1 Introduction

The Deoxyribonucleic acid was discovered in 1869 by the Swiss biochemist, F.Miescher. Then called "nuclein", the generic term "nucleic acid" will appear in 1889. At that time, the main feature of the molecule as a carrier of heredity is not suspected. On 1944 the bacteriologist O.T. Avery shows that hereditary characters are transmitted from one bacterium to another by DNA molecules purified. Biochemists have determine the structure of the molecule which constitutes a code for the mechanism of replication. From the results of the biochemist, E. Chargaff in 1950, J. D. Watson and F. Crick in 1953 derived the double helix structure of the DNA.

Physicists have a special interest in working on DNA. It is indeed a long macromolecule. Its double helix structure, following the arrangement of the four elementary molecules which constitute it, makes it more rigid than other polymers, synthetic polymers. Its behavior is similar to that of an ideal chain, mainly dominated by entropy and excluded volume interactions are generally limited because of the stiffness. With current techniques in biochemistry addition, DNA may be synthesized identical to itself so perfectly monodisperse with specificities in the arrangement of the base pairs or termination of the double helix. If the DNA is extracted from a particular strain (viruses, bacteria), the arrangement of base pairs is also identical from one molecule to the other to close the pair of bases. These elements promote the reproducibility of experiments.

1.2 The main characters of DNA

1.2.1 DNA as a biological entity

A. Primary structure

DNA result from the assembly of subunits which constitute its primary structure.

a) Nucleobases classification

The four basic elements of DNA, Adenine, Thymine, Cytosine and Guanine are from two large families of chemical compounds: purine bases derived from heterocyclic purine and pyrimidine bases, which are derived from pyrimidine. Figure 1 represents the purine and pyrimidine and numbering of the atoms of cycles is important for the orientation of the DNA chain Bases. Purine bases found in DNA are 6-aminopurine and adenine (A) and 2-amino-6-oxypurine or guanine (G), but other purine compounds exist in living beings. Pyrimidine bases of nucleic acids are 5-methyluracil or Thymine (T) and 2-keto-4-aminopyridine or Cytosine (C) [21, 1]. Figure 2 gives their representation.

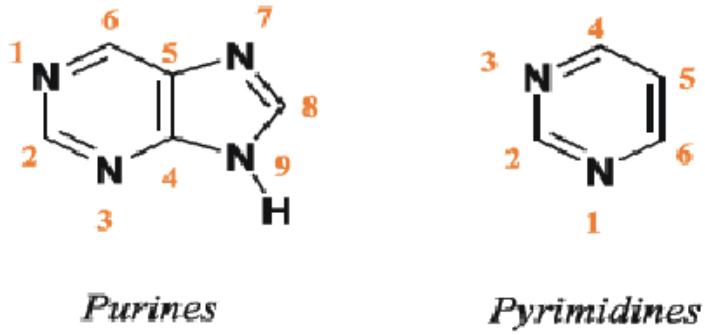

Figure 1: Numbering of purines and pyrimidines. [22].

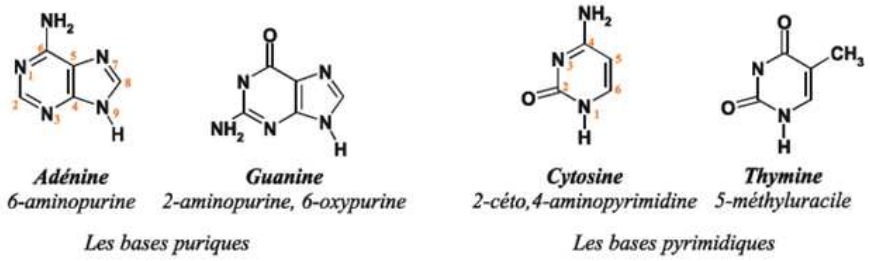

Figure 2: Representation of the purine and pyrimidine bases.[22]

b) Nucleosides and nucleotide

The upper floor of the molecular structure after the foundation is the nucleoside. It consists of the association of a base and a sugar. The sugar in DNA is deoxyribose (see Fig.3 (a)). To

distinguish them from those bases, the carbon atoms are numbered 1 'to 5'. The connection between the base and sugar is called ?-N-glycoside. In the purine nucleoside derivatives, the base is joined to the atom 1 'of the sugar by the N9 nitrogen heterocyclic. In the pyrimidine nucleoside derivatives, it is related to 1' carbon sugar in their N1. And the nucleotide is a nucleoside that has a phosphate group. The precursor's bio-synthesis of nucleic acids are phosphorylated on C5 '.

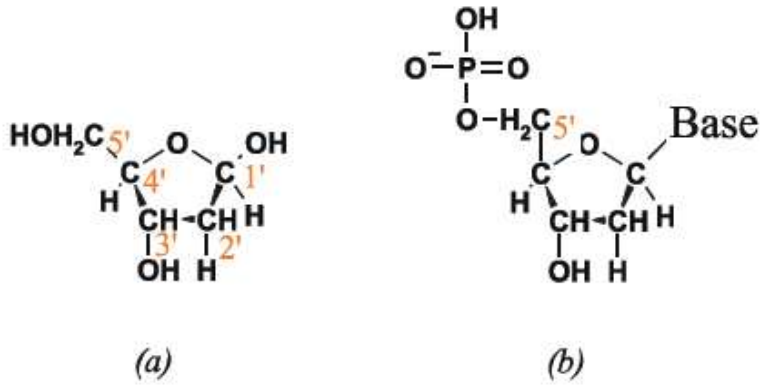

Figure 3: : (a) - Deoxyribose. The numbering of atoms is important for the orientation of the molecule. (b) - Representation of a nucleotide associated with deoxyribose. In DNA, the nucleotides are phosphorylated on C5'.[22]

c) Primary structure of nucleic acids

The nucleic acids are polymers of nucleotides. The phosphodiester bonds of a nucleotide to another are established between a nucleotide C3'OH C5'P and the next. The chain orientation is essential for the interaction of proteins with the molecule. Fig.4 gives a representation of a sequence of nucleotides in DNA.

d) Ionization of bases and nucleotides

The DNA of cells immersed in a liquid medium, said physiological. This is where the replication process occurs. The chemical characteristics of the environment such as pH or the presence of salts (ionic strength of the solution) will control the physical chemistry of the molecule. At pH <1, one base is protonated and phosphates are neutralized. As soon as the pH increases, the first deprotonations phosphates appear. Under physiological conditions in particular (pH $= 7$), the sucro phophate-chain of the molecule is negatively charged. This is what gives the chain its polyelectrolyte character. This acidic character will be responsible for its interactions with salts and ions of the physiological medium.

B. Secondary Structure

a) The model of the double helix by Watson and Crick

This structure was identified in 1953 by J.D Watson and F. Crick [1] from the operation of X-ray diffraction photographs Crick had deduced the helical structure of the molecule. Parallel work of R. Franklin had helped to highlight the following results:

*Bases are perpendicular to the axis of the helix.

*They are stacked at a distance of 0.34nm.

*A turn of the helix contains 10.4 nucleotides; the helical pitch is of the order of 3.4nm.

*The diameter of the helix is of the order of 2nm.

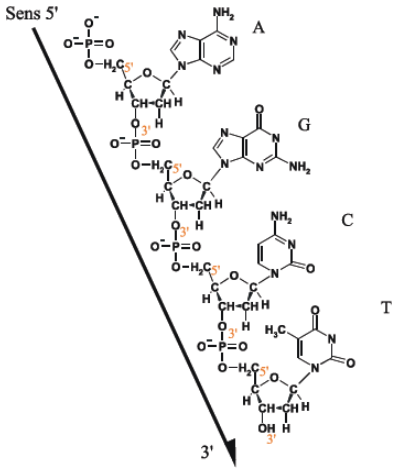

Figure 4: Sequence of nucleotides in DNA.[22]

Given the size of a nucleotide, the expected diameter of the molecule is 1 nm, where the idea of a double-stranded molecule. From these elements, Watson and Crick proposed that the bases are inside a double helix. The basics have not all the same size; they deduce that mate purine-pyrimidine pairs by hydrogen bonds to maintain a constant diameter of 2 nm. Identification of pairs AT, CG is obtained from the results of Chargaff (see fig.5). In this model, DNA consists of two chains of sugar and phosphate and antiparallel arranged helically. The bases are centrally matched pairs. The two ends of the double helix are identical and terminate in and C5'P C3'OH. The helix is right (see Fig.6).

The double helix is like a ladder whose amounts are alternating sugars and phosphates and bars base pairs (bp). Binding sites of the bars are in the plane of the base pair but not in the axis of the bar. So instead of having a regular structure, the double helix has two depressions: a large or major groove and a narrow or minor groove. Their depths are substantially equivalent widths and 1.14 and 0.6 nm. The alternation of the base pairs along the sucro-phosphate backbone

forms the genetic code. During transcription, the code is read by an enzyme, RNA polymerase, which forms a messenger RNA which produces the protein corresponding to the original code. The size of the molecules varies organizations. For humans, there are about tens to hundreds of millions of base pairs per chromosome. Each human cell has 23 pairs of chromosomes. This represents a total length of 3 meters.

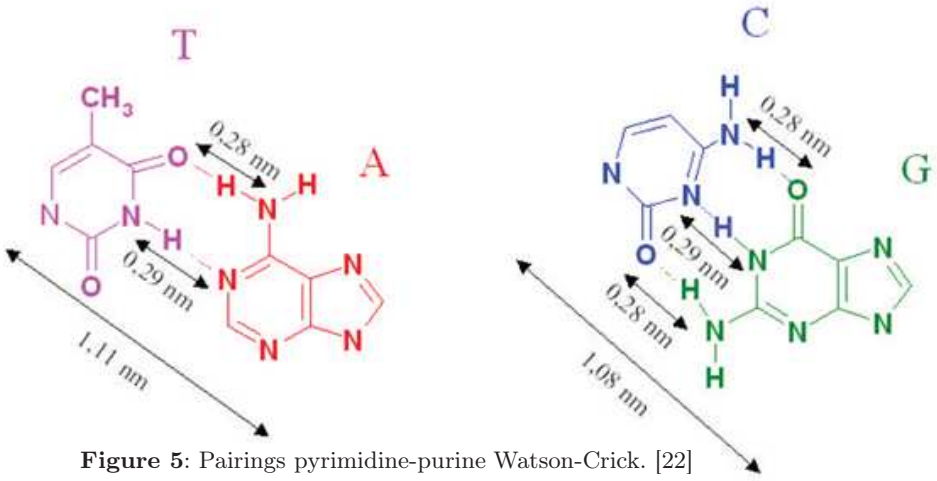

Figure 5: Pairings pyrimidine-purine Watson-Crick. [22]

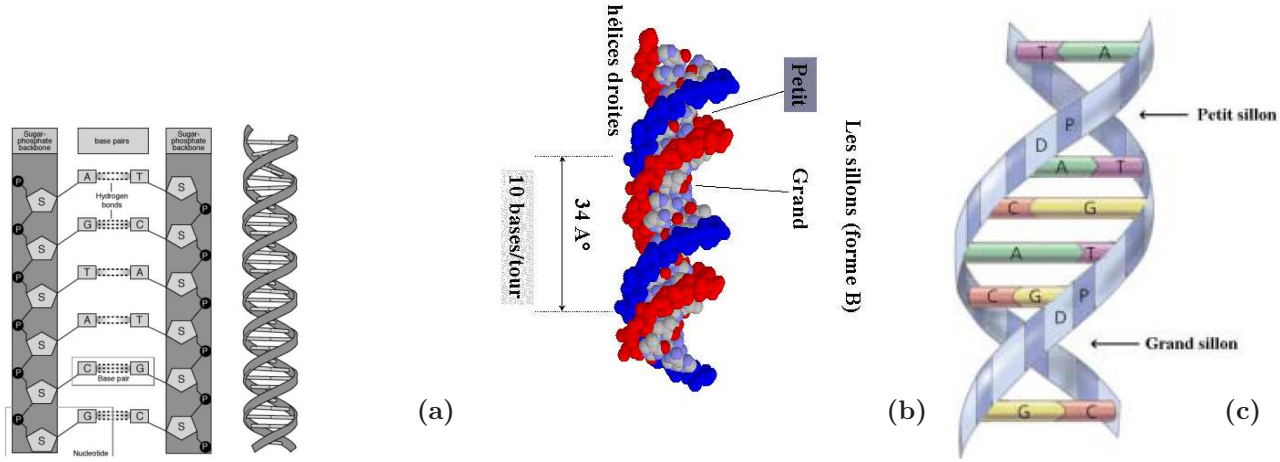

Figure 6: The double-helix model of Watson and Crick and molecular modeling. [23, 24, 25]

b) The different forms of DNA

The model described by Watson and Crick is the B structure of DNA. Under the terms

of ionic strength, hydration or mechanical, other characteristic forms of the double helix may occur. The structure B is the most common life form. The stability of these helices result of hydrogen bonds between bases but also hydrophobic interactions between trays bases which we give the name of stacking interactions ("stacking"). These are due to the fact that it is energetically favorable to hydrophobic cycles to "flatten" to each other rather than be exposed to the aqueous solution in which bathes the DNA. If the cohesion of the double helix associated with hydrogen bonds is dependent only of the composition pairs, couples AT committing two against three CG bonds, the stacking forces are related, in addition to the succession of sequences. The scale of the free energy stack according to the composition is given in Fig.7 (a).

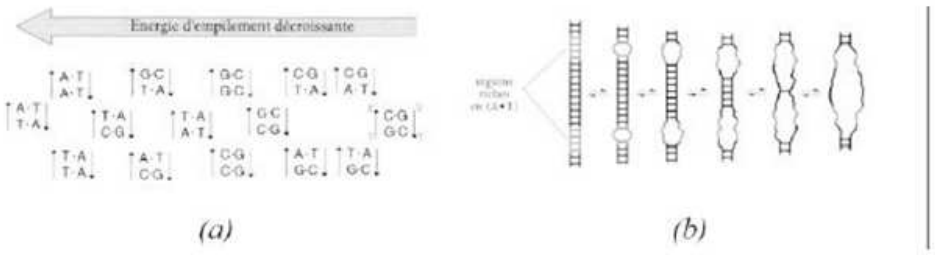

Figure 7: (a) - Free Energy stacking base pairs, according to [28]. It should be noted that the orientation of the molecule along the axis 5'-3 'leads to a different energy for couples such 5'A 3'T and 5' T-3'A. (b) - DNA aperture during thermal denaturation. The richest groups in AT areas open first.

1.2.2 DNA as a dynamic entity

When considering the structure of the molecule (see Fig. 6), we find that the genetic code carried by the foundation is well protected inside the double helix, which is certainly favorable to avoid it easily altered, but it is also a serious limitation when you have to "read" the code, that is to say, perform chemical reactions involving the bases. Access to information contained in the DNA double helix is possible only because the propeller can be opened locally. The structure is not static but dynamic contrast. We can distinguish different types of movements: those involved in the replication and transcription, and large fluctuations, known to biologists as the "breath of DNA" that occur at any time. Can be added to thermal denaturation, which is a purely physical process of heating due to the molecule which results in the destruction of the double helix.

A. Denaturation and renaturation of DNA

The double helical structure may be destabilized. Heating, varying the electrostatic repulsion between the strands by altering the pH or ionic strength of the solution, or mechanically

stressing the double helix can lead to denaturation of the molecule, that is to say to the physical separation of the two strands. It can be complete and irreversible in this case, or local, and then reversible (annealing), like a zipper that can open and close again. AT-rich regions open before GC rich regions and distortion spreads (see Fig. 7 (b)).

B. Transcription and replication.

The two basic phenomena that characterize the dynamic nature of DNA are replication and transcription. Replication completely fills the genetic information by opening the molecule as a zipper (Fig. 8 (a)). Transcription corresponds to the reading of a single strand, that is to say a few hundred or thousand base pairs. It is initiated by an enzyme, RNA polymerase which binds to the DNA to synthesize mRNA. This activation results, after a series of intermediate events, a local denaturation of the double helix (range 10 to 20 base pairs), which is the rate-limiting step in transcription. This opening is then propagated along the gene, exposing successively all its bases (Fig. 8 (b)).

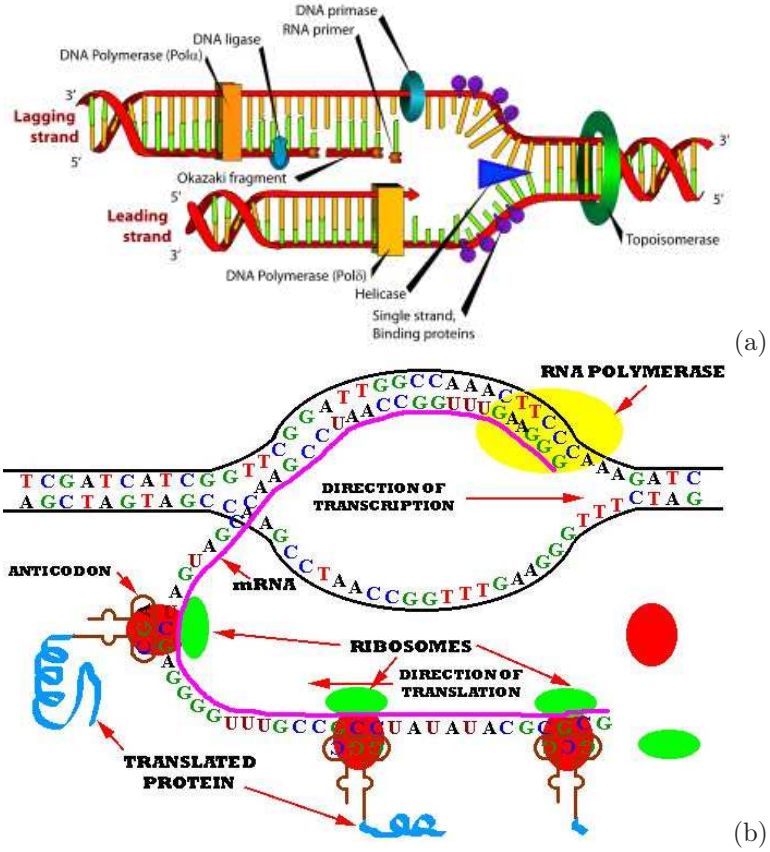

Figure 8: Réplication (a) et Transcription de l'ADN (b) [25]

C. The "breathing" of DNA

Since the structure of biological macromolecules is stabilized by weak interactions, we can expect significant fluctuations due to thermal motion. The existence of open temporary states of DNA and some double helix synthetic polynucleotides was demonstrated by measurements of proton exchange. Base pairs are separated reversibly exposing nucleotide protons to exchange with those of the solvent, and then close. These open states exist in many daris the double helix, even at room temperature. The hydrogen proton exchange cross-database links provides a more direct and non-disruptive method to study the movement of the bases. I1 can be followed by the tritium labeling (when measured by radioactivity) or by deuterium labeling (insure by optical methods compatible with rapid kinetics). These techniques were used to study the exchange of protons in homopolymers of RNA or DNA in natural DNA fragments. Nuclear magnetic resonance (NMR), which is able to identify the exchangeable protons and measure the speed of exchange, is now used in most of these studies. In the early 1980s NMR measurements [29, 30, 31] or Raman [32, 33] have revealed the presence of low frequency oscillating movements and long life in the DNA molecule. These movements, compared to breathing (the term "(breathing" was used for the first time by Von Hippel PH), were subsequently the subject of theoretical studies by the group Prohofsky [34, 35] that shown that breathers can be either highly localized or spread over a wide area of the molecule. Inspired by the theory of solitons and breathers particular, one think that breathing mode can be created by a very low energy input, the breathers could be the cause of the location of energy in the molecule and may lead to local denaturation. It should be interesting to develop a theoretical and descriptive explanation of these "bubbles" of denaturation and study their dynamics.

1.3 Mathematical models of DNA dynamics

Mathematical models of biological systems should be very complex to model the system accurately. Physicists have been very successful in modelling complex system with very simple models. The key has been to restrict the study to some particular cases, then model these cases. Finally, putting these simples models together in order to understand a complex system. In biology this method is not as simple, since this often practically would kill the organism one is studying. One therefore has to study the whole complex system, but one can restrict oneself to some particular process where one effect is believed to be the dominant one. We will use this experience from physics and use a very simple model to model the complex DNA molecule under some special assumptions.

1.3.1 Interaction in DNA

The chemical covalent (C-V) bonds between atoms of the DNA molecule have actually, as just mentioned, for the greater part of cases excitation energies well above the temperature at

which DNA lives. In these conditions, we should consider the backbone as rigid, with no "small oscillations" possible: although we are going to discuss classical mechanics models for the degrees of freedom of interest, we should not forget that the molecule obeys quantum mechanics, so that even in classical modeling it would be physically wrong to allow for motions of these "hard" degrees of freedom. Let us look more closely at the structure of DNA, with special attention to "soft" degrees of freedom, i.e. to degrees of freedom excited at body temperature. These are of three kinds [36]:

a) The H-bonds between pairing bases;

b) The bases are essentially free to rotate around the N-C bond linking them to the nucleoside (free with respect to covalent interactions; interactions of other nature-e.g. electrostatic-with the other atoms in the molecule give a restoring torque, as we will see later);

c) The sugar ring in the nucleoside has nearly degenerate equilibrium positions, separated by a potential barrier, and an tunnel between the equilibrium positions on the two sides of the plane. This is known as sugar puckering, and the excitation energy of such sugar puckering modes is similar to that of the H-bonds. Sugar puckering affects the geometry of the double helix, and one of its effects is to take apart bases in a H-bonds pair, i.e. to move radially (with respect to the axis of the double helix) the base attached to the sugar affected by puckering. The identification of these degrees of freedom as the only ones which should actually be affected by body-temperature dynamics is actually enough to introduce and justify the models we want to discuss. Indeed, due to the great complexity of the molecule, the models (and the parameters appearing in them) should be regarded as effective ones for the models of these selected degrees of freedom, i.e. we should not try to deduce details of the models and value of the parameters from first principles and the structure of the molecule, but just find a model which describes coherently with experimental observation the motion of these degrees of freedom. We will anyway mention some other details on interactions in DNA, before determining the models; this will permit to fix terminology. Usually, the interactions between bases are divided into pairing and stacking ones; the former are essentially due to H-bonds, while the latter are due to a number of effects in the molecule, and their net effect is to keep stacked one over the other the bases on each helix. The stacking interactions also greatly influence the pairing. The energy of H-bond pairing also greatly differs for the pairs (A-T) and (G-C): indeed, this is no surprise, since in one case the bases are couples by three H-bond, while in the other one by two H-bonds. The stacking interactions can be thought as responsible for the restoring forces trying to keep the bases in their equilibrium positions independently of the H-bonds, i.e. the forces opposing the "rotational" and "vibrational" movements of points b) and c) above. Indeed, one observes experimentally that once three consecutive pairs of bases are bridged by H-bonds, stacking forces to continue the closing of the double helix; this also gives a brute estimate of $1/3$ for the ratio between pairing effects due to stacking and direct pairing forces due to H-bond.

The local opening of the double helix, i.e. the breaking of the H-bonds between pairing bases,

are accessible to experimental observation. This is usually done through study of absorption of UV rays [37] for details. From our point of view, the base pair openings will be the central object of our study. It should be remarked, in relation to the above discussion of accessible degrees of freedom, that the H-bonds can be broken either by increasing the distance between pairing bases (e.g. by the geometrical effect related to sugar puckering, as described above), either by rotation of the bases around the N-C bond connecting them to the relative nucleoside. Indeed, H-bonds are often strongly directional, so that a change in direction of the bases, although comporting only a small variation in the relative distance, can be quite effective in breaking the H-bonds.

1.3.2 Common features of the DNA models

From the above short discussion, it follows that our simple modes for DNA dynamics should have several features:

a) Consider only the two degrees of freedom per helix segment, i.e. per base, considered above; from now on we will call "vibrational" the dynamics associated to sugar puckering and rectilinear (radial with respect to the axis of the double helix) separation of the bases in a pair, and "torsional" the dynamics associated to rotations of the bases around the C-N bond linking them to the sugar ring in the nucleoside.

b) Consider direct pairing and staking forces.

c) Not depend on details of the forces between bases. But only on qualitative features. On the other side, and always due to our lack of understanding of such a complex molecule, the constants (coupling constants and parameters) appearing in the model should be seen as effective ones, i.e. we have some freedom in their choice.

We will moreover choose to describe the dynamics we are interested in terms of classical mechanics rather than in quantum terms (but, as explained before, the restriction to the degrees of freedom we actually consider is justified by quantum mechanical consideration); this is admittedly a matter of preference, and other approaches would be possible, considering quantum mechanical models or even looking at the double helix as an Ising system (the two states of the "spin" at a site would correspond then to "closed" or "open" H-bonds between bases at the site), [38, 39].

Although a model having these features would already be extremely simplified (we are in fact considering by now only two degrees of freedom per base), we want to operate a further simplification. Namely, we want to consider separately models for the vibrational dynamics alone and for the torsional dynamics alone (vibrational and torsional in the sense explained above), so to have only *one* degree of freedom per base. We will moreover introduce still another further severe simplification: we will assume that all the bases are equal: i.e. they have the same mass and moment of inertia, and all couplings of the same type are equal. (We will moreover assume double helix to be of infinite length, as we suppose side effects to be inessential).

Such models were introduced by Peyrard and Bishop [40] for the vibrational dynamics, and by Yakushevich [41] for the torsional one; we will sometime refer to them as "planar" ones for reasons to be evident in the following. They will also be indicated. For short, as PB model and Y model respectively. It must be stressed that while the reduction to two degrees of freedom per base discussed above was well justified physically, the present splitting of the dynamics in two noninteracting parts is admittedly due to an attempt to deal with a manageable problem rather than to physical consideration. We will see anyway that, somehow rather surprisingly, these "one degree of freedom models" are able to capt relevant experimentally observed features of DNA dynamics; this will give a justification a posteriori of our splitting.

Let us now shortly describe some features common to all the models we are going to discuss in this section. We write down the models in term of kinetic T plus potential V energy. The hamiltonian is given by:

$$H = T(\dot{u}) + V(u), \tag{1.1}$$

where we assume

$$T(\dot{u}) = \sum_{n,i} \frac{1}{2} m(\dot{u}_n^i)^2, \tag{1.2}$$

with m the mass of the bases, according to the degree of freedom taken in consideration; $u_n^i (n = 1, 2..., i \epsilon Z)$is the generalized coordinate describing the base at site n on the ith chain of the double helix, which we suppose of infinite length. As for the potential energy, it can be divided into three parts: a pairing, or transverse, interaction energy V_T , a stacking interaction energy V_S, and a third kind of energy (helicoidal interaction energy) V_H to be discussed later on. So we have

$$V(u) = V_S(u) + V_T(u) + V_H(u). \tag{1.3}$$

If $V_H(u) = 0$ model will be called planar and we assume that

$$V_T = \sum_n U_T(u_n^1, u_n^2), \qquad V_S = \sum_n U_S(u_{n+1}^i, u_n^i). \tag{1.4}$$

We use coordinates such that $u_n^i = 0$ correspond to the equilibrium stable configuration.It should be stressed that, since the stacking is considerably stronger than H bonding, the nonlinear effects will appear essentially only in the direct pairing (transverse) interactions. This amounts to say that the dynamics stretches the stacking interactions much less that the H bonds. These observations suggest to consider an harmonic potential approximation for stacking interactions. However, a work considering anharmonic stacking interactions [41] has shown that nonlinear stacking can have a dramatic effect on the thermodynamics of the transition; anyway, it was observed from numerical simulations that it has only a small effect on the

dynamics of the nonlinear excitations, except in the immediate vicinity of the denaturation transition.

1.3.3 The simple mathematical model to describe the nonlinear dynamics of DNA

a) The Peyrard-Bishop model

The model used to describe molecule dynamics of DNA is through the whole thesis the Peyrard-Bishop model, named after its creators Michel Peyrard and Alan Bishop [40]. It has been successful in its predictions of denaturation temperature and transition curves of DNA sequences. It is applicable when the separation distance is large compared to other quantities. It seems reasonable that the PB-model could serve as a first step towards description of the transcription and replication of DNA, as well.
We consider the "vibrational" dynamics of DNA, associated to sugar puckering modes; as recalled before, this corresponds to radial motion of the bases with respect to the axis of the double helix; the coordinate x_n^i describing the position of the base will then be its distance from the axis of the double helix, or better, in order to keep x_n^ias the equilibrium configuration, this distance minus the distance corresponding to the equilibrium position (see Fig. 9). We will consider such a model, which was proposed by Peyrard and Bishop [40]; they suggested to use as pairing potential the Morse potential: namely, if x_n^i is the coordinate defined above for the nth base on the ith chain, we have

$$V_n = D[e^{-a(x_n^1 - x_n^2)} - 1]^2 = D[e^{-a\sqrt{2}\psi_n} - 1]^2, \tag{1.5}$$

where in the last expression we introduced again the coordinates

$$\phi_n = \frac{x_n^1 + x_n^2}{\sqrt{2}}; \quad \psi_n = \frac{x_n^1 - x_n^2}{\sqrt{2}}, \tag{1.6}$$

D is the dissociation energy and a a parameter homogeneous to the inverse of a length, which sets the spatial scale of the potential. Its shape is presented in Fig. 10 This expression has been chosen because it is a standard expression for chemical bonds and, moreover, it has the appropriate qualitative shape [40]:

★ it includes a strong repulsive part for $\psi_n < 0$,
corresponding to the steric hindrance between bases in a pair,

★ it has a minimum at the equilibrium position $\psi_n = 0$ and

★ it becomes flat for large un, giving a force between the bases that tends to vanish, as expected when the bases are very far apart; this feature allows a complete dissociation of the

base pair, which would be forbidden if we had chosen a simple harmonic potential. As for stacking interactions, we keep the harmonic potential approximation, which gives

$$\begin{aligned} w_n &= \frac{k}{2}[(x^1_{n+1} - x^2_n)^2 + (x^1_{n+1} - x^2_n)^2] \\ &= \frac{k}{2}[(\phi_{n+1} - \phi_n)^2 + (\psi_{n+1} - \psi_n)^2] = W(\psi_n, \psi_{n+1}) + W(\phi_n, \phi_{n+1}) \end{aligned} \tag{1.7}$$

the potential $W(\psi_n, \psi_{n+1})$ and $W(\phi_n, \phi_{n+1})$ describe the interactions between adjacent bases along the DNA molecule. It has several physical origins:

★ The presence of the sugar-phosphate strand, which is rather rigid and connects the bases. Pulling a base out of the stack in a translational motion tends to pull the neighbors due to this link. One should note, however, that we have not specified the three-dimensional motion of the bases in this simple model. An increase of the base pair stretching could also be obtained by rotating the bases out of the stack, around an axis parallel to the axis of the helix and passing through the attachment point between a base and the sugarphosphate strand. Such a motion would not couple the bases through the strands. The potential $U_S(u_n, u_{n-1})$ is an effective potential which can be viewed as averaging over the different possibilities to displace the bases.

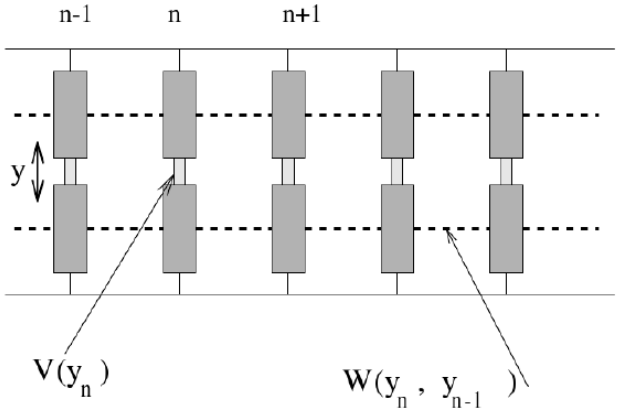

Figure 9: *The PB model, set to study the processes of transcription and replication, was also used in thermal denaturation of DNA. This model only considers short-range interaction due to the stacking of adjacent base pairs which is denoted by $W(y_n, y_{n-1})$. Since the bases are connected one to another through hydrogen bonds, the Morse potential, $V(y_n)$, is chosen because of its shape. Only the transversal displacements of the bases denoted by y_n from their equilibrium positions along the direction of the hydrogen bonds are considered [40].*

Note that the Morse potential has the important property that its derivative goes to zero as the separation, ψ_n goes to infinity, which is a necessary property for a potential that should model large separations realistically. In order to obtain the Hamiltonian for the system one also has to know the kinetic energy

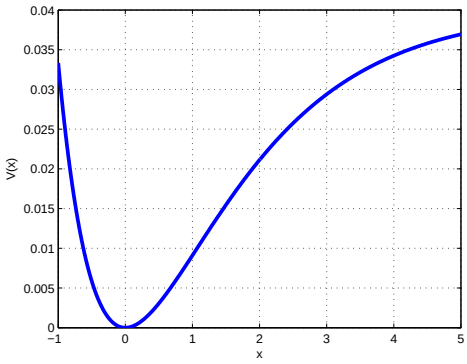

Figure 10: *The panel shows the 2D-plot of the Morse potential. This potential has been chosen because it is a standard expression for chemical bonds and, moreover, it has the appropriate qualitative shape:* ***(i)*** *it includes a strong repulsive part for $y < 0$, corresponding to the steric hindrance between bases in a pair, (ii) it has a minimum at the equilibrium position $y = 0$ and* ***(iii)*** *it becomes flat for large y, giving a force between the bases that tends to vanish, as expected when the bases are very far apart; this feature allows a complete dissociation of the base pair, which would be forbidden if we had chosen a simple harmonic potential .*

$$T_n = \frac{m}{2}((\dot{x}_n^1)^2 + (\dot{x}_n^2)^2 = \frac{m}{2}(\dot{\phi_n}^2 + \dot{\psi}_n^2), \tag{1.8}$$

of each particle, where as before dots indicates differentiation with respect to time. Hence, the Hamiltonian for this system is

$$H_n = \sum_n [\frac{m}{2}(\dot{\phi_n}^2 + \dot{\psi}_n^2) + \frac{k}{2}[(\phi_{n+1} - \phi_n)^2 + (\psi_{n+1} - \psi_n)^2] + D[e^{-a\sqrt{2}\psi_n} - 1]^2]. \tag{1.9}$$

The equations of motion for this system is then separated such that

$$m\ddot{\psi}_n = k(\psi_{n+1} - 2\psi_n + \psi_{n-1}) + 2\sqrt{(2)}aD(e^{-2a\sqrt{2}\psi_n} - e^{-a\sqrt{2}\psi_n}), \tag{1.10}$$

$$m\ddot{\phi}_n = k(\phi_{n+1} - 2\phi_n + \phi_{n-1}). \tag{1.11}$$

b) Helical geometry and helicoidal DNA models

The PB model which described up to now have been qualified as planar; this is due to the fact that it can be schematized as in Fig. (9). The PB model do not take into account the peculiar geometry of the double helix. It turns out that taking this into account, even in a "minimal" way, produces qualitative changes in the dynamics, quite relevant also in relation with "observable" properties of the model (especially in the case of the PB model). The modification we consider here was first proposed in the context of the Yakushevich model [41, 42], and then applied also to the Peyrard- Bishop one [43, 44]. The modified model in this way will be qualified as helicoidal. In the following, we will write HPB for "helicoidal Peyrard-Bishop". In a double helix (with pitch of the helix 2h in base units) it happens that bases which are half-wind of

the helix apart, i.e. h sites away, come to be spatially near, so that they can interact. It should be stressed that such an interaction is actually present in real DNA, where it is realized by bridging water filaments between the concerned bases. From the point of view of our model, and referring to the notation previously employed, w_n become:

$$w_n = \frac{k}{2}[(x_n^1 - x_n^2)^2 + (x_n^1 - x_n^2)^2] + U_H, \tag{1.12}$$

with

$$\begin{aligned} U_H = \frac{K}{2}[(x_n^1 - x_{n+h}^2)^2 + (x_n^1 - x_{n-h}^2)^2] = \frac{K}{2}[(\phi_{n+h} - \phi_n)^2 + (\psi_{n+h} + \psi_n)^2] \\ = U_H(\phi_{n+h}, \phi_n) + U_H(\psi_{n+h}, \psi_n), \end{aligned} \tag{1.13}$$

this means that the hamiltonian will now be of the form

$$\begin{aligned} H_n = \sum_n [\frac{m}{2}(\dot{\phi_n}^2 + \dot{\psi_n^2}) + \frac{k}{2}[(\phi_{n+1} - \phi_n)^2 + (\psi_{n+1} - \psi_n)^2] \\ + \frac{K}{2}[(\phi_{n+h} - \phi_n)^2 + (\psi_{n+h} + \psi_n)^2]] + D[e^{-a\sqrt{2}\psi_n} - 1]^2. \end{aligned} \tag{1.14}$$

The HPB hamiltonian above gives as equations of motion

$$\begin{aligned} m\ddot{\psi_n} = k(\psi_{n+1} - 2\psi_n + \psi_{n-1}) + K(\psi_{n+h} + 2\psi_n + \psi_{n-h}) + 2\sqrt{(}2)aD(e^{-2a\sqrt{2}\psi_n} - e^{-a\sqrt{2}\psi_n}) \\ m\ddot{\phi_n} = k(\phi_{n+1} - 2\phi_n + \phi_{n-1}) + K(\phi_{n+h} - 2\phi_n + \phi_{n-h}). \end{aligned} \tag{1.15}$$

1.3.4 A complex model of DNA dynamics

a) A model of DNA torsion dynamics

In the model proposed by L. Yakushevich [41], the pairing interaction is considered in the approximation of harmonic potential, depending on the distance between the endpoints of the bases, i.e. the atoms bridged by of an angle θ of rotation around the N-C bond, the force becomes a nonlinear function of such an angle. Here the distance l between points p_1 and p_2 satisfies

$$l^2 = [d + 2r - r(cos\theta_1 + cos\theta_2)]^2 + [r(sin\theta_1 + sin\theta_2)]^2. \tag{1.16}$$

It is then convenient to pass to coordinates

$$\varphi_\pm = \frac{\theta_1 \pm \theta_2}{2}. \tag{1.17}$$

In terms of which, by standard trigonometric identities, the distance is written as

$$l^2 = d^2 + 4r^2(1 + cos^2\varphi_- - cos\varphi_+ cos\varphi_-). \tag{1.18}$$

Yakushevich does also suggest to consider the approximation $d \to 0$. In other words we are considering the stretchning of H bond due to small rotations of the bases and extend this to

the full range $[0, 2\pi]$ of angular coordinates. Notice that we are trascurating the directionality effects, as only distance is taken into account. The potential describing the pairing interaction will then be

$$U_T = \frac{1}{2}\alpha[1 + cos^2\varphi_- - cos\varphi_+ cos\varphi_-], \tag{1.19}$$

(notice that this is $2\pi - periodic$ in both angular coordinates, as it should) As for stacking interactions, we will also a fortiori keep the harmonic approximation for them; if θ_n^i is the angular coordinate relation to the $n - th$ chain (i= 1, 2), the stacking interaction potential between bases at sites n and $n+1$ will be.

$$U_S = \frac{1}{2}\beta[(\theta_{n+1}^{(1)} - \theta_n^{(1)})^2 + (\theta_{n+1}^{(2)} - \theta_n^{(2)})^2], \tag{1.20}$$

Passing again to the coordinates

$$\theta_n^{(1)} = \theta_n^{(+)} + \theta_n^{(-)}; \quad \theta_n^{(2)} = \theta_n^{(+)} - \theta_n^{(-)}, \tag{1.21}$$

the above reads

$$U_S = \frac{1}{2}\beta[(\theta_{n+1}^{(+)} - \theta_n^{(+)})^2 + (\theta_{n+1}^{(-)} - \theta_n^{(-)})^2]. \tag{1.22}$$

In the following, in order to avoid confusion and to lighten notation, we will prefer to write $\psi = \theta^+$ and $\phi = \theta^-$ the Hamiltonian in this model is given by:

$$\begin{aligned} H &= T + U_S + U_T + U_H \\ T &= \sum_n \frac{1}{2} I[(\dot{\theta}_n^{(1)})^2 + (\dot{\theta}_n^{(2)})^2], = \sum_n \frac{1}{2} I[(\dot{\psi}_n)^2 + (\dot{\phi}_n)^2] \\ U_S &= \frac{1}{2}\beta[(\psi_{n+1} - \psi_n)^2 + (\phi_{n+1} - \phi_n)^2], \\ U_T &= \frac{1}{2}\alpha[1 + cos^2\phi_n - cos\phi_n cos\psi_n] \\ U_H &= \frac{K}{2}[(\phi_{n+h} - \phi_n)^2 + (\psi_{n+h} + \psi_n)^2]], \end{aligned} \tag{1.23}$$

where we introduced the ψ, ϕ coordinates in the kinetic term T as well. The equilibrium (stable) configuration is represented by $((\psi, \phi) = (0, 0) \forall n)$; I is the moment of inertia of the bases around the N-C bond. The above hamiltonian gives as equations of motion

$$\begin{aligned} I\ddot{\psi}_n &= \beta(\psi_{n+1} + \psi_{n-1} - 2\psi_n) + K(\psi_{n+h} + 2\psi_n + \psi_{n-h}) - \alpha sin\psi_n cos\phi_n, \\ I\ddot{\phi}_n &= \beta(\phi_{n+1} + \phi_{n-1} - 2\phi_n) + K(\phi_{n+h} - 2\phi_n + \phi_{n-h}) - \alpha sin\phi_n(cos\psi_n - cos\phi_n), \end{aligned} \tag{1.24}$$

after expanding the term in sinus and cosinus until the third order, we get the following system:

$$\begin{aligned} \ddot{\psi}_n &= K_s(\psi_{n+1} + \psi_{n-1} - 2\psi_n) + K_h(\psi_{n+h} + 2\psi_n + \psi_{n-h}) - c(\psi_n - \frac{\psi_n^3}{6} - \frac{\phi_n^2\psi_n}{2}), \\ I\ddot{\phi}_n &= K_s(\phi_{n+1} + \phi_{n-1} - 2\phi_n) + K_h(\phi_{n+h} - 2\phi_n + \phi_{n-h}) - c(\phi_n^3 - \phi_n\psi_n^2), \end{aligned} \tag{1.25}$$

with $K_s = \frac{\beta}{I}$; $K_h = \frac{K}{I}$; $c = \frac{\alpha}{I}$.

b) The DNA model with anharmonic stacking interactions

Peyrard and Bishop [38] proposed a model to describe the denaturation processes of a homogeneous DNA double helix

$$U = w(y_n, y_{n-1}) + V(y_n), \tag{1.26}$$

where, y_n is the stretching of the $n-th$ base-pair, w is the stacking interaction of the nearest neighbors n and $n+1$, and V the interaction of the $n-th$ base-pair. The PB model does not give rise to a sharp first-order-like denaturation which have been observed experimentally. This issue was addressed later by Dauxois, Peyrard and Bishop [45, 46] by the addition of an anharmonic term to the stacking interaction

$$w_{an.}(y_n, y_{n-1}) = [1 + \rho e^{-\alpha(y_n + y_{n-1})}] w_{harm.}(y_n, y_{n-1}), \tag{1.27}$$

where, $w_{harm.}$ can take several for: it is possible to improve it as follows [5]

$$w_{harm.}(y_n, y_{n-1}) = \frac{k}{2}(y_n - y_{n-1})^2. \tag{1.28}$$

When the hydrogen bonds connecting the bases are broken, there is a modification of the molecule structure leading to stacking interaction between adjacent bases. This is denoted by the known quadratic term $(y_n - y_{n-1})^2$ which is governed by the factor $\frac{k}{2}[1 + \rho e^{-\alpha(y_n + y_{n-1})}]$. This factor decreases from $\frac{1}{2}k[1+\rho]$ to $\frac{1}{2}k$, when either one or both base pair is stretched.

Gerald Weber et al. [47] proposed an alternative form for the harmonic potential [48, 49], rewriting equation (1.28)

$$w_{harm.}(y_n, y_{n-1}) = \frac{k}{2}(y_n^2 - 2y_{n-1}y_n cos\theta + y_{n-1}^2), \tag{1.29}$$

where, θ is the twist angle between neighbouring base pairs. This is motivated by 3D helicoidal models such as proposed by Barbi et al [50], as well as torsional potentials used in molecular dynamics [51]. This formulation is particularly convenient as it can be readily introduced in existing models, such as the anharmonic-Morse model [52, 53], without significantly modifying existing analytical calculations. For an angle of $\theta = 0$ the usual harmonic stacking interaction term [54] is obtained and would represent the situation of perfectly parallel neighbouring bonds. Evidently, the base pairs can only denaturate when the double helix is largely unwound and therefore we use a small, but non-zero, fixed angle of $\theta = 0.01$ rad for the calculations presented in this work.

Similar anharmonic formulations have been put forth by Joyeux and Buyukdagli [55] with the introduction of a finite stacking potential

$$w_{fin.}(y_n, y_{n-1}) = \frac{\Delta H}{2}[1 - e^{-\alpha(y_n - y_{n-1})^2}] + \frac{K_b}{2}(y_n - y_{n-1})^2, \tag{1.30}$$

where, ΔH is a finite stacking energy and the harmonic potential is used with a much smaller elastic constant K_b (about three orders of magnitude smaller than k for the HM model). Also,

Saccomandi and Sgura [56] proposed the addition of a nonlinear term to the stacking potential of polynomial form

$$w_{pol.}(y_n, y_{n-1}) = w_{harm.}(y_n, y_{n-1}) + \frac{K_{nl}}{4}(y_n - y_{n-1})^4, \tag{1.31}$$

to obtain the similar effect of sharpened transitions, where they introduced the additional parameter k_{nl}. The addition of anharmonic terms to the nearestneighbour interaction potential w is not the only form to obtain a sharp DNA denaturation. We showed that the addition of a solvent potential to the base-pair, interaction also causes such a sharp denaturation [57].

$$V(y_n) = D(1 - e^{-ay_n})^2 - f_s D[tanh(y_n/\lambda_s) + 1], \tag{1.32}$$

the first term is the usual Morse potential [40] which describes the hydrogen bonds of the base-pairs. The second term is a solvent interaction potential, adapted from Drukker et al [51], which simulates the formation of hydrogen bonds with the solvent once the base-pair hydrogen bonds are displaced by more than λ_s from their equilibrium values. For $y_n > \lambda_s$ the base pairs are pulled away from each other until the bond with the solvent is established. Once the bases are bonded to the freely moving solvent molecule they are no longer pushed to any particular direction, a situation which is represented by the potential plateau for $y_n > \lambda_s$ (see also Fig. 11)

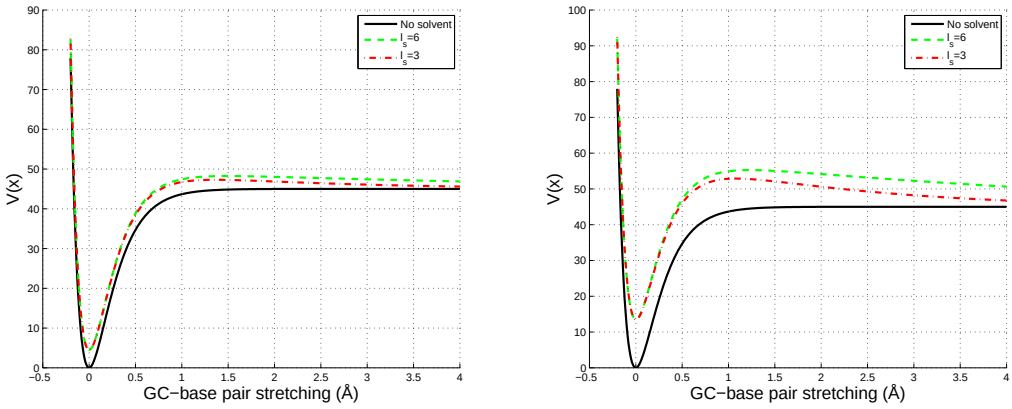

Figure 11: GC- base pair stretching (a):$f_s = 0.1$ and (b): $f_s = 0.1$

The Hamiltonian in this model is given by:

$$H = T + U. \tag{1.33}$$

In so doing, the equations describing the local stretching of the base pairs are, as a whole, given by

$$m\ddot{y}_n = -\frac{\partial w(y_n, y_{n-1})}{\partial y_n} - \frac{\partial w(y_{n+1}, y_n)}{\partial y_n} - \frac{\partial V(y_n)}{\partial y_n}. \tag{1.34}$$

1.3.5 Toward realistic models of DNA molecule

T model proposed above, introduce a one-dimensional Hamiltonian DNA model capable of reproducing the main features of the experimental denaturation curves for homogeneous and heterogeneous DNA sequences. We have shown that the sequence heterogeneity is properly taken into account by the introduction of stacking depending on the nature of the base pair energies. Despite these encouraging results, we can assume that the model of Eq. 1.27,1.30 or 1.31 is a bit simplistic. The major limitation of this model is that each degree of freedom y_n is an integer monomer, ie both the base and the sucre phosphate skeleton, then it would be desirable that the elongation of large amplitude base and the weak fluctuations skeleton are treated separately. In addition, the dissociation of the sequence is described solely in terms of the coordinated elongation, while the rotation of the bases relative to the axis of the double helix is likely to play an important role in the separation of the two strands. Sahin BUYUKDAGLI [4] provide a DNA model calling BSJ model for homogeneous and heterogeneous sequences that takes into account these additional features [58].

The improved model is shown schematically in Fig.12. Complex sugar-phosphate of each monomer is represented by a mass m, and the complexes are interconnected by harmonics "springs".

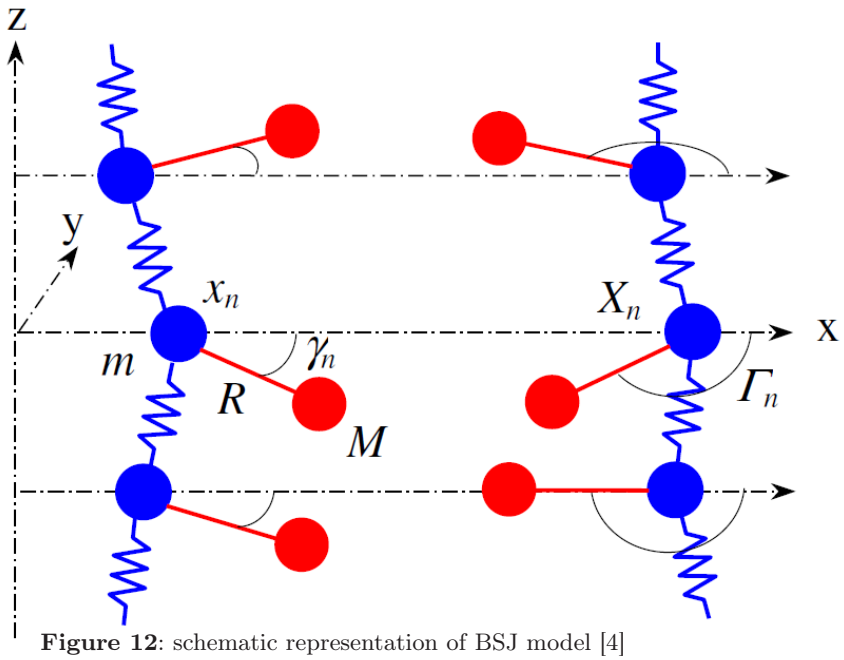

Figure 12: schematic representation of BSJ model [4]

In other to reduce the number of degrees of freedom, the masses m were regularly arranged along the axis z and their movement is restricted to the $x-axis$ that connects the two strands. Coordinates x_n and X_n indicate the respective position of the nth mass m of each strand. The bases are represented by two other point substance of mass M, each of which is rigidly

connected to a group of sugar-phosphate mass m. The distance between the R group is attached to the base and the base is free to rotate in the plane (x, y). In this model the position of each base depends on the angle of rotation γ (resp. Γ) and coordinate translation x_n (resp. X_n). The interaction of adjacent bases on the same strand is described by a potential stacking similar to the model presented in Section 1.3.4 and the bases of a pair interact via a Morse potential. If we merely these words, nothing prevents double-stranded fold compared to the propeller shaft (even at very low temperatures) so that the two sets of masses M represents the sugar skeleton/phosphate are virtually superimposed. To avoid this, it is necessary to add to the Hamiltonian an interaction term that keeps the masses m and M of each of the strands more or less aligned to the dissociation. The term function is to model the effect of the two (AT) or three (GC) hydrogen bonding of each pair of bases which, in the physical system, this provide rigidity to prevent the level of monomers and the chain to bend. Noting $u_n = x_n + Rcos\gamma_n; v_n = Rsin\gamma_n$; $U_n = X_n + Rcos\Gamma_n; V_n = Rsin\Gamma_n$; the coordinates of the masses M of each strand in the plane (x, y) and $d_n = \sqrt{(U_n - u_n)^2 + (V_n - v_n)^2}$. The distance between the bases of a pair in the plan, the proposed model Hamiltonian is written

$$\begin{aligned} H &= T + V, \\ T &= \frac{1}{2}(m+M)\sum_n(\dot{x}_n^2 + \dot{X}_n^2) + \frac{1}{2}\frac{mMR^2}{m+M}\sum_n(\dot{\gamma}_n^2 + \dot{\Gamma}_n^2), \\ V = D\sum_n \{\ 1 - exp[a(d_0 - d_n)]\}^{\ 2} &+ K_b\sum_n(2 - cos\gamma_n + cos\Gamma_n)exp[a(d_0 - d_n)] \\ &+ \frac{1}{2}\sum_n \Delta H^n\{\ 1 - exp[-b(u_n - u_{n+1})^2 - b(v_n - v_{n+1})^2]\} \\ &+ \frac{1}{2}\sum_n \Delta H^n\{\ 1 - exp[-b(U_n - U_{n+1})^2 - b(V_n - V_{n+1})^2]\} \\ &+ K_s\sum_n[(x_n - x_{n+1})^2 + (X_n - X_{n+1})^2]. \end{aligned} \tag{1.35}$$

The first term of the potential energy is the Morse potential modeling hydrogen bonds that joins bases of a same pair. The second term is the interaction that prevents the two springs to bend and the third and the fourth term represent the interaction of stacking between the adjacent bases that are on the same sprig. The last term of the Hamiltonian is the elastic energy of skeleton sugar-phosphate. The equation of motion is giving by:

$$\begin{aligned} (m+M)\ddot{x}_n &= -\frac{\partial V}{\partial x_n}; \quad (m+M)\ddot{X}_n = -\frac{\partial V}{\partial X_n}, \\ \frac{mMR^2}{m+M}\ddot{\gamma_n} &= -\frac{\partial V}{\partial \gamma_n}; \quad \frac{mMR^2}{m+M}\ddot{\Gamma_n} = -\frac{\partial V}{\partial \Gamma_n}. \end{aligned} \tag{1.36}$$

Shahin BUYUKDAGLI [4] studied the dynamics of the dissociation of the model 1.35 while

integrating numerically equations of Langevin,

$$\mu\frac{d^2q_n}{dt^2} = -\frac{\partial H}{\partial q_n} - \mu\gamma\frac{dq_n}{dt} + \sqrt{2\mu k_B T w(t)} \tag{1.37}$$

where, $\mu = m + M$ for a coordinate of elongation ($q_n = x_n$ or X_n) and $\mu = \frac{mMR^2}{m+M}$ for the rotational coordinate ($q_n = \gamma_n$ or Γ_n)

1.4 The nonlinear excitation in biomolecules

Given the complexity of biological phenomena at the molecular level, it may appear as a challenge to consider physical modeling. However, there are a number of fundamental processes, based on physic-chemical mechanisms established that one can hope to describe theoretically better understood. The approach is to develop a relatively simple model making silly adequately reflect experimental observations, it is therefore necessary to determine the dominant mechanisms in the process that is being studied. Since the early 1990s there linen craze, growing up in this type of physical modeling of biological processes due to the combination of two effects: The molecular biology has made very considerable progress.

*She can now give very detailed experimental data (especially in the structure, but sometimes the dynamics), would build models of specific bases.

*The development of the analysis of nonlinear systems since the mid-1970s introduced new concepts, such as soliton, which can provide a good starting point for modeling, although we must be careful, in their application to biological systems. Three physical processes play a very important role in the functioning of biological molecules such as proteins and DNA: - The storage and transfer of energy in many DC functions; - Changes in the conformation of molecules that are essential -transport charges (electrons as protons silly).

a) Location and energy transport in proteins

The necessary protein activity energy is often the hydrolysis of the molecule adenosine triphospliate (ATP). It binds to a particular receptor site of the protein reacts with water to release approximately 0.42 eV. This amount of energy is very high at the molecular scale (of the order of 20 kBT) but it can only be effective if it is not readily distributed to all degrees of freedom of the protein by equipartition energy, that is, if it remains localized. It could be temporarily stored in electronic form, but it is also possible that it is located by non-linear and possibly even transported as non-linear excitation effect. This hypothesis is still controversial for protein but recent experiments on molecular crystals with similar connections to the peptide bonds of proteins showed that the trapping of vibrational energy by non-linear effect could, exist in these model systems [59]. Moreover, the idea is interesting to consider, because

the corresponding model contains concepts rather general.

b) The change in conformation of biomolecules

Conformational changes (the molecules involved, meanwhile in protein dynamics, especially in the functioning of enzymes, but they are even more fundamental to the DNA because reading the genetic code could not be done without a running local of the molecule. this local opening of the double helix request breaking many hydrogen bonds (typically 50) and requires a high concentration of energy in a small area of the molecule. as it is assumed that this energy is not made by chemical reactions, it is possible to consider a phenomenon of energy localization by nonlinearity, analogous to the self-focusing process. process of transcription of a gene is, however, very complex because it involves the interaction of an enzyme with DNA is probably not yet accessible to the physical modeling but there is a physical process that comes close: forming "bubbles thermal denaturation" of DNA correspond to local opening of the double helix induced by heating. study of this phenomenon can be seen as a first step towards physical modeling of transcription and can be used to validate models of DNA. We present some recent developments this approach in chapter 3.

c) The charge transport

A third unsolved problem today is that transport proton through or along the membranes. A purely diffusive mechanism could be considered, a number of questions remain, however, unresolved. How this mechanism could assure consistency transport for biological function '? How could it be effective enough to ensure high proton fluxes may be needed? How to explain the experimental results showing that the proton transport is practically independent of the pH difference on both sides of the membrane! This result is indeed not compatible with diffusion under the influence of a concentration gradient. Can be considered a transmission channel along hydrogen bonds that extend from one side to the other of the membrane, either because they belong to transmembrane proteins, or because certain proteins, like gramicidin, form real one-dimensional channels containing chains of water molecules. Models involving coherent motion of protons in hydrogen-bonded chains have been proposed. Va1idité in their biological context is not yet established we do not present in this thesis but an introduction to these concepts can be found in the reference [60]. In all these applications the use of the concept of soliton is no doubt abuse but it provides a good basis for the development of models. I1 there is indeed little doubt that these biological processes are dominated by non-linear phenomena. Energy recycled locally by hydrolysis 1'ATP is very important at the molecular level. Similarly, rotations of 180 "base pairs of DNA are clearly not harmonic phenomena. Moreover, the large biological molecules allow collective behavior of certain groups of atoms, so that two basic ingredients for

the existence of solitons, nonlinearity and cooperatively, are present.

1.5 Propagation of twist solitons in real DNA chains

Solitonic excitations are very common in nonlinear dynamical systems. It has been proposed that they may play an important role also in functional processes of the DNA double helix such as transcription and denaturation. Since the original proposal by Englander several simplified models for the nonlinear dynamics of the DNA chain have been proposed. Most of these models allow for solitonic solutions describing stretch and/or twist excitation of the DNA chain. The models describe both the structural and dynamical features of DNA in a highly simplified way, so that it is not at all clear if solitonic excitations play a role for real DNA.

One strong objection against the existence of solitons in real DNA is represented by the observation that solitons propagate in a significant way only in the homogeneous DNA double chain, i.e. when the four nitrogen bases and their interactions are assumed to be indistinguishable. This is obviously an unrealistic assumption, as we know that real DNA is highly inhomogeneous; actually the genetic information is coded exactly in the bases sequence along the DNA double helix.

The relevance of the issue about the existence and stability of solitons in inhomogeneous media goes far beyond DNA modelling: it concerns solitonic propagation in realistic nonlinear media. Existence and stability of solitons ? in particular topological solitons (kinks) ? is well established in a broad class of nonlinear phenomena (nonlinear optics, molecular chains, ferromagnetic waves, Josephson effect etc...), but these involve an idealized homogeneous medium. Some examples of solitons propagation in inhomogeneous media have been considered both in the framework of nonlinear DNA dynamics and of generic solitonic propagation. However, these investigations either refer to localized inhomogeneities - in the form of e.g discontinuities, potential barriers, delta potentials etc.) - or else the inhomogeneities are parametrized by particular ad hoc rules. The existence of solitonic perturbations in real DNA chains and in general inhomogeneous nonlinear media still remains an involved and open question. Starting from a homogenous system for which one knows solitonic solutions exist, and introducing inhomogeneities in the system, one naturally expects that:

a) Solitons still propagate along the chain as long as the size of the soliton is substantially larger than the typical scale of the inhomogeneities;

b). The effect of the inhomogeneities on the soliton propagation will be the production of linear excitations (like phonons) which will dissipate the kinetic energy of the soliton and bring the soliton to rest (or disappear for non-topological solitons) after a finite time.

The relevant question to be asked is the following: can there be fully inhomogeneous nonlinear systems in which solitons ? of size comparable with the typical scale of the inhomogeneity ? propagate for distances which are long enough for the soliton to be relevant for the physical (or

biological) process it is assumed to describe? We will answer to this question (in the positive) for the case of soliton propagation in a real DNA chain (the Human Adenovirus 2 (HA2)) using a realistic ? albeit simplified ? model of DNA torsional dynamics.

1.6 Conclusion

In this chapter, we have given an overview of the structure of DNA molecule. The molecule has been presented as a biological entity on the one hand and as a dynamical entity on the other hand. Some, some mathematical models to study the nonlinear dynamics of the molecule have been also presented.

Chapter 2

Analytical and Numerical Methods

2.1 Introduction

It is well known that most of the phenomena that arise in mathematical physics and biophysical systems can be described by partial differential equations (PDEs). In physics for example, the heat flow and the wave propagation phenomena are well described by PDEs. In ecology, most population models are governed by PDEs. The dispersion of a chemically reactive material is characterized by PDEs. In addition, most physical phenomena of fluid dynamics, quantum mechanics, plasma physics, propagation of shallow water waves, and many other models are controlled within its domain of validity by PDEs. PDEs have become a useful tool for describing these natural phenomena of science and biophysical models. Therefore, it becomes increasingly important to be familiar with all traditional and recently developed methods for solving PDEs, and the implementation of these methods. Another simple possibility of solving PDEs is through the linear stability analysis which leads to the modulational instability (MI). This phenomenon is well known as the Benjamin-Feir MI. In this chapter, we present some method used to obtain soliton solutions of the DNA dynamics. The linear stability analysis, which is important for the characterization of the MI processes is also presented. Finally, the numerical methods used to solve the different equations are also discussed.

2.2 Perturbative methods

Nonlinear differential-difference equation cannot be solved exactly. Thus, there exist several techniques to convert them into more integrable systems [61, 62, 63, 64, 65]. In this frame, one can apply the reductive perturbation method (or multiple scales analysis) that allows the deduction of simplified equation from a basic model without losing its characteristic features. The method consists essentially in an asymptotic analysis of a perturbation series, based on the existence of different scales. More specially, the method generates a hierarchy of (small) scales for the space and time variations of the envelopes of a fundamental (linear) plane wave and all

the overtones. Moreover, the scale is directly related to the small amplitude of the wave itself. The scaling of variables is performed via a Taylor expansion of the frequency $\omega(q_0)$ in powers of a small deviation of the wave number q_0. This deviation from the linear dispersion relation is, of course, generated by the nonlinearity. There are actually three different approaches to multiple scales analysis for a discrete evolution. The first is obviously to go to the continuous limit right in the starting system, for which discreteness effects are wiped out. The second is the semi-discrete approach which consists in having a discrete carrier wave modulated by a continuous envelope. In the latter case, some discreteness aspects are preserved. The third stems from the adiabatic approximation, but the approach requires one to use the rotating wave approximation to artificially eliminate the overtones. The price to pay is that the predictions, for example the MI, are not trustworthy for large time [62, 63].

In light of the previous studies, we will recall the method of multiple scales. This method streamlines the approximation of amplitudes slowly variables. Formally, it is to seek a solution $f(t,\epsilon)$ in the field or $\bigcirc(t) \leq 1/\epsilon^M$ as form of asymptotic expansion in multiple scales $t_0, t_1, t_2..., t_M$ (considered as independent variables):

$$y(t,\epsilon) = \sum_0^M \epsilon^n y_n(t_0, t_1, ..., t_M) + \bigcirc(\epsilon t_M), \tag{2.1}$$

with

$$t_0 = t, \;\; t_1 = \epsilon t, \quad t_2 = \epsilon^2 t, ... \quad t_M = \epsilon^M t, \tag{2.2}$$

y_n functions check of partial differential equations whose solutions are such that:

-they must be such that y satisfies the boundary conditions imposed.

-the asymptotic expansion must be uniformly valid for $\bigcirc(t) \leq 1/\epsilon^M$, *i.e* $|y_{n+1}/y_n|$ remains bounded for $\bigcirc(t) \leq 1/\epsilon^M$ (each approximation cannot be more singular than the previous one).

Operations bypass write:

$$\frac{d}{dt} = \frac{\partial}{\partial t} + \epsilon\frac{\partial}{\partial t_1} + ... \quad And \quad \frac{d^2}{dt^2} = \frac{\partial^2}{\partial t^2} + 2\epsilon\frac{\partial^2}{\partial t \partial t_1} + ... \tag{2.3}$$

Thus the derivative of y

$$\frac{dy}{dt} = \frac{\partial y_0}{\partial t} + \epsilon(\frac{\partial y_1}{\partial t} + \frac{\partial y_0}{\partial t_1}) + \bigcirc(\epsilon) \quad And \quad \frac{d^2y}{dt^2} = \frac{\partial^2 y_0}{\partial t^2} + \epsilon(\frac{\partial^2 y_1}{\partial t^2} + 2\frac{\partial^2 y_0}{\partial t \partial t_1}) + \bigcirc(\epsilon). \tag{2.4}$$

2.3 The semi-discrete approximation

2.3.1 The semi-discrete approximation in the Peyrard-Bishop-Joyeux model: the nonlinear Schrödinger equation

We consider the wave propagation in DNA within the Joyeux-Buyukdagli model of DNA. This model was introduced by Joyeux and Buyukdagli to takes into account a modified stacking interaction term. From the Hamiltonian the equation that governs the local oscillations of DNA nucleotides is [66]:

$$\begin{aligned} m\ddot{y}_n =& k_b(y_{n+1} - 2y_n + y_{n-1}) - \frac{2\Delta Hb}{C}(y_n - y_{n-1}) \times e^{-b(y_n+y_{n-1})^2} \\ &+ \frac{2\Delta Hb}{C}(y_{n+1} - y_n) \times e^{-b(y_{n+1}-y_n)^2} + 2aD(e^{-ay_n} - e^{-2ay_n}). \end{aligned} \tag{2.5}$$

In the following, we consider a special collective motion of the pairs in a DNA molecule. The amplitude of the wave packet is big enough, so that the nonlinear effect plays an essential role in DNA molecules. On the other hand, it is still very small compared with the amplitude of the broken base pairs. Therefore, the base pairs in DNA molecule do not oscillate far away from the bottom of the Morse potential well. In this respect, we can assume $0 < y_n \ll 1$ and expand the terms in exponential $e^{-b(y_{n+1}-y_n)^2}$, $e^{-b(y_n-y_{n-1})^2}$ and e^{-ay_n} until the second and third orders, respectively. This leads to the modified equation

$$\begin{aligned} \ddot{y}_n =& k_2(y_{n+1} - 2y_n + y_{n-1}) - k_4[(y_{n+1} - y_{n-1})^3 - (y_n - y_{n-1})^3] \\ &- \omega_g^2(y_n + \alpha y_n^2 + \beta y_n^3). \end{aligned} \tag{2.6}$$

For the small, but yet nonlinear oscillations of the nucleotides at the position n we can assume [67, 68]

$$y_n = \epsilon\Phi_n, \quad \epsilon \ll 1, \tag{2.7}$$

we have:

$$\begin{aligned} \ddot{\Phi}_n =& k_2(\Phi_{n+1} - 2\Phi_n + \Phi_{n-1}) - \epsilon^2 k_4[(\Phi_{n+1} - \Phi_{n-1})^3 - (\Phi_n - \Phi_{n-1})^3] \\ &- \omega_g^2(\Phi_n + \epsilon\alpha\Phi_n^2 + \epsilon^2\beta\Phi_n^3), \end{aligned} \tag{2.8}$$

where, $k_2 = \frac{2(k_bC+\Delta H_n b)}{mC}$; $k_4 = \frac{2\Delta H_n b^2}{mC}$; $\alpha = -\frac{3a}{2}$; $\beta = \frac{7a^2}{6}$; $\omega_g^2 = \frac{2a^2D_n}{m}$.

To obtain the function, Φ_n we use the semi-discrete approximation [67, 69] and look for the wave solution in the form

$$\Phi_n(t) = F_1(\epsilon nl, \epsilon t)e^{i\theta_n} + \epsilon[F_0(\epsilon nl, \epsilon t) + F_2(\epsilon nl, \epsilon t)e^{2i\theta_n}] + cc + 0(\epsilon^2), \tag{2.9}$$

where $C.C$ stands for complex-conjugate. All important derivations and explanations can be found below. The functions F_0 and F_2 will be expressed through F_1, while the function F_1 is a

solution of the NLSE [67, 70] and $\theta_n = nql - \omega t$.

$$\begin{aligned}\ddot{\Phi}_n =&\epsilon^2(\ddot{F}_1 e^{i\theta_n} - 4i\omega\dot{F}_2 e^{2i\theta_n}) \\ &- \epsilon(2i\omega\dot{F}_1 e^{i\theta_n} + 4\omega^2 F_2 e^{2i\theta_n}) - \omega^2 F_1 e^{i\theta_n} + 0(\epsilon^3) + C.C,\end{aligned} \tag{2.10}$$

$$\begin{aligned}\Phi_n^2 =&\epsilon^2(F_2^{*2}e^{-4i\theta_n} + 4F_2F_0e^{i\theta_n} + 4F_0^2 + 4F_0F_2^*e^{-2i\theta_n} + 2|F_2|^2 + F_2^2e^{4i\theta_n}) \\ &\epsilon[e^{i\theta_n}(4F_0F_1 + 2F_2F_1^*) + F_1F_2e^{3i\theta_n} + F_1F_2^*e^{-i\theta_n} + F_1^*F_2^*e^{-3i\theta_n}] \\ &+ (2|F_1|^2 + F_1^2e^{2i\theta_n} + F_1^{*2}e^{-2i\theta_n}) + 0(\epsilon^3),\end{aligned} \tag{2.11}$$

$$\begin{aligned}\Phi_n^3 =&\epsilon^2(12F_0^2F_1^*e^{-i\theta_n} + 12F_2F_1^*F_0e^{i\theta_n} + 6F_1^*|F_2|^2e^{-i\theta_n} + 3F_1F_2^{*2}e^{-3i\theta_n} \\ &+ 12F_2F_1F_0e^{3i\theta_n} + 12F_1F_0^2e^{i\theta_n} + 12F_2^*F_1^*F_0e^{-3i\theta_n} + 6F_1|F_2|^2e^{i\theta_n} \\ &+ 3F_1^*F_2^2e^{3i\theta_n} + 3F_1^*F_2^{*2}e^{-5i\theta_n} + 12F_2^*F_1^*F_0e^{-i\theta_n} + 3F_1F_2^2e^{3i\theta_n}) \\ &+ \epsilon(6F_1^2F_0e^{2i\theta_n} + 3F_1^2F_2e^{4i\theta_n} + 12|F_1|^2F_0 + 3F_1^2F_2^* + 6F_1^{*2}F_0e^{-2i\theta_n} \\ &+ 6F_2^*|F_1|^2e^{-2i\theta_n} + 3F_1^{*2}F_2^*e^{-4i\theta_n} + 3F_2F_1^{*2} + 6F_2|F_1|^2e^{2i\theta_n}) \\ &+ F_1^3e^{3i\theta_n} + F_1^{*3}e^{-3i\theta_n} + 3|F_1|^2F_1e^{i\theta_n} + 3|F_1^*|^2F_1^*e^{-i\theta_n} + 0(\epsilon^3),\end{aligned} \tag{2.12}$$

$$\begin{aligned}\Phi_{n+1} + \Phi_{n-1} - 2\Phi_n =&\epsilon^2[2isin(2ql)(F_2^{'}e^{2i\theta_n} - F_2^{*'}e^{-2i\theta_n}) + cos(ql)(F_1^{"}e^{i\theta_n} + F_1^{*"}e^{-i\theta_n})] \\ &+ \epsilon[2isin(ql)(F_1^{'}e^{i\theta_n} - F_1^{*'}e^{-i\theta_n}) - 4sin^2(ql)(F_2e^{2i\theta_n} + F_2^*e^{-2i\theta_n})] \\ &- 4sin^2(\frac{ql}{2})(F_1e^{i\theta_n} + F_1^*e^{-i\theta_n}) + 0(\epsilon^3),\end{aligned} \tag{2.13}$$

$$\begin{aligned}&(\Phi_{n+1} - \Phi_{n-1})^3 - (\Phi_n - \Phi_{n-1})^3 = (F_1^3e^{3i\theta_n} + F_1^{*3}e^{-3i\theta_n})(-4sin^2(\frac{3ql}{2}) - 6cos(2ql) + 6cos(ql)) \\ &+ (24cos(ql) - 6cos(2ql) - 18)(F_1e^{i\theta_n} + F_1^*e^{-i\theta_n})|F_1|^2 + \epsilon\{6F_1^{*2}F_2^*e^{-4i\theta_n} - 6F_1^2F_2e^{4i\theta_n} \\ &+ 12[cos(ql) - cos(3ql)](F_2e^{2i\theta_n} + F_2^*e^{-2i\theta_n})|F_1|^2 + 12i[2sin(ql) - sin(2ql)](F_1^{'}e^{i\theta_n} - F_1^{*'}e^{-i\theta_n})|F_1|^2 \\ &+ 6i[sin(4ql) + sin(ql) - sin(2ql)]F_1^2F_1^{'}e^{3i\theta_n} + 6[cos(4ql) + 2cos(ql) - 2cos(3ql)]F_1^2F_2e^{4i\theta_n} \\ &+ 6[cos(4ql) + 2cos(ql) - 2cos(3ql)]F_2^*F_1^{*2}e^{-4i\theta_n} + 6i[sin(2ql) - sin(3ql) - sin(ql)]F_1^{*2}F_1^{*'}e^{-3i\theta_n} \\ &- 24|F_1|^2(F_2e^{2i\theta_n} + F_2^*e^{-2i\theta_n}) + 6[-2cos(3ql) + cos(4ql)]e^{-4i\theta_n}F_1^{*2}F_2^* - 6isin(3ql)e^{3i\theta_n}F_1^2F_1^{'}\} \\ &+ \epsilon^2(...) + 0(\epsilon^3),\end{aligned} \tag{2.14}$$

introducing the equation (2.9)-(2.14) in (2.8) one gets:

-at order $\epsilon^0 e^{i\theta_n}$

$$\omega^2 = \omega_g^2 + 4k_2sin^2(\frac{ql}{2}) \tag{2.15}$$

-at order $\epsilon e^{0i\theta_n}$

$$F_0 = -2\alpha|F_1|^2 = \mu|F_1|^2 \tag{2.16}$$

-at order $\epsilon e^{2i\theta_n}$

$$F_2 = \frac{\alpha\omega_g^2}{3\omega_g^2 + 16k_2 sin^2(\frac{ql}{2})} F_1^2 = \delta F_1^2 \tag{2.17}$$

-at order $\epsilon^2 e^{i\theta_n}$ and using equations (2.16) and (2.17) we obtain the nonlinear Schrödinger equation (NLS):

$$iF_{1\tau} + PF_{SS} + Q|F_1|^2 F_1 = 0 \tag{2.18}$$

where: $\tau = \epsilon^2 t$; $S = Z - V_g T$; $T = \epsilon t$; $V_g = \frac{d\omega}{dq} = \frac{k_2 sin(ql)}{\omega}$ who is the group velocity. P and Q are the pseudo constant given by:

$$P = \frac{d^2\omega}{dq^2} = \frac{k_2 cos(ql) - V_g^2}{2\omega} \tag{2.19}$$

$$Q = \frac{1}{2\omega}\{ -12k_4[2cos(ql) - cos^2(ql) - 1] - 2\omega_g^2\alpha(\delta + 2\mu) - 3\beta\omega_g^2\} \tag{2.20}$$

2.3.2 The semi-discrete approximation in the PB model: the cubic-quintic nonlinear Schrödinger equation

Let us consider the PB model of DNA molecule. Its equations of motion is given by

$$m\ddot{y_n} = k(y_{n+1} - 2y_n + y_{n-1}) + 2\sqrt{2}aD(e^{-2a\sqrt{2}y_n} - e^{-a\sqrt{2}y_n}), \tag{2.21}$$

we expand e^{-ay_n} until the second and third orders, respectively. This leads to the modified equation

$$\ddot{y_n} = \omega_0^2(y_{n+1} - 2y_n + y_{n-1}) - \omega_g^2(y_n + \alpha y_n^2 + \beta y_n^3), \tag{2.22}$$

where $\alpha = -\frac{3a}{\sqrt{2}}$; $\beta = \frac{7a^2}{3}$; $\omega_g^2 = \frac{4a^2 D_n}{m}$; $\omega_0^2 = \frac{k}{m}$. We use the semi-discrete approximation to obtain the short-wavelength envelope soliton. This asymptotic approach allows us to describe the envelope in the continuum approximation and to treat properly the carrier wave with its discrete character. Owing to the assumed weak nonlinearity, we expand y_n into the following asymptotic series [71]:

$$y_n(t) = \sum [\epsilon^l y_{l,m}(n,t)] e^{im\theta(n,t)} + C.C \tag{2.23}$$

Utilizing the idea developed by Taniuti and Yajima [72],the solution y_n is taken to be

$$\begin{aligned} y_n(t) =& \epsilon^{\frac{1}{2}} y_{11}(n,t)e^{i\theta} + C.C + \epsilon[y_{20} + y_{22}(n,t)e^{2i\theta} + C.C] + \epsilon^{\frac{3}{2}} y_{33}(n,t)e^{3i\theta} + C.C \\ &+ \epsilon^2[y_{42} + y_{44}(n,t)e^{4i\theta} + C.C] + \epsilon^{\frac{5}{2}}[y_{53}(n,t)e^{3i\theta} + y_{55}(n,t)e^{5i\theta} + C.C] + 0(\epsilon^{\frac{7}{2}}), \end{aligned} \tag{2.24}$$

where $C.C$ stands for complex-conjugate and $\theta_n = nql - \omega t$. The smallness parameter ϵ which ranks from 0 to 1 $0 < \epsilon \leq 1$ represents the size of the amplitude of perturbation.

In the resulting equation, there are nonzero terms $y_{lm}(n \pm 1)$, which are expanded in the continuum approximation around $y_{lm}(x,t)$, with $n = x$. So, the fast change in the phase θ in (Eq.3.147) is correctly taken into account by considering differences in the phase for the discrete variable n. We have also scaled time and space derivatives as $\frac{\partial}{\partial x} \sim 0(\epsilon)$ and $\frac{\partial}{\partial t} \sim 0(\epsilon)$, respectively, and neglected consistently high order in ϵ terms. Then, we keep up to the second derivative terms of y_n to balance dispersion and nonlinearity. Substitution of y_n and its derivatives in (Eq.3.145) yields a series of equations with respect to the power of ϵ.

From equation of $(\epsilon^{\frac{1}{2}}, e^{i\theta})$, that is, the terms of $0(\epsilon^{\frac{1}{2}})$ for the first harmonic, we obtain the linear dispersion relation

$$\omega^2 = \omega_g^2 + 4\omega_0^2 sin^2(\frac{ql}{2}), \tag{2.25}$$

from the equation of $(\epsilon^{\frac{1}{2}}, e^{0i\theta})$ we obtain the expression of the group velocity V_g defined by

$$V_g = \frac{\partial \omega}{\partial q} = \frac{4\omega_0^2 sin(ql)}{\omega}. \tag{2.26}$$

At the order of $(\epsilon, e^{0i\theta})$, we have

$$y_{20} = a_{20}|y_{11}|^2, \quad a_{20} = -2\alpha. \tag{2.27}$$

At the order of $(\epsilon, e^{2i\theta})$, we have

$$\begin{aligned} y_{22} &= a_{22} y_{11}^2, \quad with \\ a_{22} &= \frac{\alpha\omega_g^2}{4(\omega^2 - \omega_0^2 sin^2(ql)) - \omega_g^2}. \end{aligned} \tag{2.28}$$

At the order of $(\epsilon^{\frac{3}{2}}, e^{3i\theta})$, we have

$$\begin{aligned} y_{33} &= a_{33} y_{11}^3, \quad with \\ a_{33} &= a_{30}(\beta + 2\alpha a_{22}) \quad and \\ a_{30} &= \frac{\omega_g^2}{9\omega^2 - 4\omega_0^2 sin^2(\frac{3ql}{2}) - \omega_g^2}. \end{aligned} \tag{2.29}$$

At the order of $(\epsilon^2, e^{2i\theta})$, we have

$$\begin{aligned} y_{42} &= a_{42}|y_{11}|^2 y_{11}^2, \quad with \\ a_{42} &= [a_{22}(4a_{20}a_{22} + 2a_{33}) + 6\frac{\beta a_{22}}{\alpha}(a_{20} + a_{22})]. \end{aligned} \tag{2.30}$$

At the order of $(\epsilon^2, e^{4i\theta})$, we have

$$\begin{aligned} y_{44} &= a_{44} y_{11}^4, \quad with \\ a_{44} &= a_{40}[\alpha(a_{22}^2 + 2a_{33}) + 3\beta a_{22}] \quad and \\ a_{40} &= \frac{\omega_g^2}{4(4\omega^2 - \omega_0^2 sin^2(2ql)) - \omega_g^2}. \end{aligned} \tag{2.31}$$

At the order of $(\epsilon^{\frac{3}{2}}, e^{3i\theta})$, we have

$$\begin{aligned} y_{53} &= a_{53}|y_{11}|^2 y_{11}^3, \quad with \\ a_{53} &= a_{30}[\alpha(2a_{42} + 2a_{44} + 4a_{33}a_{20}) + \beta(12a_{20}a_{22} + 6a_{33} + 3a_{22}^2)]. \end{aligned} \tag{2.32}$$

At the order of $(\epsilon^{\frac{5}{2}}, e^{5i\theta})$, we have

$$\begin{aligned} y_{55} &= a_{55} y_{11}^5, \quad , a_{55} = a_{50}[2\alpha(a_{44} + a_{22}a_{33}) + 3\beta(a_{33} + a_{22}^2)] \\ a_{50} &= \frac{\omega_g^2}{25\omega^2 - 4\omega_0^2 sin^2(\frac{5ql}{2}) - \omega_g^2}. \end{aligned} \tag{2.33}$$

From the equation of $(\epsilon^{\frac{5}{2}}, e^{i\theta})$ and by going into the reference frame moving with the group velocity, the resulting equation describing the dynamics of a wave packet has the following form:

$$i\frac{\partial y_{11}}{\partial \tau} + P\frac{\partial^2 y_{11}}{\partial \xi^2} + Q_1|y_{11}|^2 y_{11} + Q_2|y_{11}|^4 y_{11} = 0, \tag{2.34}$$

where $\tau = t$, $\xi = x - V_g t$ and the subscripts τ and ξ denote partial differentiations with respect to τ and ξ.

$$\begin{aligned} P = \frac{l^2\omega_0^2 cos(ql) - V_g^2}{2\omega}; \quad Q_1 = -\frac{\omega_g^2[3\beta + 2\alpha(2a_{20} + a_{22})]}{2\epsilon\omega} \\ Q_2 = -\frac{\omega_g^2[2\alpha(a_{22}a_{33} + a_{42}) + \beta(12a_{22}a_{20} + 3a_{33} + a_{20} + 6a_{22}^2 + 12a_{20}^2)]}{2\omega}. \end{aligned} \tag{2.35}$$

Equation (2.18) is the cubic-quintic nonlinear Schrödinger equation obtained here for the DNA molecule.

2.3.3 The semi-discrete approach in the PBD model: the coupled nonlinear Schrödinger equation

We consider the "helicoidal Peyrard-Bishop" where the equation of motion in given by

$$\begin{aligned} m\ddot{\psi_n} =& k(\psi_{n+1} - 2\psi_n + \psi_{n-1}) + K(\psi_{n+h} - 2\psi_n + \psi_{n-h}) \\ &+ 2\sqrt{(2)}aD(e^{-2a\sqrt{2}\psi_n} - e^{-a\sqrt{2}\psi_n}). \end{aligned} \tag{2.36}$$

The amplitude of the wave packet is big enough, so that the nonlinear effect plays an essential role in DNA molecules. On the other hand, it is still very small compared with the amplitude of

the broken base pairs. Therefore, the base pairs in DNA molecule do not oscillate far away from the bottom of the Morse potential well. In this respect, we can assume $0 < \psi_n \ll 1$ and expand the terms in exponential $e^{-a\sqrt{2}\psi_n}$ until the third orders. This leads to the modified equation

$$\begin{aligned}\ddot{\psi}_n - K_1(\psi_{n+1} + \psi_{n-1} - 2\psi_n) + K_2(\psi_{n+h} + \psi_{n-h} + 2\psi_n) \\ + \omega_g^2(\psi_n + \alpha\psi_n^2 + \beta\psi_n^3) = 0,\end{aligned} \tag{2.37}$$

where, $\omega_g^2 = \frac{4a^2D}{m}$,$K_1 = \frac{k}{m}$, $K_2 = \frac{K}{m}$, $\alpha = -\frac{3a}{\sqrt{2}}$ and $\beta = \frac{7a^2}{3}$. The corresponding frequencies is given by

$$\omega^2 = [4K_1 \sin^2(ql/2) + 4K_2 \cos^2(qlh/2) + \omega_g^2]. \tag{2.38}$$

we assume the following reductive perturbation method [72, 73], we introduce the independent multiple-scale variables $X_i = \varepsilon^i n$ and $T_i = \varepsilon^i t$, where $\varepsilon \ll 1$. Moreover, the solution of (Eq. 2.37) is assumed to have a following form while taking $\psi_n = V_n$:

$$\begin{aligned}V_n(t) =&\varepsilon[V_{1+}(X_1, X_2, ..., T_1, T_2, ...)] \exp(i\theta_+) + \varepsilon^2[V_{2+}(X_1, X_2, ..., T_1, T_2, ...)] \exp(2i\theta_+) \\ &+ \varepsilon[V_{1-}(X_1, X_2, ..., T_1, T_2, ...)] \exp(i\theta_-) + \varepsilon^2[V_{2-}(X_1, X_2, ..., T_1, T_2, ...)] \exp(2i\theta_-) + c.c.,\end{aligned} \tag{2.39}$$

where the carrier phases are $\theta_+ = qn - \omega t$ and $\theta_- = -qn - \omega t$, and c.c. represents the complex conjugate of the preceding terms. The second-harmonic terms $V_2\pm$ are added to the fundamental ones $V_1\pm$ in order to take the asymmetry of the persistence-length into account.

$$\begin{aligned}\ddot{V}_n =&\epsilon(e^{i\theta_+}\frac{\partial^2 V_{1+}}{\partial T_0^2} + e^{i\theta_-}\frac{\partial^2 V_{1-}}{\partial T_0^2} - 2i\omega\frac{\partial V_{1+}}{\partial T_0}e^{i\theta_+} - 2i\omega\frac{\partial V_{1-}}{\partial T_0}e^{i\theta_-} - \omega^2 V_{1+}e^{i\theta_+} - \omega^2 V_{1-}e^{i\theta_-}) \\ &+ \epsilon^2(2e^{i\theta_+}\frac{\partial^2 V_{1+}}{\partial T_0 \partial T_1} + 2e^{i\theta_-}\frac{\partial^2 V_{1-}}{\partial T_0 \partial T_1} + e^{2i\theta_+}\frac{\partial^2 V_{2+}}{\partial T_0^2} + e^{2i\theta_-}\frac{\partial^2 V_{2-}}{\partial T_0^2} - 2i\omega\frac{\partial V_{1+}}{\partial T_1}e^{i\theta_+} \\ &- 2i\omega\frac{\partial V_{1-}}{\partial T_1}e^{i\theta_-} - 4i\omega\frac{\partial V_{1+}}{\partial T_0}e^{2i\theta_+} - 4i\omega\frac{\partial V_{2-}}{\partial T_0}e^{2i\theta_-} - 4\omega^2 V_{2+}e^{2i\theta_+} - 4\omega^2 V_{2-}e^{2i\theta_-})) \\ &+ \epsilon^3(e^{i\theta_+}\frac{\partial^2 V_{1+}}{\partial T_1^2} + e^{i\theta_-}\frac{\partial^2 V_{1-}}{\partial T_1^2} + e^{i\theta_+}\frac{\partial^2 V_{1+}}{\partial T_0 \partial T_2} + e^{i\theta_-}\frac{\partial^2 V_{1-}}{\partial T_0 \partial T_2} - 2i\omega\frac{\partial V_{1+}}{\partial T_2}e^{i\theta_+} \\ &- 2i\omega\frac{\partial V_{1-}}{\partial T_2}e^{i\theta_-} - 4i\omega\frac{\partial V_{2+}}{\partial T_1}e^{2i\theta_+} - 4i\omega\frac{\partial V_{2-}}{\partial T_1}e^{2i\theta_-} + 0(\epsilon^4) + C.C,\end{aligned} \tag{2.40}$$

and

$$
\begin{aligned}
V_n^2 =&\epsilon^2(V_{1+}^2e^{2i\theta_+}+V_{1-}^2e^{2i\theta_-}+V_{1+}^{*2}e^{-2i\theta_+}+2V_{1-}^{*2}e^{-2i\theta_-}+2V_{1+}V_{1-}e^{i(\theta_++\theta_-)}+2|V_{1+}|^2+2|V_{1-}|^2\\
&+2V_{1+}V_{1-}^*e^{i(\theta_+-\theta_-)}+2V_{1+}^*V_{1-}^*e^{-i(\theta_++\theta_-)}+2V_{1+}^*V_{1-}e^{-i(\theta_+-\theta_-)})\\
&+\epsilon^3(2V_{1+}^*V_{2-}^*e^{-i(\theta_++2\theta_-)}+2V_{1-}^*V_{2+}^*e^{-i(2\theta_++\theta_-)}+2V_{1-}V_{2+}e^{i(2\theta_++\theta_-)}\\
&+2V_{1+}V_{2+}e^{3i\theta_+}+2V_{1+}V_{2-}e^{i(\theta_++2\theta_-)}+2V_{2+}V_{1-}e^{i(2\theta_++\theta_-)}+2V_{1+}V_{2-}^*e^{-i(\theta_+-2\theta_-)}\\
&+2V_{2+}V_{1-}^*e^{-i(\theta_++2\theta_-)}+2V_{1+}^*V_{2+}^*e^{-3i\theta_+}+2V_{1-}V_{2-}^*e^{-i\theta_-}+2V_{1-}^*V_{2-}e^{i\theta_-}\\
&+2V_{1+}^*V_{2-}e^{-i(2\theta_--\theta_+)}+2V_{1+}^*V_{2+}e^{i\theta_+}+2V_{1+}V_{2+}^*e^{-i\theta_+}+2V_{1-}^*V_{2-}^*e^{-3i\theta_-}\\
&+2V_{1-}V_{2+}^*e^{-i(\theta_--2\theta_+)}+2V_{1-}V_{2-}e^{3i\theta_-})+0(\epsilon^4),
\end{aligned}
\tag{2.41}
$$

and

$$
\begin{aligned}
V_n^3 =&\epsilon^3(V_{1+}^3e^{3i\theta_+}+3V_{1+}V_{1+}^{*2}e^{-3i\theta_+}+V_{1+}^{*3}e^{-3i\theta_+}+V_{1-}^{*3}e^{-3i\theta_-}\\
&+3V_{1+}V_{1-}^{*2}e^{i(\theta_+-2\theta_-)}+3V_{1-}V_{1-}^{*2}e^{-i\theta_-}+V_{1-}^3e^{3i\theta_-}\\
&+3V_{1+}^*V_{1-}^2e^{-i(\theta_+-2\theta_-)}+3V_{1-}V_{1+}^{*2}e^{i(\theta_--2\theta_+)}+6e^{i\theta_+}|V_{1-}|^2V_{1+}+6e^{-i\theta_-}|V_{1+}|^2V_{1-}^*\\
&+3e^{i\theta_+}|V_{1+}|^2V_{1+}+3V_{1+}V_{1-}^2e^{-i(\theta_++2\theta_-)}+3V_{1-}^{*2}V_{1+}^*e^{-i(\theta_++2\theta_-)}+3V_{1+}^2V_{1-}e^{i(2\theta_++\theta_-)}\\
&+6e^{i\theta_-}|V_{1+}|^2V_{1-}+3V_{1+}^2V_{1-}^*e^{-i(2\theta_+-\theta_-)}+6e^{-i\theta_+}|V_{1-}|^2V_{1+}^*\\
&+3e^{i\theta_-}|V_{1-}|^2V_{1-}+3V_{1+}^{*2}V_{1+}^*e^{-i(2\theta_+-\theta_-)})+0(\epsilon^4),
\end{aligned}
\tag{2.42}
$$

Using the Eqs.(2.3) and (2.4) we obtain:

$$
\begin{aligned}
V_{n+1}+V_{n-1}-2V_n =&2isin(q)\big\{\epsilon(\frac{\partial V_{1+}}{\partial X_0}e^{i\theta_+}-\frac{\partial V_{1-}}{\partial X_0}e^{i\theta_-})+\epsilon^2(\frac{\partial V_{2+}}{\partial X_0}e^{2i\theta_+}-\frac{\partial V_{2-}}{\partial X_0}e^{2i\theta_-}\\
&+\frac{\partial V_{1+}}{\partial X_1}e^{i\theta_+}-\frac{\partial V_{1-}}{\partial X_1}e^{i\theta_-})+\epsilon^3(\frac{\partial V_{1+}}{\partial X_2}e^{i\theta_+}-\frac{\partial V_{1-}}{\partial X_2}e^{i\theta_-})\big\}+2cos(q)\big\{\epsilon(\frac{\partial^2V_{1+}}{\partial X_0^2}e^{i\theta_+}\\
&+\frac{\partial^2V_{1-}}{\partial X_0^2}e^{i\theta_-})+\epsilon^2(\frac{\partial^2V_{2+}}{\partial X_0^2}e^{2i\theta_+}+\frac{\partial^2V_{2-}}{\partial X_0^2}e^{2i\theta_-}+2\frac{\partial^2V_{1+}}{\partial X_0\partial X_1}e^{i\theta_+}+2\frac{\partial^2V_{1-}}{\partial X_0\partial X_1}e^{i\theta_-})\\
&+\epsilon^3(2\frac{\partial^2V_{2+}}{\partial X_0\partial X_1}e^{2i\theta_+}+2\frac{\partial^2V_{2-}}{\partial X_0\partial X_1}e^{2i\theta_-}+2\frac{\partial^2V_{1+}}{\partial X_0\partial X_2}e^{i\theta_+}+2\frac{\partial^2V_{1-}}{\partial X_0\partial X_2}e^{i\theta_-})+\frac{\partial^2V_{1+}}{\partial X_1^2}e^{i\theta_+}\\
&+\frac{\partial^2V_{1-}}{\partial X_1^2}e^{i\theta_-}\big\}+0(\epsilon^4)+C.C,
\end{aligned}
\tag{2.43}
$$

and the similar style, we have:

$$\begin{aligned}V_{n+h}+V_{n-h}-2V_n =&2hisin(q)\big\{\epsilon(\frac{\partial V_{1+}}{\partial X_0}e^{i\theta_+}-\frac{\partial V_{1-}}{\partial X_0}e^{i\theta_-})+\epsilon^2(\frac{\partial V_{2+}}{\partial X_0}e^{2i\theta_+}-\frac{\partial V_{2-}}{\partial X_0}e^{2i\theta_-}\\&+\frac{\partial V_{1+}}{\partial X_1}e^{i\theta_+}-\frac{\partial V_{1-}}{\partial X_1}e^{i\theta_-})+\epsilon^3(\frac{\partial V_{1+}}{\partial X_2}e^{i\theta_+}-\frac{\partial V_{1-}}{\partial X_2}e^{i\theta_-})\big\}+2h^2cos(q)\big\{\epsilon(\frac{\partial^2 V_{1+}}{\partial X_0^2}e^{i\theta_+}\\&+\frac{\partial^2 V_{1-}}{\partial X_0^2}e^{i\theta_-})+\epsilon^2(\frac{\partial^2 V_{2+}}{\partial X_0^2}e^{2i\theta_+}+\frac{\partial^2 V_{2-}}{\partial X_0^2}e^{2i\theta_-}+2\frac{\partial^2 V_{1+}}{\partial X_0\partial X_1}e^{i\theta_+}+2\frac{\partial^2 V_{1-}}{\partial X_0\partial X_1}e^{i\theta_-})\\&+\epsilon^3(2\frac{\partial^2 V_{2+}}{\partial X_0\partial X_1}e^{2i\theta_+}+2\frac{\partial^2 V_{2-}}{\partial X_0\partial X_1}e^{2i\theta_-}+2\frac{\partial^2 V_{1+}}{\partial X_0\partial X_2}e^{i\theta_+}+2\frac{\partial^2 V_{1-}}{\partial X_0\partial X_2}e^{i\theta_-})+\frac{\partial^2 V_{1+}}{\partial X_1^2}e^{i\theta_+}\\&+\frac{\partial^2 V_{1-}}{\partial X_1^2}e^{i\theta_-}\big\}+0(\epsilon^4)+C.C.\end{aligned} \tag{2.44}$$

Inserting (Eq. 2.39) to 2.44 in (Eq. 2.36) yields, after some standard calculations and While considering the terms of $\epsilon^3 e^{i\theta_+}$ and $\epsilon^3 e^{i\theta_-}$, to a set of two CNLS equations [74] :

$$\begin{aligned}&i\frac{\partial V_{1+}}{\partial T_2}+iV_g\frac{\partial V_{1+}}{\partial X_2}+P\frac{\partial^2 V_{1+}}{\partial X_1^2}+[Q_1|V_{1+}|^2+Q_2|V_{1-}|^2]V_{1+}=0,\\&i\frac{\partial V_{1-}}{\partial T_2}-iV_g\frac{\partial V_{1-}}{\partial X_2}+P\frac{\partial^2 V_{1-}}{\partial X_1^2}+[Q_1|V_{1-}|^2+Q_2|V_{1+}|^2]V_{1-}=0,\end{aligned} \tag{2.45}$$

where, $V_g=\frac{d\omega}{dq}=\frac{K_1\sin(q)-hK_2\sin(qh)}{\omega}$ is the velocity and $P=\frac{d^2\omega}{dq^2}=\frac{K_1\cos(q)-K_2h^2\cos(qh)-V_g^2}{2\omega}$, the group velocity dispersion. The nonlinear coefficients Q_1 and Q_2 are, respectively,

$$Q_1=-\frac{\omega_g^2\beta}{\omega},\quad Q_2=-\frac{3\omega_g^2\beta}{2\omega} \tag{2.46}$$

Physically, the set of two variables ($t=T_2$ and $x=X_1=X_2$) is sufficient to describe the evolution of the envelopes, which correspond to letting ε tend to unity. Let us assume $V_{1+}=\psi_1$ and $V_{1-}=\psi_2$; (Eq. 2.45) can be rewrite has:

$$\begin{aligned}&i\frac{\partial\psi_j}{\partial t}+iV_{g,j}\frac{\partial\psi_j}{\partial x}+P\frac{\partial^2\psi_j}{\partial x^2}+[Q_j|\psi_j|^2+Q_l|\psi_l|^2]\psi_j=0\\&l\neq j=1,2\quad V_{g,1}=-V_{g,2}\end{aligned} \tag{2.47}$$

Equation (2.47) is a set of coupled nonlinear Schrödinger (CNLS) equations. The CNLS equations are very important because they can be used to model a great variety of physical systems. Solitary waves in these equations are often called vector solitons in the literature since they are generically described by two-component wave functions.[74, 75] One of the simplest vector solitons is known as shapepreserving, self-localized solution of coupled nonlinear evolution equations.[74] The CNLSE may also model beam propagation inside crystals as well as water wave interactions, and in fiber communication system, such equations have been shown to govern pulse propagation along orthogonal polarization axes in nonlinear optical fibers and in wavelength-division- multiplexed systems.[76, ?] So, Eq. (2.47) can also be used to describe solitons of two-component in the case of the PBD model.

2.4 The multiple scale analysis

2.4.1 Discrete multiple scaling

Let us perform the multiple scale analysis of the discrete evolution equation. The physical problem we are concerned with is the following: the first particle of the chain (say, n=0) is given an oscillation (or submitted to an external force) at frequency Ω. In a linear chain, this oscillation would propagate without distortion as the plane wave $e^{i(\Omega t+Knd)}$, where d is the lattice spacing. However, the nonlinearity induces some deviations from the value Ω, namely, the wave propagates with actual frequency ω and wave number k that is defined as [78]

⋆ ***Representation by the frequency of the wave***

Consider the following wave packet:

$$U_n(t) = \int_{paquet} \hat{u}(\omega) e^{i(knd+\omega t)} d\omega, \tag{2.48}$$

The Taylor expansion is used to express the wave number based on the frequency as follows, where f is any function. We can write

$$f(x) = f(x_0) + \frac{(x-x_0)}{1!}\frac{\partial f}{\partial x}|_{x_0} + \frac{(x-x_0)^2}{2!}\frac{\partial^2 f}{\partial x^2}|_{x_0} + ..., \tag{2.49}$$

is then

$$\begin{aligned} k(\omega) =& k(\Omega) + \frac{(\omega-\Omega)}{1!}\frac{\partial k}{\partial \omega}|_{\Omega} + \frac{(\omega-\Omega)^2}{2!}\frac{\partial^2 k}{\partial \omega^2}|_{\Omega} + ... \\ =& K + \epsilon\nu\frac{\partial k}{\partial \omega}|_{\Omega} + \frac{(\epsilon\nu)^2}{2}\frac{\partial^2 k}{\partial \omega^2}|_{\Omega} + ..., \end{aligned} \tag{2.50}$$

Ultimately, the wave number is:

$$\omega = \Omega + \epsilon\lambda, \quad k = K + \epsilon\frac{\nu}{\nu_g} + \epsilon^2\gamma\nu^2 + ..., \tag{2.51}$$

For simplicity, we asked

$$\frac{1}{\nu_g} = \frac{\partial k}{\partial \omega}|_{\Omega}, \quad 2\gamma = \frac{\partial^2 k}{\partial \omega^2}|_{\Omega}. \tag{2.52}$$

By introducing equation (2.51) in equation (2.48), we obtain:

$$\begin{aligned} U_n(t) &= \int \hat{u}(\nu) e^{i\left[(K+\epsilon\frac{\nu}{\nu_g}+\epsilon^2\gamma\nu^2)nd+(\Omega+\epsilon\lambda)t\right]}\epsilon d\nu \\ &= \epsilon e^{i(Knd+\Omega t)} \int \hat{u}(\nu) e^{i\left[\epsilon^2\gamma nd\nu^2+(t+\frac{nd}{\nu_g})\epsilon\nu\right]} d\nu \\ &= \epsilon e^{i(Knd+\Omega t)} \int \hat{u}(\nu) e^{i(\nu^2\gamma\xi_n+\nu\tau_n)} d\nu, \end{aligned} \tag{2.53}$$

To simplify, let $\gamma = 1$, which does not restrict the generalization of this approach. The previous relationship can also take the form:

$$\begin{aligned} &U_n(t) = A(n,t)\psi(\xi_n,\tau_n) \quad with \\ &A(n,t) = e^{i(Knd+\Omega t)} \quad and \quad \psi(\xi_n,\tau_n) = \epsilon \int \hat{u}(\nu) e^{i(\nu^2\gamma\xi_n+\nu\tau_n)} d\nu. \\ &\tau_n = \epsilon(t + \frac{nd}{\nu_g}), \quad \xi_n = nd\epsilon^2. \end{aligned} \tag{2.54}$$

⋆ ***Representation by the wave number***

The wave packet is defined by:

$$U_n(t) = \int_{paquet} \hat{u}(k) e^{i(knd+\omega t)} dk, \tag{2.55}$$

Both ω and k values are this time expressed in terms of changes in the wave number. By analogy with the above reasoning, we can write:

$$\omega = \Omega + \epsilon\nu_g\lambda + \epsilon^2 p\lambda^2 + ..., \quad k = K + \epsilon\lambda \tag{2.56}$$

with

$$\nu_g = \frac{\partial\omega}{\partial k}|_k, \quad 2p = \frac{\partial^2\omega}{\partial k^2}|_k, \tag{2.57}$$

ν_g is the group velocity and $2p$ the group velocity dispersion. Taking into account the previous development, the relationship (2.55) becomes:

$$\begin{aligned} U_n(t) &= \int_{paquet} \hat{u}(\lambda) e^{i[(K+\epsilon\lambda)nd+(\Omega+\epsilon\nu_g\lambda+\epsilon^2 p\lambda^2+...)t]} d\lambda \\ &= \epsilon e^{i(Knd+\Omega t)} \int \hat{u}(\lambda) e^{i[nd\epsilon\lambda+(\epsilon\nu_g\lambda+\epsilon^2 p\lambda^2+...)t]} d\lambda. \end{aligned} \tag{2.58}$$

Then

$$\begin{aligned} &U_n(t) = B(n,t)\phi(Z_n,T) \quad with \\ &B(n,t) = e^{i(Knd+\Omega t)} \quad and \quad \phi(Z_n,T) = \epsilon \int \hat{u}(\lambda) e^{i(\lambda Z_n+\lambda^2 Tp)} d\lambda. \\ &Z_n = \epsilon(nd + \nu_g t), \quad T = \epsilon^2 t. \end{aligned} \tag{2.59}$$

The function ϕ represents the envelope of the waveform.

⋆ ***discrete scale***

Equation (2.54) has a clear physical meaning: one considers long distance (ϵ^{-2}) effects in the retarded time to give the input disturbance enough time to reach the observed lattice point. In such a situation, the lattice is excited at one end. This corresponds, in other words, to a boundary value problem. The quantity $\psi(\xi_n, \tau_n)$ defines the slow modulation. In order to keep discreteness in space variable for the envelope $\psi(\xi_n, \tau_n)$ one fixes the small parameters as [78, 79]

$$\epsilon^2 = \frac{1}{N} \tag{2.60}$$

and, for any given n, we shall consider only the set of points $..., n-N, n, n+N, ...$ of a large grid indexed by the slow variable m, that is,

$$...(n-N) \to (m-1), \quad n \to m, \quad (n+N) \to (m+1)... \tag{2.61}$$

As a consequence, we can index the variable ξ_n by m in the new grid; we can call m a given point n and $m+j$ the points $n+jN$ for all j. [78, 79]. To simplify the notation, we shall be using everywhere

$$\psi(\xi_j, \tau_j) = \tilde{\psi}_j, \quad \psi(\xi_j, \tau_n) = \psi_j. \tag{2.62}$$

For a given point n and for all j, we have $\tilde{\psi}_j = \psi_j$. Indeed $\tilde{\psi}_n = \psi(\xi_n, \tau_n)$. However $\psi_n = \psi(\xi_n, \tau_j)$ $\Rightarrow \tilde{\psi}_j = \psi_j$.

With the grid defined above, we express the different terms depending, $\psi_m = \psi(m, \tau)$ as follows:

$$\psi_{n-N} = \psi_{m-1}, \quad \psi_n = \psi_m, \quad \psi_{n+N} = \psi_{m+1}. \tag{2.63}$$

The problem is now to express the various different operators occurring in nonlinear evolutions for the product, $A(n,t)\psi_m$ in terms of different operators for ψ_m. The traditional approach to multiple scaling for continuous media originates from water wave theory for which the physical problem is usually that of the evolution of an initial disturbance (e.g., of the surface). In this case, the observer has to follow the deformation at the (linear) group velocity. This operation corresponds to making, in the general Fourier transform solution, the expansion of, $\omega(k)$, around small deviations of k from the linear dispersion law.

We now have to obtain the analogous relations for the product, $U_n(t) = A(n,t)\psi(\xi_n, \tau_n) = A_n\psi_m$, appearing in definition (2.48). The quantities, $U_{n+1}+U_{n-1}-2U_n$, and $U_{n+h}+U_{n-h}-2U_n$ are factorized as follows: [78]

$$\begin{aligned} U_{n+1} + U_{n-1} - 2U_n =& [A_{n+1} + A_{n-1} - 2A_n]\psi_m + \epsilon[A_{n+1} - A_{n-1}](\frac{d}{\nu_g})\frac{\partial \psi_m}{\partial \tau} \\ &+ \frac{\epsilon^2}{2}[A_{n+1} + A_{n-1}](\frac{d}{\nu_g})^2\frac{\partial^2 \psi_m}{\partial \tau^2} + \frac{\epsilon^2}{2}[A_{n+1} - A_{n-1}][\psi_{m+1} - \psi_{m-1}] + \vartheta(\epsilon^3) \end{aligned} \tag{2.64}$$

$$\begin{aligned} U_{n+h} + U_{n-h} - 2U_n =& [A_{n+1} + A_{n-1} - 2A_n]\psi_m + \epsilon[A_{n+h} - A_{n-h}](\frac{hd}{\nu_g})\frac{\partial \psi_m}{\partial \tau} \\ &+ \frac{\epsilon^2}{2}[A_{n+h} + A_{n-h}](\frac{hd}{\nu_g})^2\frac{\partial^2 \psi_m}{\partial \tau^2} + \frac{\epsilon^2}{2}[A_{n+h} - A_{n-h}][\psi_{m+h} - \psi_{m-h}] + \vartheta(\epsilon^3) \end{aligned} \tag{2.65}$$

2.4.2 Application of the discrete multiple scale analysis to the Yakushevich model

We consider the Yakushevich model given by

$$\begin{aligned}\ddot{\psi}_n &= K_s(\psi_{n+1}+\psi_{n-1}-2\psi_n)+K_h(\psi_{n+h}+2\psi_n+\psi_{n-h})-c(\psi_n-\frac{\psi_n^3}{6}-\frac{\phi_n^2\psi_n}{2})\\ I\ddot{\phi}_n &= K_s(\phi_{n+1}+\phi_{n-1}-2\phi_n)+K_h(\phi_{n+h}-2\phi_n+\phi_{n-h})-c(\phi_n^3-\phi_n\psi_n^2),\end{aligned} \tag{2.66}$$

with $K_s=\frac{\beta}{I}$; $K_h=\frac{K}{I}$; $c=\frac{\alpha}{I}$. We look for solutions in the form of a Fourier expansion in harmonics of the fundamental, $e^{i(knd+\Omega t)}$, where the Fourier components are developed in a Taylor series in powers of the small parameter, ϵ, measuring the amplitude of the initial wave [78]

$$\psi(t)=\sum_{p=1}^{\infty}\epsilon^p\sum_{l=-p}^{p}A_{\psi}^{(l)}(n,t)u_p^{(l)}(m,\tau)\qquad \phi(t)=\sum_{p=1}^{\infty}\epsilon^p\sum_{l=-p}^{p}A_{\phi}^{(l)}(n,t)v_p^{(l)}(m,\tau), \tag{2.67}$$

with, $A_{\psi}^{(l)}(n,t)=e^{il(knd+\Omega_\psi t)}$, $A_{\phi}^{(l)}(n,t)=e^{il(knd+\Omega_\phi t)}$, and $u_p^{(-l)}=(u_p^{(l)})^*$, $v_p^{(-l)}=(v_p^{(l)})^*$. Inserting the above expression in Eq.(2.66) we get the following system:

$$\begin{aligned}&\sum_{p=1}^{\infty}\epsilon^p\sum_{l=-p}^{p}[\epsilon^2\partial_{\tau\tau}u_p^{(l)}(m,\tau)+2i\epsilon l\Omega\partial_\tau u_p^{(l)}(m,\tau)-(l\Omega)^2u_p^{(l)}(m,\tau)]A_{\psi}^{(l)}(n,t)\\
&-K_s\sum_{p=1}^{\infty}\epsilon^p\sum_{l=-p}^{p}[(e^{ilqd}+e^{-ilqd}-2)u_p^{(l)}(m,\tau)+\epsilon(\frac{d}{\nu_g})(e^{ilqd}-e^{-ilqd})\partial_\tau u_p^{(l)}(m,\tau)\\
&+\frac{\epsilon^2}{2}(\frac{d}{\nu_g})^2(e^{ilqd}+e^{-ilqd})\partial_{\tau\tau}u_p^{(l)}(m,\tau)+\frac{\epsilon^2}{2}(e^{ilqd}-e^{-ilqd})(u_p^{(l)}(m+1,\tau)-u_p^{(l)}(m-1,\tau))]A_{\psi}^{(l)}(n,t)\\
&-K_h\sum_{p=1}^{\infty}\epsilon^p\sum_{l=-p}^{p}[(e^{ihlqd}+e^{-ihlqd}-2)u_p^{(l)}(m,\tau)+\epsilon(\frac{hd}{\nu_g})(e^{ihlqd}-e^{-ihlqd})\partial_\tau u_p^{(l)}(m,\tau)\\
&+\frac{\epsilon^2}{2}(\frac{hd}{\nu_g})^2(e^{ihlqd}+e^{-ihlqd})\partial_{\tau\tau}u_p^{(l)}(m,\tau)+\frac{\epsilon^2}{2}(e^{ihlqd}-e^{-hilqd})(u_p^{(l)}(m+h,\tau)-u_p^{(l)}(m-h,\tau))]A_{\psi}^{(l)}(n,t)\\
&-c[\sum_{p=1}^{\infty}\epsilon^p\sum_{l=-p}^{p}A_{\psi}^{(l)}(n,t)u_p^{(l)}(m,\tau)-\frac{1}{6}(\sum_{p=1}^{\infty}\epsilon^p\sum_{l=-p}^{p}A_{\psi}^{(l)}(n,t)u_p^{(l)}(m,\tau))^3\\
&-\frac{1}{2}(\sum_{p=1}^{\infty}\epsilon^p\sum_{l=-p}^{p}A_{\psi}^{(l)}(n,t)u_p^{(l)}(m,\tau))\times(\sum_{p=1}^{\infty}\epsilon^p\sum_{l=-p}^{p}A_{\phi}^{(l)}(n,t)v_p^{(l)}(m,\tau))^2]=0,\end{aligned} \tag{2.68}$$

$$\sum_{p=1}^{\infty}\epsilon^p\sum_{l=-p}^{p}[\epsilon^2\partial_{\tau\tau}v_p^{(l)}(m,\tau)+2i\epsilon l\Omega_\phi\partial_\tau v_p^{(l)}(m,\tau)-(l\Omega_\phi)^2v_p^{(l)}(m,\tau)]A_\phi^{(l)}(n,t)$$
$$-K_s\sum_{p=1}^{\infty}\epsilon^p\sum_{l=-p}^{p}[(e^{ilqd}+e^{-ilqd}-2)v_p^{(l)}(m,\tau)+\epsilon(\frac{d}{\nu_g})(e^{ilqd}-e^{-ilqd})\partial_\tau v_p^{(l)}(m,\tau)$$
$$+\frac{\epsilon^2}{2}(\frac{d}{\nu_g})^2(e^{ilqd}+e^{-ilqd})\partial_{\tau\tau}v_p^{(l)}(m,\tau)+\frac{\epsilon^2}{2}(e^{ilqd}-e^{-ilqd})(v_p^{(l)}(m+1,\tau)-v_p^{(l)}(m-1,\tau))]A_\phi^{(l)}(n,t)$$
$$-K_h\sum_{p=1}^{\infty}\epsilon^p\sum_{l=-p}^{p}[(e^{ihlqd}+e^{-ihlqd}-2)v_p^{(l)}(m,\tau)+\epsilon(\frac{hd}{\nu_g})(e^{ihlqd}-e^{-ihlqd})\partial_\tau v_p^{(l)}(m,\tau)$$
$$+\frac{\epsilon^2}{2}(\frac{hd}{\nu_g})^2(e^{ihlqd}+e^{-ihlqd})\partial_{\tau\tau}v_p^{(l)}(m,\tau)+\frac{\epsilon^2}{2}(e^{ihlqd}-e^{-hilqd})(v_p^{(l)}(m+h,\tau)-v_p^{(l)}(m-h,\tau))]A_\phi^{(l)}(n,t)$$
$$-c[-(\sum_{p=1}^{\infty}\epsilon^p\sum_{l=-p}^{p}A_\psi^{(l)}(n,t)u_p^{(l)}(m,\tau))^2\times(\sum_{p=1}^{\infty}\epsilon^p\sum_{l=-p}^{p}A_\phi^{(l)}(n,t)v_p^{(l)}(m,\tau))$$
$$(\sum_{p=1}^{\infty}\epsilon^p\sum_{l=-p}^{p}A_\phi^{(l)}(n,t)v_p^{(l)}(m,\tau))^3]=0. \tag{2.69}$$

We obtain that the coefficients of the constant term give at different orders of ϵ

$$\begin{aligned}&\epsilon:u_1^{(0)}=v_1^{(0)}=0;\quad \epsilon^2:u_2^{(0)}=v_2^{(0)}=0;\quad \epsilon^3:u_3^{(0)}=v_3^{(0)}=0\\ &\Omega_\psi^2=c+4K_ssin^2(\frac{qd}{2})+4K_hcos^2(\frac{hqd}{2});\quad \Omega_\phi^2=4K_ssin^2(\frac{qd}{2})+4K_hsin^2(\frac{hqd}{2}).\end{aligned} \tag{2.70}$$

The coefficients of $A_\psi^{(1)}$ and $A_\phi^{(1)}$ at different order of ϵ give:

$$\epsilon^2:\nu_{g\psi}=\frac{d[K_ssin(qd)-hK_hsin(hqd)]}{\Omega_\psi};\quad \nu_{g\phi}=\frac{d[K_ssin(qd)-hK_hsin(hqd)]}{\Omega_\phi}, \tag{2.71}$$

$$\begin{aligned}&\epsilon^3:[1-K_s(\frac{d}{\nu_{g\psi}})^2cos(qd)-K_s(\frac{hd}{\nu_{g\psi}})^2cos(hqd)]\frac{\partial^2u_1^{(1)}}{\partial\tau^2}-iK_ssin(qd)[u_1^{(1)}(m+1)-u_1^{(1)}(m-1)]\\ &-iK_hsin(hqd)[u_1^{(1)}(m+h)-u_1^{(1)}(m-h)]-\frac{c}{2}[|u_1^{(1)}|^2+3|v_1^{(1)}|^2]u_1^{(1)}=0\\ &[1-K_s(\frac{d}{\nu_{g\phi}})^2cos(qd)-K_s(\frac{hd}{\nu_{g\phi}})^2cos(hqd)]\frac{\partial^2v_1^{(1)}}{\partial\tau^2}-iK_ssin(qd)[v_1^{(1)}(m+1)-v_1^{(1)}(m-1)]\\ &-iK_hsin(hqd)[v_1^{(1)}(m+h)-v_1^{(1)}(m-h)]+c[3|v_1^{(1)}|^2-2|u_1^{(1)}|]v_1^{(1)}=0.\end{aligned} \tag{2.72}$$

The last equation in ϵ^3 of the above set writes

$$\begin{aligned}
&\frac{i}{2}(\chi_{m+1}-\chi_{m-1})+\frac{iP}{2}(\chi_{m+h}-\chi_{m-h})+Q_\psi\frac{\partial^2\chi_m}{\partial\tau^2}+[\gamma_{11}|\chi_m|^2+\gamma_{12}|\eta_m|^2]\chi_m=0\\
&\frac{i}{2}(\eta_{m+1}-\eta_{m-1})+\frac{iP}{2}(\eta_{m+h}-\eta_{m-h})+Q_\phi\frac{\partial^2\eta_m}{\partial\tau^2}+[\gamma_{21}|\chi_m|^2+\gamma_{22}|\eta_m|^2]\eta_m=0,
\end{aligned} \tag{2.73}$$

where, $u_1^{(1)}=\chi_m$ and $v_1^{(1)}=\eta_m$, with

$$\begin{aligned}
&P=\frac{K_h\sin(hqd)}{K_s\sin(qd)};\quad \gamma_{11}=\frac{c}{2K_s\sin(qd)},\quad \gamma_{12}=\frac{3c}{2K_s\sin(qd)};\quad \gamma_{21}=\frac{-3c}{K_s\sin(qd)};\quad \gamma_{22}=-\frac{2c}{K_s\sin(qd)}\\
&Q_\psi=\frac{1}{K_s\sin(qd)}[K_s(\frac{d}{\nu_{g\psi}})^2\cos(qd)+K_s(\frac{hd}{\nu_{g\psi}})^2\cos(hqd)-1]\\
&Q_\phi=\frac{1}{K_s\sin(qd)}[K_s(\frac{d}{\nu_{g\phi}})^2\cos(qd)+K_s(\frac{hd}{\nu_{g\phi}})^2\cos(hqd)-1].
\end{aligned} \tag{2.74}$$

2.4.3 The Fourier series expansion method for the PBD model

We consider the DPB model with the Hamiltonian:

$$H=\sum_{n=1}^{N}[\frac{m\dot{y}_n^2}{2}+V(y_n,y_{n-1})+w_{an}(y_n,y_{n-1})], \tag{2.75}$$

where

$$V(y_n)=D(1-e^{-ay_n})^2-f_sD[tanh(y_n/\lambda_s)+1], \tag{2.76}$$

and

$$w_{an}(y_n,y_{n-1})=\frac{k}{2}(y_n^2-2y_{n-1}y_ncos\theta+y_{n-1}^2)(y_n-y_{n-1})^2. \tag{2.77}$$

We derive from the Hamiltonian, the equation that governs the local oscillations of DNA nucleotides

$$\begin{aligned}
\mu\ddot{y}_n=&K(y_{n+1}+y_{n-1}-2y_n)-2Ksin^2(\frac{\theta}{2})(y_{n+1}+y_{n-1})\\
&-K\rho[(y_n-y_{n-1})e^{-\alpha(y_n+y_{n-1})}-(y_{n+1}-y_n)e^{-\alpha(y_n+y_{n+1})}]\\
&+\frac{bK\rho}{2}[(y_n-y_{n-1})^2e^{-\alpha(y_n+y_{n-1})}+(y_{n+1}-y_n)^2e^{-\alpha(y_n+y_{n+1})}]\\
&-2K\rho sin^2(\frac{\theta}{2})(1-by_n)[y_{n-1}e^{-\alpha(y_n+y_{n-1})}+y_{n+1}e^{-\alpha(y_n+y_{n+1})}]\\
&+\frac{D_nf_s}{l_s}sech^2(\frac{y_n}{l_s})-2aD_n(e^{-ay_n}-e^{-2ay_n}),
\end{aligned} \tag{2.78}$$

In the following, we consider a special collective motion of the pairs in a DNA molecule. The amplitude of the wave packet is big enough, so that the nonlinear effect plays an essential role in DNA molecules. On the other hand, it is still very small compared with the amplitude of the broken base pairs. Therefore, the base pairs in DNA molecule do not oscillate far away

from the bottom of the Morse potential well. In this respect, we can assume, $0 < y_n \ll 1$, and expand the terms in exponential $e^{(y_n+y_{n-1})}$, $e^{(y_n+y_{n+1})}$, and e^{-ay_n} until the second and third orders, respectively. This leads to the modified equation:

$$\begin{aligned}\ddot{y}_n = K_1(y_{n+1}+y_{n-1}-2y_n) - S_1(y_{n+1}+y_{n-1}) - K_2[(y_n+y_{n-1})^2+(y_n+y_{n+1})^2] \\ +K_3y_n(y_{n+1}^2+y_{n-1}^2) - S_3[(y_n+y_{n-1})^3+(y_n+y_{n+1})^3] + K_4y_n^2 - K_5y_n^3 - \omega_0^2y_n.\end{aligned} \tag{2.79}$$

where, $S_1 = \frac{S(1+\rho)}{\mu}$, $S_2 = \frac{S\rho\alpha}{\mu}$, $S_3 = \frac{S\rho\alpha^2}{2\mu}$, $S = 2Ksin^2(\frac{\theta}{2})$, $K_1 = \frac{K(1+\rho)}{\mu}$, $K_2 = \frac{K\rho\alpha}{2\mu} - S_2$, $K_3 = \frac{K\rho\alpha^2}{\mu} - S_3$, $K_4 = \frac{4K\rho\alpha}{\mu} - \gamma\omega_g^2 + \frac{24D_nf_s}{\mu l_s^3} - 2S_2$, $K_5 = \frac{2K\rho,\alpha^2}{\mu} + \beta\omega_g^2 + \frac{112D_nf_s}{3\mu l_s^4} - 2S_3$, $\gamma = -\frac{3a}{2}$, $\beta = -\frac{7a^2}{6}$,$\omega_g^2 = \frac{2a^2D_n}{\mu}$, $\omega_0^2 = \omega_g^2 - \frac{8D_nf_s}{\mu l_s^2}$.

Linearizing (Eq.2.79) yields plane wave solutions with wavenumber k and frequency, $\omega(k)$, given by the dispersion relation, $\omega^2 = \omega_0^2+2S_1cos(ql)+4K_1sin^2(\frac{ql}{2})$. For the nonlinear (Eq.2.79), we search for small-amplitude time-periodic solutions as [80]

$$y_n = \sum_{-\infty}^{+\infty} a_n^{(p)} e^{ip\omega_b t} \tag{2.80}$$

where, ω_b is close to some linear oscillation frequency and the Fourier coefficients are slowly depending on time, $a_n^{(p)}(\epsilon^2 t)$, we have defined the smallness implicit parameter, $\epsilon = \sqrt{K_1}/\omega_g$. Due to exponential decay of the Fourier coefficients in p, they must satisfy, $a_n^{(p)} \sim \epsilon^p$ for $p > 0$, while $a_n^{(0)} \sim \epsilon^2$. Moreover, $a_n^{(p)} \sim a_n^{(-p)*}$, since y_n is real. This allows, for a slow time dependence of the Fourier coefficients $a_n^{(p)}$, a DNLS equation for the dominating coefficient, $a_n^{(1)}$, describing the leading-order nonlinear effects.[80]. Defining, $a_n^{(1)}$ as

$$a_n^{(1)} = (-1)^n\sqrt{\frac{2\omega_b}{3K_5+6S_3}}\psi_n \times exp(i\frac{\omega_0^2-\omega_b^2+2K_1}{2\omega_b}), \tag{2.81}$$

the modified DNLS equation of the DNA model reads

$$\begin{aligned}i\frac{d\psi}{dt} + P(\psi_{n+1}+\psi_{n-1}) + Q_1|\psi_n|^2\psi_n + Q_2[2\psi_n(|\psi_{n+1}|^2+|\psi_{n-1}|^2) + \psi_n^*(\psi_{n+1}^2+\psi_{n-1}^2)] + \\ Q_3[|\psi_{n+1}|^2\psi_{n+1} + |\psi_{n-1}|^2\psi_{n-1} + \psi_n^2(\psi_{n+1}^*+\psi_{n-1}^*) + 2|\psi_n^2|(\psi_{n+1}+\psi_{n-1})] = 0\end{aligned} \tag{2.82}$$

where, $P = \frac{K_1-S_1}{2\omega_b}$; $Q_1 = \frac{K_5-2S_3}{K_5+2S_3}$; $Q_2 = \frac{3S_3-K_3}{3K_5+6S_3}$; $Q_3 = \frac{-2S_3}{K_5+2S_3}$. P, Q_1, Q_2, and Q_3, are the coefficients of the generalized DNLS equation.

2.5 The linear stability analysis

2.5.1 The linear stability analysis for the CQNLS equation

We present the linear stability (LS) analysis of the plane waves in the context of the cubic quintic nonlinear Schrödinger equation. While putting $y_{11}(\xi,t) = \psi(X,t)$ with $\xi = X$ we obtain the general CQNS equation:

$$i\psi_t + P\,\psi_{XX} + Q_1|\psi|^2\psi + Q_2|\psi|^4\psi = 0. \tag{2.83}$$

P, Q_1, and Q_1 are define is (3.150). We assume that the amplitude of the wave is time-independent during propagation in the system. This amounts to consider the plane waves of the form

$$\psi(x,t) = A_0 \exp[i(kx - \tilde{\omega}t], \tag{2.84}$$

where, $\tilde{\omega} = \omega + kV_g$ and A_0 is a real constant. Replacing this solution into Eq. (2.83) yields the associated nonlinear dispersion relation

$$\tilde{\omega} = P\,k^2 - Q_1 A_0^2 - Q_2 A_0^4. \tag{2.85}$$

In the LS framework the MI is examined using the linearization. Then, we use the ansatz

$$\psi(x,t) = [A_0 + \varepsilon\phi(x,t)] \exp[i(kx - \tilde{\omega}t)]. \tag{2.86}$$

In this ansatz, $\phi(x,t)$ is a small perturbation, say $\phi \ll A_0$, $qx - \tilde{\omega}t$, is the modulation phase in which k and $\tilde{\omega}$ are, respectively, the wave number and frequency of the modulation. We substitute the perturbed plane wave (2.86) in Eq. (2.83) considering the above dispersion relation. Then, neglecting terms of order higher than $\mathrm{O}(\varepsilon)$, we obtain the equation describing the dynamics of the perturbation $\phi(x,t)$:

$$i\phi_t = -P\phi_{xx} - 2iPq\phi_x - \Delta(\phi + \phi^*), \tag{2.87}$$

where, ϕ^* is the complex conjugate of ϕ, and $\Delta = Q_1 A_0^2 + 2Q_2 A_0^4$. We consider a perturbation of the form $\phi = u(x,t) + iv(x,t)$. Then the real and imaginary parts of ϕ obey the coupled set of equations:

$$\begin{aligned} &u_t + Pv_{xx} + 2Pku_x = 0, \\ &v_t - Pu_{xx} + 2Pkv_x - 2\Delta u = 0. \end{aligned} \tag{2.88}$$

We suppose that the perturbation is a plane wave defined according to the following expressions:

$$\begin{aligned} u &= \mathrm{Re}\{U \exp[i(Kx - \Omega t]\}, \\ v &= \mathrm{Im}\{V \exp[i(Kx - \Omega(s)t]\}. \end{aligned} \tag{2.89}$$

Plugging Eq. (2.89) into Eq. (2.88) we obtain a system of first order equations in U, V:

$$\begin{aligned} &[\Omega - 2PkK]\,U - PK^2 V = 0, \\ &[2\Delta + PK^2]\,U - [\Omega - 2PkK]\,V = 0. \end{aligned} \tag{2.90}$$

Such a system may have solutions only if its determinant is zero. This corresponds to the following explicitly time-dependent dispersion relation for the parameters of the perturbation

$$\Omega^2 - 4PkK\Omega + PK^2[4Pk^2 + 2\Delta - PK^2] = 0. \tag{2.91}$$

From this relation we can derive the condition of occurrence of the modulational instability. In fact the perturbation may undergo the exponential growth if the modulation frequency Ω is a

complex with positive imaginary part. This condition should be realized when the discriminant of the above quadratic equation in Ω is negative, say

$$PK^2 - 2Q_1A_0^2 - 4Q_2A_0^4 < 0. \tag{2.92}$$

This condition relates the perturbation wave number K to the amplitude A_0 of the initial plane wave and the strengths of cubic-quintic nonlinearity. Under this condition, the MI sets in within the system under study with a gain (or instability growth rate) $G = |\mathrm{Im}(\Omega)|$ given by

$$G = |K|\sqrt{-P^2K^2 + 2PQ_1A_0^2 + 4PQ_2A_0^4}. \tag{2.93}$$

One realizes that the MI gain does not depend on the wave number k of the initial plane wave. Hence a linear stability analysis with $k = 0$, as it is the case in numerous works, does not loss generality. The linear stability analysis is useful in purposes such as the investigation of modulational instability where it provides the instability criterion, growth rate and domains. However it cannot give us the time evolution of any parameter of the modulational perturbations, notably its amplitude and phase.

2.5.2 The linear stability analysis for the CNLS equation

In order to investigate the MI of a two-component waves, we shall first seek an equilibrium state in the form $\psi_j = \psi_{j0}\exp(i\varphi_j(t))$ (for j = 1, 2), where ψ_{j0} is a constant real amplitude and $\varphi_j(t)$ is the phase. Using this relation into Eqs. 2.47 leads to a monochromatic (fixed-frequency) solution of the form $\varphi_j(t) = \Omega_{j0}t$, where $\Omega_{j0} = Q_j\psi_{j0}^2 + Q_l\psi_{l0}^2$ $(for j \neq l = 1, 2,)$. Considering a small perturbation around equilibrium, we take $\psi_j = (\psi_{j0} + \delta\psi_j)\exp(i\varphi_j(t))$, where $\delta\psi_j = \varepsilon\psi_{j1}(r,t)$ is a small ($\varepsilon \ll 1$, $\psi_{j1} = a_j + ib_j$) complex amplitude perturbation of the wave amplitudes. We substitute this expression into (Eqs. 2.47) and separate the real and imaginary parts. The first order terms $(in\ \ \varepsilon)$ yields to [81]

$$\begin{aligned} -\frac{\partial b_j}{\partial t} - V_{g,j}\frac{\partial b_j}{\partial x} + P\frac{\partial^2 a_j}{\partial x^2} + 2Q_j\psi_{j0}^2a_j + 2Q_l\psi_{j0}\psi_{l0}a_l = 0, \\ \frac{\partial a_j}{\partial t} + V_{g,j}\frac{\partial a_j}{\partial x} + P\frac{\partial^2 b_j}{\partial x^2} = 0. \end{aligned} \tag{2.94}$$

Equation (2.94) can be simplified and we obtain

$$[(\frac{\partial}{\partial t} - V_{g,j}\frac{\partial}{\partial x})^2 + P(P\frac{\partial^2}{\partial x^2} + 2Q_1\psi_{10}^2)\frac{\partial^2}{\partial x^2}]a_1 + 2Q_2\psi_{10}\psi_{20}\frac{\partial^2 a_2}{\partial x^2} = 0. \tag{2.95}$$

Let us use $a_j = a_{j0}\exp[i(Kx - \Omega t)]$ + c.c where K and Ω are the wavevector and the frequency of the perturbation, respectively, viz. $\frac{\partial}{\partial t} \to -i\Omega$ and $\frac{\partial}{\partial x} \to iK$. We get the following equation:

$$\begin{bmatrix} (\Omega - KV_g)^2 - \Omega_1^2 & 2K^2PQ_2\psi_{10}\psi_{20} \\ 2K^2PQ_2\psi_{10}\psi_{20} & (\Omega + KV_g)^2 - \Omega_2^2 \end{bmatrix} \begin{bmatrix} a_{10} \\ a_{20} \end{bmatrix} = 0, \tag{2.96}$$

where $\Omega_1^2 = PK^2(PK^2 - 2Q_1\psi_{10}^2)$ and $\Omega_2^2 = PK^2(PK^2 - 2Q_1\psi_{20}^2)$. Non trivial solutions is obtained if the determinant of matrix is different of zero. So, this implies that:

$$[(\Omega - KV_g)^2 - \Omega_1^2][(\Omega + KV_g)^2 - \Omega_2^2] - \Omega_c^4 = 0, \tag{2.97}$$

where $\Omega_c^4 = (2K^2PQ_2\psi_{10}\psi_{20})^2$. This dispersion relation is a 4th order polynomial in Ω.

2.5.3 The linear stability analysis for the discrete NLS equation

We begin our analysis by considering the linear dispersion properties of the modified DNLS equation Eq. (2.82). In so doing, we write $\psi_n = \psi_0 e^{i(qn-\Lambda t)}$, where the wavenumber q, the angular frequency Λ and the amplitude ψ_0 satisfy the dispersion relation

$$\Lambda = -2Pcos(q) - \psi_0^2[Q_1 + 2Q_2(2 + cos(2q)) + 8Q_3cos(q)]. \tag{2.98}$$

To examine the LS of the initial plane waves, we look for a solution of the form

$$\psi_n = \psi_0(1 + B_1e^{i(Qn-\Omega t)} + B_2^*e^{-i(Qn-\Omega^* t)})e^{i(qn-\Lambda t)}, \tag{2.99}$$

where the asterisk denotes complex conjugation. B_1 and B_2 are complex constant and stand for perturbation amplitudes. K and Ω represent the wavenumber and the angular frequency of the perturbation, respectively. We obtain the linear homogeneous system for B_1 and B_2

$$\begin{pmatrix} a_{11} + \Omega & a_{12} \\ a_{21} & a_{22} - \Omega \end{pmatrix} \begin{pmatrix} B_1 \\ B_2 \end{pmatrix} = \begin{pmatrix} 0 \\ 0 \end{pmatrix}, \tag{2.100}$$

with

$$\begin{aligned} a_{11} &= 2P(cos(Q+q) - cos(q)) + \psi_0^2[Q_1 + 2Q_2(1 - sin(Q)sin(2q)) + Q_3(8cos(q+Q) - cos(q))], \\ a_{22} &= 2P(cos(Q-q) - cos(q)) + \psi_0^2[Q_1 + 2Q_2(1 + sin(Q)sin(2q)) + Q_3(8cos(Q-q) - cos(q))], \\ a_{12} &= a_{21} = \psi_0^2[Q_1 + 2Q_2(2cos(Q) + cos(2q)) + 8Q_3cos(q)cos^2(\frac{Q}{2})]. \end{aligned} \tag{2.101}$$

The condition for the existence of non trivial solutions of the above linear homogenous system is given by a second order equation for the frequency Ω, that is

$$\Omega^2 + (a_{11} - a_{22})\Omega + a_{12}^2 - a_{11}a_{22} = 0, \tag{2.102}$$

the discriminative of equation (15) is given by

$$\Delta = 16(A + \psi_0^2 D_1)(A - \psi_0^2 D_2) \tag{2.103}$$

whit, $A = 2Pcos(q)sin^2(\frac{Q}{2})$, $D_1 = [2Q_2(cos(Q) - sin^2(q)) + Q_3]$, $D_2 = [Q_1 + 2Q_2(cos(Q) + cos^2(q)) + \frac{3}{2}Q_3cos(q)(4cos(Q) + 1)]$. MI will develop in the molecule if Δ is negative.

2.6 The Variational Approach

The variational approximation (VA) was first introduced for solitons in plasmas in the cornerstone paper by Bondeson *et al* [82]. Then following this pattern, the VA has been developed for solitons in other physical media (chiefly, optical fibers) [83]. The VA technique for optical solitons was further developed in an important paper by Anderson *et al* [83]. In a work by Malomed [84], a review of variational approximation is addressed and it is demonstrated that a combination of the variational approximation with direct numerical simulations is the most natural and efficient approach to many problems in nonlinear optics and other areas of physics which are based on nonlinear PDEs. These works became the basis for the rapid development of analytical methods in the fields of nonlinear system based on VA. The variational approximation turns out to be a very efficient technique, as it is, as a matter of fact, the only consistent approximation producing analytical or semi-analytical results for complex dynamical models.

An alternative method to study the modulational instability of plane waves in the context of NLS equation is a variational approximation, the so-called variational approach (VA). It is also used in the study of solitons at the classical level [84] as well as quantum level [85]. The VA is a dynamical system's type approach [86] which allows us to derive in a simple way not only the MI condition, but also the Euler-Lagrange equations for the time evolution of the perturbation ansatz parameters. The distinguishing characteristics of the VA amongst the other similar approaches are as follows:

- The VA uses the MI-motivated ansatz,
- The VA uses the variational formulation of the three-mode approximation problem (instead of the application of the three-mode ansatz in the dynamical equation in the context of Ref. [87]),
- In the VA we perturb around an exact plane wave solution, while in the case of Ref. [87], the plane wave is an additional mode in the relevant expansion.

The approximation begins with postulating an ansatz, i.e., a trial analytical form of the field configuration sought for. In most cases, the configuration is a solitary wave or a plane wave. In the case of the NLS equation (2.83), commonly adopted ansatz approximate a perturbed soliton or plane wave on the respective forms

$$\psi(x,t) = A_0 \mathrm{sech}\left(\frac{x}{a}\right) e^{\mathrm{i}[f(t)x^2+b(t)]}, \tag{2.104}$$

$$\psi(x,t) = \{A_0 + a_1(t)e^{\mathrm{i}[Kx+b_1(t)]} + a_2(t)e^{\mathrm{i}[-Kx+b_2(t)]}\}\, e^{\mathrm{i}[kx-\tilde{\omega}t]}. \tag{2.105}$$

The functional form of the ansatz is fixed as concerns its x-dependence, while it contains several free parameters, for instance the real amplitude A_0, width a, phase b, and the chirp f in the case of the ansatz (2.104). The free parameters are allowed to be functions of the evolutional variable, which is t in the case of Eq. (2.83). Equations governing the evolution

of these variational parameters in t can be derived in a natural way, provided that the underlying equation(s) can be derived by means of the standard variational procedure, equating to zero the variational derivative $\delta S/\delta\psi^*$ of the corresponding action functional $S\{\psi,\psi^*\}$ (the asterisk stands for complex conjugation). The variational representation is usually available for conservative models, including those with an explicit coordinate dependence. This allows the variational approach to be applicable to the Gross-Pitaevskii equation which is very useful in the field of Bose-Einstein condensates. However in some special cases, dissipative models also admit a natural variational representation, see [84].

The action is represented in the form $S=\int L\mathrm{d}t$, where t is considered as the evolutional variable, and L is a Lagrangian, which is represented in its own integral form,

$$L=\int \mathcal{L}\mathrm{d}\vec{r}\mathrm{d}x, \tag{2.106}$$

where $\mathcal{L}$ is a Lagrangian density, that must be real, and $\vec{r}$ is the vector set of transverse coordinates (implying the possibility to consider spatiotemporal evolution of fields in two- and three-dimensional dispersive nonlinear media). If the transverse coordinates are present, the ansatz must be a definite function of both x and $\vec{r}$. In the case of the nonlinear Schrödinger equation (2.83), the Lagrangian density reads

$$\mathcal{L}(\psi)=\frac{1}{2}\mathrm{i}(\psi^*\frac{\partial\psi}{\partial t}-\psi\frac{\partial\psi^*}{\partial t})-P|\frac{\partial\psi}{\partial x}|^2+\frac{1}{2}Q_1|\psi|^4+\frac{1}{3}Q_2|\psi|^6, \tag{2.107}$$

and $\mathrm{d}\vec{r}$ is dropped in Eq. (2.106). More generally, in the case of a system of NLS-like equations for complex variables $\psi_n(x,t,\vec{r})$, the density is

$$\mathcal{L}=\mathcal{L}\big(\psi_n,\psi_n^*,(\psi_n)_x,(\psi_n^*)_x,(\psi_n)_t,(\psi_n^*)_t,\nabla\psi_n,\nabla\psi_n^*\big), \tag{2.108}$$

where $(\psi_n)_x$ stands for the derivative of ψ_n with respect to x, and ∇ is the gradient with respect to the transverse coordinates. In this case, the equations following from the variational principle, $\delta S/\delta\psi_n^*=0$, take the form

$$\frac{\partial}{\partial t}\frac{\partial\mathcal{L}}{\partial[(\psi_n^*)_t]}+\frac{\partial}{\partial x}\frac{\partial\mathcal{L}}{\partial[(\psi_n^*)_x]}+\nabla\cdot\left[\frac{\partial\mathcal{L}}{\partial(\nabla\psi_n^*)}\right]=\frac{\partial\mathcal{L}}{\partial(\nabla\psi_n^*)}. \tag{2.109}$$

The Lagrangian representation of the nonlinear wave equations is related to their Hamiltonian representation, which, for a broad class of equations of the NLS type, is

$$\frac{\partial\psi_n}{\partial t}=-\mathrm{i}\frac{\delta H}{\delta\psi_n^*}, \tag{2.110}$$

with the functional $H\{\psi_n,\psi_n^*\}$ being the Hamiltonian. In particular, for the NLS equation (2.83), it is given by the expression

$$H=\int_{-\infty}^{+\infty}\left[P|\frac{\partial\psi}{\partial x}|^2-\frac{1}{2}Q_1|\psi|^4-\frac{1}{3}Q_2|\psi|^6\right]\mathrm{d}x. \tag{2.111}$$

In order to apply VA to a given problem, one should insert the adopted ansatz into the expression (2.106) and calculate the integral in an analytical form. The necessity to perform the integration analytically imposes conditions on the choice of the ansatz. Let $m_j(t)$ be the set of free parameters that the ansatz contains. The calculation of the integral (2.106) after the substitution of the ansatz yields an effective Lagrangian, L, which is a function of the parameters m_j and their t-derivatives $\dot{m}_j$ (the derivatives appear because of the presence of the t-derivatives in the Lagrangian density). For example, the effective Lagrangian obtained by substitution of the ansatz (2.105) into the NLS Lagrangian corresponding to the density (2.107) can be easily calculated analytically. Here we rather consider an annular geometry, which is a one-dimensional geometry that imposes periodic boundary conditions on the wave function $\psi(x,t)$ and integration limits $0 \leq x < 2\pi$ in Eq. (2.106). This leads to the quantization of the wave numbers i.e. $k, K = 0, \pm 1, \pm 2, \pm 3, ...$ However, our results can be generalized to the case of an infinite open system and to higher dimensions. We obtain the effective Lagrangian :

$$\begin{aligned} L = -\pi\big\{ & 2(a_1^2\dot{b}_1 + a_2^2\dot{b}_2) + 2(PK^2 - Q_1A_0^2 - 2Q_2A_0^4)(a_1^2 + a_2^2) + 4PkK(a_1^2 - a_2^2) \\ & -(Q_1 + 6Q_2A_0^2)(a_1^4 + a_2^4 + 4a_1^2a_2^2) \\ & +A_0^4(Q_1 + \frac{4}{3}Q_2A_0^2) - \frac{2}{3}Q_2(a_1^6 + a_2^6 + 9a_1^4a_2^2 + 9a_1^2a_2^4) \\ & -4A_0^2(Q_1 - 2Q_2A_0^2)a_1a_2\cos(b_1 + b_2) - 12Q_2A_0^2(a_1^2 + a_2^2)a_1a_2\cos(b_1 + b_2)\big\}. \end{aligned} \tag{2.112}$$

The effective Lagrangian gives rise to a set of variational equations for the variables $m_j(t)$,

$$\frac{\mathrm{d}}{\mathrm{d}t}\frac{\partial L}{\partial \dot{m}_j} - \frac{\partial L}{\partial m_j} = 0, \tag{2.113}$$

which can then be solved by means of analytical or numerical methods. First of all, one should find fixed points (FPs) of the ordinary differential equation (ODE) system (2.113), $\mathrm{d}m_j/\mathrm{d}t = 0$, which correspond to a stationary soliton of the underlying model. Next, stability of the fixed points against small perturbations can be analyzed, linearizing Eqs. (2.113) near the FP solutions, which should predict whether the soliton is expected to be dynamically stable. Full dynamical solutions to Eqs. (2.113) (rather than linearization around the fixed points), that correspond to a strong perturbation of the solitons, may also be of interest from the viewpoint of the underlying model. Thus, the essence of VA is approximating an unknown field configuration by an appropriate ansatz, whose free parameters evolve in t according to the system of ODEs (2.113).

It is necessary to stress that there is no direct formal relation between the underlying PDEs (for instance, the NLS equation) and the system of variational equations (2.113). Thus, VA is always based, to a large extent, on physical intuition rather than on rigorous mathematical arguments, and the relevance of the application of a particular variational ansatz to a given problem can only be checked *a posteriori* by comparison of the results with direct numerical simulations of the underlying PDEs. Comparison with direct simulations is especially necessary

if one is dealing with the stability problem. Actually while the shape of a static soliton may be readily mimicked by a reasonably chosen ansatz, the approximation can miss a specific perturbation mode leading to an instability of the soliton. Moreover, VA can sometimes introduce a false instability that the soliton in fact does not have.

2.7 The solution soliton for the DNA molecule

We seek soliton solution for the NLS equation in the form

$$\psi(x,t) = \phi(x,t)e^{i\theta(x,t)}, \tag{2.114}$$

where, θ and ϕ are real functions. By suitably choosing the factor Phase ϕ, it can be restricted to positive values for the amplitude θ. Referring this ansatz in the NLS equation (**??**), and separating real and imaginary parts, one obtains the following system of equations:

$$\begin{aligned} -\phi\theta_t + P\phi_{xx} - P\phi\theta_x^2 + Q\phi^3 = 0, \\ \phi_t + P\phi\theta_{xx} + 2P\theta_x\phi_x = 0. \end{aligned} \tag{2.115}$$

We will seek a particular solution whose carrier θ spreads the speed u_p keeping its shape and the casing ϕ propagates at the speed u_e also keeping its shape. That is to say that we seek a solution as

$$\phi(x,t) = \phi(x - u_e t) \quad and \quad \theta(x,t) = \theta(x - u_p t) \tag{2.116}$$

Finally the following solution is obtained for the NLS equation

$$\psi(x,t) = \phi_0 sech[\sqrt{\frac{Q}{2P}}\phi_0(x - u_e t)]e^{i\frac{u_e}{2P}}(x - u_p t), \tag{2.117}$$

with

$$\phi_0 = \sqrt{\frac{u_e^2 - 2u_e u_p}{2PQ}}, \quad PQ > 0, \quad and \quad u_e^2 - 2u_e u_p > 0. \tag{2.118}$$

Note that we do not get a solution $u = u_p$, which means that is not possible to obtain a solution with a constant profile for the equation NLS. One can also write the solution as

$$\psi(x,t) = \phi_0 sech(\frac{x - u_e}{L_e})e^i(\kappa x - \mu t), \tag{2.119}$$

where

$$L_e = \frac{1}{\phi_0}\sqrt{\frac{Q}{2P}}, \quad \kappa = \frac{u_e}{2P} \quad and \quad \mu = \frac{u_e u_p}{2P}. \tag{2.120}$$

2.8 The numerical analysis

According to the analytical study presented in the previous section, we perform numerical integrations of the nonlinear partial differential equations governing the wave propagation in the network, which are an approximation of the exact equation governing modulated wave propagation in the network. The fourth-order Runge-Kutta scheme is used with normalized integration time step.

For our study, the number of cells N is chosen to be equal to 1600 and we have used periodic boundary conditions so that we do not encounter the wave reflection at the end of the line. At the input of the line, we apply a slowly modulated signal. In other hand, to perform our analytical results, we are tested by direct numerical simulation the analytical solutions.

2.9 Conclusion

This chapter was concerned with the analytical and numerical methods used in the study of DNA dynamics. They are the perturbation method (semi-discrete expansion, the multiple scale analysis...) transformation, the Fourier series expansion method, the linear stability analysis, the time-dependent variational approach, and the numerical procedure. We have developed the semi-discrete and discrete multiple scaling transformation and in the PB model and his extension models as well as in the Yakushevich to get the NLSE, the CQNLSE and the CNLSE. Using the Fourier series expansion method we obtained the general DNLS equation.

Chapter 3

Results and Discussions

3.1 Introduction

One of the most fascinating problems in molecular biology is that the interactions between proteins and nucleic acids whose role is crucial in the process of replication, transcription, and storage of DNA in cells. The study of these interactions is very complex and only a precise knowledge on the atomic scale three-dimensional structures of the molecules studied, their flexibility and energy terms involved, can help to understand the nature and the mechanism of these interactions. From a purely structural point of view it has been observed on many complex, the fixing of a protein could lead to large deformations of the DNA molecule. Although some of these deformations are directly induced by the protein, it is now recognized that the base sequence of DNA itself influences the structure and flexibility of the double helix. Initially seen as a regular and rigid molecule, the DNA double helix has in fact a strong structural and dynamic in terms of its base sequence and its environment heterogeneity. These properties play a major role in recognition processes involving proteins that target the double helix. We must therefore take into account all the dynamic characteristics intrinsic to the DNA molecule to really understand how a protein can recognize and interact with a specific site of the double helix and thus grow in the knowledge of essential biological processes. Nevertheless, it is still difficult to predict this behavior because obtaining such properties present several experimental problems related to the shape and flexibility of the DNA molecule.

The goal of this work is precisely to study the dynamical processes taking place in DNA, and specifically the processes mentioned above, namely the motion of the transcription and replication bubble with the use some of the nonlinear dynamical models proposed so far. The chapter is divided into two part: the first part is based on the study of modulational instability (MI) through some of the models presented in chapter one while the second part is devoted to derive excat soliton solutions of the DNA models.

3.2 Modulational instability through the Peyrard-Bishop model

The PB model considers a simplifed geometry for the DNA chain. The chain consists of a sequence of base pairs as described in chapter one. Each base pair includes two degrees of freedom. They correspond to the displacements of the bases from their equilibrium positions along the direction of the hydrogen bonds that connect two bases in a pair. In this work, we pay attention to the out-of-phase dynamics because it describes nonlinear waves. The equation of the out-of-phase motion is written as

$$m\ddot{y_n} = S(y_{n+1} - 2y_n + y_{n-1}) + 2\sqrt{2}aD(e^{-2a\sqrt{2}y_n} - e^{-a\sqrt{2}y_n}). \tag{3.1}$$

We expand e^{-ay_n} until the second and third orders, respectively. This leads to the modified equation

$$\ddot{y_n} = \omega_0^2(y_{n+1} - 2y_n + y_{n-1}) - \omega_g^2(y_n + \alpha y_n^2 + \beta y_n^3), \tag{3.2}$$

where, $\alpha = -\frac{3a}{\sqrt{2}}$; $\beta = \frac{7a^2}{3}$; $\omega_g^2 = \frac{4a^2D_n}{m}$; $\omega_0^2 = \frac{S}{m}$.

We use the semi-discrete approximation to obtain the short-wavelength envelope soliton. This asymptotic approach allows us to describe the envelope in the continuum approximation and to treat properly the carrier wave with its discrete character. Owing to the assumed weak nonlinearity, we expand y_n into the following asymptotic series [65] :

$$y_n(t) = \sum [\epsilon^l y_{l,m}(n,t)]e^{im\theta(n,t)} + C.C. \tag{3.3}$$

Utilizing the idea developed by Taniuti and Yajima [72],the solution y_n is taken to be

$$\begin{aligned} y_n(t) =& \epsilon^{\frac{1}{2}} y_{11}(n,t)e^{i\theta} + C.C + \epsilon[y_{20} + y_{22}(n,t)e^{2i\theta} + C.C] + \epsilon^{\frac{3}{2}} y_{33}(n,t)e^{3i\theta} + C.C \\ &+ \epsilon^2[y_{42} + y_{44}(n,t)e^{4i\theta} + C.C] + \epsilon^{\frac{5}{2}}[y_{53}(n,t)e^{3i\theta} + y_{55}(n,t)e^{5i\theta} + C.C] + 0(\epsilon^{\frac{7}{2}}), \end{aligned} \tag{3.4}$$

where, $C.C$ stands for complex-conjugate and $\theta_n = nql - \omega t$. The smallness parameter ϵ which ranks from 0 to 1 $0 < \epsilon \leq 1$ represents the size of the amplitude of perturbation. Using the method of the section 2.3.2 we obtain the Cubic Quintic Nonlinear Schrödinger (CQNLS) equation

$$i\frac{\partial y_{11}}{\partial \tau} + P\frac{\partial^2 y_{11}}{\partial \xi^2} + Q_1|y_{11}|^2 y_{11} + Q_2|y_{11}|^4 y_{11} = 0, \tag{3.5}$$

where $\tau = t$, $\xi = x - V_g t$ and the subscripts τ and ξ denote partial differentiations with respect to τ and ξ. While putting $y_{11}(\xi, t) = \psi(X, t)$ with $\xi = X$ we obtain the general CQNS equation:

$$i\psi_t + P\,\psi_{XX} + Q_1|\psi|^2\psi + Q_2|\psi|^4\psi = 0. \tag{3.6}$$

$$\begin{aligned} P = \frac{l^2\omega_0^2 cos(ql) - V_g^2}{2\omega}; \quad Q_1 = -\frac{\omega_g^2[3\beta + 2\alpha(2a_{20} + a_{22})]}{2\epsilon\omega}, \\ Q_2 = -\frac{\omega_g^2[2\alpha(a_{22}a_{33} + a_{42}) + \beta(12a_{22}a_{20} + 3a_{33} + a_{20} + 6a_{22}^2 + 12a_{20}^2)]}{2\omega}, \end{aligned} \tag{3.7}$$

P, Q_1, Q_2, are respectively, the dispersion coefficient, the cubic nonlinear coefficient as well as the the quintic nonlinear coefficient. Figure. (13) shows the parameters of equation (3.6)

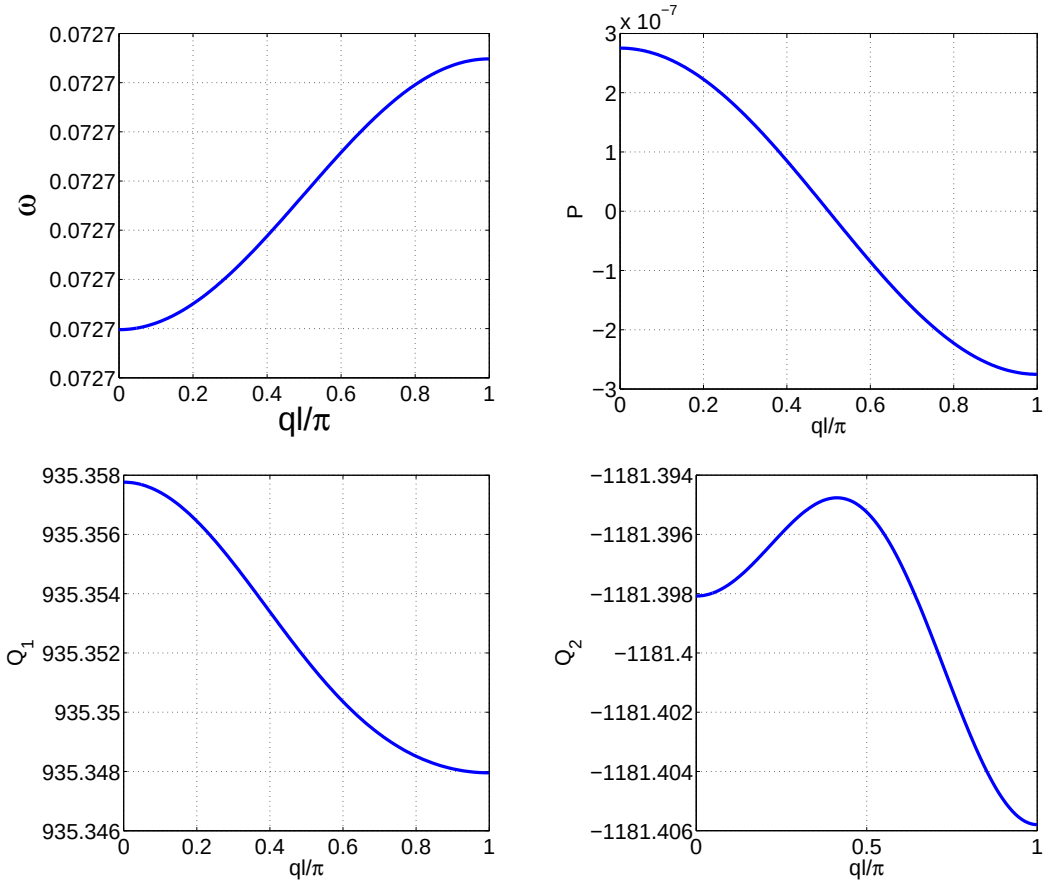

Figure 13: Parameters of CQNLS equation

The NLS is used for the modeling of wave processes in different physical systems such as nonlinear optics [88, 89], circular polarized Alfven waves in plasma [90], Stokes waves in fluids of finite depth, etc. In nonlinear optics [92], the NLS equation can be derived from a systematic way by means of the reductive perturbation scheme as a model for single mode propagation. In the context of waveguides as optical fibers, t usually corresponds to the propagation distance of the electric field envelope ψ of an optical beam along the fiber, x plays the role of the time, in most natural cases, one assumes that the term $Q_1|\psi|^2\psi$ corresponds to self-focusing ($Q_1 > 0$) cubic (Kerr) nonlinearity competing with its self-focusing ($Q_2 < 0$) quintic counterpart. Here, we have obtained the CQNLS equation for the PB model.

In order to examine the MI of the DNA dynamic through the linear stability framework, we may use the ansatz

$$\phi(x,t) = (A_0 + \delta\phi)\exp(-i\Lambda t), \tag{3.8}$$

where, Λ is a nonlinear frequency shift, A_0 is a real constant and $\delta\phi$ is the amplitude perturba-

tion. Substituting Eq. (3.8) into Eq. (3.6), neglecting second order terms in $\delta\phi$ and its complex conjugate $\delta\phi^*$, we take

$$\Lambda = -A_0^2[\,Q_1 + Q_2 A_0^2], \tag{3.9}$$

to obtain the following equation describing the dynamics of the perturbation:

$$i\frac{\partial\,\delta\phi}{\partial t} = -P\frac{\partial^2\delta\phi}{\partial x^2} + \Delta(\delta\phi + \delta\phi^*). \tag{3.10}$$

In Eq. (3.10), $\Delta = -A_0^2[\,Q_1 + 2Q_2A_0^2]$. Let u_1 and u_2 be respectively, the real and imaginary parts of $\delta\phi$. Then Eq. (3.10) is transformed into the following two coupled equations:

$$\frac{\partial u_1}{\partial t} + P\frac{\partial^2 u_2}{\partial x^2} = 0, \tag{3.11}$$

$$-\frac{\partial u_2}{\partial t} + P\frac{\partial^2 u_1}{\partial x^2} - 2\Delta u_1 = 0. \tag{3.12}$$

Now, we consider that the variation of the perturbation obeys the expression:

$$\begin{aligned} u_1 &= \mathrm{Re}\{U_1 \exp\big[i\big(Kx - \Omega t\big)\big]\}, \\ u_2 &= \mathrm{Im}\big\{U_2 \exp\big[i\big(Kx - \Omega t\big)\big]\}, \end{aligned} \tag{3.13}$$

where $Kx - \Omega t$ is the modulation phase in which K and Ω are respectively, the wave number and frequency of the modulation. After some calculations, we obtain the following explicitly time-dependent dispersion relation:

$$\Omega^2 = PK^4 - K^2[2Q_1A_0^2 + 4Q_2A_0^4]. \tag{3.14}$$

This relation can easily been rewritten on the following form

$$\Omega^2 = K^4[P - 2\big(\frac{A_0}{K}\big)^2(\,Q_1\ + 2Q_2A_0^2)]. \tag{3.15}$$

For the MI to occur, the frequency of modulation must be complex with nonzero imaginary part. Such a condition may be simply realized if the right-hand side of Eq. (3.15) is negative ; that is,

$$-2Q_1\big(\frac{A_0}{K}\big)^2\ - 4Q_2A_0^2\big(\frac{A_0}{K}\big)^2 + P < 0. \tag{3.16}$$

In that case, the local growth rate of instability is given by the relation

$$G = |K|\sqrt{-P^2K^2 + 2PQ_1A_0^2 + 4PQ_2A_0^4}. \tag{3.17}$$

Figure (14) shows the regions of MI obtained from the analytical study. In this figure, we plot the wave number K as functions of wave number q, we therefore obtain three zones of instability and stability in the plane (q, K). for $0 < q < 0.5\pi$, the MI may develop as soon as the experiment begins; for $0.5\pi < q < \pi$,the system is expected to be modulationally stable.

We plot in figure (15) the initial gain of MI in the system for points labeled in the (q, K) plane.

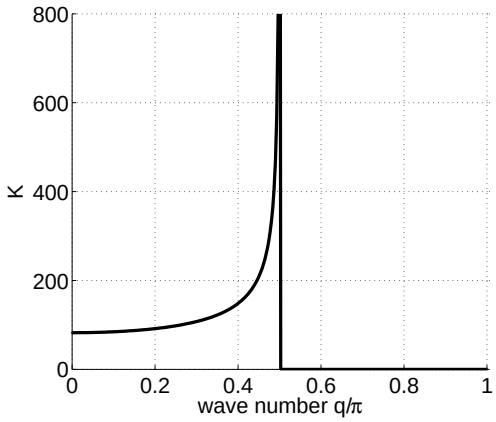

Figure 14: Regions of modulational stability and instability in the (q, K) plane. The parameters used are :m=300; D=0.04; a=4.45; S=0.06; $A_0 = 0.001$; $\epsilon = 0.01$

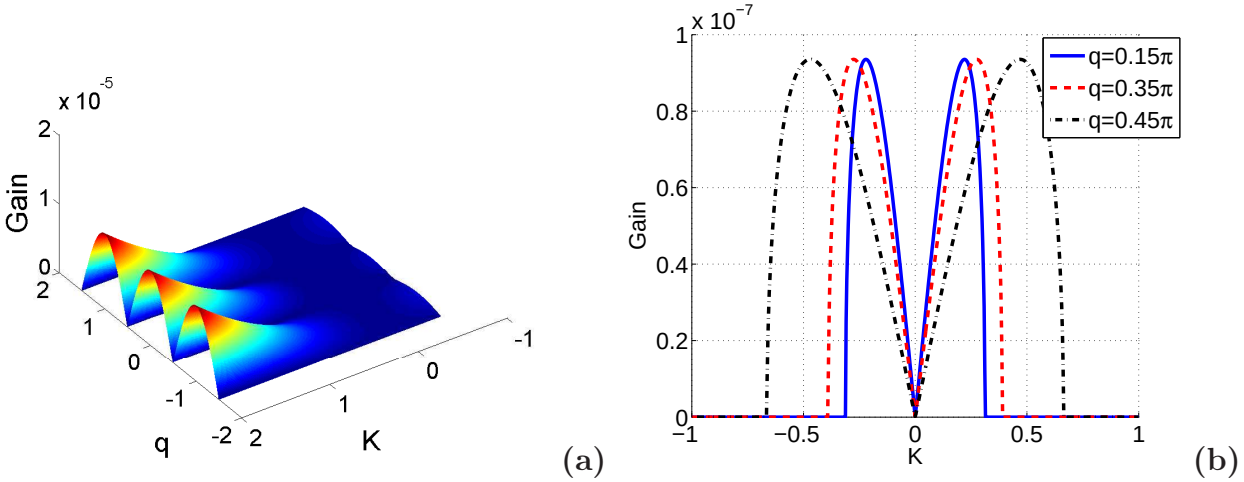

Figure 15: Modulational instability gain as a function of (a) the wave number K and the wave number q; (b) the wave number K for three values of the q $q = 0.15\pi$ (solid blue line), $q = 0.35\pi$ (red dashed line) and $q = 0.45\pi$ (black dash-dotted line). The parameters are m=300; D=0.04; a=4.45; S=0.06; $A_0 = 0.000001$; $\epsilon = 0.01$.

Panel (a) shows the MI gain spectrum for various values of the wave number K. We observe from panel (b) that the induced MI gain is relatively higher for the higher value of wave number q

3.3 Modulational instability through variational approach for the DNA molecule

We examine MI using a time-dependent variational approach (TDVA), and study the result in comparison with the standard linear stability (LS) calculations. It should be mentioned that the use of TDVA for the study of solitons at the classical [91] and even at the quantum [93]

level is not new.

3.3.1 Variational approach to modulational instability

Let us reconsider the nonlinear Schrödinger equation (2.83). Apart from the arbitrary diffusion constant c, this equation is very similar to Eq. (3.6). The investigation of MI through the time-dependent variational approach starts by finding the Lagrangian density that generates equation (3.6), which is

$$\pounds(\psi) = \frac{\mathrm{i}}{2}(\psi^*\frac{\partial\psi}{\partial t} - \psi\frac{\partial\psi^*}{\partial t}) - P|\frac{\partial\psi}{\partial x}|^2 - \frac{1}{2}Q_1|\psi|^4 - \frac{1}{3}Q_2|\psi|^6. \tag{3.18}$$

An exact solution of the cubic-quintic NLS equation (2.83) is the plane wave in Eq. (2.84), to which is associated the dispersion relation (2.85). We may use, as variational ansatz for the wave function of the condensate, a modulation of the solution (2.84) defined by:

$$\begin{aligned}\psi(x,t) = \{&A_0 + a_1(t)\exp[i(Kx + b_1(t))] \\ &+ a_2(t)\exp[i(-Kx + b_2(t))]\}\ \exp[i(kx - \tilde{\omega}t)].\end{aligned} \tag{3.19}$$

Following the standard procedure given in Ref. [84], we should insert the variational ansatz into the density (3.18) and calculate the effective Lagrangian,

$$L = \int_{-\infty}^{+\infty}\mathcal{L}(\psi)\mathrm{d}x. \tag{3.20}$$

But here, we consider an annular (one-dimensional) geometry, which imposes periodic boundary conditions on the wave function $\psi(x,t)$ and integration limits $0 \leq x < 2\pi$ in Eq. (3.20). This leads to the quantization of the wave numbers i.e. $k, K = 0, \pm1, \pm2, \pm3, ...$ However, our results can be generalized to the case of an infinite open system and to higher dimensions. Let's substitute the ansatz (3.19) into Eqs. (3.18) and (3.20) considering the new geometry. We obtain the effective Lagrangian :

$$\begin{aligned}L = -\pi\big\{&2(a_1^2\dot{b}_1 + a_2^2\dot{b}_2) + 2(PK^2 - Q_1A_0^2 - 2Q_2A_0^4)(a_1^2 + a_2^2) + 4PkK(a_1^2 - a_2^2) \\ &-(Q_1 + 6Q_2A_0^2)(a_1^4 + a_2^4 + 4a_1^2a_2^2) \\ &+A_0^4(Q_1 + \frac{4}{3}Q_2A_0^2) - \frac{2}{3}Q_2(a_1^6 + a_2^6 + 9a_1^4a_2^2 + 9a_1^2a_2^4) \\ &-4A_0^2(Q_1 - 2Q_2A_0^2)a_1a_2\cos(b_1 + b_2) - 12Q_2A_0^2(a_1^2 + a_2^2)a_1a_2\cos(b_1 + b_2)\big\}.\end{aligned} \tag{3.21}$$

From this Lagrangian, we may interpret the pair $b_1(t), b_2(t)$ as the generalized coordinates of the system, while the pair $A_1(t), A_2(t)$, with $A_1(t) = 2a_1^2(t)$ and $A_2(t) = 2a_2^2(t)$, is formed of the corresponding momenta. The expression of the Hamiltonian of the system is

$$H_s = -L + \int_{-\infty}^{+\infty}\frac{\mathrm{i}}{2}(\psi^*\frac{\partial\psi}{\partial t} - \psi\frac{\partial\psi^*}{\partial t})\mathrm{d}x, \tag{3.22}$$

that is, in the new geometry,

$$\begin{aligned}H_s = \pi\big\{ & A_0^2[2Pk^2 - Q_1A_0^2 - \frac{2}{3}Q_2A_0^4] + [PK^2 + Pk^2 - 2Q_1A_0^2 - 3Q_2A_0^4](A_1 + A_2) \\ & +2PkK(A_1 - A_2) - \frac{1}{4}[Q_1 + 6Q_2A_0^2](A_1^2 + A_2^2 + 4A_1A_2) \\ & -\frac{1}{12}Q_2(A_1^3 + A_2^3 + 9A_1A_2^2 + 9A_1^2A_2) - 2A_0^2[Q_1 + 2Q_2A_0^2]\sqrt{A_1}\sqrt{A_2}\cos(b_1 + b_2) \\ & -3Q_2A_0^2(A_1 + A_2)\sqrt{A_1}\sqrt{A_2}\cos(b_1 + b_2)\big\}.\end{aligned} \tag{3.23}$$

But, in particular, the pairs $A_1(t), b_1(t)$ and $A_2(t), b_2(t)$ are canonically conjugate with respect to the effective Hamiltonian H (i.e $\frac{\partial A_i}{\partial t} = -\frac{\partial H}{\partial b_i}$ and $\frac{\partial b_i}{\partial t} = \frac{\partial H}{\partial A_i}$) given by :

$$\begin{aligned}H = \big\{ & [PK^2 - Q_1A_0^2 - 2Q_1A_0^4](A_1 + A_2) + 2PkK(A_1 - A_2) \\ & -\frac{1}{4}[Q_1 + 6Q_2A_0^2](A_1^2 + A_2^2 + 4A_1A_2) - \frac{1}{12}Q_2(A_1^3 + A_2^3 + 9A_1A_2^2 + 9A_1^2A_2) \\ & -2A_0^2[Q_1 + 2Q_2A_0^2]\sqrt{A_1}\sqrt{A_2}\cos(b_1 + b_2) - 3Q_2A_0^2(A_1 + A_2)\sqrt{A_1}\sqrt{A_2}\cos(b_1 + b_2)\big\}.\end{aligned} \tag{3.24}$$

This effective Hamiltonian is an exact integral of motion on the subspace spanned by the ansatz (3.19).

To derive the evolution equations for the time-dependent parameters of Eq. (3.19), we use the corresponding Euler-Lagrange equations based on the variational Lagrangian L. In the generalized form, these equations are :

$$\frac{\mathrm{d}}{\mathrm{d}t}\frac{\partial L}{\partial \dot{\xi}_i} - \frac{\partial L}{\partial \xi_i} = 0, \tag{3.25}$$

where, ξ_i is the generalized coordinate and $\dot{\xi}_i$ is the corresponding generalized momentum. Then, the evolution equation corresponding to the coordinate $a_1(t)$ is

$$\begin{aligned}\frac{\mathrm{d}b_1}{\mathrm{d}t} = & C_1 + C_2\frac{a_2}{a_1}\cos(b_1 + b_2) \\ & +\{\frac{1}{3}C_3[1 + 2(\frac{a_2}{a_1})^2] + \frac{1}{2}C_4\frac{a_2}{a_1}[3 + (\frac{a_2}{a_1})^3]\cos(b_1 + b_2)\}\, a_1^2 \\ & +\frac{1}{10}C_5[1 + 6(\frac{a_2}{a_1})^2 + 3(\frac{a_2}{a_1})^4]\, a_1^4.\end{aligned} \tag{3.26}$$

The parameters, $C_i, i = \overline{1,5}$ are given by: $C_1 = Q_1A_0^2 + 2Q_2A_0^4 - PK^2 - 2PkK$, $C_2 = Q_1A_0^2 + 2Q_2A_0^4$, $C_3 = 3Q_1 + 18Q_2A_0^2$, $C_4 = +6Q_2A_0^2$, $C_5 = 10Q_2$ and we let $C_6 = Q_1A_0^2 + 2Q_2A_0^4 - PK^2 + 2PkK$.

For the coordinate $b_1(t)$, we have :

$$\frac{\mathrm{d}a_1}{\mathrm{d}t} = \{C_2a_2 + \frac{1}{2}C_4[1 + (\frac{a_1}{a_2})^2]a_2^3\}\sin(b_1 + b_2). \tag{3.27}$$

The coordinate $a_2(t)$ yields the evolution equation :

$$\begin{aligned}\frac{\mathrm{d}b_2}{\mathrm{d}t} &= C_6 + C_2\frac{a_1}{a_2}\cos(b_1+b_2)\\ &+\{\frac{1}{3}C_3[1+2(\frac{a_1}{a_2})^2]+\frac{1}{2}C_4\frac{a_1}{a_2}[3+(\frac{a_1}{a_2})^3]\cos(b_1+b_2)\}\,a_2^2\\ &+\frac{1}{10}C_5[1+6(\frac{a_1}{a_2})^2+3(\frac{a_1}{a_2})^4]\,a_2^4.\end{aligned} \tag{3.28}$$

The evolution of the variational parameter $a_2(t)$ is provided by the coordinate $b_2(t)$:

$$\frac{\mathrm{d}a_2}{\mathrm{d}t} = \{C_2a_1+\frac{1}{2}C_4[1+(\frac{a_2}{a_1})^2]a_1^3\}\sin(b_1+b_2). \tag{3.29}$$

For simplicity, we may use a variant of the ansatz (3.19) for which

$$a_2 = a_1 \equiv a. \tag{3.30}$$

Then adding together Eqs. (3.26) and (3.28), we obtain with Eq. (3.27) (or Eq. (3.29)), under the condition (3.30), the system of equations:

$$\begin{aligned}\frac{\mathrm{d}a}{\mathrm{d}t} &= (C_2\,a + C_4\,a^3)\sin b\\ \frac{\mathrm{d}b}{\mathrm{d}t} &= (C_1+C_6)+2[C_2\cos b+(C_3+2C_4\cos b)\,a^2+C_5\,a^4],\end{aligned} \tag{3.31}$$

where, $b = b_1(t)+b_2(t)$. Keeping only terms to $\mathbf{0}(a)$, this system yields equations:

$$\frac{\mathrm{d}a}{\mathrm{d}t} = C_2\,a\sin b, \tag{3.32}$$

and:

$$\frac{\mathrm{d}b}{\mathrm{d}t} = (C_1+C_6)+2C_2\cos b. \tag{3.33}$$

To obtain the modulational instability criterion, we rewrite the effective Hamiltonian (3.3.1) considering Eq. (3.30). Then, with $A = 2a^2$, we have

$$\begin{aligned}H(A) = \big\{2[PK^2-Q_1A_0^2-2Q_2A_0^4]A-\frac{3}{2}[Q_1+6Q_2A_0^2]A^2\\ -\frac{5}{3}Q_2A^3-2A_0^2[Q_1+2Q_2A_0^2]A\cos b-6Q_2A_0^2A^2\cos b\big\}.\end{aligned} \tag{3.34}$$

Using $A(t=0)=0$ (without loss of generality) in Eq. (3.34) yields $H_0 = H(A(t=0)) = 0$. Since the Hamiltonian is conserved, $H_0 = H(A)$ and thus, we obtain

$$\begin{aligned}2[-Q_1A_0^2-2Q_2A_0^4+PK^2]A-\frac{3}{2}[Q_1+6Q_2A_0^2]A^2-\frac{5}{3}Q_2A^3\\ -2A_0^2[Q_1+2Q_2A_0^2+3Q_2A]\,A\cos[b(t)]=0.\end{aligned} \tag{3.35}$$

Rewriting the first equation of (3.31) in terms of A and eliminating $b(t)$ between the resultant equation and Eq. (3.35) leads us to the following *energy equation* for A :

$$\frac{1}{2}\dot{A}^2 + V = 0, \tag{3.36}$$

where the effective potential

$$\begin{aligned} V = \big\{ & 2PA^2K^2[PK^2 - 2Q_1A_0^2 - 4Q_2A_0^4] + 3A^3[PK^2(-Q_1 - 6Q_2A_0^2) \\ & +4Q_1A_0^4Q_2 + Q_1^2A_0^2 + 4Q_2^2A_0^6] + A^4[\frac{101}{6}Q_1A_0^2Q_2 + \frac{9}{8}Q_1^2 \\ & +\frac{175}{6}Q_2^2A_0^4 - \frac{10}{3}PK^2Q_2] + \frac{5}{2}A^5Q_2[Q_1 + 6Q_2A_0^2] + \frac{25}{18}A^6Q_2^2\big\}. \end{aligned} \tag{3.37}$$

The evaluation of the curvature of the potential at $A = 0$ may determine whether the dynamics is stable or not. Indeed, the potential will be convex (corresponding to a stable dynamics) for $\frac{\partial^2 V}{\partial A^2}|_{A=0} > 0$, while for $\frac{\partial^2 V}{\partial A^2}|_{A=0} < 0$ it will be concave (unstable dynamics). Thus as we have $\frac{\partial^2 V}{\partial A^2}|_{A=0} = 4PK^2[PK^2 - 2Q_1A_0^2 - 4Q_2A_0^4]$ with $K^2 > 0$, the instability region for Eq. (2.83) appears for perturbation wave numbers verifying the time-dependent condition:

$$PK^2 - 2Q_1A_0^2 - 4Q_2A_0^4 < 0. \tag{3.38}$$

This is nothing but the explicitly time-dependent MI condition (3.16) obtained within the framework of the linear stability analysis. Of course this is true when $P > 0$.

Similarly as in the case of the LS analysis, the MI gain can easily been deduced. Thus the TDVA provides the effective potential which can be used to study the derive the MI criterion and then the MI gain. Moreover the equations of evolution of the perturbation parameters $a(t)$ and $b(t)$ can be obtained.

In solving Eqs. (3.32) and (3.33), to obtain the expressions of the modulational parameters $a(t)$ and $b(t)$, two different cases arise :

When $PK^2 - 2C_2 > 0$ (case where the instability criterion is not satisfied), the solutions are :

$$b(t) = 2\,\arctan\left[\sqrt{1 - \frac{2C_2}{PK^2}}\;\tan\sqrt{K^2(PK^2 - 2C_2)}\,t\right], \tag{3.39}$$

for the phase, and

$$a(t) = a_0 \exp\left\{\left[\frac{-PK^2\sqrt{1 - \frac{2C_2}{PK^2}}}{4C_2}\right]\ln\left[\frac{\left(1 + (1 - \frac{2C_2}{PK^2})\;\tan^2\left(\sqrt{K^2(PK^2 - 2C_2)}\,t\right)\right)}{\left(1 + \tan^2(\sqrt{K^2(PK^2 - 2C_2)}\,t)\right)}\right]\right\} \tag{3.40}$$

for the amplitude. When $PK^2 - 2C_2 < 0$ (case where the instability criterion is satisfied), the solutions are :

$$b(t) = 2\,\arctan\left[\sqrt{-1 + \frac{2C_2}{PK^2}}\;\tanh\sqrt{K^2(-PK^2 + 2C_2)}\,t\right], \tag{3.41}$$

for the phase, and

$$a(t) = a_0 \exp\left\{\left(\frac{PK^2\sqrt{-1+\frac{2C_2}{PK^2}}}{4C_2}\right)t\right\} \times \left[\frac{1+(-1+\frac{2C_2}{PK^2})\tanh^2\left(\sqrt{PK^2(-PK^2+2C_2)}t\right)}{1+\tanh(\sqrt{PK^2(-PK^2+2C_2)}t)}\right]^{\frac{1}{2}} \tag{3.42}$$

for the amplitude. These solutions clearly indicate the occurrence of the MI when crossing the threshold wave numbers defined by $PK^2 = 2C_2$ is crossed (passing from higher to lower perturbation wave numbers).

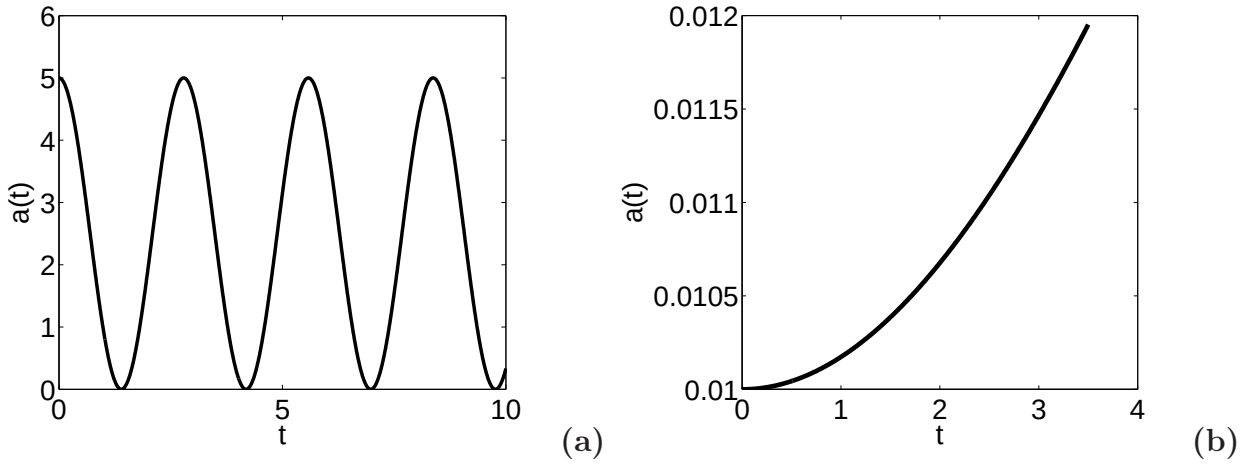

Figure 16: (a)The time evolution of the modulational perturbation $a(t)$ in the stable oscillatory case, the parameters are $A_0 = 2.5$; $\epsilon = 0.01$; K=2.5; $q = 0.15\pi$. (b)The time evolution of the modulational perturbation $a(t)$ in the unstable case, the parameters are $A_0 = 0.01$; $\epsilon = 0.01$; K=1; $q = 0.15\pi$.

Figs.16a and 16b show the time evolution of $a(t)$ in accordance with solutions Eqs. (3.40) and (3.42), respectively.

we see on fig.16a that the modulational perturbation a(t) oscillates in time, showing the stability of the DNA molecule.

fig.16b show that The modulational perturbation $a(t)$ exponentially grows in the time, from its initial value 0.01, characterizing the instability of the DNA molecule.

3.3.2 Numerical results

According to the above analytical results based on linear stability analysis, the stability condition of an extended nonlinear plane wave has been determined for the cubic-quintic NLS equation. Linear stability analysis can determine the instability domain in the parameter space

and predict qualitatively how the amplitude of a modulation sideband evolves at the onset of the instability. However, such an analysis is based on the linearization around the unperturbed carrier wave, which is valid only when the amplitude of perturbation is small in comparison with that of the carrier wave. Clearly, the linear approximation must fail at large time scales as the amplitude of unstable sideband growths exponentially. Furthermore, the linear stability analysis neglects additional combination waves generated through wave-mixing process which, albeit small at the initial stage can become significant at large time scales if the system is in the unstable regime. Linear stability analysis therefore cannot tell us the long-time evolution of a modulated extended nonlinear wave. In order to check the validity of our analytical analysis and to investigate the time evolution of modulated nonlinear plane waves, we carried out numerical experiments on Eq. (3.6). The fourth-order Runge-Kutta scheme with normalized integration time step $h_0 = 0.005$ and space step $h_1 = 5$ has been used to integrate the system. The simulations have been performed with periodic boundary conditions. As localized initial condition, in accordance with the analytical part, we take the modulated wave solution Eq. (3.19).

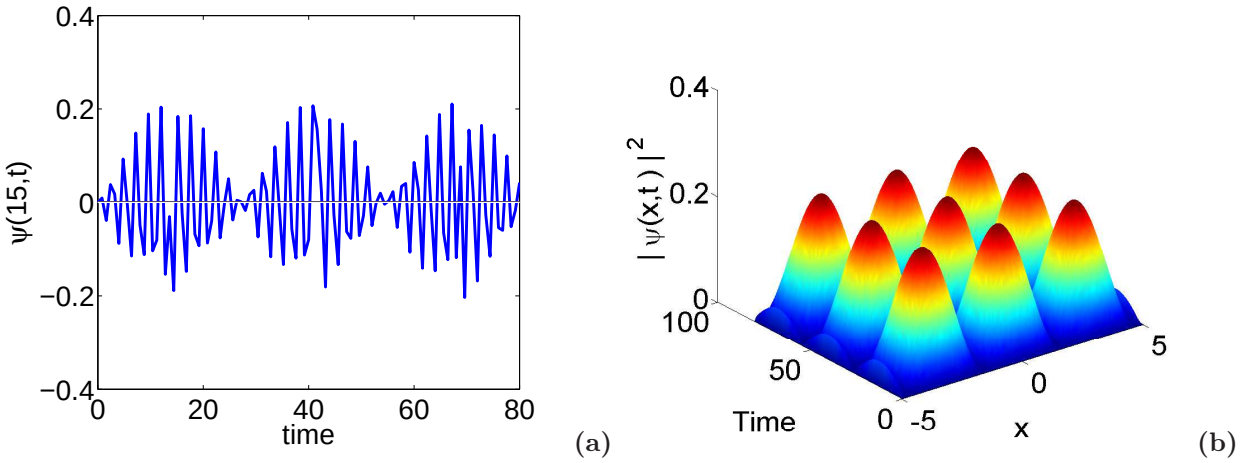

Figure 17: Wave train: (a) the amplitude of waves appears as a train of soliton-like objects at position x =15.(b) modulational instability has broken the initial wave into pulse, the parameters are $A_0 = 0.01$; $\epsilon = 0.01$; K=1; $q = 0.15\pi$.

In Fig. 17, we present the evolution of wave at different position of the system. Modulational instability is the prerequisite for the formation of spatial or temporal patterns. In the DNA molecule where the field evolution is described by the NLS equation, MI of a continuous wave can be employed for the generation of pulse trains with high repetition rate [94, 95, 96]. We present such a case in Fig. 17a. The initial modulated plane wave has been broken in term of a train of small-amplitude short waves. In these figures, each element of the train has the shape of a soliton object. These excitations have envelope functions with shape familiar from the theory of soliton-like objects, but in contrast to solitons they emerge as solutions of the time-dependent classical equations of motion. This point is well illustrated in 17b, where we

see that the initial waves evolve with a pulse shape for cubic quintic NLS equation.

We have examined the MI of nonlinear wave in cubic-quintic NLS equation. For this purpose, we have derived the nonlinear dispersion relation from the cubic-quintic NLS equation by using two different approaches, namely, the standard linear stability analysis and the variational approach. It is found that the quintic term can be used to reduce the magnitude of waves and hence to stabilize the propagation of waves in the system. The theoretical findings have been numerically tested through direct simulations of the behavior of the system predicted by analytical results. Excellent agreement has been obtained between analytical predictions and numerical experiments.

3.4 Modulational instability of two-component Peyrard-Bishop-Dauxois model

The dynamics of two counter-propagating waves in the Peyrad-Bishop-Dauxois model is investigated. We have shown using the reductive perturbation method that the dynamics of the system can be described by a set of coupled nonlinear Schrödinger equations. This model can be used to describe a two degrees of freedom of each DNA monomer, namely: (i) transverse backbone displacements and (ii) torsional oscillations of nucleosides considered as rigid bodies. The relevant MI scenarios are explored and we note that the system is stable under the modulation for certains parameters value of the Peyrad-Bishop-Dauxois model. We also point out the impact of the group velocity on the stability of the system.

3.4.1 The model

It is well known that the DNA molecule is a double helix, which consists of two strands. Only the nearest-neighbour harmonic interaction along the chain is assumed, as well as the same coupling constant k along each strand. Also, a common mass m=5.1 10-25 kg is used for all the nucleotides [97, 98]. This can be justified by the fact that the nucleotide masses differ from the average value for $-6.4\%(Cytosine)$, $-1.6\%(Thymine)$, $1.4\%(Adenine)$ and $6.6\%(Guanine)$ [99, 100]. All this means that the DNA chain is treated as a perfectly periodic structure with the period l. As was mentioned above, the PBD model takes the helicoidal structure into consideration. This means that the nucleotide at a site n of one strand interacts with both (n+h)th and (n-h)th nucleotides of the other strand. As if the helix has a helical pitch of about 10 bps per turn, as was stated above, we assume h=5. The strands are coupled to each other through hydrogen bonds, connecting A-T or C-G base pairs, and the corresponding potential

energy is modeled by a Morse potential. The Hamiltonian for the DNA chain has the form [97].

$$\begin{aligned} H = \sum_{n=1}^{N} [\frac{1}{2} m(\dot{u}_n^2 + \dot{v}_n^2) + \frac{1}{2} k[(u_n - u_{n-1})^2 + (v_n - v_{n-1})^2] \\ + \frac{1}{2} K[(u_n - v_{n+h})^2 + (u_n - v_{n-h})^2] + V(u_n - v_n)], \end{aligned} \tag{3.43}$$

where, u_n and v_n are transversal displacements of nucleotides of different strands at the site n from their equilibrium positions. Parameters k and K are harmonic constants of the longitudinal and the helicoidal spring, respectively. Hence, the third term in Eq. (3.43) represents a twisting of the DNA molecule and does not exist in the PB model. The last term in Eq. (3.43)is the Morse potential, representing transversal hydrogen bonds between nucleotides of different strands (fig. 1). Parameters D and a are the depth and the inverse width of the Morse potential. Using coordinates U_n and V_n for in-phase and out-ofphase motions, defined as:

$$U_n = (u_n + v_n)/\sqrt{2}, \qquad V_n = (u_n - v_n)/\sqrt{2}, \tag{3.44}$$

we obtain two perfectly decoupled dynamical equations of motion, as follows

$$\ddot{U}_n - K_1(U_{n+1} + U_{n-1} - 2U_n) - K_2(U_{n+h} + U_{n-h} - 2U_n) = 0, \tag{3.45}$$

$$\begin{aligned} \ddot{V}_n - K_1(V_{n+1} + V_{n-1} - 2V_n) + K_2(V_{n+h} + V_{n-h} + 2V_n) \\ + \omega_g^2(V_n + \alpha V_n^2 + \beta V_n^3) = 0, \end{aligned} \tag{3.46}$$

where, $\omega_g^2 = \frac{4a^2 D}{m}$,$K_1 = \frac{k}{m}$, $K_2 = \frac{K}{m}$, $\alpha = -\frac{3a}{\sqrt{2}}$ et $\beta = \frac{7a^2}{3}$. Equation (3.45) desrcribes usual linear waves (phonon) while Eq. (3.46) describes nonlinear breathers. So, we restrict our attention on the second nonlinear equation. In other words, we assume that the oscillations of bases are larges enough to be harmonic but still small enough so that the plateau of the Morse potential is not yet reached.

A rather tedious derivation brings about two dispersion relations, pertaining to the decoupled degrees of freedom [97, 98].. The corresponding frequencies, being acoustical for the in-phase and optical for the out of-phase motions, are

$$\begin{aligned} \omega_x^2 = [4K_1 \sin^2(ql/2) + 4K_2 \sin^2(qlh/2)], \\ \omega_y^2 = [4K_1 \sin^2(ql/2) + 4K_2 \cos^2(qlh/2) + \omega_g^2]. \end{aligned} \tag{3.47}$$

The method used in ref [101, 102] to obtain the short wavelength envelope solitons is the semi-discrete approximation. That is, the continuum approximation is only introduced for the envelope while a completely discrete description is used for the carrier wave, the wave-vector of which can range over the entire Brillouin zone. The idea is to investigate how the plane wave is

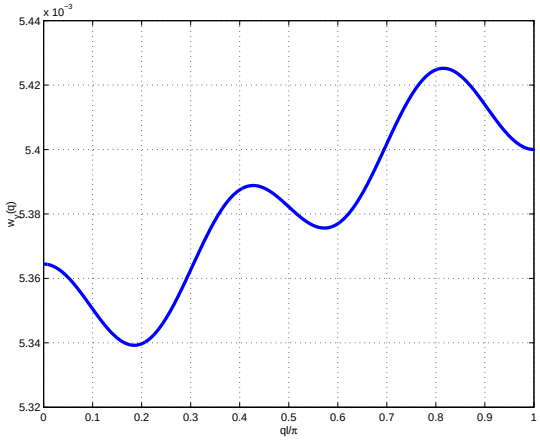

Figure 18: Linear dispersion curves as a function of the wave number q for $0 \leq ql \leq \pi$ with k=1.5/m; K=0.7/m

modulated by nonlinear effects. Now, we assume the following reductive perturbation method [72, 73], we introduce the independent multiple-scale variables $X_i = \varepsilon^i n$ and $T_i = \varepsilon^i t$, where $\varepsilon \ll 1$. Moreover, the solution of Eq. (3.46) is assumed to have a following form:

$$\begin{aligned} V_n(t) = &\varepsilon[V_{1+}(X_1, X_2, ..., T_1, T_2, ...)] \exp(i\theta_+) + \varepsilon^2[V_{2+}(X_1, X_2, ..., T_1, T_2, ...)] \exp(2i\theta_+) \\ &+ \varepsilon[V_{1-}(X_1, X_2, ..., T_1, T_2, ...)] \exp(i\theta_-) + \varepsilon^2[V_{2-}(X_1, X_2, ..., T_1, T_2, ...)] \exp(2i\theta_-) + c.c., \end{aligned} \tag{3.48}$$

where the carrier phases are $\theta_+ = kn - \omega t$ and $\theta_- = -kn - \omega t$, and c.c. represents the complex conjugate of the preceding terms. The second-harmonic terms $V_2\pm$ are added to the fundamental ones $V_1\pm$ in order to take the asymmetry of the persistence-length into account.

Inserting Eq. (3.48) in Eq. (3.46) yields, after some standard calculations, to a set of two CNLS equations [75, 74] :

$$\begin{aligned} i\frac{\partial V_{1+}}{\partial T_2} + iV_g\frac{\partial V_{1+}}{\partial X_2} + P\frac{\partial^2 V_{1+}}{\partial X_1^2} + [Q_1|V_{1+}|^2 + Q_2|V_{1-}|^2]V_{1+} = 0, \\ i\frac{\partial V_{1-}}{\partial T_2} - iV_g\frac{\partial V_{1-}}{\partial X_2} + P\frac{\partial^2 V_{1-}}{\partial X_1^2} + [Q_1|V_{1-}|^2 + Q_2|V_{1+}|^2]V_{1-} = 0, \end{aligned} \tag{3.49}$$

where, $V_g = \frac{d\omega}{dq} = \frac{K_1 \sin(q) - hK_2 \sin(qh)}{\omega}$ is the group velocity and the group velocity dispersion $P = \frac{d^2\omega}{dq^2} = \frac{K_1 \cos(q) - K_2 h^2 \cos(qh) - V_g^2}{2\omega}$ is calculated from Eq. (3.47). The nonlinear coefficients Q_1 and Q_2 are, respectively,

$$Q_1 = -\frac{\omega_g^2 \beta}{\omega}, \quad Q_2 = -\frac{3\omega_g^2 \beta}{2\omega}. \tag{3.50}$$

Physically, the set of two variables ($t = T_2$ and $x = X_1 = X_2$) is sufficientto describe the evolution of the envelopes, which correspond to letting ε tend to unity. Let us assume $V_{1+} = \psi_1$

and $V_{1-} = \psi_2$; Eq. (3.49) can be rewrite has:

$$\begin{aligned} & i\frac{\partial \psi_j}{\partial t} + iV_{g,j}\frac{\partial \psi_j}{\partial x} + P\frac{\partial^2 \psi_j}{\partial x^2} + [Q_j|\psi_j|^2 + Q_l|\psi_l|^2]\psi_j = 0 \\ & l \neq j = 1,2 \quad V_{g,1} = -V_{g,2} \end{aligned} \tag{3.51}$$

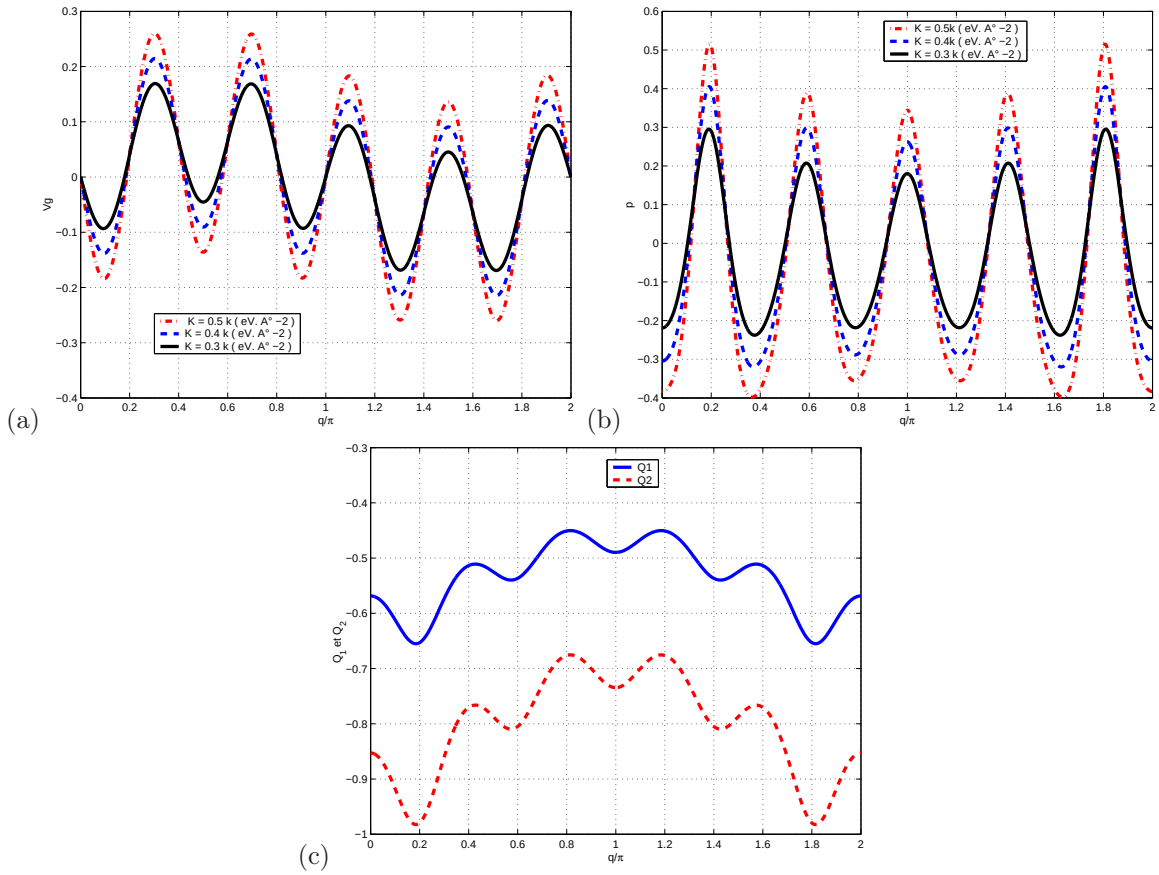

Figure 19: (a)the group velocity;(b)the group velocity dispersion for differents values of the springiness constant (K); (c)The nonlinear coefficients Q_1 and Q_2

Equation (3.51) is a set of coupled nonlinear Schrödinger (CNLS) equations. The CNLS equations are very important because they can be used to model a great variety of physical systems. Solitary waves in these equations are often called vector solitons in the literature since they are generically described by two-component wave functions [75, 74]. One of the simplest vector solitons is known as shape-preserving, self-localized solution of coupled nonlinear evolution equations [75]. The CNLSE may also model beam propagation inside crystals as well as water wave interactions, and in fiber communication system, such equations have been shown to govern pulse propagation along orthogonal polarization axes in nonlinear optical fibers and in wavelength-division- multiplexed systems [76, 77]. So, Eq. (3.51) can be used to describe solitons of two-component in the case of the PBD model.

3.4.2 Linear stability analysis of the two-component system.

Let us first briefly recall some results of the linear stability analysis in the case of a single-component. In this case the system is derived by setting $V_{1-} = \psi_2 = 0$ in Eqs. (3.49): the (single) NLS equation is thus obtained. According to the standard formalism [103, 104], $V_{1+} = \psi_1$ (dropping the index in this paragraph we choose to write ψ). The system is modulationally unstable (stable) if PQ > 0 (PQ < 0). This result can easily obtained by using a plane wave solution of the form $\psi(x,t) = \exp(iQ|\psi_0|^2 t)$, where ψ_0 is a constant (real) amplitude. The standard stability analysis then shows that the dispersion relation is given by: $(\Omega - V_g K)^2 = PK^2(PK^2 - 2Q|\psi_0|^2)$. The system exhibits a growing unstable mode if $K \leq K_{cr,0} = \sqrt{2Q/P}|\psi_0|$ (hence only if PQ > 0). The growth rate $\sigma = Im\Omega$ attains a maximum value $\sigma_{max} = Q|\psi_0|^2$ at $K_{cr,0}/\sqrt{2}$ For PQ < 0, on the other hand, the wave is stable to external perturbations. We note that stability is obtained for PQ <0, however Q is already negative; therefore we can say that a sufficient condition for the stability, is simply given by P>0.

In order to investigate the MI of a two-component waves, we shall first seek an equilibrium state in the form $\psi_j = \psi_{j0}\exp(i\varphi_j(t))$ (for j = 1, 2), where ψ_{j0} is a constant real amplitude and $\varphi_j(t)$ is the phase. Using this relation into Eqs. (3.51) leads to a monochromatic (fixed-frequency) solution of the form $\varphi_j(t) = \Omega_{j0}t$, where $\Omega_{j0} = Q_j\psi_{j0}^2 + Q_l\psi_{l0}^2$ $(for j \neq l = 1, 2,)$. Considering a small perturbation around equilibrium, we take $\psi_j = (\psi_{j0} + \delta\psi_j)\exp(i\varphi_j(t))$, where $\delta\psi_j = \varepsilon\psi_{j1}(r,t)$ is a small ($\varepsilon \ll 1$, $\psi_{j1} = a_j + ib_j$) complex amplitude perturbation of the wave amplitudes. We substitute this expression into Eqs. (3.51) and separate the real and imaginary parts. The first order terms $(in\ \ \varepsilon)$ yields to [77]

$$\begin{aligned} -\frac{\partial b_j}{\partial t} - V_{g,j}\frac{\partial b_j}{\partial x} + P\frac{\partial^2 a_j}{\partial x^2} + 2Q_j\psi_{j0}^2 a_j + 2Q_l\psi_{j0}\psi_{l0}a_l = 0, \\ \frac{\partial a_j}{\partial t} + V_{g,j}\frac{\partial a_j}{\partial x} + P\frac{\partial^2 b_j}{\partial x^2} = 0. \end{aligned} \tag{3.52}$$

Equation (3.52) can be simplified and we obtain

$$[(\frac{\partial}{\partial t} - V_{g,j}\frac{\partial}{\partial x})^2 + P(P\frac{\partial^2}{\partial x^2} + 2Q_1\psi_{10}^2)\frac{\partial^2}{\partial x^2}]a_1 + 2Q_2\psi_{10}\psi_{20}\frac{\partial^2 a_2}{\partial x^2} = 0. \tag{3.53}$$

Let us use $a_j = a_{j0}\exp[i(Kx - \Omega t)]$ + c.c where K and Ω are the wavevector and the frequency of the perturbation, respectively, viz. $\frac{\partial}{\partial t} \to -i\Omega$ and $\frac{\partial}{\partial x} \to iK$. We get the following equation:

$$\begin{bmatrix} (\Omega - KV_g)^2 - \Omega_1^2 & 2K^2PQ_2\psi_{10}\psi_{20} \\ 2K^2PQ_2\psi_{10}\psi_{20} & (\Omega + KV_g)^2 - \Omega_2^2 \end{bmatrix} \begin{bmatrix} a_{10} \\ a_{20} \end{bmatrix} = 0, \tag{3.54}$$

where $\Omega_1^2 = PK^2(PK^2 - 2Q_1\psi_{10}^2)$ and $\Omega_2^2 = PK^2(PK^2 - 2Q_1\psi_{20}^2)$. Non trivial solutions is obtained if the determinant of matrix is different of zero. So, this implies that:

$$[(\Omega - KV_g)^2 - \Omega_1^2][(\Omega + KV_g)^2 - \Omega_2^2] - \Omega_c^4 = 0, \tag{3.55}$$

where $\Omega_c^4 = (2K^2PQ_2\psi_{10}\psi_{20})^2$. This dispersion relation is a 4th order polynomial in Ω.

A. Weak group velocity

For weak group velocity V_g, one has: $\Omega + KV_g \to \Omega$ and $\Omega - KV_g \to \Omega$. Equation (3.55) is reduced to

$$\Omega^4 - T\Omega^2 + D = 0, \tag{3.56}$$

where $T = \Omega_1^2 + \Omega_2^2$ and $D = \Omega_1^2\Omega_2^2 - \Omega_c^4$ are, respectively, the trace and the determinant of the matrix. Eq. (3.56) admits solutions of the form

$$\Omega^2 = \frac{1}{2}[T \pm (T^2 - 4D)^{1/2}], \quad \Omega_\pm^2 = \frac{1}{2}(\Omega_1^2 + \Omega_2^2) \pm \frac{1}{2}[(\Omega_1^2 - \Omega_2^2)^2 + 4\Omega_c^4]^{1/2}. \tag{3.57}$$

Stability is ensured (for any wavenumber K) if (and only if) both of the (two) solutions of (3.56), say $\Omega_\pm^2$, are positive (real) numbers. So, the right-hand side has to be real. The discriminant $\Delta = T^2 - 4D = (\Omega_1^2 - \Omega_2^2)^2 + 4\Omega_c^4$ has to be positive. Furthermore, recalling that the roots of the polynomial p(x)=$x^2 - Tx + D$, say $r = r_{1,2}$ satisfy $T = r_1 + r_2$ and $D = r_1r_2$, the stability requirement is tantamount to the following three conditions being satisfied simultaneously: T>0, D>0 and $\Delta = T^2 - 4D > 0$

The first stability condition, namely the positivity of the trace T:

$$T = K^2[2P^2K^2 - 2PQ_1(\psi_{10}^2 + \psi_{10}^2)] > 0, \tag{3.58}$$

depends on (the sign of) the quantity $q_1 = 2PQ_1(\psi_{10}^2 + \psi_{10}^2)$, which has to be negative for stability. The only case ensuring absolute stability (for any ψ_{j0} and K) is

$$PQ_1 < 0 \tag{3.59}$$

Otherwise, T becomes negative (and thus either $\Omega_-^2 < 0 < \Omega_+^2$ or $\Omega_-^2 < \Omega_+^2 < 0$) for K below a critical value $K_{cr,1} = [\frac{Q_1(\psi_{10}^2+\psi_{10}^2)}{P}]^{1/2} > 0$ (cf. the single wave criterion above); this is always possible for a sufficiently large perturbation amplitude $|\psi_{20}|$ if $PQ_1 > 0$. Therefore, only a pair of two individually stable waves can be stable, or the presence of a single unstable wave may de-stabilize its counterpart.

The second stability condition, namely positivity of the determinant D, amounts to

$$D(K^2) = P^2K^4[(P^2K^2 - 2PQ_1\psi_{10}^2)(P^2K^2 - 2PQ_1\psi_{20}^2) - 4Q_2^2\psi_{10}^2\psi_{20}^2] > 0. \tag{3.60}$$

Let's put $q_2 = 2P^3Q1(\psi_{10}^2 + \psi_{10}^2)$ and $q_3 = 4P^2(Q_1^2 - Q_2^2)$. D can be written as follow $D(K^2) = K^4(P^2K^4 - q_2K^2 + q_3)$; the discriminant of this equation is given by: $\Delta' = q_2^2 - 4P^4q_3 = 4P^4[PQ_1(\psi_{10}^2 - \psi_{10}^2)^2 + 4P^2Q_2^2\psi_{10}^2\psi_{20}^2]$. We note therefore that this discriminant is strictly positive, then $D(K^2)$ admits two distinct reals solutions $K_{D,1/D,2}^2 = \frac{1}{P^4}[q_2^2 \mp (q_2^2 - 4P^4q_3)^{1/2}]$; $q_3 < 0$ ((regardless of q_2) , then $K_{D,1}^2 < 0 < K_{D,2}^2$, and the wave pair is unstable to a perturbation with $K^2 < K_{D,2}^2$. The last stability condition regards the positivity of the discriminant quantity

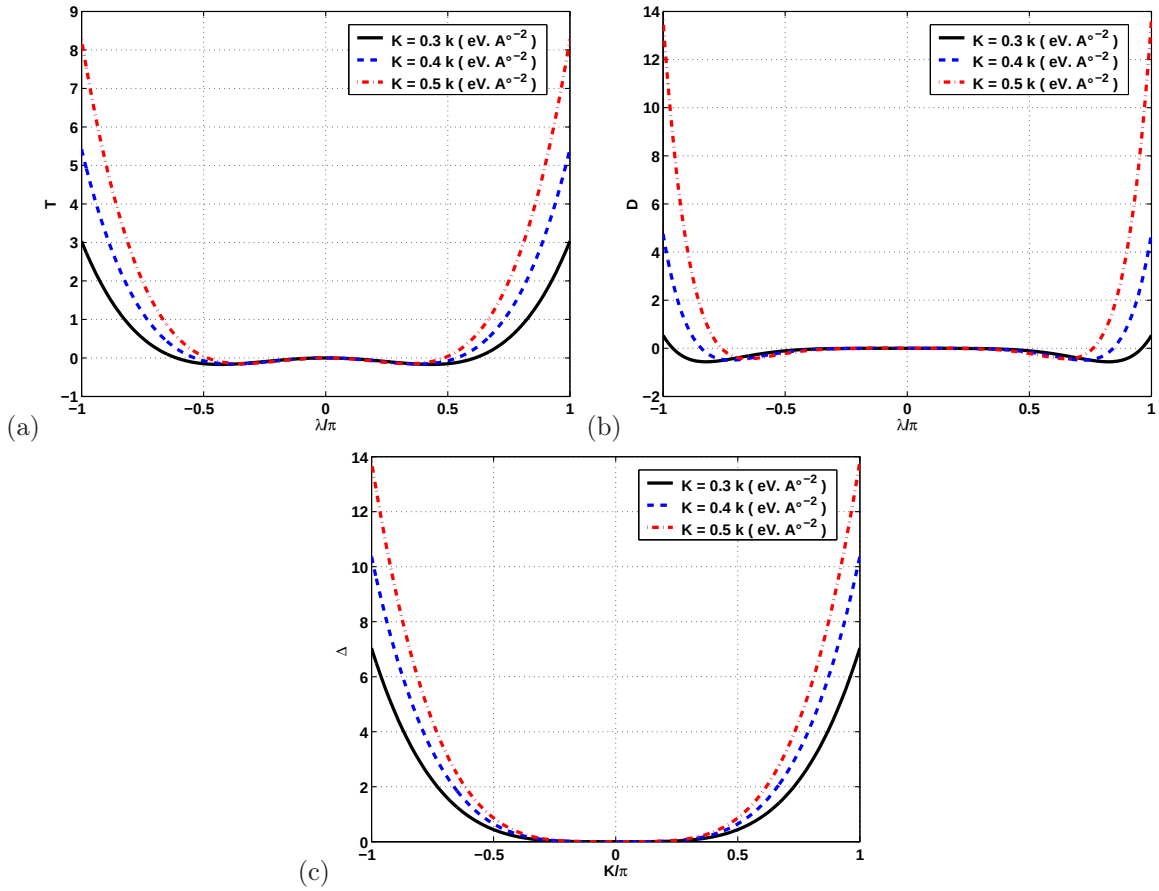

Figure 20: representation of the parameters T (a), D (b), Δ (c) according to the wavevector and for different values of the harmonic constant K .

$\Delta = T^2 - 4D > 0$

$$\Delta = 4K^4P^2[Q_1^2(\psi_{10}^2 - \psi_{10}^2)^2 + 4Q_2^2\psi_{10}^2\psi_{20}^2] > 0. \tag{3.61}$$

This last necessary condition for stability is always fulfilled. Instability is manifested as a purely growing mode, when one or more of the above conditions are violated. In specific, if T < 0 and/or D < 0, then one (or both) of the solutions of the dispersion relation (3.56) (for Ω^2), becomes negative, say $\Omega_-^2 < 0$ [given by (3.57)]; the instability growth rate in this case is given by $\sigma \equiv \sqrt{-\Omega_-^2}$, and is manifested in the wavenumber ranges $[0, K_{cr,1}]$ and either $[0, K_{D,2}]$ or $[K_{D,1}, K_{D,2}]$ (depending on parameter values; see the definitions above)[77]. fig.21.

B. The role of the group velocity misfit.

It may be interesting to discuss the role of the group velocity opposed, in a coupled wave system. Keeping the discussion qualitative, we shall avoid to burden the presentation with tedious numerical calculations. One may rather point out the role of the group velocity misfit via simple geometric arguments. Inspired by an idea proposed in Ref. [105], we may express

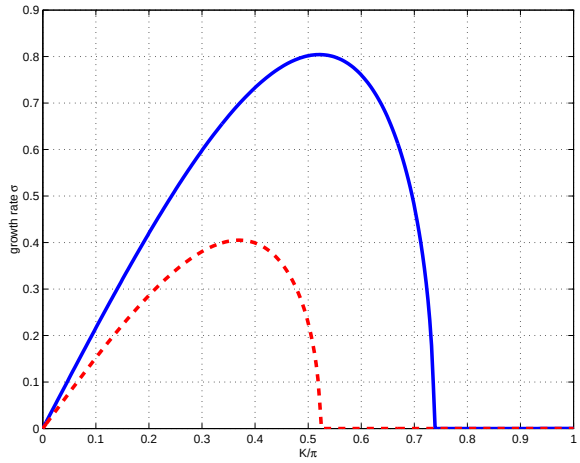

Figure 21: The square of the instability growth rate $\sigma = \sqrt{-\Omega_-^2}$ is depicted versus the perturbation wavenumber K (arbitrary parameter values). Notice the difference from the single wave case (lower curve).

the general dispersion relation (3.55) in the form

$$f_1(x) = f_2(x) \tag{3.62}$$

where we have defined the functions $f_1(x) = (x - x_1)^2 + A$ and $f_2(x) = \frac{C}{(x-x_2)^2+B}$, and the real quantities $x_j = KV_{g,j}$, $A = -\Omega_1^2$, $B = -\Omega_2^2$ and $C = \Omega_c^4$; x denote Ω. The stability profile is determined by the number of real solutions of Eq. (3.175), an integer, say r, between 0 and 4. For absolute stability (for any K, $|\psi_{j0}|$), we need to have 4 real solutions; in any other case, i.e. if $r < 4$, the (imaginary part of) the $4 - r$ complex solutions determine(s) the growth rate of the instability. Note that $x_1 \neq x_2$ expresses the group velocity mismatch $V_{g,1} \neq V_{g,2}$. Negative A (B) means that wave 1 (2) alone is stable, and vice versa.
we see that $C > 0$. We shall study the curves representing the functions $f_1(x)$ and $f_2(x)$ on the xy plane. The former one is a parabola, with a minimum at (x_1, A). The latter one is characterized by a local maximum ($C > 0$) at $(x_1, C/B)$, in addition to a horizontal asymptote (the x-axis), since $f_2(x) \to 0$ for $x \to \pm\infty$. Furthermore, for $B < 0$ (only), $f_2(x)$ has two vertical asymptotes (poles) at $x = x_2 \pm \sqrt{|B|}$ (see Fig22(a,d)). Now, for a stable - stable wave pair (i.e. for $A, B < 0$), we have seen that the dispersion relation (3.46) predicted stability. This result regarded the equal (or vanishing) group velocity case,$V_{g,1} = V_{g,2} = 0$, and may be visualized by plotting $f_1(x)$ and $f_2(x)$ for $x_1 = x_2 = 0$ and A,B < 0; thus, 4 points of intersection exist, (cf. Fig.22a); this fact ensures stability. Now, considering $V_{g,1} = -V_{g,2}$ results in a horizontal shift between the two curves (cf. Fig.22d), which may exactly result in reducing the number of intersection points from 4 to 2 (enabling instability). Therefore, a pair of stable waves may be destabilized due to a finite difference in group velocity.

Still for a stable-stable wave pair ($A, B < 0$), let us assume that $D = AB - C < 0$, implying (for $B < 0$) that $A > C/B$. Thus, the minimum of $f_1(x)$ here lies above the local maximum of

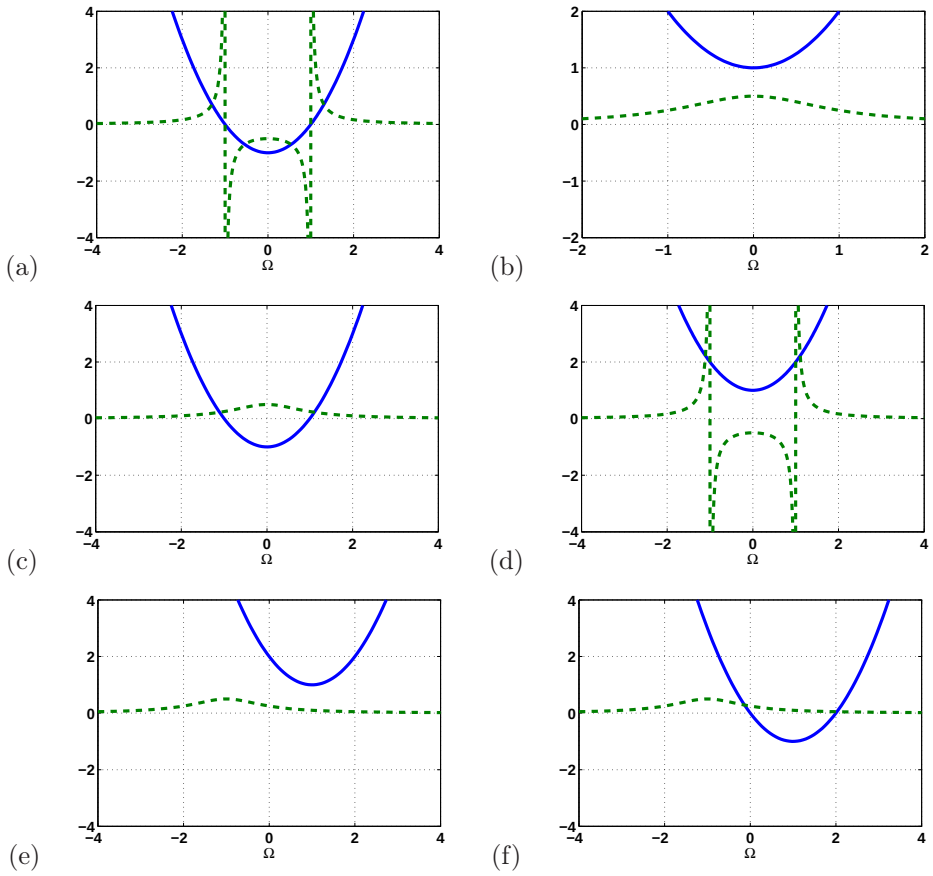

Figure 22: (a) The functions $f_1(x)$ (parabola) and $f_2(x)$ (rational function, two vertical asymptotes) defined in the text are depicted, vs. $x, for A = B = -1, C = 0.5$ (so that $D = AB - C = +0.5 > 0$), $x_1 = x_2 = 0$ (equal group velocities). Note that a group velocity mismatch (a horizontal shift) may destabilize a pair of (stable, separately) waves (i.e. reduce the intersection points from 4 to 2); (b) The functions $f_1(x)$ and $f_2(x)$ are depicted, for $A = B = +1, C = 0.5$ (so that $D = AB - C > 0$), and $x_1 = x_2 = 0$. At most 2 intersection points may occur by translation. A pair of (unstable, separately) waves is always unstable; (c) $D < O, A = -1, B = +1, C = 0.5$, and $x_1 = x_2 = 0$; (d) $D < O, A = +1, B = -1, C = 0.5$, and $x_1 = x_2 = 0$; (e) $D > O, A = +1, B = +1, C = 0.5$, and $x_1 = -x_2 = 1$; (f) $D < O, A = +1, B = -1, C = 0.5$, and $x_1 = -x_2 = 1$;

$f_2(x)$, and only 2 points of intersection now exist, (shift the parabola upwards in Fig22c to see this); this fact imposes instability (for $D < 0$), as predicted above. Considering an unstable - unstable wave pair ($i.e. A > 0$ and $B > 0$) with $D = AB - C > 0$ ($A > C/B$). Plotting $f_1(x)$ and $f_2(x)$ for $x_1 = x_2$ and $A, B > 0$ (see Fig22b), we see that the minimum of $f_1(x)$ lies above the local maximum of $f_2(x)$. No points of intersection exist, a fact which prescribes instability. Considering $V_{g,1} = -V_{g,2}$ simply results in a horizontal shift between the two curves, which does not affect this result at all. On the other hand (still for $A > 0$ and $B > 0$), now assuming that $D = AB - C < 0$, $i.e. A < C/B$, results in a vertical shift downwards of the parabola in Fig.22f; at least 2 complex solutions obviously exist, hence instability. Therefore, a pair of unstable waves is always unstable ($forall V_{g,1}, V_{g,2}$). Still for $C > 0$, one may consider a stable

- unstable wave pair (say, for $A < 0$ and $B > 0$, with no loss of generality): the plot of f_1 and f_2 (here omitted) would look like Fig.22e upon a strong vertical translation of the parabola downwards (so that the minimum lies in the lower half-plane, since $A < 0$). Instability ($r = 2$) dominates this case also.

We have investigated the occurrence of modulational instability in a pair of coupled waves, co-propagating in the PBD model of DNA. This two-component model of DNA can be used to investigate the idea that a breather mechanism could ensure signal propagation in a chain of biological macromolecule supported by the mechanism of two-component breathers within the the nonlinear PBD model of DNA. The injection of an unsettled solution permitted us to study conditions of stability of the macromolecule according to parameters of the problem. The dynamical profile is determined by the wave dispersion laws (i.e., the group velocities and the group velocity dispersion terms) and the nonlinearity and coupling coefficients, on which no assumption is made. We have also studied the influence of the group velocities on the dynamics of the system.

3.5 The twisted DNA with solvent interaction

We investigate the generation of soliton-like pulses along a DNA chain which takes into account both torsional and solvent interaction effects. Interactions between neighboring base pairs are described by a twist angle. Twisting is essential in the model to capture the importance of nonlinear effects on the thermodynamical properties. The nonlinear dynamics of the DNA is then modeled in the Hamiltonian approach by the generalized Dauxois-Peyrard-Bishop model. We introduce the generalized discrete nonlinear Schrödinger equation describing the dynamics of modulated wave through the twisted DNA with solvent interaction. The MI is studied and we present an analytical expression for the MI gain to show the effects of twist angle on MI gain spectra as well as on stability diagram. With the increase of the twist angle the MI gain decreases then increases. Some interesting MI phenomena appear with an additional new MI region as the twist angle increases. The instability/stability diagrams are also affected. Numerical simulations are carried out to show the validity of the analytical approach. It results that the initial wave breaks into a train of ultrashort pulses with repetition rates, which are trapped in some sites. The impact of the twist angle is investigated and we obtain that the twist angle affects the dynamics of stable patterns generated through the molecule. Thereafter, we study energy localization in the framework of twisted DNA with solvent interaction. While the twist angle leads to a stronger localization of energy, the solvent interaction delocalizes energy along the molecule.

3.5.1 The generalized discrete nonlinear Schrödinger equation to describe the twisted DNA with solvent interaction

The DPB Hamiltonian for a system of N base pairs assumes the pair mates separation y_n (for the nth base pair) with respect to the ground state position as the relevant degree of freedom. The longitudinal base displacements along the molecule backbone are neglected as they are much smaller than the transverse stretching y_n; hence, the model Hamiltonian is essentially one-dimensional. The general form of the DPB Hamiltonian which incorporates, nonlinearities both in the inter-base pair interactions and in the coupling between neighboring base along the two strands, helicity and solvent interaction is considered. The Hamiltonian is composed of the following elements

$$U = w(y_n, y_{n-1}) + V(y_n), \tag{3.63}$$

where, y_n is the stretching of the $n-th$ base-pair, $w(y_n, y_{n-1})$ is the stacking interaction of the nearest neighbors n and $n+1$, and $V(y_n)$ the interaction of the $n-th$ base-pair. In this work, we consider two terms for the base-pair interaction,

$$V(y_n) = D_n(exp(-ay_n) - 1)^2 - D_n f_s(tanh(y_n/l_s) - 1). \tag{3.64}$$

The first term is the usual Morse potential [106] which describes the hydrogen bonds of the base-pairs. The second term is a solvent interaction potential, adapted from Drukker et al. [107], which simulates the formation of hydrogen bonds with the solvent once the base-pair hydrogen bonds are stretched by more than a value l_s from their equilibrium values. The solvent interaction potential is a function which varies smoothly from $f_s D$ at $y_n < -l_s$ to zero for $y_n > l_s$. For $y_n < l_s$, the base-pairs are pulled away from each other until the bond with the solvent is established. Once the bases are bonded to the freely moving solvent molecule they are no longer pushed to any particular direction, a situation which is represented by the potential plateau for $y_n > l_s$. The solvent potential combined with the Morse potential results in a single barrier of height and width of the orders of $f_s D$ and l_s, respectively, as shown in fig.11. We will refer to the Hamiltonian with the base-pair interaction of eq.(3.64) as to the Morse-solvent Hamiltonian. The harmonic stacking interaction is considered in a modified form,

$$w(y_n, y_{n-1}) = \frac{K}{2}(y_n^2 - 2y_n y_{n-1} cos\theta + y_{n-1}^2), \tag{3.65}$$

θ, is the twist angle between neighboring base-pairs. Torsional effects have been included in several mesoscopic studied, ranging from molecular dynamics simulations [107, 19] to extensions of DPB model [50, 61] and of Ising-like model [108]. The role of the helicoidal geometry on the denaturation pattern is still unclear. For an angle of $\theta = 0$ the usual harmonic stacking interaction term [109] is obtained and would represent the situation of perfectly parallel neighboring bonds. Evidently, the base-pairs can only denaturate when the double helix is largely uncoiled and therefore we use a small angle . However, since the divergence is actually caused by the

stacking interaction $w(y_n, y_{n-1})$ when $y_n = y_{n+1}$, i.e. when neighboring bonds are stretching by exactly the same amount, it seems more appropriate to remove this divergence by modifying the term which is causing it. For comparison, the anharmonic Hamiltonian proposed by Dauxois et al. [109] has been considered, and modify to take into account the same torsion angle dependence as in Eq. (3.65) for the stacking interaction,

$$w_{an}(y_n, y_{n-1}) = \frac{K}{2}(1 + \rho exp[-\alpha(y_n + y_{n-1})])(y_n^2 - 2y_n y_{n-1} cos\theta + y_{n-1}^2). \tag{3.66}$$

Thus generalizing the DPB Hamiltonian to the following expression:

$$H = \sum_{n=1}^{N}[\frac{m\dot{y}_n^2}{2} + V(y_n, y_{n-1}) + w_{an}(y_n, y_{n-1})], \tag{3.67}$$

K, is the harmonic stacking related to μ by $K = \mu\nu^2$, ν being the frequency of the phonon mode. ρ and α are the anharmonic stacking parameters which are also assumed independent of the type of base at the n and n-1 sites. The AT and GC base are comparable in size and weight with their effective masses usually taken as $\mu = 300amu$. From this Hamiltonian, an equation governing the local oscillations of DNA nucleotides is derived

$$\begin{aligned}
\mu\ddot{y}_n &= K(y_{n+1} + y_{n-1} - 2y_n) - 2Ksin^2(\frac{\theta}{2})(y_{n+1} + y_{n-1}) \\
&- K\rho[(y_n - y_{n-1})e^{-\alpha(y_n+y_{n-1})} - (y_{n+1} - y_n)e^{-\alpha(y_n+y_{n+1})}] \\
&+ \frac{bK\rho}{2}[(y_n - y_{n-1})^2 e^{-\alpha(y_n+y_{n-1})} + (y_{n+1} - y_n)^2 e^{-\alpha(y_n+y_{n+1})}] \\
&- 2K\rho sin^2(\frac{\theta}{2})(1 - by_n)[y_{n-1}e^{-\alpha(y_n+y_{n-1})} + y_{n+1}e^{-\alpha(y_n+y_{n+1})}] \\
&+ \frac{D_n f_s}{l_s} sech^2(\frac{y_n}{l_s}) - 2aD_n(e^{-ay_n} - e^{-2ay_n})
\end{aligned} \tag{3.68}$$

In the following, we consider a special collective motion of the pairs in a DNA molecule. The amplitude of the wave packet is big enough, so that the nonlinear effect plays an essential role in DNA molecules. On the other hand, it is still very small compared with the amplitude of the broken base pairs. Therefore, the base pairs in DNA molecule do not oscillate far away from the bottom of the Morse potential well. In this respect, we can assume $0 < y_n \ll 1$ and expand the terms in exponential $e^{(y_n+y_{n-1})}, e^{(y_n+y_{n+1})}$ and e^{-ay_n} until the second and third orders, respectively. This leads to the modified equation:

$$\begin{aligned}
\ddot{y}_n &= K_1(y_{n+1} + y_{n-1} - 2y_n) - S_1(y_{n+1} + y_{n-1}) \\
&- K_2[(y_n + y_{n-1})^2 + (y_n + y_{n+1})^2] \\
&+ K_3 y_n(y_{n+1}^2 + y_{n-1}^2) - S_3[(y_n + y_{n-1})^3 + (y_n + y_{n+1})^3] \\
&+ K_4 y_n^2 - K_5 y_n^3 - \omega_0^2 y_n.
\end{aligned} \tag{3.69}$$

where, $S_1 = \frac{S(1+\rho)}{\mu}$, $S_2 = \frac{S\rho\alpha}{\mu}$, $S_3 = \frac{S\rho\alpha^2}{2\mu}$, $S = 2Ksin^2(\frac{\theta}{2})$, $K_1 = \frac{K(1+\rho)}{\mu}$, $K_2 = \frac{K\rho\alpha}{2\mu} - S_2$, $K_3 = \frac{K\rho\alpha^2}{\mu} - S_3$, $K_4 = \frac{4K\rho\alpha}{\mu} - \gamma\omega_g^2 + \frac{24D_nf_s}{\mu l_s^3} - 2S_2$, $K_5 = \frac{2K\rho,\alpha^2}{\mu} + \beta\omega_g^2 + \frac{112D_nf_s}{3\mu l_s^4} - 2S_3$, $\gamma = -\frac{3a}{2}$, $\beta = -\frac{7a^2}{6}$,$\omega_g^2 = \frac{2a^2D_n}{\mu}$, $\omega_0^2 = \omega_g^2 - \frac{8D_nf_s}{\mu l_s^2}$.

Linearizing Eq. (3.69) yields plane wave solutions with wavenumber k and frequency $\omega(k)$ given by the dispersion relation $\omega^2 = \omega_0^2 + 2S_1cos(ql) + 4K_1sin^2(\frac{ql}{2})$. For the nonlinear Eq. (3.69), we search for small-amplitude time-periodic solutions as[34 38]

$$y_n = \sum_{-\infty}^{+\infty} a_n^{(p)} e^{ip\omega_b t} \tag{3.70}$$

where, ω_b is close to some linear oscillation frequency and the Fourier coefficients are slowly depending on time, $a_n^{(p)}(\epsilon^2 t)$; we have defined the smallness implicit parameter $\epsilon = \sqrt{K_1}/\omega_g$. Due to exponential decay of the Fourier coefficients in p, they must satisfy $a_n^{(p)} \sim \epsilon^p$ for $p > 0$, while $a_n^{(0)} \sim \epsilon^2$. Moreover . $a_n^{(p)} \sim a_n^{(-p)*}$, since y_n is real. This allows, for a slow time dependence of the Fourier coefficients $a_n^{(p)}$, a MDNLS equation for the dominating coefficient $a_n^{(1)}$ describing the leading-order nonlinear effects. Defining $a_n^{(1)}$ as

$$a_n^{(1)} = (-1)^n \sqrt{\frac{2\omega_b}{3K_5 + 6S_3}} \psi_n \times exp(i\frac{\omega_0^2 - \omega_b^2 + 2K_1}{2\omega_b}) \tag{3.71}$$

the modified DNLS equation of the DNA model reads

$$\begin{aligned} &i\frac{d\psi}{dt} + P(\psi_{n+1} + \psi_{n-1}) + Q_1|\psi_n|^2\psi_n + Q_2[2\psi_n(|\psi_{n+1}|^2 + |\psi_{n-1}|^2) + \psi_n^*(\psi_{n+1}^2 + \psi_{n-1}^2)] \\ &+ Q_3[|\psi_{n+1}|^2\psi_{n+1} + |\psi_{n-1}|^2\psi_{n-1} + \psi_n^2(\psi_{n+1}^* + \psi_{n-1}^*) + 2|\psi_n^2|(\psi_{n+1} + \psi_{n-1})] = 0 \end{aligned} \tag{3.72}$$

where, $P = \frac{K_1 - S_1}{2\omega_b}$; $Q_1 = \frac{K_5 - 2S_3}{K_5 + 2S_3}$; $Q_2 = \frac{3S_3 - K_3}{3K_5 + 6S_3}$; $Q_3 = \frac{-2S_3}{K_5 + 2S_3}$.

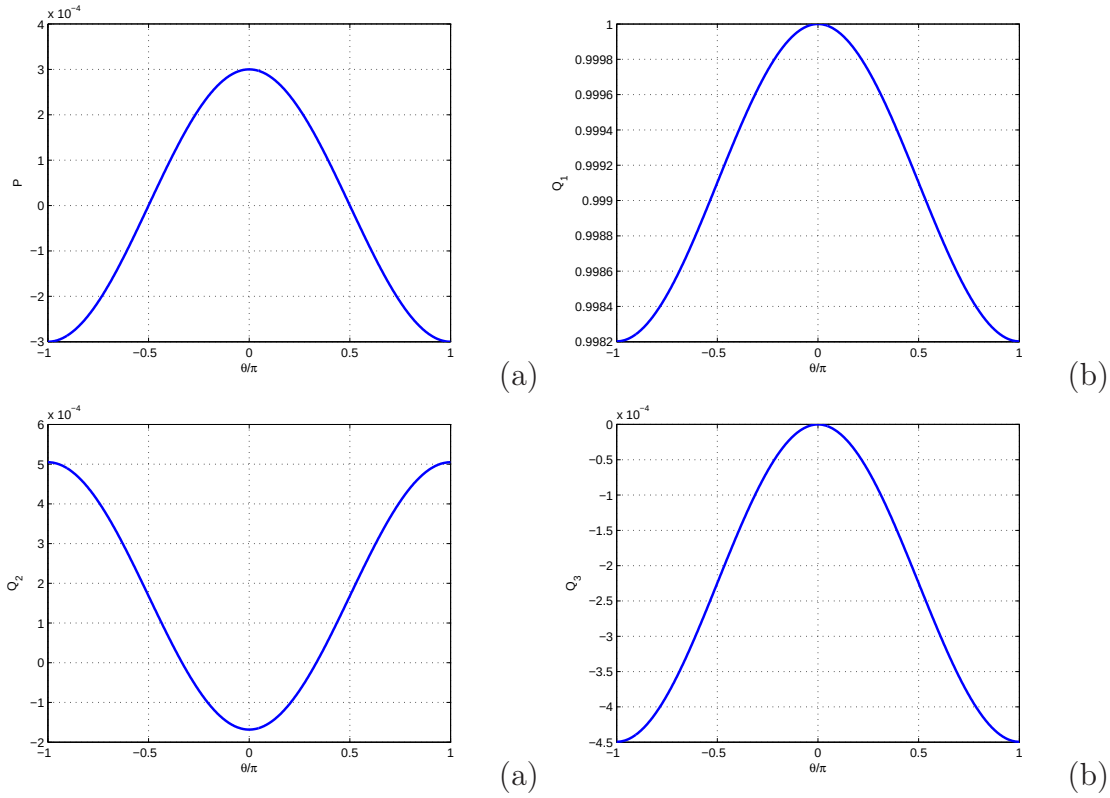

Figure 23: The parameters of equation for $\omega_b = 1$, $\rho = 2$ D $= 0.05$ eV , $\alpha = 0.35$Å, K=60mev.Å^{-2}, $f_s = 0.3$, and $l_s = 3$Å.

For $\theta = 0$ we have $Q_1 = 1$, $Q_3 = 0$, $P = \frac{K_1}{2\omega_b}$ and $Q_2 = \frac{-K_3}{3K_5+6S_3}$, equation (3.72) becomes as the one studied in [37]. For $\theta = \frac{\pi}{3}$, $Q_2 = 0$, $Q_1 > 0$ and $Q_3 < 0$, we have here also the modified DNLS equation. in the case where $\theta \neq 0$ and $\theta \neq \frac{\pi}{3}$ equation (3.72) is a modified DNLS equation, we will take her as a basis to study the instability in our model.

3.5.2 Linear stability analysis

In order to study the MI of the DNA molecule, we use the standard linear stability analysis. For this, we consider the propagation of wave signal along the molecule. The corresponding wave can be written as,$\psi_n = \psi_0 e^{i(qn-\Lambda t)}$, where the wavenumber q, the angular frequency Λ and the amplitude ψ_0 satisfy the dispersion relation

$$\Lambda = -2Pcos(q) - \psi_0^2[Q_1 + 2Q_2(2 + cos(2q)) + 8Q_3cos(q)] \tag{3.73}$$

To examine the linear stability of the initial plane waves, we look for a solution of the form

$$\psi_n = \psi_0(1 + B_1 e^{i(Qn-\Omega t)} + B_2^* e^{-i(Qn-\Omega^* t)})e^{i(qn-\Lambda t)} \tag{3.74}$$

where the asterisk denotes complex conjugation. B_1 and B_2 are complex constant and stand for perturbation amplitudes. K and Ω represent the wavenumber and the angular frequency of the perturbation, respectively. We obtain the linear homogeneous system for B_1 and B_2

$$\begin{pmatrix} a_{11}+\Omega & a_{12} \\ a_{21} & a_{22}-\Omega \end{pmatrix} \begin{pmatrix} B_1 \\ B_2 \end{pmatrix} = \begin{pmatrix} 0 \\ 0 \end{pmatrix} \tag{3.75}$$

with

$$\begin{aligned} a_{11} &= 2P(\cos(Q+q)-\cos(q)) + \psi_0^2[Q_1 + 2Q_2(1-\sin(Q)\sin(2q)) + Q_3(8\cos(q+Q)-\cos(q))] \\ a_{22} &= 2P(\cos(Q-q)-\cos(q)) + \psi_0^2[Q_1 + 2Q_2(1+\sin(Q)\sin(2q)) + Q_3(8\cos(Q-q)-\cos(q))] \\ a_{12} &= a_{21} = \psi_0^2[Q_1 + 2Q_2(2\cos(Q)+\cos(2q)) + 8Q_3\cos(q)\cos^2(\frac{Q}{2})] \end{aligned} \tag{3.76}$$

The condition for the existence of non trivial solutions of the above linear homogenous system is given by a second order equation for the frequency Ω, that is

$$\Omega^2 + (a_{11}-a_{22})\Omega + a_{12}^2 - a_{11}a_{22} = 0 \tag{3.77}$$

the discriminative of equation (3.77) is given by

$$\Delta = 16(A+\psi_0^2 D_1)(A-\psi_0^2 D_2) \tag{3.78}$$

with $A = 2P\cos(q)\sin^2(\frac{Q}{2})$, $D_1 = [2Q_2(\cos(Q)-\sin^2(q)) + Q_3]$,
$D_2 = [Q_1 + 2Q_2(\cos(Q)+\cos^2(q)) + \frac{3}{2}Q_3\cos(q)(4\cos(Q)+1)]$. If Δ is negative, The perturbed wave can then be unstable. Hence, two complex numbers are solution of the above equation. The MI is measured by the power gain and it is defined at any wave number by $\sigma(q,Q) = 2Im(\Omega)$. The corresponding growth is given by

$$\sigma(q,Q) = \sqrt{16(A+\psi_0^2 D_1)(A-\psi_0^2 D_2)}, \tag{3.79}$$

On the other hand, it becomes possible to express the initial amplitude $\psi_0|$ with respect to a threshold amplitude $\psi_0 cr$. Therefore, a plane wave introduced in the molecule will be unstable if the initial amplitude $|\psi_0|$ exceeds the threshold amplitude $|\psi_0 cr|$ defined as follows

$$|\psi_0|^2 \geq |\psi_0 cr|^2 = \frac{P\cos(q)\sin^2(\frac{Q}{2})}{[Q_1 + 2Q_2(\cos(Q)+\cos^2(q)) + \frac{3}{2}Q_3\cos(q)(4\cos(Q)+1)]}, \tag{3.80}$$

For all those cases, it is necessary that $D_1 > 0$, for it, $\theta < \frac{\pi}{3}$ and

$$Q > Q_{cr} = \arccos(\sin^2(q) - \frac{Q_3}{2Q_2}) \tag{3.81}$$

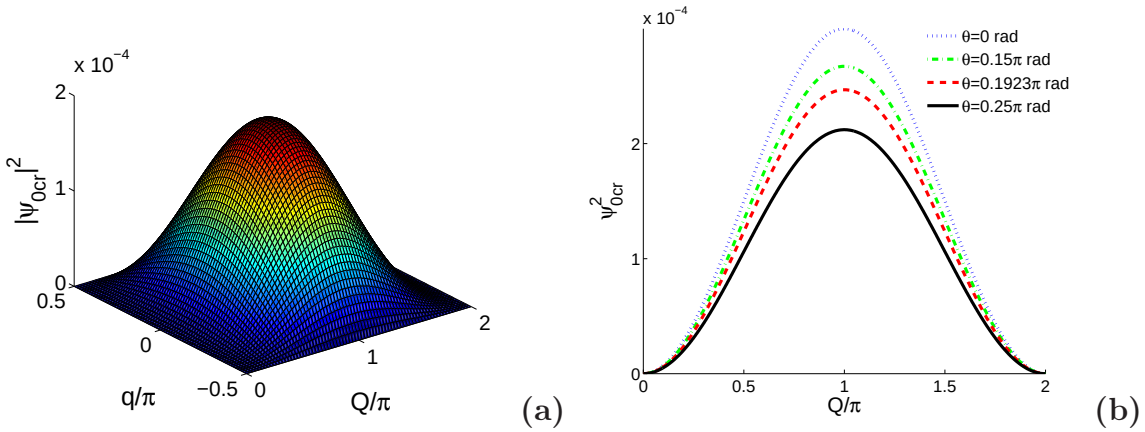

Figure 24: The panels shows the plot of the threshold amplitude.In panel (a), $|\psi_0 cr|^2$ has been plotted for $\theta = 0.4 * \pi$.In panel (b), we have plot the threshold amplitude for three values of θ and for $\omega_b = 1$, $\rho = 2$ D = 0.05 eV , $\alpha = 0.35$Å, K=60mev.Å^{-2}, $f_s = 0.3$, and $l_s = 3$Å. It appears that the amplitude is a decreasing function of θ

The evolution of the threshold amplitude versus the perturbation wave numbers Q is shown in Fig. 24a for any value of the wave number q of the carrier wave. We notice that the more discreteness effects are important ($q = \pi$) the higher the necessary amplitude leading to MI. The impact of the twist angle on the threshold amplitude is studied in Fig.24b. We observe that the threshold amplitude decreases as the twist angle θ increases. So, the magnitude of the threshold amplitude could be controlled through the twist angle (we have set $q = 0$ in Fig. 24b) 23

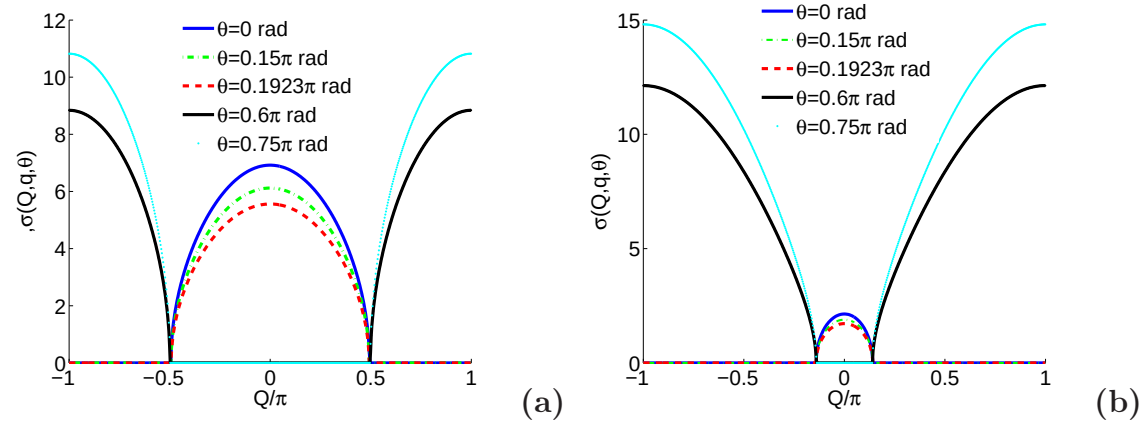

Figure 25: Growth rate versus the wavenumber of the perturbation Q for $q = 0$ (a), $q = 0.6\pi$ (b) and for $\omega_b = 1$, $\rho = 2$ D = 0.05 eV , $\alpha = 0.35$Å, K=60mev.Å^{-2}, $f_s = 0.3$, and $l_s = 3$Å. This has been plotted for three values of the θ. It is obvious that the increase of θ significantly increase the region of instability as also shown in Figure 1

Figure 25 displays the combine effect of the twist angle and the wave number q of the carrier wave on the growth rate of instability. Let us first present in Fig. 25a the MI gain for $q = 0$. One obtain that for θ lower than 0.5π, the MI gain decreases with increasing θ as in Fig.24b for the threshold amplitude, but for θ greater than 0.5π we observe the presence of an additional new

MI region and the MI gain has increased with θ. Figure 25b shows the growth rate of MI for non nil value of the wave number q ($q \neq 0$). The presence of q drastically change the maximum peak of the growth rate. One observe that for θ lower than 0.5π, the MI gain still a decreasing function of θ, but the peak of MI gain is less compare to the one of Fig. 25a. For θ greater than 0.5π, the new additional MI region still presents, but the peak of the MI gain is higher than the one of Fig. 25a (obtained for $q = 0$). Similar results have been obtained in optical fiber, where the additional MI region is due to the presence of the fourth-order dispersion [110]. So, the presence q has a double effect, while for $\theta < 0.5\pi$, the MI gain is a decreasing function of θ, for $\theta > 0.5\pi$ the MI gain is an increasing fonction of θ. The bandwidth of the MI decreases with the presence of q for $\theta < 0.5\pi$, while it increases due to q for$\theta > 0.5\pi$ (see Fig.25b)

Another main features of the MI is highlighted in Fig. 26. Thus, the instability/stability diagram is plotted in the (q, Q) plane. White regions represent zone of stability, while dark one indicates the zone of instability. Dark regions correspond to the regions of instability in which the amplitude of any waves would be expected to suddenly display an exponential growth.

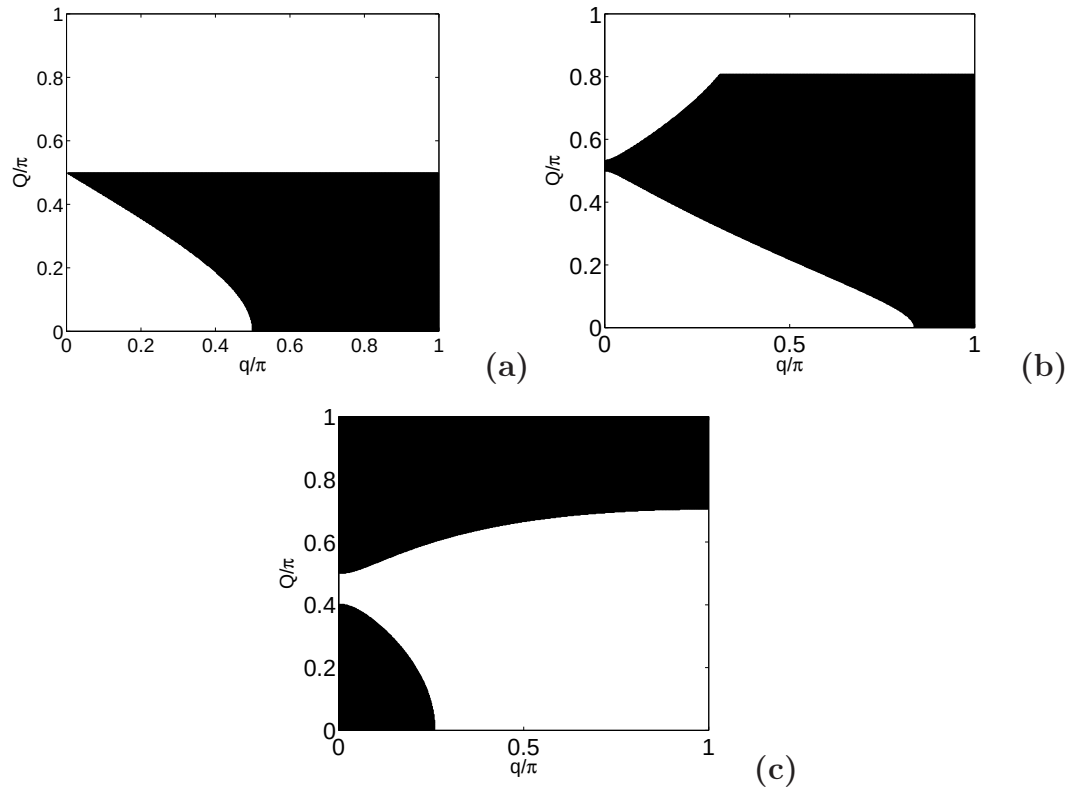

Figure 26: Panels show the stability/ instability diagrams in the (Q, q) plane for $\omega_b = 1$, $\rho = 2$ D = 0.05 eV , $\alpha = 0.35$Å, K=60mev.Å^{-2}, $f_s = 0.3$, and $l_s = 3$Å and $\theta = 0$ (a), $\theta = 0.15\pi$ (b), $\theta = 0.25\pi$ (c). One clearly sees that the instability region becomes hight for higher values of θ

Figure 26a displays the MI diagram for $\theta = 0$. Figures 26b and 26c have been plotted for $\theta = \theta_{eq}$ and $\theta = 0.60\pi$, respectively. As θ grows, regions of MI increase, but if θ becomes greater

than 0.5π, one observe an additional MI region. So, the presence of the twist angle θ increases the bandwidth of MI diagram. We have noted that the solvent interaction (f_s) doesn't influence on zones of stability.

3.5.3 Generation of soliton-like structures through the twisted DNA with solvent interaction

To study the creation of localized structures in the finite stacking enthalpy model, it is not enough to formulate the problem in terms of the modified DNLS Eq. (3.72) that governs the dynamics of the modulated wave (3.70). The transformation from the equation of motion of the base pairs Eq (3.68)to Eq. (3.72) involves some approximations. So, Eq. (3.72) has simply been used to predict and determine regions of MI and those analytical results must be verified through direct numerical simulations in the generic anharmonic model to Eq. (3.72), with corresponding values of parameters. In order to check the validity of our analytical approach and to determine the evolution of the system taking into account the instability zone, we have performed numerical simulations of the equation of motion (3.72) with a given initial condition. They are integrated with a fourth-order Runge-Kutta scheme with a time step chosen to conserve the energy to an accuracy better than 5×10^{-3}. Most of the simulations are performed with a molecule of 300 base pairs with periodic boundary conditions; so that the wavenumbers q and Q must necessarily assume the form $q = 2\pi l/N$ and $Q = 2\pi L/N$, where l and L are integers lower than N/2. We chose as the initial condition a linear wave with a slightly modulated amplitude [30,31,32]

$$\begin{aligned} y_n(t=0) &= \psi_0[1 + 0.01\cos(Qn)]\cos(qn), \\ \dot{y}_n(t=0) &= \psi_0[1 + 0.01\cos(Qn)]\omega\sin(qn). \end{aligned} \tag{3.82}$$

Our aim in this numerical analysis is to point out the impact of the twist angle θ and solvent interaction barrier factors fs on the occurrence of solitonlike objects induced by MI. As a first case, we set $\theta = 0$ (the system becomes the PBD model) with wave numbers $q = 0.45\pi and$ $Q = 0.98\pi$ (the corresponding point lies in an instability region of Fig. 26) and $\psi_0 = 0.002$. We observe in Fig. 27a that as the time increases, the initial condition tends to disintegrate during the propagation leading to the break-up of waves into localized patterns with small-amplitude. Each element of the train has the shape of a soliton object. In fact, nonlinear interactions can give rise to very stable excitations, called solitons, which can travel without changing their shape. These excitations are very robust and important in the coherent transfer of energy. For realistic interatomic potentials the solitary waves are compressive and supersonic. They propagate without energy loss, and their collisions are almost elastic. This feature is depicted in Fig. 27. One can conclude that MI is the most standard mechanism through which bright solitons or solitary structures can appear in physical systems. Now, let us take into account the twist angle. Figure 27b displays the disintegration of the wave for $\theta = \theta_{eq}$, we obrserve that

the number of waves train decreases with time, but the maximum amplitude increases. For $\theta = 0.60\pi$ and $\theta = 0.60\pi$ that are plotted in Fig. 27c and Fig. 27d, respectively, the number of waves train continuous to decrease with time, but the maximum amplitude increases. So, on can conclude that by increasing the the twist angle one can control the number of localized patterns generated. Dauxois et al. [111, 112, 113] have suggested that, such localized oscillations can be precursors of bubbles that appear in the thermal denaturation of DNA. In this framework, they can be good candidates for transporting energy and charge in discrete lattices in general and in DNA in particular. It is clear that θ influences the number of the sites oscillating with soliton shape in the train. Also, intrinsic fluctuations of DNA in the form of vibrational energy itself might be trapped in soliton excitations as a result of a balance between dispersion and nonlinearity, which leads to localized base-pair opening. These fluctuations act as a source for DNA denaturation.

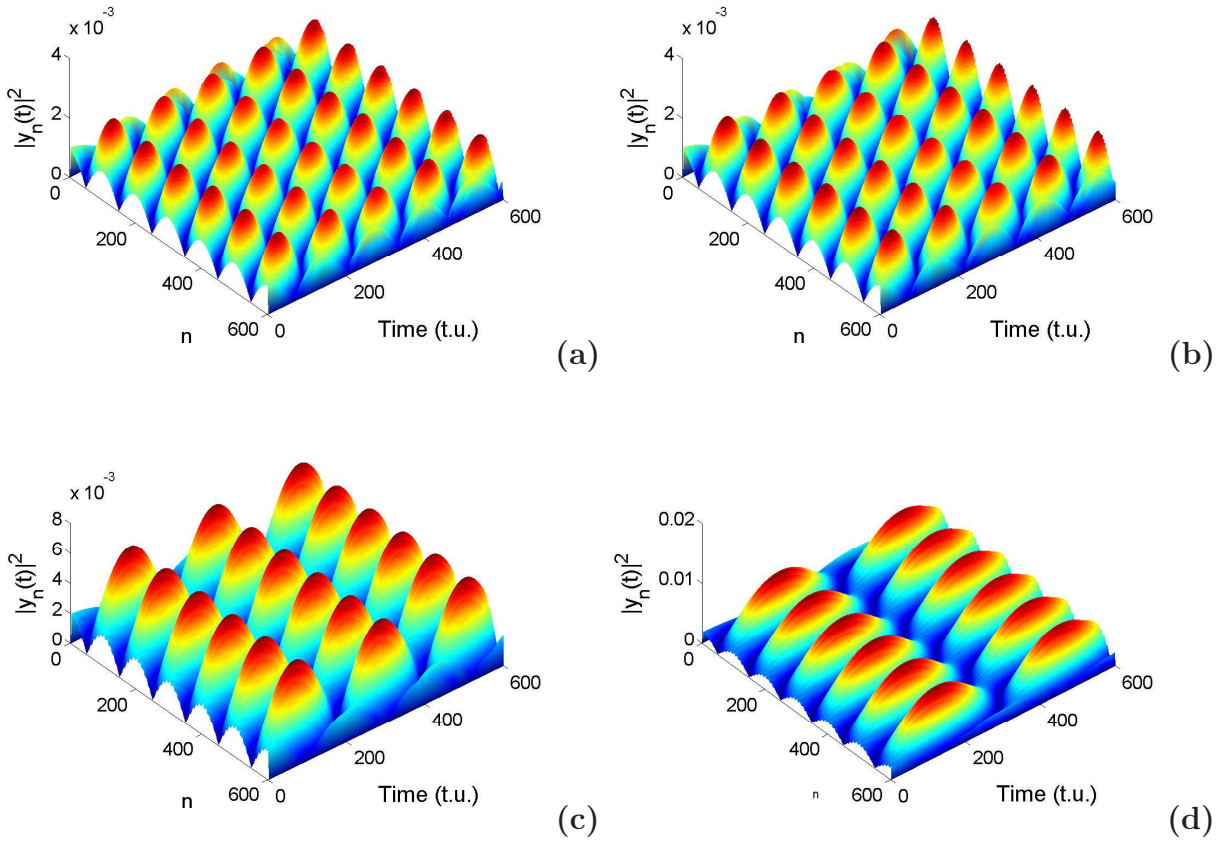

Figure 27: (Color online) Temporal evolution of waves trough the lattice. The initial plane waves solution break into waves train in the DNA molecule, as predicted by the analytical studies, for $\omega_b = 1$, $\rho = 2$ D $= 0.05$ eV , $\alpha = 0.35$Å, K=60mev.Å^{-2}, $f_s = 0$, and $l_s = 3$Å and $\theta = 0$ (a), $\theta = 0.45\pi$ (b), $\theta = 0.55\pi$ (c), $\theta = 0.75\pi$ The width of localized patterns increase and their number over the time decreases when θ grows. This confirms the fact that the value of the twisted angle influences the number of modulated waves oscillating over the time in the DNA model.

In Fig. 28, we study the localization of energy along the twisted DNA with solvent interaction. The energy density of the molecule is given by

$$\begin{aligned} E_n =& \sum_{n=1}^{N}[\frac{m\dot{y}_n^2}{2} + \frac{K}{2}(1+\rho e^{-\alpha(y_n+y_{n-1})})(y_n^2 - 2y_n y_{n-1}\cos\theta + y_{n-1}^2) \\ &+ \frac{K}{2}(1+\rho e^{-\alpha(y_{n+1}+y_n)})(y_{n+1}^2 - 2y_n y_{n+1}\cos\theta + y_n^2) \\ &+ D_n(e^{-ay_n}-1)^2 - D_n f_s(\tanh(y_n/l_s)-1)]. \end{aligned} \tag{3.83}$$

Figure 28 shows localization of energy in the molecule for different values of the twist angle. The energy density is plotted in this figure with the same parameters as in Fig. 27. The energy is located in some particular sites. We see that the energy density is coherently localized in space and time. The twist angle has an effect on the number of sites where energy is been localized. The width of the energy pattern increases has the twist angle increases. The energy is uniformly localized with a certain recurrence in the molecule. The localization of energy becomes strong enough when θ grows.

For $\theta = 0$, the density of energy is $E_n = 1.2 \times 10^{-4}$ eV (see Fig. 28a), for $\theta = 0.45\pi$ rad,$E_n = 1.8 \times 10^{-4}$ eV (see Fig. 28b), for $\theta = 0.55\pi$ rad, $E_n = 3.2 \times 10^{-4}$ eV (see Fig. 28c) and for $\theta = 0.75\pi$ rad $E_n = 5.5 \times 10^{-4}$ eV (see Fig. 28d)(in blue regions $E_n = 0$). In general, increasing θ makes possible a strong localization of energy in the DNA lattice. In consequence, the features displayed by the whole Fig. 28 imply that the twist angle can be used as a theoretical tool to control the density of energy and the amplitude of oscillations of the hydrogen bonds. These oscillations can be a better way to transport information and charge in the double helical structure. So, increasing θ makes a small number of base pairs to participate in the formation of open-state configuration. We can conjecture that vibrations remain affecting only to a small number of consecutive base pairs when θ grows, this can initiate denaturation or transcription bubbles. The above study have been done without the solvent interaction effect. Let us study the combine impact of the solvent interaction and twist angle along the molecule. Let us recall that Figs. 28a and 28a have been plotted for the DPB model (that is $\theta = 0$, $f_s = 0$). Figures 29a and 29b have been

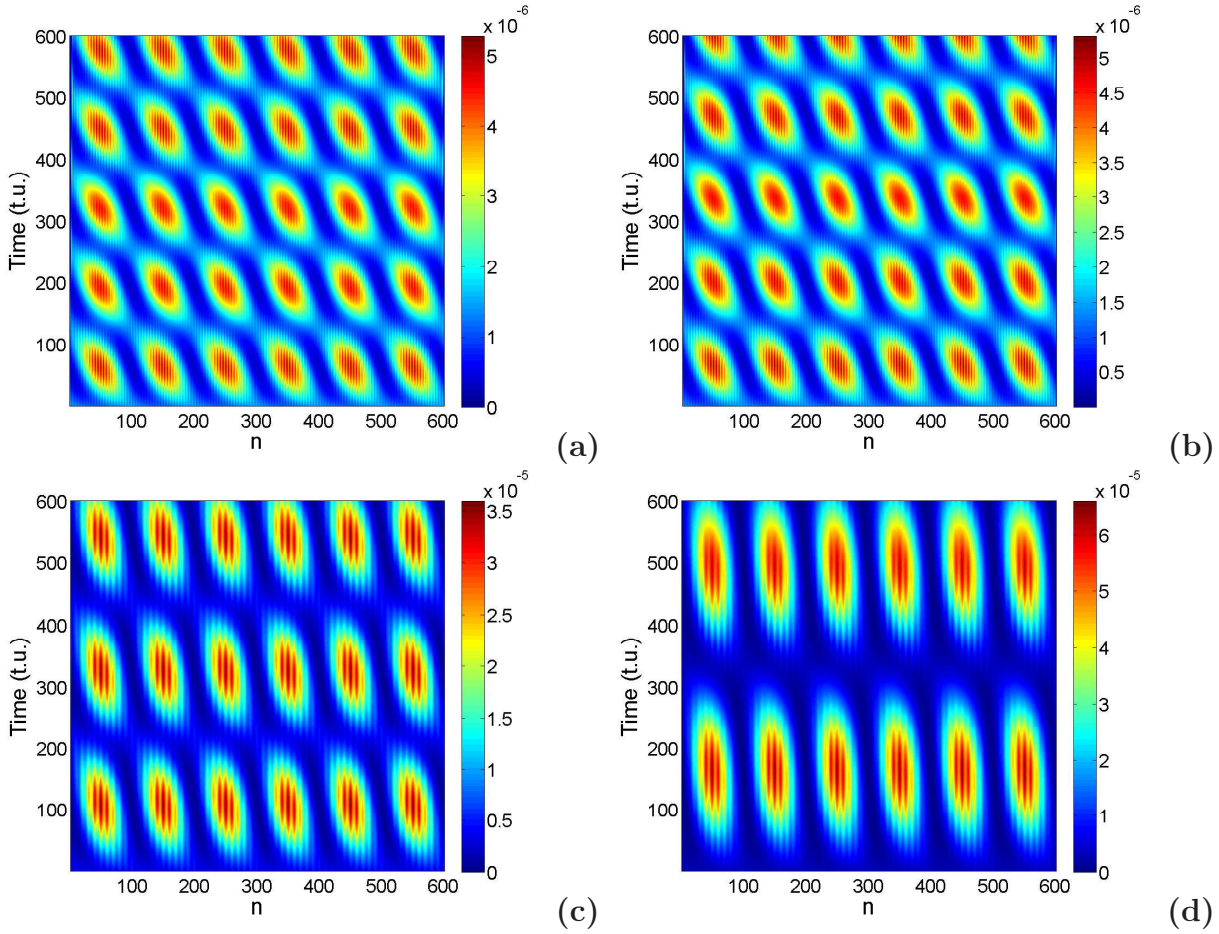

Figure 28: (Color online) Energy localization for the twisted DNA for different value of θ. Same parameter as in Fig.27 . $\theta = 0$ (a), $\theta = 0.45\pi$ (b), $\theta = 0.55\pi$ (c), $\theta = 0.75\pi$ (d). We observe that the localization of energy increases with time as θ increases.

obtained for $f_s = 0.1$ and $f_s = 0.3$, respectively, and $\theta = \theta_{eq}$. Compare with Fig. 27b (that is $f_s = 0$), one sees that the waves train become compact while the oscillation amplitude increases with fs. Let us now consider in Figs. 29c and 29d the molecule with, respectively, $f_s = 0.1$ and $f_s = 0.3$, for $\theta = 0.60\pi$. Compare with Fig. 27c (that is in the absence of solvent interaction, $f_s = 0$), we conclude that, as fs and θ increase the number of waves train in the molecule decreases. So, the presence of the solvent through the system will twin some waves train, while the amplitude of oscillation will increases. During our simulations, we have obtain that energy is not localized in any particular sites due to the presence of the solvent interaction.

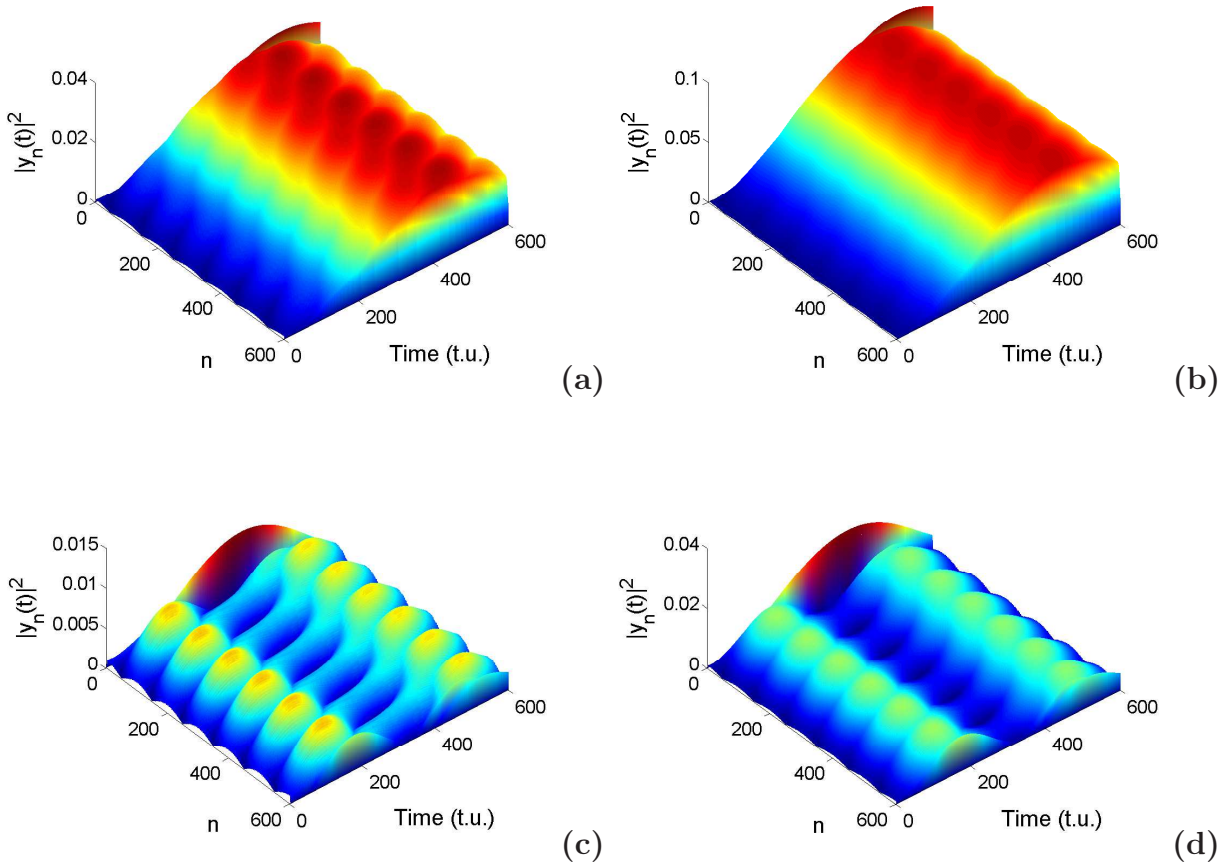

Figure 29: (Color online) Effect of the solvent interaction along the molecule for $\omega_b = 1$, $\rho = 2$ D $= 0.05$ eV , α= 0.35Å, K=60mev.Å^{-2}, and $l_s = 3$Å $\theta = \theta_{eq}$ and $f_s = 0.1$ (a); (b) $\theta = \theta_{eq}$ and $f_s = 0.3$ $\theta = 0.60\pi$ and $f_s = 0.1$ (c); (d) $\theta = 0.60\pi$ and $f_s = 0.3$. One clearly observes that the magnitude amplitude of waves increases with the solvent interaction, while the number of localized patterns decreases with time.

We have consider a twisted DNA molecule with solvent interaction, looking to very interesting MI phenomena. MI is one of the principal mechanisms which leads to the emergence of localized coherent nonlinear structures and the formation of a train of ultrashort pulses. Based on the DPB model of twisted DNA molecule, the generalized DNLS equation governing the dynamics of the twisted DNA molecule with solvent interaction has been derived. This model describes in a simplified way, the hydrogen bond and has been used successfully in numerous applications such as energy localization or to calculate solitonic speed. We mainly studied the effect of the twist angle and solvent interaction on the MI gain as well as on the propagation of envelope bright solitary wave. The linear stability analysis has been performed, the threshold amplitude and MI gain derived. We have seen that for $\theta < 0.5\pi$, increases θ will decreases the MI gain. But for $\theta > 0.5\pi$, we observe an additional new region of MI. Such features has been obtained in the case of optical fiber, where addition region of MI is due to the presence of the fourth-order dispersion. We have also seen that the wave number of the carrier wave q affect

the MI gain as well as the bandwidth. The diagram of instability/stability has been also plotted in the (q, Q) plane and we find that is sensitive to the value of θ.

Numerical verifications performed in the generic equation of motion confirmed our analytical predictions due to the effective bearing of localized structures from a nonsoliton initial condition. The possibility that nonlinear effects might focus the vibrational energy of twisted DNA with solvent interaction into localized coherent structures has been expressed here with the generation of pulse waves. Energy has been localized in some sites and therefore can be stored in the hydrogen bond. We have seen that this localization of energy depends on the twist angle. When θ grows, energy becomes more localized along the molecule. Numerical simulations have shown that discrete breathers, which are spatially localized nonlinear oscillations, can appear in models of crystals, biomolecules, and many others nonlinear discrete systems [114, 115]. It is well known that discrete breathers can be static, but they can also move under certain physical conditions [116], constituting a mechanism for the transport of energy and information along discrete system. On the other hand, we have seen that the presence of the solvent interaction spreads the energy along the molecule, while it increases the amplitude of oscillations.

The present theoretical studies can suggest interesting experiments in order to improve the physical knowledge of nonlinear waves in twisted DNA with solvent interaction. It is, however, important to point out that applications of these results in biology must be done with prudence. From a theoretical point of view, it is known that the stability and lifetime of localized solutions are very sensitive to properties of the thermal fluctuations such as viscosity and temperature [117, 118]. The DNA is in contact with a thermal bath in the cell. Therefore, the friction and thermal forces play an important role in its internal dynamics.

3.6 Effect of the torsion on the dynamics of the DNA molecule

Modulational instability (MI) is explored in the framework of the base-rotor model of DNA dynamics. We show, in fact, that the helicoidal coupling introduced in the spin model of DNA reduces the system to a discrete CNLS equation. Also, the competitive effects of the harmonic longitudinal and helicoidal constants on the dynamics of the system are notably pointed out. In the same way, it is shown that MI can lead to energy localization which becomes high for some values of the helicoidal coupling constant. The base-rotor model, where we introduce the helicoidal coupling, is addressed and our results show that the interplay between stacking and helicoidal couplings can give rise to highly localized structures with a consequence on energy localization.

3.6.1 Model and dynamical equations

In the model proposed by L. Yakushevich [41], the pairing interaction is considered in the approximation of harmonic potential, depending on the distance between the endpoints of the

bases, i.e. the atoms bridged by of an angle θ of rotation around the N-C bond, the force becomes a nonlinear function of such an angle. Here the distance l between points p_1 and p_2 satisfies.

$$l^2 = [d + 2r - r(\cos\theta_1 + \cos\theta_2)]^2 + [r(\sin\theta_1 + \sin\theta_2)]^2. \tag{3.84}$$

It is then convenient to pass to coordinates

$$\varphi_\pm = \frac{\theta_1 \pm \theta_2}{2}. \tag{3.85}$$

In terms of which, by standard trigonometric identities, the distance is written as

$$l^2 = d^2 + 4r^2(1 + \cos^2\varphi_- - \cos\varphi_+ \cos\varphi_-). \tag{3.86}$$

Yakushevich also suggested to consider the approximation $d \to 0$. In other words we are considering the stretchning of H bond due to small rotations of the bases and extend this to the full range $[0, 2\pi]$ of angular coordinates. Notice that we are trascurating the directionality effects, as only distance is taken into account. The potential describing the pairing interaction will then be

$$U_T = \frac{1}{2}\alpha[1 + cos^2\varphi_- - cos\varphi_+ cos\varphi_-], \tag{3.87}$$

(notice that this is $2\pi - periodic$ in both angular coordinates, as it should). As for stacking interactions, we will also a fortiori keep the harmonic approximation for them; if θ_n^i is the angular coordinate relation to the $n - th$ chain (i= 1, 2), the stacking interaction potential between bases at sites n and $n + 1$ will be

$$U_S = \frac{1}{2}\beta[(\theta_{n+1}^{(1)} - \theta_n^{(1)})^2 + (\theta_{n+1}^{(2)} - \theta_n^{(2)})^2]. \tag{3.88}$$

Passing again to the coordinates

$$\theta_n^{(1)} = \theta_n^{(+)} + \theta_n^{(-)}; \quad \theta_n^{(2)} = \theta_n^{(+)} - \theta_n^{(-)}, \tag{3.89}$$

the above reads

$$U_S = \frac{1}{2}\beta[(\theta_{n+1}^{(+)} - \theta_n^{(+)})^2 + (\theta_{n+1}^{(-)} - \theta_n^{(-)})^2]. \tag{3.90}$$

In the following, in order to avoid confusion and to lighten notation, we will prefer to write $\psi = \theta^+$ and $\phi = \theta^-$ the Hamiltonian in this model is given by:

$$\begin{aligned} H &= T + U_S + U_T + U_H, \\ T &= \sum_n \frac{1}{2} I[(\dot{\theta}_n^{(1)})^2 + (\dot{\theta}_n^{(2)})^2] = \sum_n \frac{1}{2} I[(\dot{\psi}_n)^2 + (\dot{\phi}_n)^2], \\ U_S &= \frac{1}{2}\beta[(\psi_{n+1} - \psi_n)^2 + (\phi_{n+1} - \phi_n)^2], \\ U_T &= \frac{1}{2}\alpha[1 + \cos^2\phi_n - \cos\phi_n \cos\psi_n] \\ U_H &= \frac{K}{2}[(\phi_{n+h} - \phi_n)^2 + (\psi_{n+h} + \psi_n)^2]], \end{aligned} \tag{3.91}$$

where we introduced the ψ, ϕ coordinates in the kinetic term T as well. The equilibrium (stable) configuration is represented by $((\psi, \phi) = (0, 0)\forall n)$; I is the moment of inertia of the bases around the N-C bond. The above hamiltonian gives as equations of motion

$$\begin{aligned} I\ddot{\psi_n} &= \beta(\psi_{n+1} + \psi_{n-1} - 2\psi_n) + K(\psi_{n+h} + 2\psi_n + \psi_{n-h}) - \alpha \sin\psi_n \cos\phi_n, \\ I\ddot{\phi_n} &= \beta(\phi_{n+1} + \phi_{n-1} - 2\phi_n) + K(\phi_{n+h} - 2\phi_n + \phi_{n-h}) - \alpha \sin\phi_n(\cos\psi_n - \cos\phi_n), \end{aligned} \tag{3.92}$$

after expanding the term in sinus and cosinus until the third order, we get the following system:

$$\begin{aligned} \ddot{\psi_n} &= K_s(\psi_{n+1} + \psi_{n-1} - 2\psi_n) + K_h(\psi_{n+h} + 2\psi_n + \psi_{n-h}) - c(\psi_n - \frac{\psi_n^3}{6} - \frac{\phi_n^2\psi_n}{2}) \\ I\ddot{\phi_n} &= K_s(\phi_{n+1} + \phi_{n-1} - 2\phi_n) + K_h(\phi_{n+h} - 2\phi_n + \phi_{n-h}) - c(\phi_n^3 - \phi_n\psi_n^2) \end{aligned} \tag{3.93}$$

with, $K_s = \frac{\beta}{I}$; $K_h = \frac{K}{I}$; $c = \frac{\alpha}{I}$. In the form of a Fourier expansion in harmonics of the fundamental $e^{i(knd+\Omega t)}$where the Fourier components are developed in a Taylor series in powers of the small parameter ϵ, measuring the amplitude of the initial wave [78]

$$\psi(t) = \sum_{p=1}^{\infty} \epsilon^p \sum_{l=-p}^{p} A_\psi^{(l)}(n,t) u_p^{(l)}(m,\tau) \qquad \phi(t) = \sum_{p=1}^{\infty} \epsilon^p \sum_{l=-p}^{p} A_\phi^{(l)}(n,t) v_p^{(l)}(m,\tau) \tag{3.94}$$

with $A_\psi^{(l)}(n,t) = e^{il(knd+\Omega_\psi t)}$, $A_\phi^{(l)}(n,t) = e^{il(knd+\Omega_\phi t)}$ and $u_p^{(-l)} = (u_p^{(l)})^*$, $v_p^{(-l)} = (v_p^{(l)})^*$. Inserting the above expression in Eq.(3.92) we get the following system (To find details of calculation to the chapter2):

$$\begin{aligned} \frac{i}{2}(\chi_{m+1} - \chi_{m-1}) + \frac{iP}{2}(\chi_{m+h} - \chi_{m-h}) + Q_\psi \frac{\partial^2\chi_m}{\partial\tau^2} + [\gamma_{11}|\chi_m|^2 + \gamma_{12}|\eta_m|^2]\chi_m = 0, \\ \frac{i}{2}(\eta_{m+1} - \eta_{m-1}) + \frac{iP}{2}(\eta_{m+h} - \eta_{m-h}) + Q_\phi \frac{\partial^2\eta_m}{\partial\tau^2} + [\gamma_{21}|\chi_m|^2 + \gamma_{22}|\eta_m|^2]\eta_m = 0, \end{aligned} \tag{3.95}$$

where, $u_1^{(1)} = \chi_m$, and $v_1^{(1)} = \eta_m$, with

$$\begin{aligned} &P = \frac{K_h \sin(hqd)}{K_s \sin(qd)}; \quad \gamma_{11} = \frac{c}{2K_s \sin(qd)} \quad \gamma_{12} = \frac{3c}{2K_s \sin(qd)}; \quad \gamma_{21} = \frac{-3c}{K_s \sin(qd)}; \quad \gamma_{22} = -\frac{2c}{K_s \sin(qd)}, \\ &Q_\psi = \frac{1}{K_s \sin(qd)}[K_s(\frac{d}{\nu_{g\psi}})^2 \cos(qd) + K_h(\frac{hd}{\nu_{g\psi}})^2 \cos(hqd) - 1], \\ &Q_\phi = \frac{1}{K_s \sin(qd)}[K_s(\frac{d}{\nu_{g\phi}})^2 \cos(qd) + K_h(\frac{hd}{\nu_{g\phi}})^2 \cos(hqd) - 1], \end{aligned} \tag{3.96}$$

and

$$\begin{aligned} \Omega_\psi^2 &= c + 4K_s \sin^2(\frac{qd}{2}) + 4K_h \cos^2(\frac{hqd}{2}), \\ \Omega_\phi^2 &= 4K_s \sin^2(\frac{qd}{2}) + 4K_h \sin^2(\frac{hqd}{2}), \end{aligned} \tag{3.97}$$

Fig.30 shows the abve frequencies while Fig.31 plots the parameters of the system.

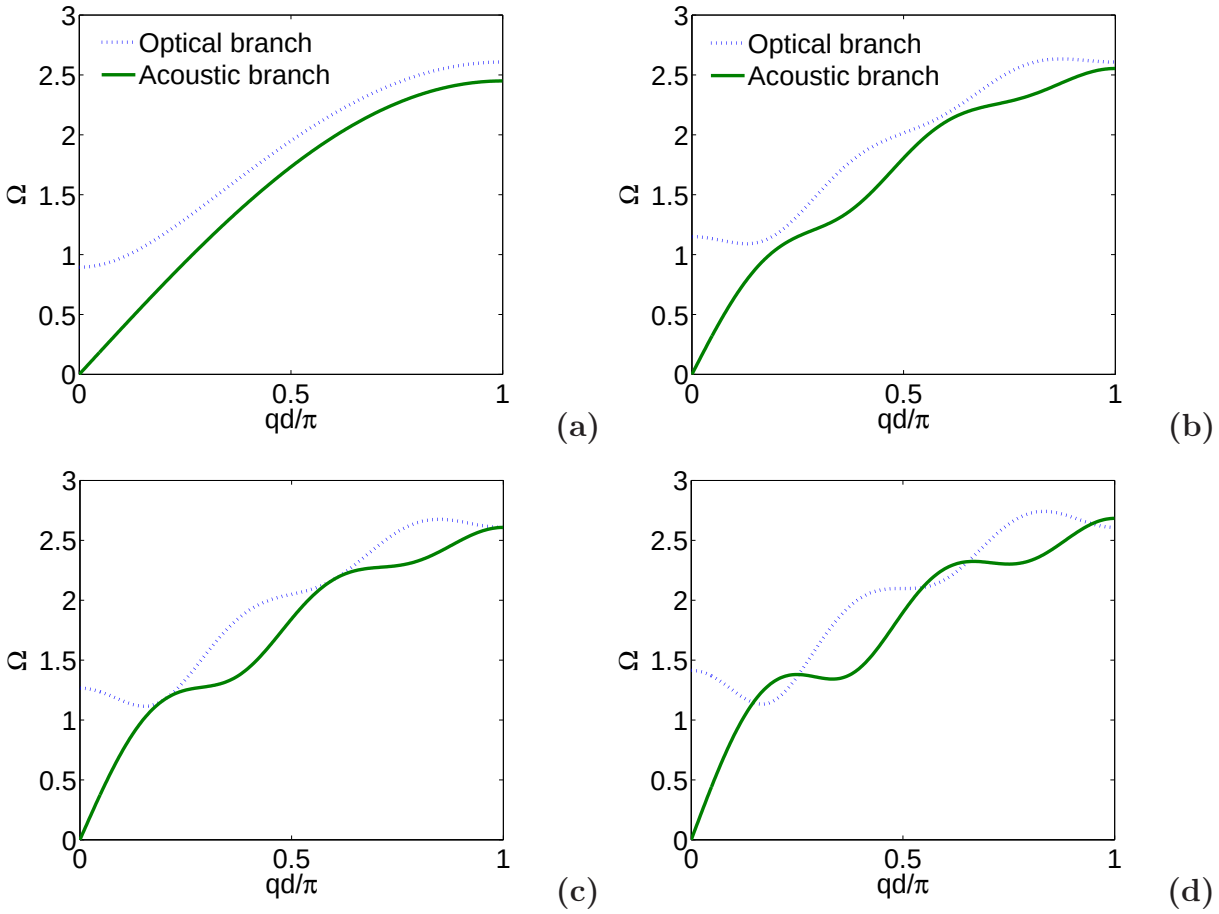

Figure 30: (Color online) Optical and acoustic frequencies as a function qd and for different values of K, $\beta = 1.5$ and $\alpha = 0.8$: Panel (a) shows the dispersion curves for $K = 0$. The curves are similar to those obtained for the modified discrete SG model. For $K = 0.13 < K_{cr}$, we have the configuration of panel (b). The dispersion curves oscillate and there is no crossing point between the optical and the acoustic curves. When $K = 0.2 = K_{cr}$, there is one crossing point. Panel (d) shows the dispersion curves for $K = 0.3 > K_{cr}$. In this case, there are two crossing points between the optical and the acoustic curves.

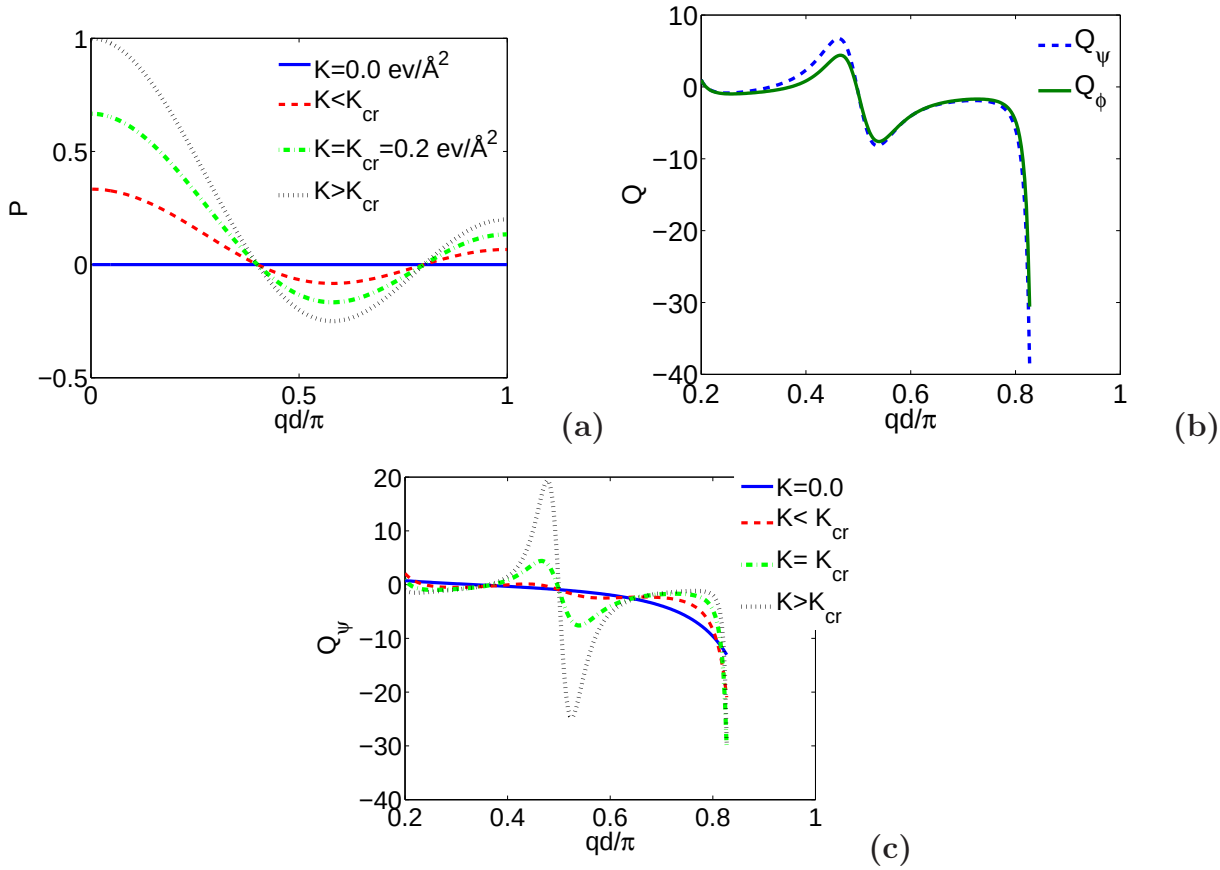

Figure 31: paramerters P and Q for different values of K

As for the dimensional parameters appearing in the model, we adopt those suggested in [Yam], i.e. $\alpha = 0.8$ eV/Å^2, $\beta = 1.5$ eV/Å^2; d=3.4Å.

3.6.2 Linear stability analysis of the single-mode excitation

In the single excitation mode, we decouple the two discrete CNLS equations by setting one of the components to zero. Thus, the system is described by only one discrete NLS equation. Taking, $\eta_m = 0$ leads us to the following single DNLS equation:

$$\frac{i}{2}(\chi_{m+1} - \chi_{m-1}) + \frac{iP}{2}(\chi_{m+h} - \chi_{m-h}) + Q_\psi \frac{\partial^2 \chi_m}{\partial \tau^2} + \gamma_{11}|\chi_m|^2\chi_m = 0. \tag{3.98}$$

From relation (3.94a), the approximate solution $\psi_n(t)$ of Eq. (3.92a) can be written as

$$\psi_n(t) = \epsilon\, \chi_m(\tau)\, \exp\{i(qnd - \Omega t)\} + \vartheta(\epsilon^2), \tag{3.99}$$

where, $\chi_m(\tau) = u_1^{(1)}(m, \tau)$. Note that the higher order correction to $\psi_n(t)$ is either explicitly expressed in terms of χ through expression up $u_1^{(1)}(m, \tau)$or by linear inhomogeneous differential

equations. This means that the theory is self-consistent and, in particular, that the overtones are by no means neglected.

The continuous version in Eq. (3.98) is a well-known model for boundary value problems in optical fibers.[119] Its discrete version (without the second term) has been found by Leon and Manna [78] using the same technique. The found modified equation thus takes helicity into consideration. For instance, in our knowledge, the DNA dynamics is the only system to be described by such an equation. Thus, it has stationary solutions in the form [78]

$$\chi_m = D \exp\left\{i(\delta m - \varrho\tau)\right\}. \tag{3.100}$$

This plane wave solution obeys the dispersion relation

$$\varrho^2 = -\frac{1}{Q_\psi}\left[\sin(\delta) - P\sin(h\delta) + \gamma_{11}|D|^2\right]. \tag{3.101}$$

By replacing P and γ_{11} by their expressions, we get the above nonlinear dispersion relation in the form

$$\varrho^2 = -\frac{1}{Q_\psi}\left[\sin(\delta) - \left(\frac{K_h\sin(hqd)}{K_s\sin(qd)}\right)\sin(h\delta) + \frac{c}{2K_s\sin(qd)}|D|^2\right]. \tag{3.102}$$

As we are considering a boundary value problem, ϱ and B are the given frequency and amplitude of the modulation. Modulated waves are then expected in the DNA model under study if the right-hand side of Eq.(3.102) is negative. In this frame, there is no real solution δ if

$$Q_\psi < 0, \quad |D|^2 > \frac{2}{c}\left[K_s\sin(qd)\sin(\delta) - K_h\sin(hqd)\sin(h\delta)\right] = D_{cr}^2. \tag{3.103}$$

The above relation represents the condition for a plane wave to be unstable in the modified discrete Yakushevich-like models. It is also a modification of the condition predicted by Leon and Manna [78] for a discrete Yakushevich-like models without the term of helicity.

In the case of the simple discrete Yakushevich-like model (without helicity) obtained for K=0, the highest value of the threshold amplitude is obtained for $\sin(\delta) = -1$.[78] In the case where helicity is taken into account, for $h = 5$, the right-hand side of Eq. (3.103) is positive for $\sin(\delta) = \sin(h\delta) = 1$, i.e.$\delta = \pi/2$. This means that

$$|D|^2 > \frac{2}{c}\left[K_s\sin(qd) - K_h\sin(hqd)\right] = D_{cr}^2. \tag{3.104}$$

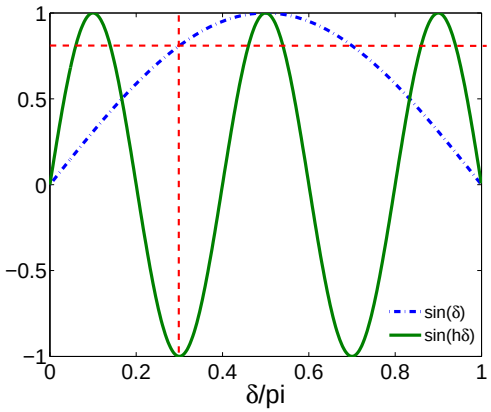

Figure 32: (Color online) The panel shows the plot of the functions $\sin(h\delta)$ (solid green curve) and $\sin(\delta)$ (dotted-dashed blue curve). The possible value of δ, which leads to the highest value of the threshold amplitude, is the one situated at the crossing point of the two red dashed lines,$\delta = 3\pi/10$.

However, this does not guarantee that the right-hand side of Eq.(3.103) is the highest for $\sin(\delta) = \sin(h\delta) = 1$. For example, it is possible that the expression in brackets is higher if $\sin(\delta)$ is a little bit smaller than 1 and $\sin(h\delta)$ is negative. To clarify this issue, we have plotted in Fig. 32 the functions $\sin(\delta)$ and $\sin(h\delta)$. The crossing point of the two red dashed lines indicates that the value which better satisfies our needs is $\delta = 3\pi/10$. For this value, $\sin(\delta)$ is 0.8 and $\sin(\delta)$ is -1. The corresponding threshold amplitude is therefore given by

$$|D|^2 > \frac{1.6}{c}\left[4K_s \sin(qd) + 5K_h \sin(hqd)\right] = D_{cr}^2. \tag{3.105}$$

The behaviors of the threshold amplitude will then be discussed with respect to the critical value K_{cr} derived in precedent section. Thus, our analysis will be based on two cases: when $K < K_{cr}$ and when $K > K_{cr}$. Therefore, the following manifestations of MI are observed:

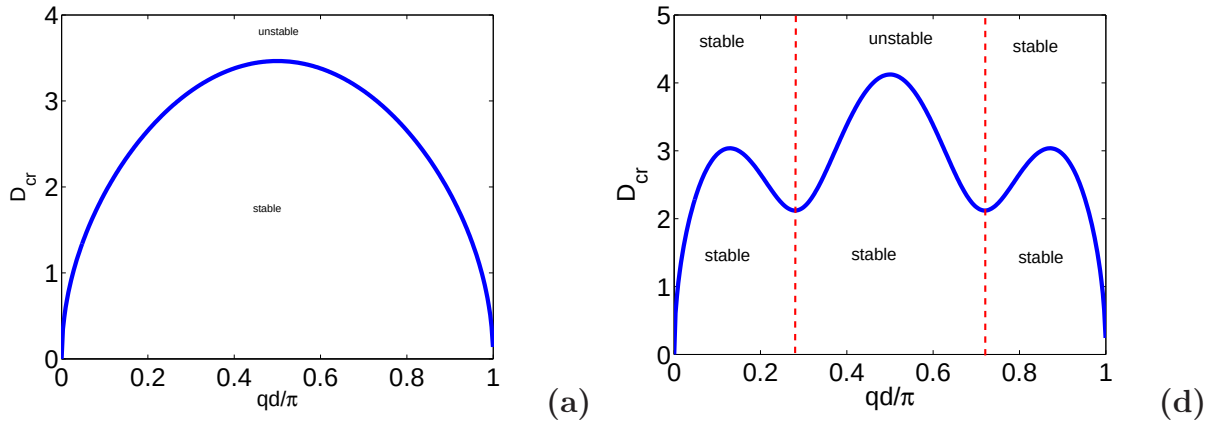

Figure 33: (Color online) The panels show the threshold amplitude Dcr for $\beta = 1.5$ and c=0.8: (a) $K = 0$. The result is similar to the one obtained by Leon and Manna (Ref. 27) for the discrete sG model. In the second panel, the threshold amplitude is plotted for $K = 0.5 > K_{cr}$. The amplitude has increased and the region of instability has been reduced due to helicity. The result is similar to the one obtained by Tabi et al. [120]

⁎ For $K = 0$, the system is described by Fig.33a The instability region belongs to the whole interval $[0, \pi]$ and there is only one sideband. These features confirm the results by Leon and Manna.[78]

⁎ For $K = 0.5 > K_{cr}$, we first observe that helicity breaks the instability domain into satellite sidebands (see Fig.33b), where the region between the two red dashed lines is the region of instability. Furthermore the instability region is reduced by the helicoidal structure of the molecule. Furthermore it is obvious that the amplitude has increased. We can say that the spiral effect reduces the stability zones. These features confirm the results by Tabi et al..[120]. Furthermore, we observe through the figure (34) that when the coefficient "c" increases the critical wave amplitude decreases and the stability zones are not changed. We can conclude that when the matching coefficient between the base pairs is high, the molecule vibrates with small amplitude, which increases the duration of denaturation.

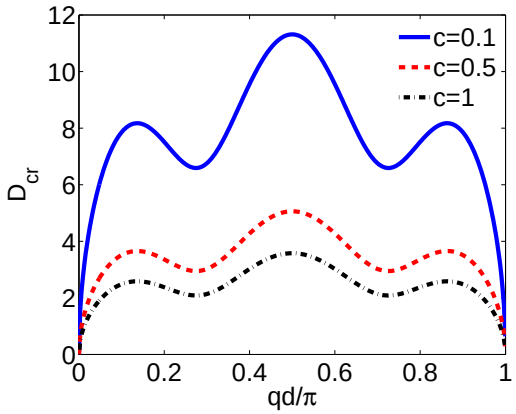

Figure 34: (Color online) The panels show the threshold amplitude Dcr vs qd for $\beta = 1.5$, $K = 0.5$ and for different values of c: The amplitude has decreased and the region of instability has been reduced due to pairing constant.

The behaviors displayed by the model under study show that this model can support large amplitude oscillation depending on the value of the helicoidal coupling constant K and the pairing coupling constant α. Such results prove that the present model is much richer than the simple discrete sG model,[121, 122, 123, 124] which only consider stacking interactions between neighboring pairs and which can be recovered here by letting $K = 0$ and $\alpha = 1$. In the framework of the PBD model, [127] it has also been shown that helicity can deeply modify the instability criterion (in comparison to the works of Peyrard and co-workers [125]) and can give rise to important behaviors in the process of soliton bearing through MI.

3.6.3 Modulational instability in the coupled-mode excitations

The most interesting dynamics of our model could be described through the coupled mode, which is the main concern of this work. The coupled mode imposes $\chi_m \neq 0$ and $\eta_m \neq 0$. We can reconsider the set of equations (3.95) being the coefficients of the discrete CNLS equations, which are plotted in figure34 versus qd

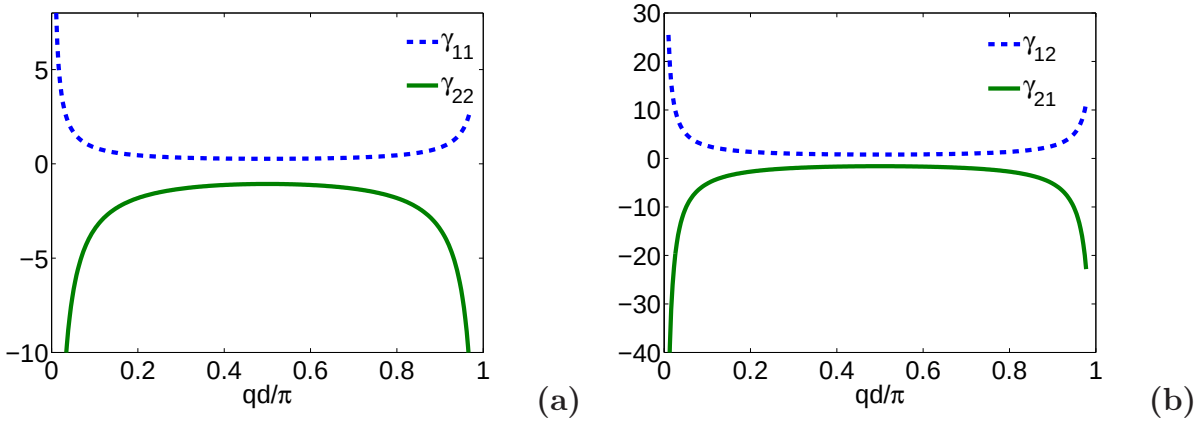

Figure 35: The plot of the coefficients γ_{ij} versus qd for $\alpha = 0.8$, $\beta = 1.5$

Eqs. (3.95) have an exact monochromatic wave solutions of the form

$$\chi_m = \chi_0 \exp i(q_\chi m - \omega_\chi t), \qquad \eta_m = \eta_0 \exp i(q_\eta m - \omega_\eta t), \tag{3.106}$$

which lead to dispersion relations

$$\begin{aligned} \omega_\chi^2 &= \frac{1}{Q_\psi}\left(\sin(q_\chi) + P\sin(hq_\chi) + \gamma_{11}\chi_0^2 + \gamma_{12}\eta_0^2\right), \\ \omega_\eta^2 &= \frac{1}{Q_\phi}\left(\sin(q_\eta) + P\sin(hq_\eta) + \gamma_{21}\chi_0^2 + \gamma_{22}\eta_0^2\right). \end{aligned} \tag{3.107}$$

For simplicity, we set $\omega_\chi^2 = \omega_\eta^2 = \omega^2$ and $q_\chi = q_\eta = k$. This gives rise to the following relation between χ_0 and η_0 putting $\sigma_\psi = \frac{1}{Q_\psi}$ and $\sigma_\phi = \frac{1}{Q_\phi}$:

$$\chi_0^2 = \frac{1}{\sigma_\phi\gamma_{21} - \sigma_\psi\gamma_{11}}\left[(\sin(k) + P\sin(hk))(\sigma_\psi - \sigma_\phi) + \eta_0^2(\sigma_\psi\gamma_{12} - \sigma_\phi\gamma_{22})\right]. \tag{3.108}$$

To examine the stability of the initial plane waves, we substitute

$$\chi_m = \chi_0\left[1 + \varepsilon_m(t)\right]\exp i(km - \omega t), \qquad \eta_m = \eta_0\left[1 + \xi_m(t)\right]\exp i(km - \omega t), \tag{3.109}$$

into Eq. (3.95), and we obtain a system of two coupled linearized equations for perturbations ε_m and ξ_m:

$$\begin{aligned} &i(\varepsilon_{m+1} - \varepsilon_{m-1})\cos(k) - (\varepsilon_{m+1} + \varepsilon_{m-1} + 2\varepsilon_m)\sin(k) \\ &+ P\left[i(\varepsilon_{m+h} - \varepsilon_{m-h})\cos(kh) - (\varepsilon_{m+h} + \varepsilon_{m-h} + 2\varepsilon_m)\sin(hk)\right] \\ &- Q_\psi(2i\omega\dot{\varepsilon}_m + \omega^2\varepsilon_m) + \gamma_{11}\chi_0^2(\varepsilon_m + \varepsilon_m^*) + \gamma_{12}\eta_0^2(\xi_m + \xi_m^*) = 0, \\ &i(\xi_{m+1} - \xi_{m-1})\cos(k) - (\xi_{m+1} + \xi_{m-1} + 2\xi_m)\sin(k) \\ &+ P\left[i(\xi_{m+h} - \xi_{m-h})\cos(kh) - (\xi_{m+h} + \xi_{m-h} + 2\xi_m)\sin(hk)\right] \\ &- Q_\phi(2i\omega\,\dot{\xi}_m + \omega^2\xi_m) + \gamma_{21}\chi_0^2(\xi_m + \xi_m^*) + \gamma_{22}\eta_0^2(\varepsilon_m + \varepsilon_m^*) = 0. \end{aligned} \tag{3.110}$$

Furthermore, we assume a general solution of the above-mentioned system as

$$\varepsilon_m = D_1 e^{i(Qm-\Omega t)} + D_2^* e^{-i(Qm-\Omega^* t)}, \qquad \xi_m = D_3 e^{i(Qm-\Omega t)} + D_4^* e^{-i(Qm-\Omega^* t)}, \tag{3.111}$$

where, Q and Ω are the wave number and frequency of perturbation, respectively. We arrive at a set of four homogeneous equations for D_1, D_2, D_3 and D_4. This set of homogeneous equations can be written in matrix form as

$$M \times (D_1, D_2, D_3, D_4)^T = 0, \tag{3.112}$$

where M is a 4×4 matrix given by

$$M = \begin{pmatrix} a_{11}+\Omega & a_{12} & a_{13} & a_{14} \\ a_{21} & a_{22}-\Omega & a_{23} & a_{24} \\ a_{31} & a_{32} & a_{33}+\Omega & a_{34} \\ a_{41} & a_{42} & a_{43} & a_{44}-\Omega \end{pmatrix}, \tag{3.113}$$

with

$$\begin{aligned}
a_{11} &= \frac{\sigma_\psi}{2\omega}\big[-2\sin(Q)\cos(k) - 4\sin(k)\cos^2(\frac{Q}{2}) \\
&- P(2\sin(Qh)\cos(hk) + 4\sin(hk)\cos^2(\frac{hQ}{2})) - Q_\psi\omega^2 + \gamma_{11}\chi_0^2\big], \\
a_{12} &= a_{21} = \gamma_{11}\chi_0^2, \quad a_{13} = a_{14} = a_{23} = a_{24} = \gamma_{12}\eta_0^2 \\
a_{22} &= \frac{\sigma_\psi}{2\omega}\big[2\sin(Q)\cos(k) + 4\sin(k)\cos^2(\frac{Q}{2}) \\
&+ P(2\sin(Qh)\cos(hk) + 4\sin(hk)\cos^2(\frac{hQ}{2})) - Q_\psi\omega^2 + \gamma_{11}\chi_0^2\big], \\
a_{33} &= \frac{\sigma_\phi}{2\omega}\big[-2\sin(Q)\cos(k) - 4\sin(k)\cos^2(\frac{Q}{2}) \\
&- P(2\sin(Qh)\cos(hk) + 4\sin(hk)\cos^2(\frac{hQ}{2})) - Q_\phi\omega^2 + \gamma_{21}\chi_0^2\big], \\
a_{34} &= a_{43} = \gamma_{21}\chi_0^2, \quad a_{31} = a_{32} = a_{41} = a_{42} = \gamma_{22}\eta_0^2, \\
a_{44} &= \frac{\sigma_\phi}{2\omega}\big[2\sin(Q)\cos(k) + 4\sin(k)\cos^2(\frac{Q}{2}) \\
&+ P(2\sin(Qh)\cos(hk) + 4\sin(hk)\cos^2(\frac{hQ}{2})) - Q_\phi\omega^2 + \gamma_{21}\chi_0^2\big].
\end{aligned} \tag{3.114}$$

The dispersion relation, which determines Ω as a function of Q and k, and parameters system, including the MI diagram , is obtained from the condition of the existence of nontrivial solutions of the algebraic linear homogeneous system $det(M) = 0$, which amounts to a quartic equation for

Ω. Thereafter, we solve the condition of the existence of nontrivial solutions using a MATLAB code and we represent the stability/instability diagram give by the fig. 36

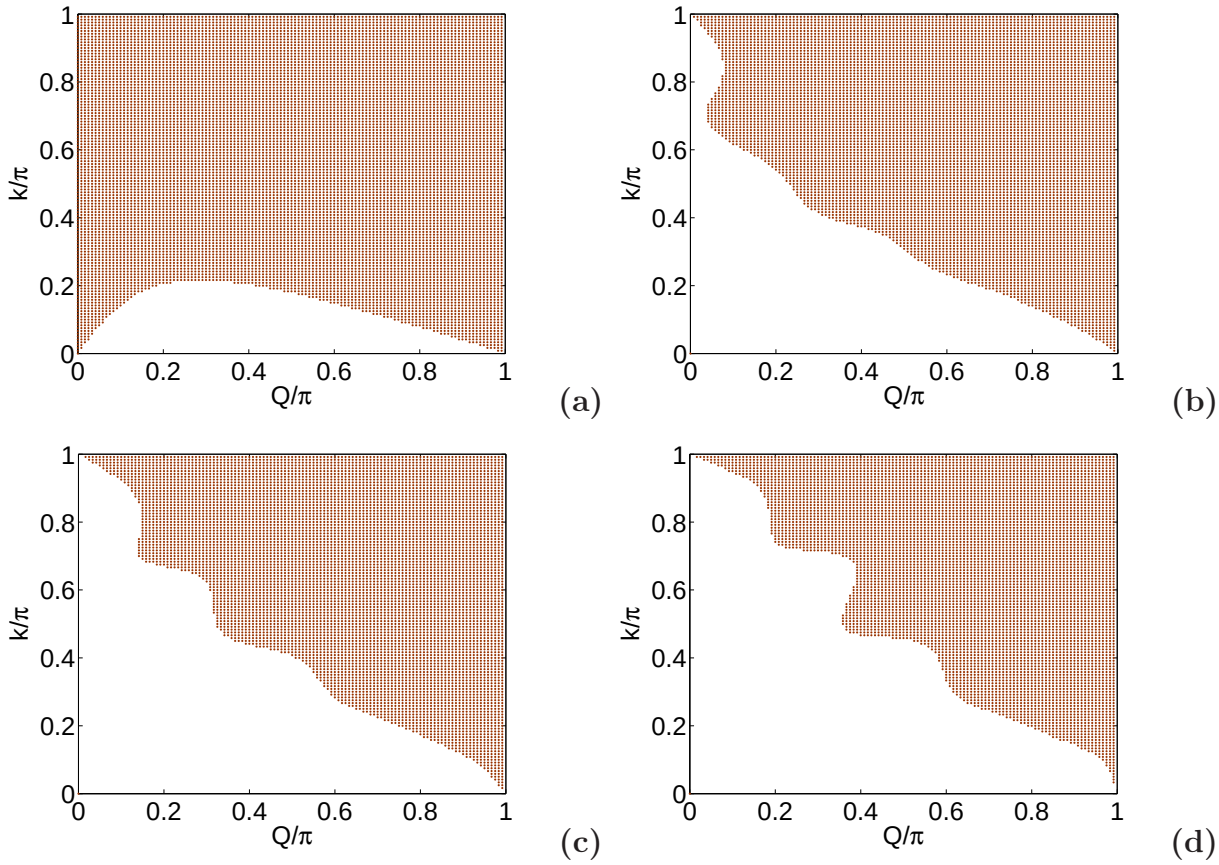

Figure 36: (Color online) Stability/ instability diagrams in the (Q, k) plane for (a) K=0; (b) $K < K_{cr}$; (c) $K = K_{cr}$; (d) $K > K_{cr}$ an for $\alpha = 0.8$, $\beta = 1.5$, $qd = 0.7\pi$

Another main features of the MI is highlighted in Fig. 36. Thus, the instability/stability diagram is plotted in the (K,Q) plane. White regions represent zone of stability, while dark one indicates the zone of instability.

Figure 35(a) displays the MI diagram for $K = 0$. Figures 36(b) and 36(c) have been plotted for $K < K_{cr}$ and $K = K_{cr}$, respectively; figure 36(d) have been plotted for $K > K_{cr}$. We observe in these figure that, as K grows, regions of MI increase.

3.6.4 Numerical analysis of modulational instability

Considering the equation system 3.92, and asking $\phi_n = 0$ in both equations we get the modified sG equation. due to the interaction between nonlinearity and dispersion effect, the main effects of MI which refers to very large growth of certain modulation wave side bands flat nonlinear propagating in a dispersive medium is generating structure located. We will therefore make numerical simulations of the instability of a plane wave in the modified sG equation to

highlight some features of MI in the model of DNA studied (Yakusevich model). In this simulation, we focus particularly on the result of the interaction between the stack and helical effect in the bearing patterns of localized waves, then comparisons are made between the numerical results and the analytical predictions made in section **??**. However, it is important to emphasize that this is when the amplitude of the disturbance is small compared with that of the carrier wave that the linear stability analysis is based on linearization around the carrier undisturbed. Anyway, when the amplitude of an unstable sideband grows exponentially, the nonlinear approximation should failed to time scale. In addition, the linear stability analysis neglects additional combination of waves generated by a wave mixing process, which, though small at the initial stage, can become significant at large time scales if the wave number is in an area of instability. Linear stability analysis, therefore, can not tell us the evolution of long of a plane wave modulated nonlinear.

In this frame, we have performed numerical simulations of the modified discrete sG equation (3.92a) with $\phi_n = 0$ using the standard fourth-order Runge-Kutta scheme with an integration time scale $\Delta t = 0.5$. The initial condition in accordance with Eq. (3.99) is a modulated wave. The number of base pairs has been chosen so that we do not encounter wave reflection at the end of the molecule and periodic boundary conditions have been used. As already announced, two cases have been considered: the case $K \leq K_{cr}$ and the case $K > K_{cr}$. For the two cases, we have chosen $\epsilon = 0.01$, $qd = 0.4\pi$, and $\varrho = 0.3\pi$.

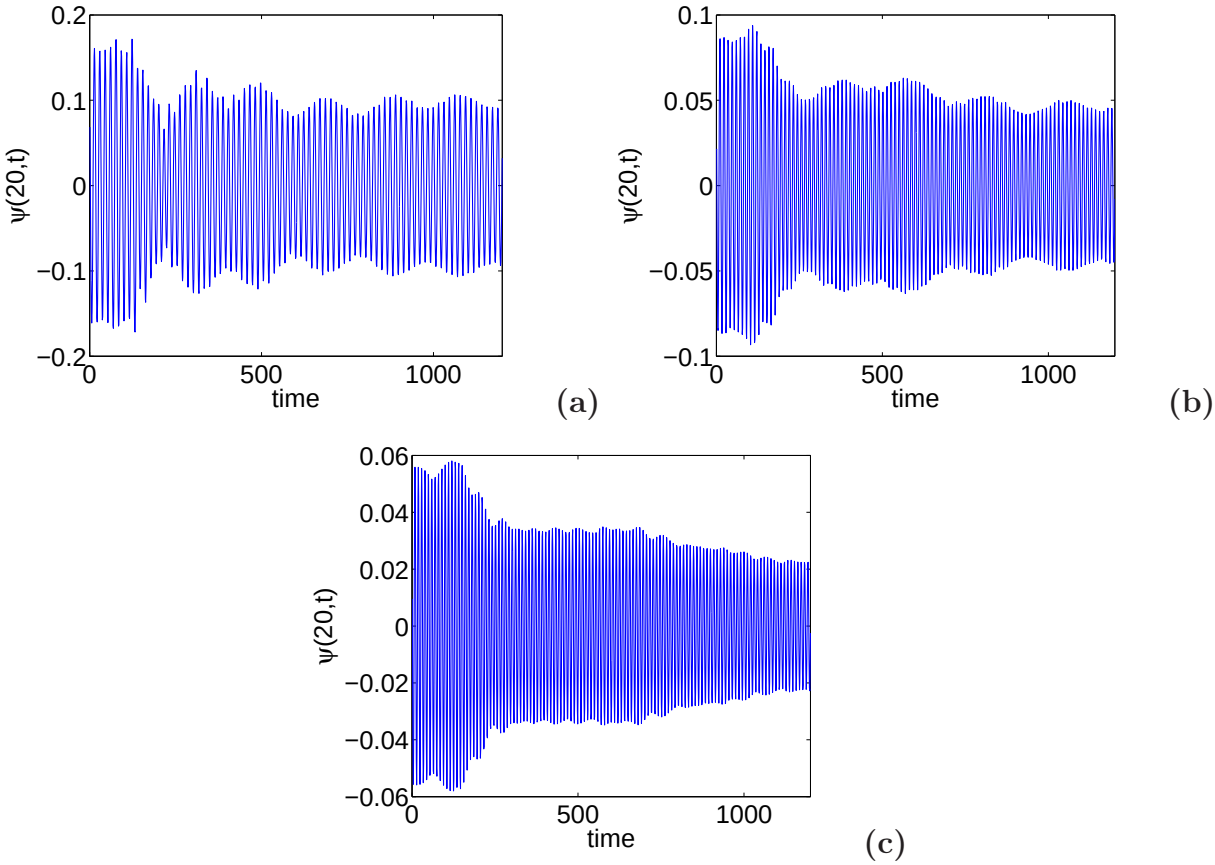

Figure 37: (Color online) Dynamics of modulated waves as a function of time units (t.u.) showing the MI of slowly modulated plane waves for $K \leq K_{cr}$. Solitonlike objects at the base pair 20 for (a) c=0.1; (b) c=0.5 and (c) c=1. The system undergoes slight oscillations which mitigates for large values of coefficient c. So, for the considered case, modulations are not efficient and cannot ensure better transmission of information within the double helical structure.

When the nearest-neighbor effect is more important in the system, i.e., $K \leq K_{cr}$, we have the features displayed in Fig. 36. We see that the plane wave excitation breaks into trains of waves, which have the appearance of multisoliton shapes with breathing motion. Attention is paid to the oscillations of the bases 20 . We observe that the oscillations disappear when the pairing coefficient increase, also the amplitude decrease when this coefficient increse . This confirms our analytical predictions and once more shows that MI is a crucial issue for soliton instability, and is also considered a precursor to soliton formation because it typically occurs in the same parameter region as that where solitons are observed. When the effect of the helicoidal coupling becomes important, i.e., $K > K_{cr}$, one obtains the results depicted in Fig. 37. Even in this case, the plane wave breaks into trains of solitonlike structures. But the amplitude of waves is higher than in the first case and oscillations are obvious. At base pair n=7, one clearly observes that the wave pattern dis-played is that of an extended wave that propagates with a breathing motion. in this case, the modulation is more important.

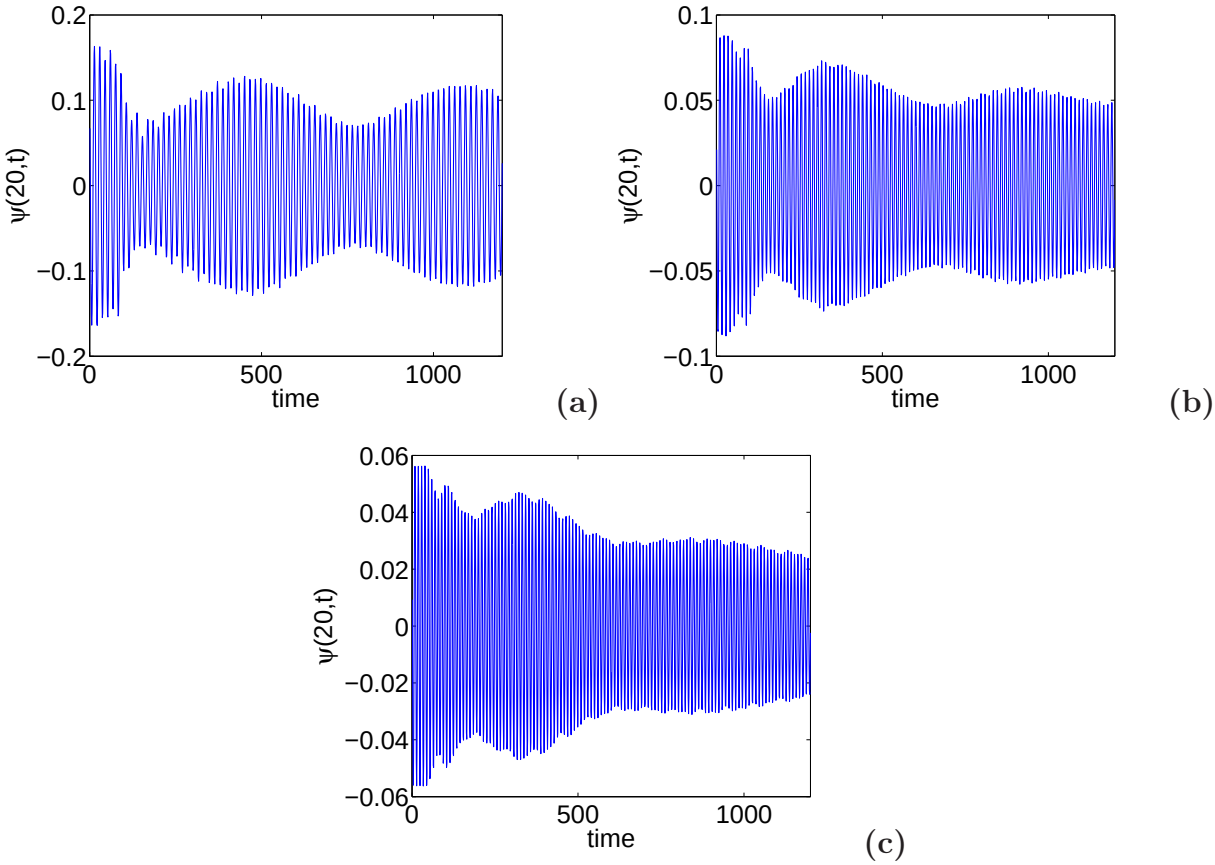

Figure 38: (Color online) Dynamics of modulated waves as a function of time units (t.u.) showing the MI of slowly modulated plane waves for $K > K_{cr}$. Solitonlike objects at the base pair 20 for (a) c=0.1; (b) c=0.5 and (c) c=1. Solitonlike objects at the base pair 10. Oscillations for this case are more efficient, but which mitigates for large values of coefficient c and clearly show that when $K > K_{cr}$, data are better transmitted within the DNA model. This brings out the importance of helicoidal models over the simple model that only take into consideration nearest-neighbor coupling.

One could then relate these exact breathing motions and the increasing of the amplitude to the presence of helicoidal terms. The corresponding values of the helicoidal coupling parameter $K > K_{cr}$ cause better and more efficient modulation of waves. This simply means that when such a condition is fulfilled, there is a better information transfer through the molecule. Also, such behaviors cannot be observed for $K \leq K_{cr}$, which, once more, suggest the importance of the helicoidal stacking interactions. on the other hand, the pairing interaction cause rather the disappear of oscillation; this means that, on should chose the small values of c for the better information transfer through the molecule.

As part of this work, we left the model of Yakusevich (DNA torsional dynamic), taking into account the helical part of the molecule, we obtained the Hamiltonian (3.91) deriving this Haliltonien, we obtained the equation (3.92) and by the limited development of thermal cosine and sine up to order 3 system, we got the equation (3.93). To investigate MI, we have first derived from the original mode simpler limit equation, all which results to be the discrete NLS

equation in discrete space and with space and time exchanged. This universal limit is obtained by a very general approach called expired multiple scale perturbation analysis. This study leads us to discrete CNLS equation (3.95). We first study the linear stability by putting $\Phi_n = 0$. The MI criterion has-been reported about to be a modification of the one reported by Leon and Manna [78] due to the presence of helical terms and by Tabi et al. due to the presence of pairing coefficient [120].

A critical value of the helical coupling parameter has-been derived and on the basis of the chosen parameter values, there has been established a relationship betweens MI and the critical value K_{cr} of K. It has, been found that for $K \leq K_{cr}$, the system does not feel the presence of helical term. When $K > K_{cr}$, the analytical analysis predicts MI wide amplitude oscillations as seen in the framework of the PBD model. Other hand, the MI criterion has been plotted in function of pairing coefficient, and we see that the critical amplitude decrease when the coefficient c increases. From the diagram stability/instability, it has been found that, the helical term decreases of instability zone.

Numerical experiments have been carried out in order to confirm the analytical predictions. It has been observed that in the case where $K \leq K_{cr}$, there is MI since the initial modulated plane wave breaks into train of extended solitons and solitonlike objects. When $K > K_{cr}$, the amplitude of the waves is higher than in the first case and the oscillations is more important. In both previous cases, not only the oscillations tend to disappear, the wave amplitude decreases as rapidly as c increases. This can be analyzed as the action of the waves flowing in the molecule and which plays an important role in the conformational concerns taking place in the B-DNA molecule. On the other hand, the increase in the amplitude of the waves trains mainly with helical coefficient describes the action of RNA polymerase, which breaks progressively the hydrogen bonds for the messenger RNA to come and copy the genetic code, And decreasing the amplitude of the pairing coefficient reflects the interaction of the wave with many loads (phonon) within the molecule. We believe that the existence and the formation of solitons in the DNA molecule could be a proper candidate to explain how data are exchanged during basic biological phenomena such as transcription and replication. As it is well known, for the hydrogen bonds to be broken, there should be a concentration of the enzyme and of the energy brought through the hydrolysis of adenosine triphosphate (ATP) [120].

3.7 Coherent modes and parameter selection in DNA models with finite stacking enthalpy

We analyze the possibility of coherent modes for DNA dynamics in a general model recently proposed by Joyeux and Florescu [129]. We show that the value they used for their results are not suitable to describe wave propagation in DNA. We therefore investigate parameter values in order to obtain coherent solitary waves with characteristics that are know experimentally.

We consider the Joyeux- Buyukdagli model of DNA. This model, introduced recently by Joyeux and Buyukdagli,[130, 131, 110] brings about a modified stacking interaction term. In fact, more than 19 years ago, Peyrard and Bishop [40] showed that stacking interaction are of importance in the process of transcription.

From the Hamiltonian of this model and following the process developed in the chapter 2, we got the NLS equation:

$$iF_{1\tau} + PF_{SS} + Q|F_1|^2F_1 = 0, \tag{3.115}$$

where, $\tau = \epsilon^2 t$; $S = Z - V_g T$; $T = \epsilon t$; the group velocity $V_g = \frac{d\omega}{dq} = \frac{k_2 sin(ql)}{\omega}$. P and Q are the pseudo constant given by:

$$P = \frac{d^2\omega}{dq^2} = \frac{k_2 cos(ql) - V_g^2}{2\omega}, \tag{3.116}$$

$$Q = \frac{1}{2\omega}\{ -12k_4[2cos(ql) - cos^2(ql) - 1] - 2\omega_g^2\alpha(\delta + 2\mu) - 3\beta\omega_g^2\}. \tag{3.117}$$

The solution of Eq.(3.115) exists if PQ>0, and is given by

$$y_n(t) = 2\varepsilon A sech[\varepsilon(nl - Vet)/Le][cos(\Theta nl - \Omega t) + 1/2\mu\varepsilon A sech[\varepsilon(nl - Vet)/Le] + \delta cos[2(\Theta nl - \Omega t)]], \tag{3.118}$$

where

$$Ve = Vg + \varepsilon u_e, \quad \Theta = q + \frac{\varepsilon u_e}{2p}, \quad p = \frac{l^2 k_2 cos(x) - v_g^2}{2\omega},; \quad mu = -2\alpha, \quad \delta = \frac{\alpha\omega_g^2}{3\omega_g^2 + 16k_2(sin(ql/2))^4}$$
$$\Omega = \omega + \frac{\varepsilon u_e(Vg + \varepsilon u_e)}{2p}, \quad A = \sqrt{\frac{ue^2 - 2u_e u_c}{2PQ}}, \quad Le = \frac{2P}{\sqrt{u_e^2 - 2u_e u_c}},$$
$$\omega = \sqrt{\omega_g^2 + 4k_2(sin(ql/2))^2}, \quad v_g = \frac{lk_2 sin(ql)}{\omega}, \tag{3.119}$$

u_e, and u_c being the velocity of the envelope and the carrier waves, respectively. The model under our study depends on two groups of parameters. Some of them are coming from the mathematical procedure: ϵ, u_e, and u_c. We can therefore introduce parameters U_e and η defined as

$$U_e = \epsilon u_e, \qquad \eta = \frac{u_c}{u_e}. \tag{3.120}$$

This allows us to reduce the number of parameters to be studied in this work. ϵA and L/ϵ can therefore be written as

$$\epsilon A = A_0 = U_e\sqrt{\frac{1 - 2\eta}{2PQ}}, \qquad \frac{L_e}{\epsilon} = L = \frac{2P}{U_e\sqrt{1 - 2\eta}}. \tag{3.121}$$

The above notations are possible if $\eta \in [0;\ 0.5]$. In their recent works, Zdravkovic et al.[132] showed that the requirements for the coherent mode can be fulfilled if

$$V_e = v_g + U_e = \frac{\Omega}{\Theta}, \tag{3.122}$$

Table 1: values of y_m, Λ and V_e for different values of $N(ql = 2\pi/N)$ and for a=4.45Å^{-1}, m=300 a.m.u., D=0.04 eV, $k_b = 10^{-5}$ eV.Å^{-2},$\Delta H = 0.44eV$, b=0.10Å^{-2}, and C=2

N	y_m(Å)	$\lambda(m)$	$V_e(m.s^{-1})$
6	0.3530	0.7	317.3358
7	0.3538	0.8642	345.7395
8	0.3555	0.9206	362.3898
...	...	...	...
12	0.3624	1.0108	390.7933
...	...	...	...
20	0.3701	1.0463	403.5260

.

An expression for the velocity, $Ue = \epsilon ue$ can consequently be written as

$$U_e = \frac{Pq}{1-\eta}\left[\sqrt{1 + \frac{2(1-\eta)(\omega - qv_g)}{Pq^2}} - 1\right]. \tag{3.123}$$

This allows us to delete the most troublesome dimensionless parameter ϵ. Furthermore, from Eqs. 3.118 and 3.121, the wave amplitude will be given by

$$y_m = 2A_0\left[1 + A_0\left(\frac{\mu}{2} + \delta\right)\right]. \tag{3.124}$$

Finally, the coherence of the soliton solution of the model we study will be effective if the number of the nucleotide pairs covered by a single soliton is known. In this frame, the corresponding density is given by

$$\Lambda = \frac{2\pi L}{l} = \frac{4\pi P}{U_e l\sqrt{1-2\eta}}. \tag{3.125}$$

It was shown in Refs. [132, 133], that q is a wavenumber of the carrier component of the soliton. Assuming that the wave covers an integer number of nucleotides, we also introduce an integer number N such that

$$ql = \frac{2\pi L}{N}. \tag{3.126}$$

The second group of parameters is so called intrinsic parameters. They describe chemical interactions and geometry of the DNA molecule. These parameters are:

- the above defined wavenumber q of the linear approximation
- a harmonic stacking constant K_b which describes the stiffness of nucleotides
- the stacking enthalpy $\Delta H/C$
- the depth of the Morse potential D
- the inverse width of the Morse potential a.

Table 2: values of y_m, Λ and V_e for different values of $N(ql = 2\pi/N)$ and for a=6Å^{-1}, m=300 a.m.u., D=0.048 eV, $k_b = 4.0.10^{-4}$ eV.Å^{-2},$\Delta H = 0.409eV$, b=0.80Å^{-2}, and C=4

N	y_m(Å)	$\lambda(m)$	$V_e(m.s^{-1})$
6	0.2559	1.0085	625.870
7	0.2564	1.1385	678.7463
8	0.2579	1.2152	711.0676
...	...	...	...
12	0.2642	1.3347	763.9569
...	...	...	...
20	0.2715	1.3781	784.5250

.

As announced in the beginning of this paper, two groups of values have been proposed by Joyeux and Florescu [130]. The corresponding set of parameter values are 1. C=2, $\Delta H = 0.44eV$, D=0.048 eV, a=4.45Å^{-1} $k_b = 10^{-5}$eV.Å^{-2} b=0.80Å^{-2}, a=6Å^{-1}, D=0.048 eV, $k_b = 4.0.10^{-4}$ eV.Å^{-2},$\Delta H = 0.409eV$, b=0.80Å^{-2}, and C=4.

The only unknown parameters are q and η. Since we deal with an homopolymer, all the bases have the same mass m = 300 amu. For that reason, we have investigated the values of the three important parameters y_m, Λ and V_e for different values of the integer N and we have fixed $\eta = 0.47$. [132] From Tables I and II, we see that the requirement presented so far are not fulfilled. This is sufficient to conclude that those values are not suitable for the description of the coherent mode in DNA.

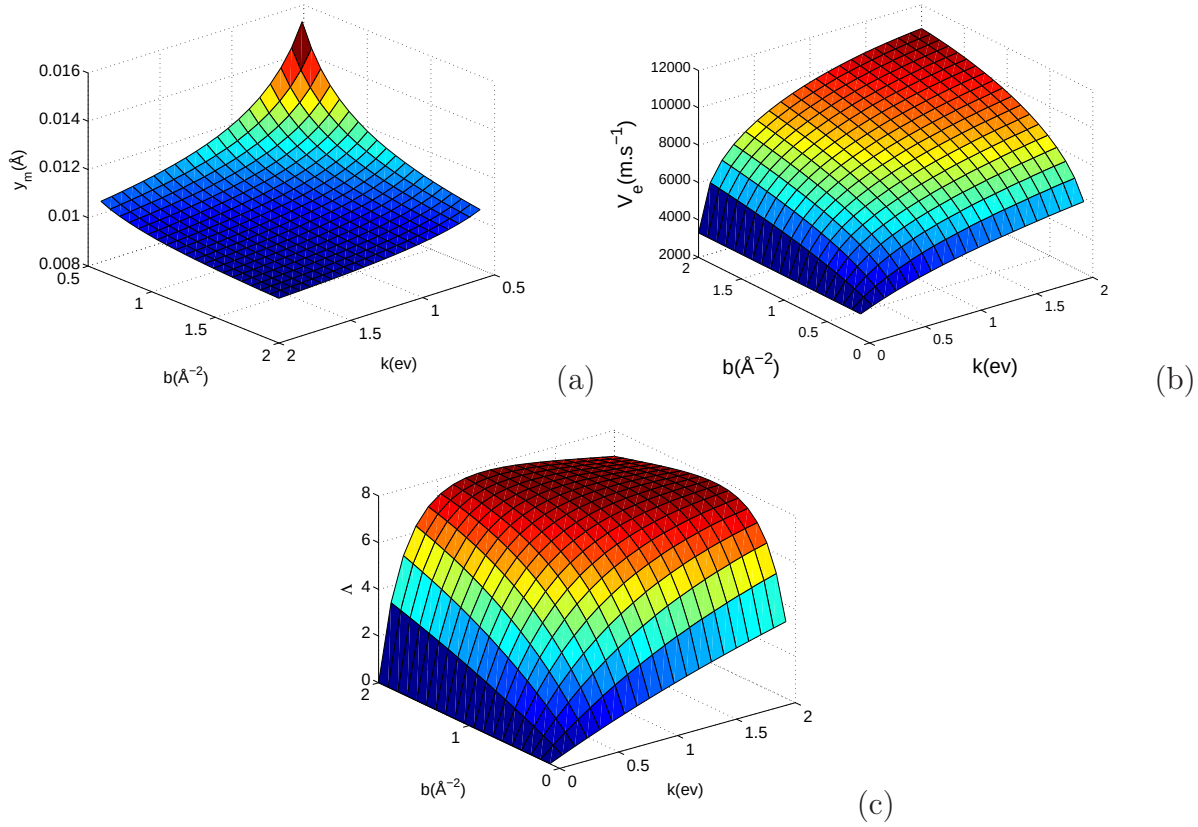

Figure 39: The panels show the surface plot of: (a) the wave amplitude y_m, (b) velocity V_e and (c) width Λ for a=1.2Å^{-1}, m = 300 amu., D=0.07 eV, $k_b = 4.0.10^{-4}$ eV.Å^{-2}

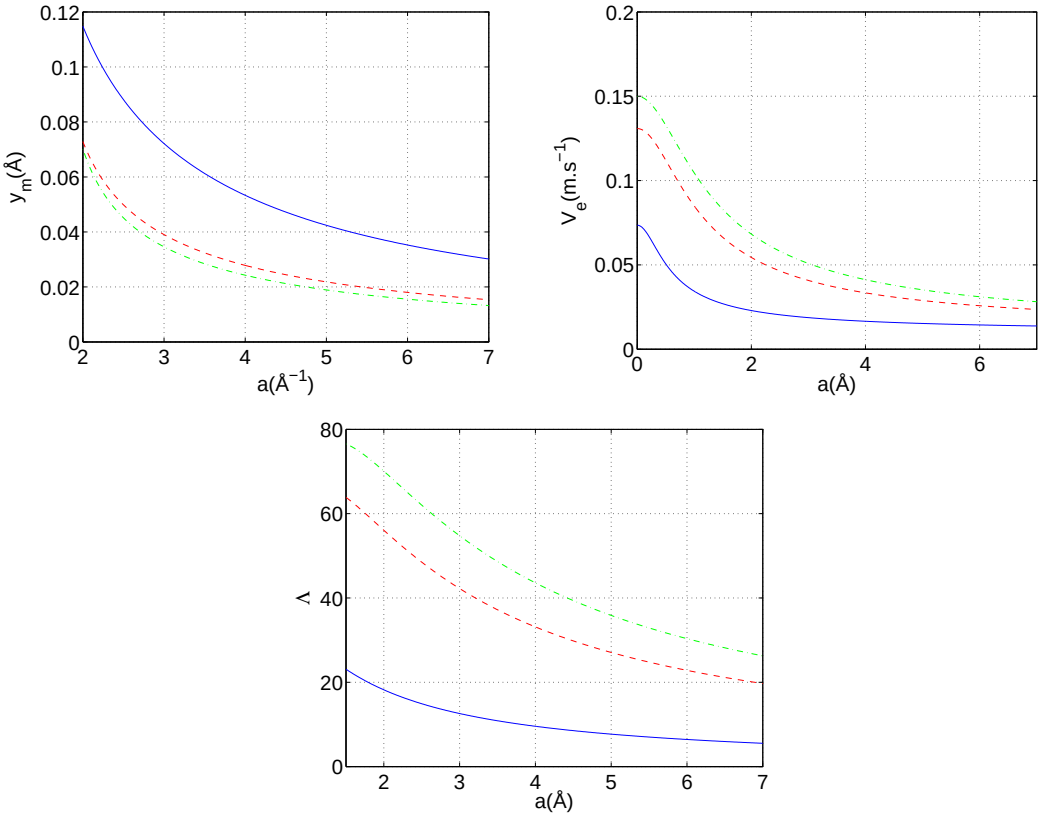

Figure 40: The panels show the plot of the three parameters y_m V_e and Λ versus a for three values of k: $k = 0.22eV$(blue line) $k = 0.80eV$ (red dashed line), and $k = 1.074eV$ (green dotted-dashed line),with N=20, m = 300 amu., D=0.07 eV, $k_b = 4.0.10^{-4}$ eV.Å^{-2} b=0.25Å^{-2}

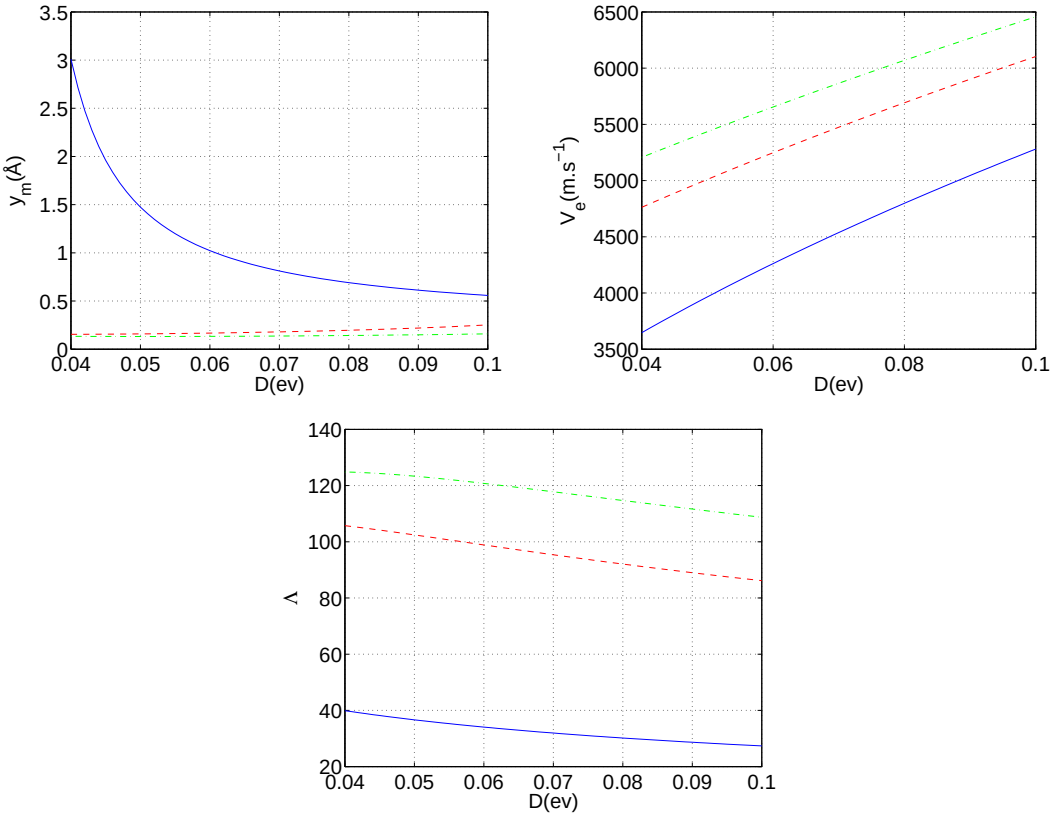

Figure 41: The panels show the plot of the three parameters y_m V_e(a) and Λ versus D for three values of k: $k = 0.22eV$(blue line) $k = 0.80eV$ (red dashed line), and $k = 1.074eV$ (green dotted-dashed line),with N=20, m = 300 amu., $k_b = 4.0.10^{-4}$ eV.Å^{-2} b=0.25Å^{-2}

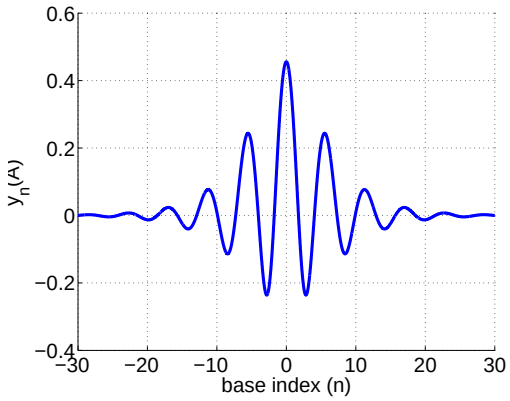

Figure 42: The nucleotide pair stretching for $k = 1.074eV$, m=300 amu., $k_b = 4.0.10^{-4}$ eV.Å^{-2} a=1.2Å^{-1}, $D = 0.07eV$, b=0.25Å^{-2}

It therefore becomes of interest to propose other parameter values in order to obtain the expected characteristics. As proposed in Ref. 11, 12, we fix $N = 20$ and introduce a parameter $k = \Delta H/C$ Furthermore, let us for example use the values of a and D proposed by Zdravkovi‘c

et al.,[132, 134] i.e., a=1.2Å^{-1}, D=0.07 eV, We also keep the stiffness parameter with the value $k_b = 4.0.10^{-4}$ eV.Å^{-2}. We have therefore plotted the three important parameters as functions of b and k. The corresponding surface plots show that it is possible to find values for b and k that give rise to the expected values for y_m V_e(a) and Λ and These values for b and k are found in the intervals [0, 0.5] and [0.80, 1.5], respectively. For the rest of the paper, we fix b = b=0.25Å^{-2} and we look for the value of k that can be used to explain DNA breathing using the model under our study. For this purpose,we also fix $D = 0.07eV$ and we plot y_m V_e and Λ versus a, for different values of k.

It comes out that the value of $k = 1.074eV$ is the one leading to expected characteristics for $a \in [1, 1.5]$, as depicted in Figure 40. If we take the value a=1.2Å^{-1} for example, we get: $y_m = 0.2448$Å, $Ve = 1740.5m.s^{-1}$, and $\Lambda = 35.6l$.

The same procedure has been adopted to investigate the interval where the suitable value for D can be found. We have therefore fixed a=1.2Å^{-1} and the interval [0.07, 0.1], for $k = 1.074eV$, has been revealed to be the most probable. Fixing $D = 0.07$, we have confirmed that $k = 1.074eV$ is the value of the stacking enthalpy where coherent localized modes could be observed in the present anharmonic model of DNA dynamics. In order to confirm our investigations, we have plotted, in Figure 42, the corresponding solution (3.118) for the proposed value of k, with a=1.2Å^{-1} $D = 0.07eV$. It displays the expected features of DNA breathing.

We have pointed out that the values proposed by Joyeux and Florescu are not suitable to describe DNA breathing and base pair oscillations in terms of solitonic waves. We have therefore investigated parameter values in order for the conditions on the wave amplitude, velocity and width to be fulfilled. It was reported that a transcription bubble covers about 17 nucleotides, RNA-DNA hybrid about 8, while RNA-polymerase covers about 35 nucleotides. On the other hand, the corresponding velocity ranks from 1740 to 2040 m/s, while the amplitude of the wave is to be found between 0.18 to 0.3 Å.

3.8 Soliton like solution of the DNA molecule

We study soliton solutions of the DNA molecule which takes into account helicity and solvent interaction. The small amplitude dynamics of the model is described by envelope solutions. The stability of the solutions has been checked through numerical simulations.

3.8.1 Model and twist effect on breather-like solutions

Let us start by considering the so-called B-form of the DNA molecule described in section (3.5). Our starting point is Eq. (3.69). For the small, but yet nonlinear oscillations of the nucleotides at the position n we can assume [135, 136]

$$y_n = \epsilon \Phi_n, \qquad \epsilon \ll 1, \tag{3.127}$$

which means that the nucleotides oscillate around the bottom of the Morse potential well. However, those oscillations are still large enough to be enharmonic. To obtain the function Φ_n, we use the semi-discrete approximation [135, 137] and look for the wave solution to be a modulated solitonic wave

$$\Phi_n(t) = F_1(\epsilon nl, \epsilon t)e^{i\theta_n} + \epsilon[F_0(\epsilon nl, \epsilon t) + F_2(\epsilon nl, \epsilon t)e^{i2\theta_n}] + cc + (\epsilon^2), \tag{3.128}$$

where cc stands for the complex conjugate and $\theta_n = nql - \omega t$, l is the distance between neighboring nucleotides of the same strand, ω is the optical frequency of the linear approximation, $q = 2\pi/\lambda$ is the wave number of a carrier wave. The functions F_0 and F_2 can be expressed through F_1, while the function F_1 is a solution of the following equation [135, 138]

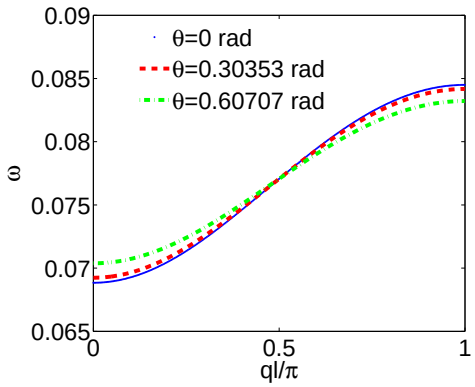

Figure 43: Dispersion curve as a function of the wave number q for different values of θ. K=60meV.Å^{-2}, $f_s = 0.3$, $l_s = 3$Å

$$iF_{1\tau} + PF_{SS} + Q|F_1|^2F_1 = 0, \tag{3.129}$$

where τ and S are rescaled time and space variables. Equation (3.129) is the nonlinear Schrödinger equation. The coefficients of Eq. (3.129) are given by

$$\begin{aligned} P &= \frac{l^2(K_1 - S_1)\cos(ql) - v_g^2}{2\omega}, \\ Q &= \frac{1}{2\omega}[2K_3(2 + cos(2ql)) - 6S_3(3 + \cos(2ql) + 4\cos(ql)) \\ &- 3K_5 + \chi(4K_4 - 32\cos^2(\frac{ql}{2})) + \delta(2K_4 - 8K_2(\cos(ql) + \cos^2(ql))], \end{aligned} \tag{3.130}$$

with $\chi = \frac{K_4 - 8K_2\cos^2(\frac{ql}{2})}{\omega_0^2 + 2S_1}$, $v_g = \frac{l(K_1 - S_1)sin(ql)}{\omega}$, $\delta = \frac{K_4 - 4K_2(\cos(ql) + \cos^2(ql))}{\omega_0^2 - 4\omega^2 + 4K_1\sin^2(ql) + 2S_1\cos(2ql)}$ and, $\omega^2 = \omega_0^2 + 2S_1\cos(ql) + 4K_1\sin^2(\frac{ql}{2})$.

Figure 43 plots the dispersion relation versus the wave number q for different values of the twist angle θ. Let us use the standard semi-discrete approximation [135] i.e., restrict ourselves to excitations that consist of a slowly varying envelope solution by modulating a carrier wave, with the dispersion relation of a nonlinear wave.

Figure 44 depicts for different value of θ, the dispersion coefficient P (Fig. 44(a)), the nonlinear coefficient Q (Fig. 44(b)) and product PQ (Fig. 44(c)), as a function of the wave number of the carrier wave q.

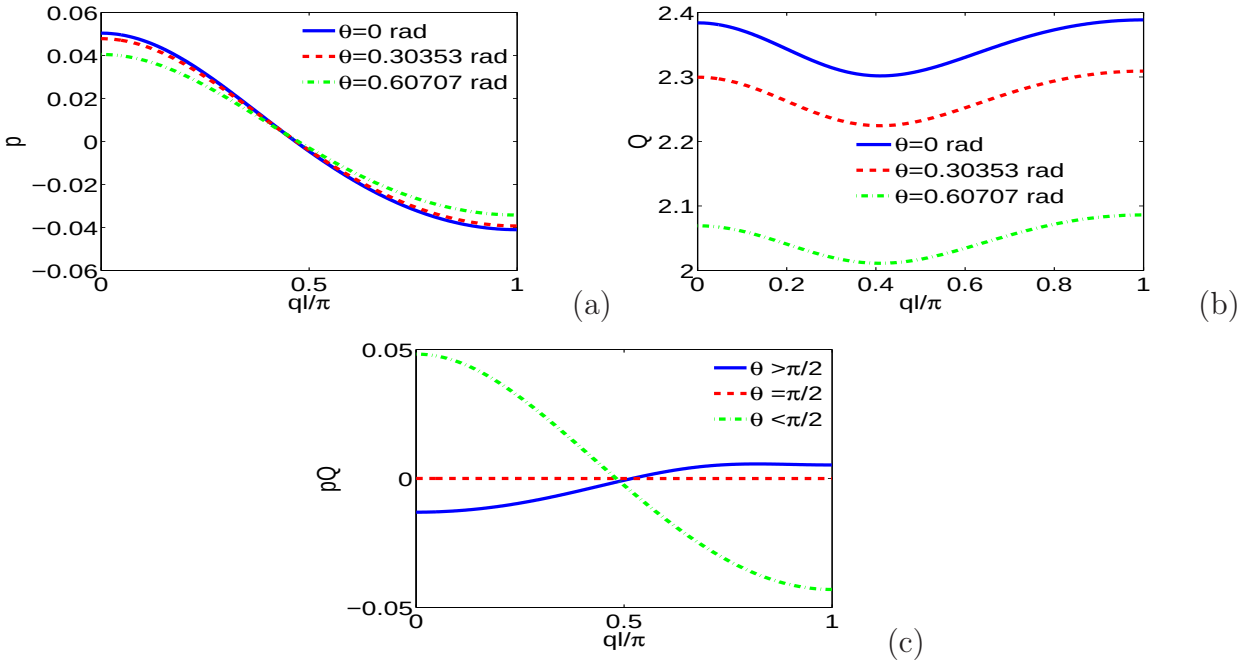

Figure 44: Coefficients of the NLS equation as a function of the wave number (a) Dispersion parameter P (b) The nonlinear coefficients Q (c) The product PQ. K=60meV.Å^{-2}, $f_s = 0.3$, $l_s = 3$Å

From Fig. 44(c) we note that, for $\theta < \frac{\pi}{2}$ the product PQ > 0 in the range $0 < ql < \frac{\pi}{2}$, while it becomes negative in the range $\frac{\pi}{2} < ql \leq \pi$. Besides, PQ=0 for $\theta = \frac{\pi}{2}$. But, for $\theta > \frac{\pi}{2}$, one has an inverse phenomenon. We have noted that the parameters l_s and f_s don't influence on the sign of the product PQ. Also, one can see in Fig. 44(c) that this product depends on θ Analytic solutions of the NLS equation depend on the signs of PQ. Negative values of PQ lead to a finite-amplitude plane wave called dark-soliton (or an envelope hole) which does not correspond to the small amplitude limit of breather modes. For positive PQ, one has the following solution

$$y_n(t) = 2\epsilon A sech[\frac{\epsilon(nl - V_e)}{L_e}] \times \{\cos(\Theta nl - \Omega t) + \epsilon A sech[\frac{\epsilon(nl - V_e)}{L_e}] \times (\frac{\chi}{2} + \delta\cos(2\Theta nl - 2\Omega t))\} + 0(\epsilon^3), \tag{3.131}$$

where the amplitude A and the width L_e have the forms

$$A = \sqrt{\frac{u_e^2 - 2u_e u_c}{2PQ}}, \quad L_e = \frac{2P}{\sqrt{u_e^2 - 2u_e u_c}}, \tag{3.132}$$

with

$$V_e = v_g + \epsilon u_e, \quad \Theta = q + \frac{\epsilon u_e}{2P}, \quad \Omega = \omega + \frac{\epsilon u_e}{2P}(v_g + \epsilon u_c), \tag{3.133}$$

v_g is the group velocity, u_e and u_c are the velocity of the envelope and the carrier waves, respectively. As DNA is a dispersive system the group velocity v_g can be obtained from the dispersion relation $\omega = \omega(q)$. Solutions (3.132) are plane wave solutions, which are unstable because of modulation (or Benjamin-Feir) instability, and a local envelope solution with a vanishing amplitude at the wing. Such a solution has the appropriate shape to represent breathing modes in DNA. One notes that this solution depends on the twist angle as well as on the solvent interaction term.

Let us use the parameters U_e and η defined as:

$$U_e = \epsilon u_e; \qquad \eta = \frac{u_c}{u_e}. \tag{3.134}$$

The parameter η represents a measure for modulation. The width L_e and the amplitude A_0 can be rewritten as

$$\epsilon A = A_0 = U_e \sqrt{\frac{1 - 2\eta}{2PQ}}; \quad \frac{L_e}{\epsilon} = L = \frac{2P}{U_e\sqrt{1 - 2\eta}}. \tag{3.135}$$

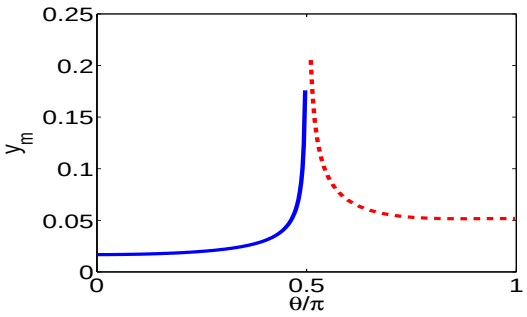

Figure 45: The maximum amplitude y_m as a function of θ. K=60meV.Å^{-2}, $f_s = 0.3$, $l_s = 3$Å

From this equation one sees that η belongs to the interval $[0; 0.5]$. The signal is modulated if η is close to its limits of 0.5. To determine the value of of the parameter U_e, one assumes a coherent mode [136, 138] for which the envelope and the carrier wave velocities are equal, i.e.

$$V_e = U_e + v_g = \frac{\Omega}{\Theta}. \tag{3.136}$$

Consequently, the function $y(t)$ is the same at any position n. The wave preserves its shape in time. We can easily obtain U_e as follows

$$U_e = \frac{Pq}{1-\eta}[\sqrt{1+\frac{2(1-\eta)(\omega-qv_g)}{Pq^2}}-1]. \tag{3.137}$$

The amplitude will be given by

$$y_m = 2A_0[1+A_0(\frac{\chi}{2}+\delta)]. \tag{3.138}$$

The amplitude y_m is shown in Fig. (45) for different valuer of q as a function of θ. Figure (45) shows that the maximum amplitude increases with increasing value of θ provided that $q < \pi/2$. But, the maximum amplitude is a decreasing function of θ for $q > \pi/2$. For angles around 0.5π, the amplitude increases/decreases exponentially and one can observe big fluctuation describing openings/closing of bases pairs, even to weak temperature. The twist θ_{eq} is found to yield the highest stability also for other sequences obtained by varying order and relative content of AT- and GC-pairs. The equality of velocities defined in Eq. (13) brings about the equality of the densities of internal oscillation D_0 as [136, 138]

$$D_0 = \frac{\Lambda}{\lambda_c}, \tag{3.139}$$

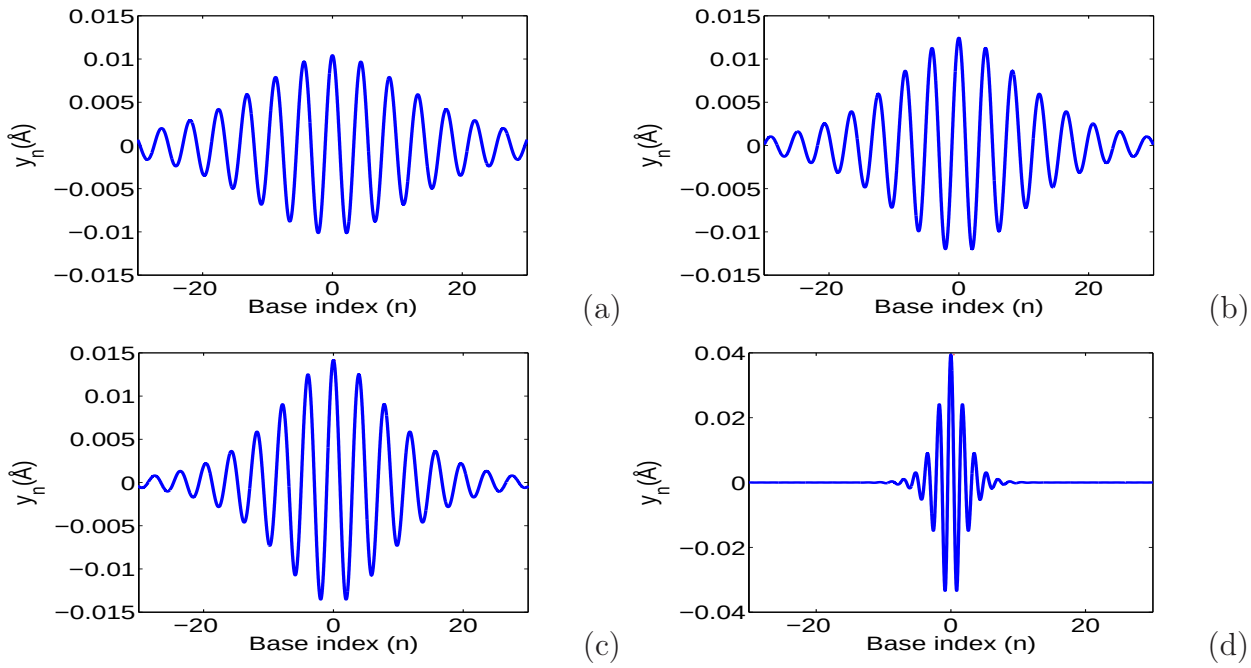

Figure 46: The nucleotide pair stretching for (a) $\theta = 0$, (b) $\theta = \theta_{eq} = 0.1923\pi$,(c) $\theta = 0.25\pi$; (d) $\theta = 0.45\pi$. K=60meV.Å^{-2}, $f_s = 0.3$, $l_s = 3$Å

where, Λ and λ_c are the length of the envelope and the wavelength of the carrier wave, respectively. To be more precise, this is a number of the carrier wavelengths per an envelope

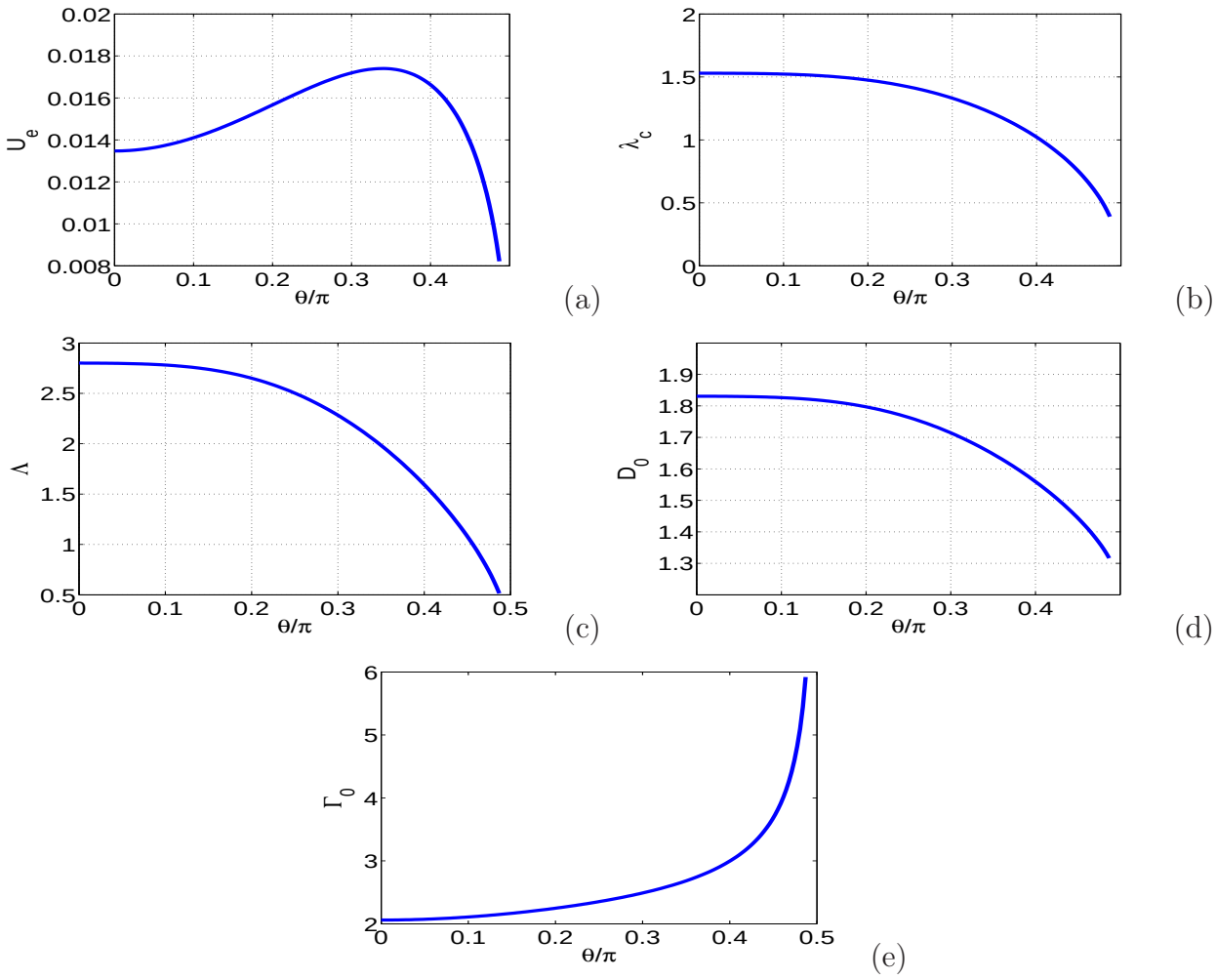

Figure 47: (a) Parameter U_e as a function of θ, (b) Parameter λ_c as a function of θ, (c) Parameter Λ as a function of θ, (d) Parameter D_0 as a function of θ, (e) Parameter Γ_0 as a function of θ.

$$\Lambda = \frac{2\pi L_e}{\epsilon} = \frac{2\pi P}{U_e\sqrt{1-2\eta}}, \qquad \lambda_c = \frac{2\pi}{\Theta} = \frac{2\pi}{q + \frac{\epsilon u_e}{2P}}. \tag{3.140}$$

So, Eq. (3.140) takes the form

$$D_0 = 1 + \frac{2qP}{\epsilon u_e}. \tag{3.141}$$

D_0 describes the solitonic solution $y(nl)$ which is Eq. ((3.132)), for a particular value of t. One can also define the density of internal oscillations (density of carrier wave oscillations) Γ_0 as a ratio of two periods

$$\Gamma_0 = \frac{\Omega}{\epsilon V_e/L_e}. \tag{3.142}$$

But, for $v_g \gg \epsilon u_e$, which might not be always correct, one easily obtains

$$\Gamma_0 = 1 + \frac{2\omega P}{\epsilon u_e v_g}. \tag{3.143}$$

Figure 46 displays the spatial evolution of the transverse stretching y_n for different value of the twist angle. These breather-like solutions have been previously obtained through the DNA molecule [137]. One see in this case that the dynamics of the breather-like solutions depend on the twist angle. Numerical simulations have shown that discrete breathers, which are spatially localized nonlinear oscillations, can appear in models of crystal, biomolecules, and many others nonlinear discrete systems [139, 140], he constituting a mechanism for the transport of energy and information along discrete systems[141].

Figure 47 illustrates the dependence of U_e, λ_c, Λ, D_0 and Γ_0 with the twist angle θ. We remark that all these quantities which characterize the breather-like solutions are function of the twist angle.

3.8.2 Numerical analysis and twist angle/solvent effect

The results discussed in the previous section are only approximated ones since they are obtained not from the initial equations of motion (**??**) but from the NLS equation (6) derived after some hypothesis. The behavior of solutions through the entire network is studied while integrating the equation (**??**) by the iterative method of fourth-order Runge-Kutta scheme. We choose absorbing boundary conditions to avoid an artificial large amount of radiations that can affect the creation process and the dynamics of localized structures. Under these boundary conditions, the time step has been chosen to conserve the energy to an accuracy better than 10^{-6} over a complete run. Most of the simulations are performed with a molecule of N = 600 base pairs and we use initial conditions given by Eq. (3.132)

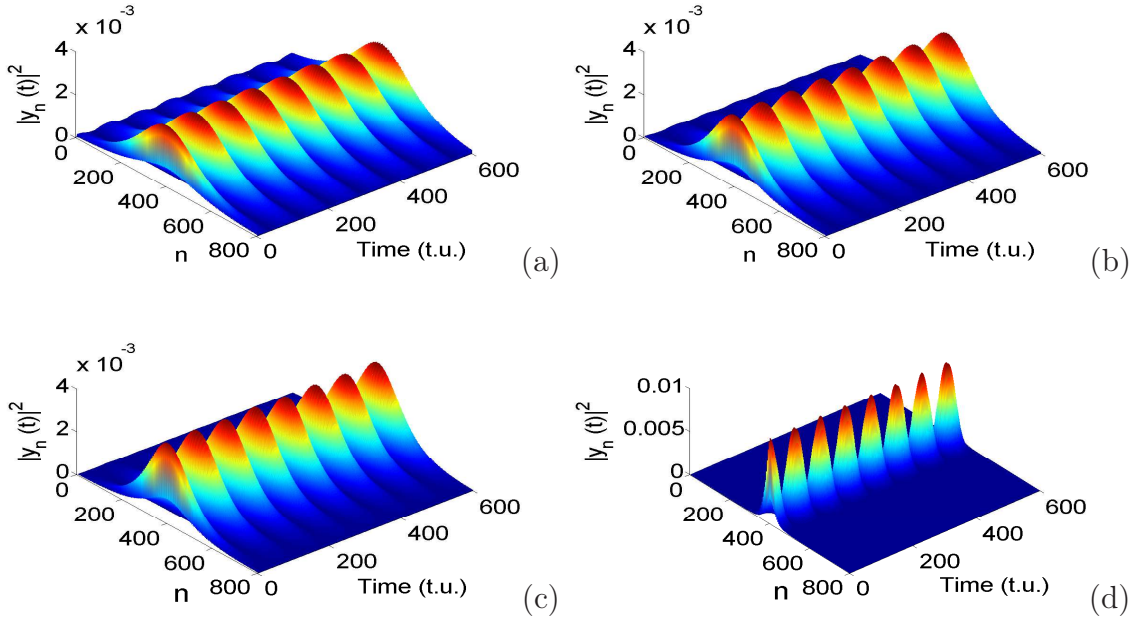

Figure 48: (Color online) Temporal behavior of breather-like solution for different value of the twist angle θ. (a) $\theta = 0$, (b) $\theta = \theta_{eq}$; (c) $\theta = 0.25\pi$; (d) $\theta = 0.45\pi$. K=60meV.Å^{-2}, $l_s = 3$Å.

It was explained above that the main purpose of this paper was to bring out the impact twist angle and the one of solvent interaction. As a first case, let us study the effect of θ on the dynamics of the system ($f_s = 0$). Figure 48 shows the temporal behavior of the breather solution through the twisted DNA molecule for different values of the twisted angle θ. Figure 48(a) represents the untwisted DNA molecule ($\theta = 0$), Fig. 48(b), 48(c) and 48(d), have been, respectively, plotted for $\theta = \theta_{eq}$, $\theta = 0.25\pi$ and $\theta = 0.45\pi$. The temporal evolution of waves depict that, as θ increases, the width of the pulse becomes more narrow while the amplitude of the pulse grows. The transmission of conformational changes over large distances along the double helix have been discussed by Polozov and Yakushevich[142]. They show that nonlinear solitary waves are a suitable model for describing the transmission. Also, nonlinear solitary waves can be used as regulatory signals propagating along DNA to the problem of gene regulation.

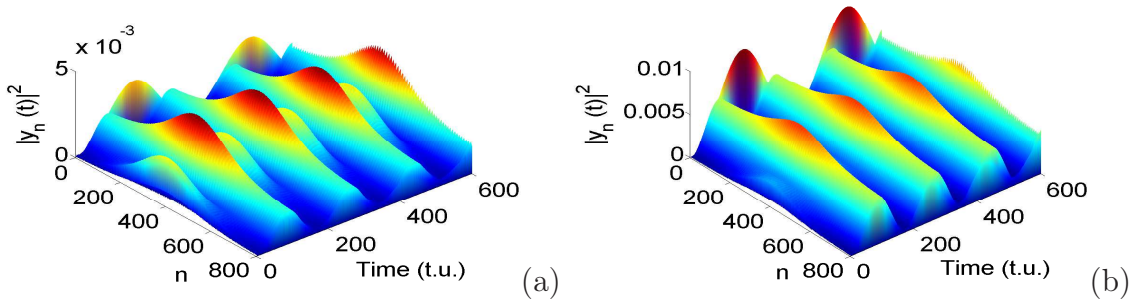

Figure 49: (Color online) Time evolution of breather-like solution for different value of the solvent interaction. (a) $f_s = 0.1$, (b) $f_s = 0.3$. K=60meV.Å^{-2}, $\theta = 0$ $l_s = 3$Å.

we note through this figure that the introduced solutions change in discreet breathers. Indeed, the existence of breathers in the discreet networks had been suggested by Dauxois [143] and later, of the numeric simulations made by Dauxois [127] proved that the localized oscillations, as those that we got, are precursors and describe bubbles observed at the time of the thermal denaturation of the DNA better. It testifies of more than once the action of RNA-polymerase and the energy generated by the hydrolysis of the Triphosphate Adenosine (ATP) that contribute to break links hydrogens binding the two sprigs. it is otherwise fame that the discreet breathers are very steady and doesn't know any modifications during the time. They are therefore some valid candidates to transport the energy and loads in general in the discreet networks and in biomolecules in particular.

Let us now examine the effect of the solvent interaction along the molecule ($\theta = 0$). Figure 8 shows the results of this study. If we compare Fig. 48(a) ($\theta = f_s = 0$), we see that the solvent interaction bring a modulation between pulses, while only the maximum amplitude of the pulses were uniform, the solvent interaction increases the width of pulses while the amplitude certain pulses increases with time as shown in Fig. 49(a). As f_s increases, the number of pulses decrease with time as depicted in Fig. 49(b). The base pair displacements should become large enough to yield those fluctuational openings which are peculiar of the double helix dynamics and, at the same time, too large base pair fluctuations should be discouraged as they destabilize the system already at room temperature. The stacking potential has the capability to select the appropriate fluctuation amplitudes as a function of the twist.

Now, we study the combine effect of the twist angle and solvent interaction on the twisted DNA with solvent interaction ($\theta \neq 0$ and $f_s \neq 0$). Figure 50 presents the results of this study for different values of θ and f_s. One sees in Fig. 50 that, the combine effect of these two terms are recovered along the molecule. When f_s is took into account, the pulses become broad. While θ increases, the width of the pulses becomes narrow and the amplitude of increases. Figure 50(a) and 50(b) have been plotted for $\theta = 0.25\pi$ and $f_s = 0.1$, $f_s = 0.3$, respectively. While Fig. 50(c) and 50(d) have been obtained for $\theta = 0.45\pi$ and $f_s = 0.1$, $f_s = 0.3$, respectively.

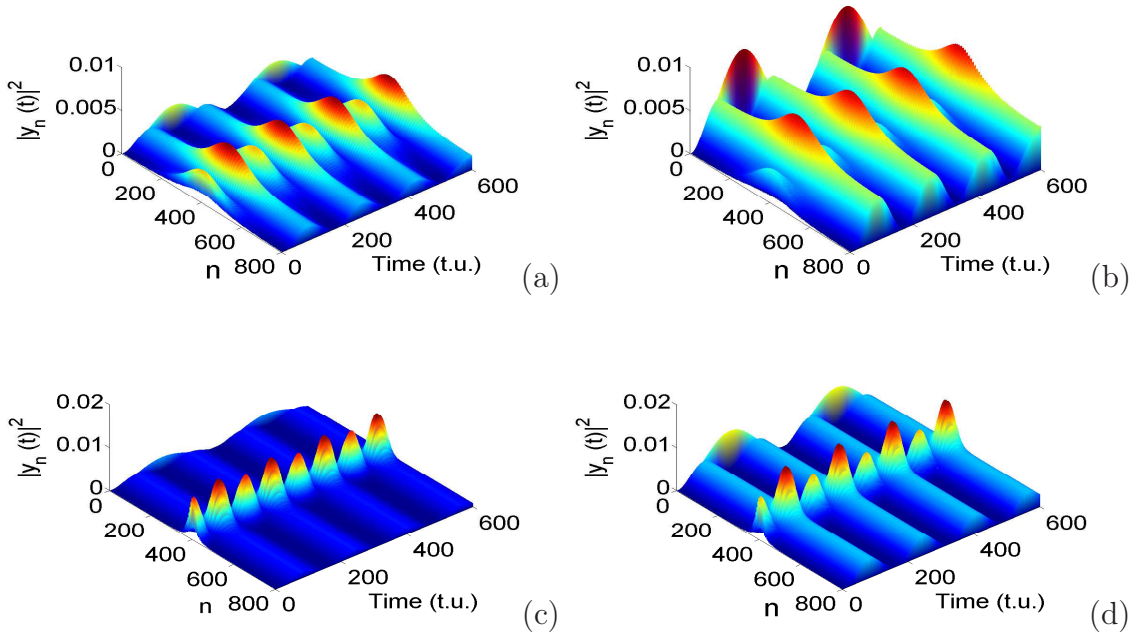

Figure 50: (Color online) Combine effect of twist angle and solvent interaction on the time evolution of breather-like solution. (a) $f_s = 0.1$, $\theta = 0.25\pi$; (b) $f_s = 0.3$, $\theta = 0.25\pi$; (c) $f_s = 0.1$, $\theta = 0.45\pi$; (d) $f_s = 0.3$, $\theta = 0.45\pi$and for K=60meV.Å^{-2}, $\theta = \theta_{eq}$ $l_s = 3$Å.

We have considered the twisted DNA with solvent, looking for solitary wave excitations. In the semi-discrete approximation, the motion equation of the molecule has been reduced to the NLS equation. The twist angle and the solvent interaction term introduce some modification in the nonlinear coefficient Q as well in the dispersion parameter P. Then, envelope soliton solutions of the NLS equation have been obtained. The condition for the existence of these solutions have been obtained and depend on θ. These solutions have been affected by the presence of the twist angle. Increasing θ decreases the width of the pulse while the amplitude increases. Numerical experiments have been carried out in order to verify the analytical predictions. It has been observe that the obtained solutions are stable during the propagation. The impact of the twist angle as well as the one of the solvent interaction term have been investigated. It is found that while increasing θ leads to ultra short pulses, f_s leads to broad oscillations which correspond better to the fluctuational openings of DNA.

The fig.46 and fig.48 show that, for the small twist models, $\theta \ll \theta_{eq}$, large fluctuations are possible; Hence, such large fluctuations do contribute to denaturation of molecule. It follows that molecules with small twist have scarce stability and begin to denaturate below room temperature [144]. On the other hand, in large twist models with $\theta \gg \theta_{eq}$ small fluctuations have stacking energies which are higher than the hydrogen bonds dissociation energy hence, their contributions to the denaturation become vanishingly small.

3.9 Bright and dark structures of the DNA molecule with higher-order effects

The study of solitary wave solutions is of prime significance for nonlinear physical systems. The Peyrard-Bishop model for DNA dynamics is generalized specifically to include the difference among bases pairs. The small amplitude dynamics of the model is studied analytically and reduced to the CQNLS equation and the exact bright and dark soliton solutions is obtained through the DNA molecule. These amplitude solutions are made of bubble solitons. The impact of elasticity on DNA dynamic is also presented. The profile of solitary wave structures is displayed for some fixed parameters.

3.9.1 Model and equation of motion

We consider the PB model as described in section 1 and 2 with the equations of motion given by

$$m\ddot{y_n} = k(y_{n+1} - 2y_n + y_{n-1}) + 2\sqrt{2}aD(e^{-2a\sqrt{2}y_n} - e^{-a\sqrt{2}y_n}). \tag{3.144}$$

We expand e^{-ay_n} until the second and third orders, respectively. This leads to the modified equation

$$\ddot{y_n} = \omega_0^2(y_{n+1} - 2y_n + y_{n-1}) - \omega_g^2(y_n + \alpha y_n^2 + \beta y_n^3), \tag{3.145}$$

where, $\alpha = -\frac{3a}{\sqrt{2}}$; $\beta = \frac{7a^2}{3}$; $\omega_g^2 = \frac{4a^2D_n}{m}$; $\omega_0^2 = \frac{k}{m}$. We use the semi-discrete approximation to obtain the short-wavelength envelope soliton. This asymptotic approach allows us to describe the envelope in the continuum approximation and to treat properly the carrier wave with its discrete character. Owing to the assumed weak nonlinearity, we expand y_n into the following asymptotic series [65] :

$$y_n(t) = \sum [\epsilon^l y_{l,m}(n,t)]e^{im\theta(n,t)} + C.C \tag{3.146}$$

Utilizing the idea developed by Taniuti and Yajima [72],the solution y_n is taken to be

$$\begin{aligned} y_n(t) =& \epsilon^{\frac{1}{2}} y_{11}(n,t)e^{i\theta} + C.C + \epsilon[y_{20} + y_{22}(n,t)e^{2i\theta} + C.C] + \epsilon^{\frac{3}{2}} y_{33}(n,t)e^{3i\theta} + C.C \\ &+ \epsilon^2[y_{42} + y_{44}(n,t)e^{4i\theta} + C.C] + \epsilon^{\frac{5}{2}}[y_{53}(n,t)e^{3i\theta} + y_{55}(n,t)e^{5i\theta} + C.C] + 0(\epsilon^{\frac{7}{2}}) \end{aligned} \tag{3.147}$$

where, $C.C$ stands for complex-conjugate and $\theta_n = nql - \omega t$. The smallness parameter ϵ which ranks from 0 to 1 $0 < \epsilon \leq 1$ represents the size of the amplitude of perturbation. Using the method of the section 2.3.2 we obtain the cubic quintic nonlinear Schrödinger (CQNLS) equation

$$i\frac{\partial y_{11}}{\partial \tau} + P\frac{\partial^2 y_{11}}{\partial \xi^2} + Q_1|y_{11}|^2 y_{11} + Q_2|y_{11}|^4 y_{11} = 0, \tag{3.148}$$

where $\tau = t$, $\xi = x - V_g t$ and the subscripts τ and ξ denote partial differentiations with respect to τ and ξ. While putting $y_{11}(\xi, t) = \psi(X, t)$ with $\xi = X$ we obtain the general CQNS equation:

$$i\psi_t + P\,\psi_{XX} + Q_1|\psi|^2\psi + Q_2|\psi|^4\psi = 0. \tag{3.149}$$

$$\begin{aligned} P &= \frac{l^2\omega_0^2 cos(ql) - V_g^2}{2\omega}; \quad Q_1 = -\frac{\omega_g^2[3\beta + 2\alpha(2a_{20} + a_{22})]}{2\epsilon\omega} \\ Q_2 &= -\frac{\omega_g^2[2\alpha(a_{22}a_{33} + a_{42}) + \beta(12a_{22}a_{20} + 3a_{33} + a_{20} + 6a_{22}^2 + 12a_{20}^2)]}{2\omega} \end{aligned} \tag{3.150}$$

The parameters of equation (3.6) is ploted on fig. (13)

3.9.2 The bright soliton solutions

In order to obtain the bright soliton solution to (3.149), the starting hypothesis is taken to be [4]

$$\begin{aligned} \psi(X,t) &= \frac{A\ \exp i\varphi}{[D_1 + \cosh(\tau)]^u}, \qquad where \\ \varphi(X,t) &= -\kappa X + \varpi t + \theta \qquad \tau = B(X - \nu t), \end{aligned} \tag{3.151}$$

Here, in (3.151), A is the amplitude of the soliton, while ν is the velocity and B is the inverse width of the soliton. Also, κ is the frequency of the soliton, while ϖ is the wave number of the soliton and θ is the phase constant. The exponent p is unknown at this point and its value will fall out in the process of deriving the solution of this equation. Also D_1 is a constant whose value in terms of the known parameters will be determined during the course of derivation of the soliton solution. Thus from ansatz (3.151)

$$\psi_t = \left\{ \frac{pB\nu A\sinh(\tau)}{[D_1 + \cosh(\tau)]^{u+1}} + \frac{i\varpi A}{[D_1 + \cosh(\tau)]^u} \right\} e^{i\varphi}, \tag{3.152}$$

$$\psi_{XX} = \left\{ \frac{u(u+1)B^2A(D_1^2 - 1)}{[D_1 + \cosh(\tau)]^{u+2}} + \frac{Au^2B^2}{[D_1 + \cosh(\tau)]^u} - \frac{u(2u+1)B^2AD_1B^2A}{[D_1 + \cosh(\tau)]^{u+1}} \right\} e^{i\varphi}. \tag{3.153}$$

Substituting (3.151-3.153) into (3.149) yields

$$\begin{aligned} &-\frac{\varpi A + PA\kappa^2 - PAu^2B^2}{[D_1 + \cosh(\tau)]^u} - \frac{-Pu(2u+1)AB^2D_1 + iuB\nu A\ \sinh(\tau) + 2P\kappa iuBA\ \sinh(\tau)}{[D_1 + \cosh(\tau)]^{u+1}} \\ &+ \frac{Pu(p+1)B^2A(D_1^2 - 1)}{[D_1 + \cosh(\tau)]^{u+2}} + \frac{Q_1A^3}{[D_1 + \cosh(\tau)]^{3u}} + \frac{Q_2A^5}{[D_1 + \cosh(\tau)]^{5u}} = 0, \end{aligned} \tag{3.154}$$

Now, separating the real and imaginary parts in Eq. (3.154), we get the following pair of relations:

$$\frac{uBA(\nu + 2P\kappa)\sinh(\tau)}{[D_1 + \cosh(\tau)]^{u+1}} = 0, \tag{3.155}$$

$$
\begin{aligned}
&-\frac{\varpi A+PA\kappa^2-PAu^2B^2}{[D_1+\cosh(\tau)]^u}-\frac{Pu(2u+1)AB^2D_1}{[D_1+\cosh(\tau)]^{u+1}}+\frac{Pu(p+1)B^2A(D_1^2-1)}{[D_1+\cosh(\tau)]^{u+1}}\\
&+\frac{Q_1A^3}{[D_1+\cosh(\tau)]^{3u}}+\frac{Q_2A^5}{[D_1+\cosh(\tau)]^{5u}}=0,
\end{aligned}
\tag{3.156}
$$

From (3.155), the velocity of the soliton is given by

$$
\nu=-2\kappa P. \tag{3.157}
$$

From the real part equation (3.156), equating the exponents $u+2$ and 5u gives $u+2=5u$ which implies $u=\frac{1}{2}$. The same value of u is also obtained when the exponents $u+1$ and $3u$ are equated against each other. Now, from (3.156), the linearly independent functions are $1/[D_1+\cosh(\tau)]^{u+j}$ for $j=0,1,2$. Therefore, setting their respective coefficients to zero yields

$$
\begin{aligned}
&\varpi A+PA\kappa^2-PAu^2B^2=0,\\
&Pu(2u+1)AB^2D_1+Q_1A^3=0,\\
&Pu(u+1)B^2A(D_1^2-1)Q_2A^5=0.
\end{aligned}
\tag{3.158}
$$

Solving the above equations gives

$$
\begin{aligned}
\varpi&=\frac{PB^2-4P\kappa^2}{4}\\
A&=\sqrt{B}\left[\frac{Q_1^2}{P^2B^2}+\frac{4Q_2}{3P}\right]^{-\frac{1}{4}}\\
D_1&=\frac{Q_1}{PB}\left[\frac{Q_1^2}{P^2B^2}+\frac{4Q_2}{3P}\right]^{-\frac{1}{2}}
\end{aligned}
\tag{3.159}
$$

As seen from (3.158) and (3.159), the soliton pulse will exist for $P\neq 0$. Thus, the bright soliton solution to the CQNLS equation (3.149) is given by

$$
\psi(X,t)=\frac{Ae^{i(-\kappa X+\varpi t+\theta)}}{[D_1+\cosh(\tau)]^{\frac{1}{2}}}, \tag{3.160}
$$

where, the velocity ν is given by (3.157), the wave number ϖ, the amplitude A of the soliton and the parameter D_1 is given by (3.159). Note that this solution exists provided that the constraint equations between the model coefficients $P\neq 0$ is satisfied. Solution (3.160) is a bright soliton as displayed by figure 51.

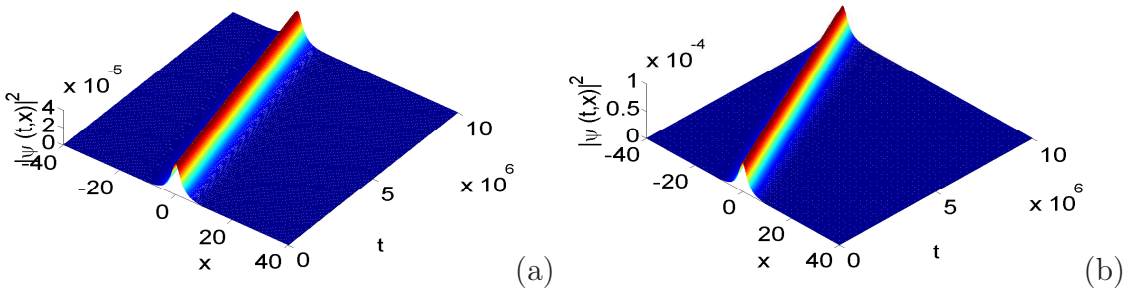

Figure 51: profile on bright siliton in the PB model in DNA dynamic. (a) S=0.04 and (b) S=0.06 and for B=1; $\kappa = 0.7$; m=300; D=0.04; a=4.45

3.9.3 Dark soliton solutions

Now we are looking to exact dark soliton solutions for the considered CQNLS equation (3.149). Dark solitons are known as topological optical solitons in the context of Theoretical Physics. The starting ansatz is

$$\psi(X,t) = [A + \lambda \tanh(\tau)]^u \, e^{i\varphi}, \tag{3.161}$$

where, τ and θ, are the same as in (3.151). Here in (3.161), A, λ and B are unknown free parameters and v is the velocity of the wave. In this case, the unknown exponent u will also fall out during the course of the derivation of the soliton solution to (3.149). From the ansatz (3.151), we get

$$\begin{aligned}\psi_t = &\left[\frac{Bu\nu}{\lambda^2}\left\{[A + \lambda \tanh(\tau)]^{u+1} - 2A\,[A + \lambda \tanh(\tau)]^u - (\lambda^2 - A^2)\,[A + \lambda \tanh(\tau)]^{u-1}\right\}\right] e^{i\varphi} \\ &+ [i\varpi\,[A + \lambda \tanh(\tau)]^u]\, e^{i\varphi}\end{aligned} \tag{3.162}$$

$$\begin{aligned}\psi_{XX} = &\Big\{\frac{B^2u\nu}{\lambda^4}\Big\{(u-1)(\lambda^2 - A^2)\,[A + \lambda \tanh(\tau)]^{u-2} - (p+1)\,[A + \lambda \tanh(\tau)]^{u+2} \\ &- 2A(2A+1)\,[A + \lambda \tanh(\tau)]^{u+1} + 2A(2u-1)(\lambda^2 - A^2)\,[A + \lambda \tanh(\tau)]^{u-1} \\ &+ 2u(3A^2 - \lambda^2)\,[A + \lambda \tanh(\tau)]^u - \kappa^2\,[A + \lambda \tanh(\tau)]^u\Big\} \\ &- \frac{2i\kappa Bu\nu}{\lambda^2}\Big\{(\lambda^2 - A^2)\,[A + \lambda \tanh(\tau)]^{u-1} + 2A\,[A + \lambda \tanh(\tau)]^u - [A + \lambda \tanh(\tau)]^{u+1}\Big\}\Big\} e^{i\varphi}\end{aligned} \tag{3.163}$$

Substituting (3.161-3.163) into (3.149), and then separating the real and imaginary parts, we can obtain the following pair of equations:

$$\frac{\left\{PuB^2(u-1)(\lambda^2-A^2)\left[A+\lambda\tanh(\tau)\right]^{u-2}\right\}}{\lambda^4}+\frac{\left\{2PuB^2A(2u-1)(\lambda^2-A^2)\left[A+\lambda\tanh(\tau)\right]^{u-1}\right\}}{\lambda^4}$$
$$-\frac{\left\{PuB^2(u+1)\left[A+\lambda\tanh(\tau)\right]^{u+2}\right\}}{\lambda^4}\left\{\frac{\{2APuB^2(2u+1)(\lambda^2-A^2)\}}{\lambda^4}\right\}\left[A+\lambda\tanh(\tau)\right]^{u+1}$$
$$+\left\{\frac{2Pu^2B^2(3A^2-\lambda^2)}{\lambda^4}-P\kappa^2-\varpi\right\}\left[A+\lambda\tanh(\tau)\right]^{u}+Q_1\left[A+\lambda\tanh(\tau)\right]^{3u}$$
$$+Q_2\left[A+\lambda\tanh(\tau)\right]^{5u}=0, \tag{3.164}$$

and

$$\frac{Bu(\nu+2P\kappa)}{\lambda^2}\left[\left(A+\lambda\tanh(\tau)\right)^{u+1}-2A\left(A+\lambda\tanh(\tau)\right)^{u}-(\lambda^2-A^2)\left(A+\lambda\tanh(\tau)\right)^{u-1}\right]=0. \tag{3.165}$$

From the imaginary part equation (3.165), the soliton velocity is the same as in the case of bright solitons that is given by (3.157). From the real part equation (3.164), equating the exponents of $\left[A+\lambda\tanh(\tau)\right]^{5u}$ and $\left[A+\lambda\tanh(\tau)\right]^{u+2}$ terms in Eq. (3.166), one again obtains $u=\frac{1}{2}$.

Now, from (3.164), the linearly independent functions are $\left[A+\lambda\tanh(\tau)\right]^{u+1}$ for $j=0,\pm1,\pm2$. Therefore, setting their respective coefficients to zero yields the following system of algebraic equations:

$$\begin{aligned}
\left\{PuB^2(u-1)\right\}(\lambda^2-A^2)^2&=0,\\
\left\{2PuB^2A(2u-1)\right\}(\lambda^2-A^2)&=0,\\
-\frac{PuB^2(u+1)}{\lambda^4}+Q_2&=0,\\
-\frac{-2PuB^2A(2u+1)}{\lambda^4}+Q_1&=0,\\
\frac{2Pu^2B^2(3A^2-\lambda^2)}{\lambda^4}-P\kappa^2-\varpi&=0.
\end{aligned} \tag{3.166}$$

Let study the following two cases:

Case I:$\lambda^2-A^2\neq0$. In the case,

$$\begin{aligned}
\varpi&=\frac{PB^2(3A^2-\lambda^2)-2P\lambda^4\kappa^2}{2\lambda^4},\\
A&=\frac{Q_1\lambda^4}{5PB^2-4Q_2\lambda^4},
\end{aligned} \tag{3.167}$$

the solution is plotted in figure 52

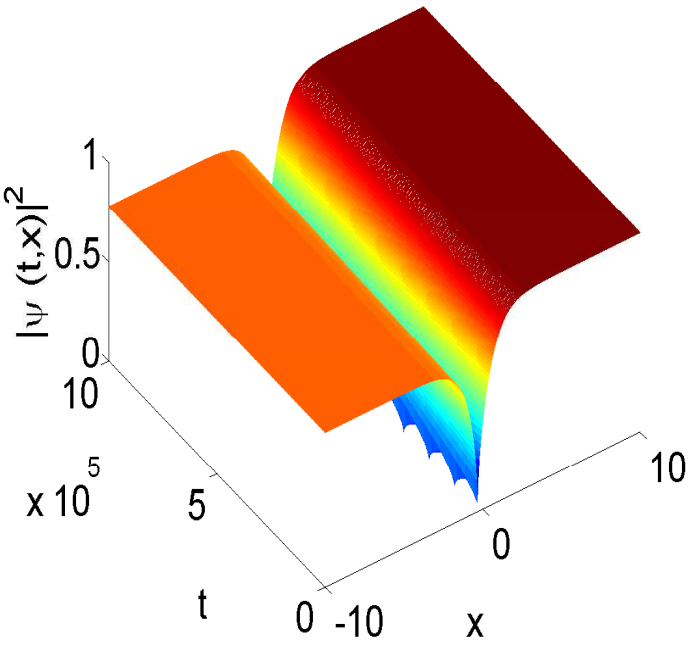

Figure 52: The dynamics of a dark-like solitary wave given by Eq. (3.161) in the PB model in DNA dynamic. S=0.06 and for $\lambda = -0.8$ B=0.75; $\kappa = 0.7$; m=300; D=0.04; a=4.45

Case II:$\lambda^2 - A^2 = 0$. In the case,

$$\begin{aligned} \varpi &= \frac{PB^2 - P\lambda^2\kappa^2}{2\lambda^4}, \\ A &= \frac{Q_1\lambda^4}{5PB^2 - 4Q_2\lambda^4}, \end{aligned} \tag{3.168}$$

the solution is plotted in figure 53.

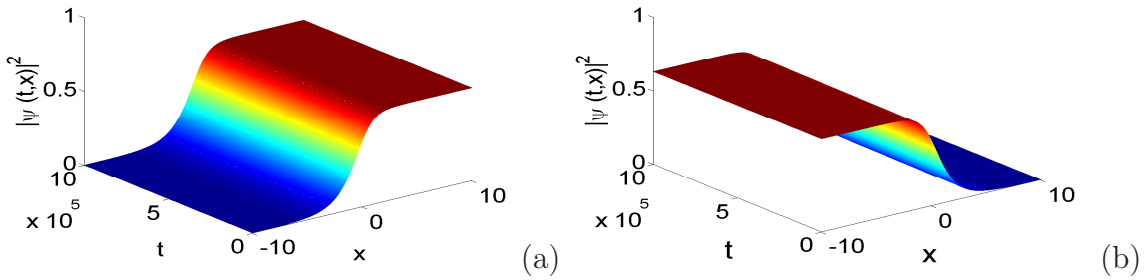

Figure 53: The dynamics of the solitary waves given by Eq. (3.161) , in the PB model in DNA dynamic. (a) give the evolution of the kink-like for $\lambda = A$ and (b) give the evolution of the antikink-like for $\lambda = -A$ and for B=0.75; S=0.06; $\kappa = 0.7$; m=300; D=0.04; a=4.45

In this section, both bright and dark 1-soliton solutions were obtained. The parameter re-

strictions in all four cases were laid down that fell out automatically from the soliton parameters.

3.10 The Jacobian elliptic function approach to derive exact soliton solutions of the DNA molecule

Several powerful methods have been proposed to solve differential-difference equations and to obtain exact solutions to the nonlinear partial differential equation. One can think of the inverse scattering method [145], the tanh method [146], the Jacobian elliptic function method [147], the multilinear variable separation, homogeneous balance method [148], the Backlund transformation method and so on. Cadoni et al [128] have performed numerical analyses which show the existence of a solitonic solution of the composite Yakushevich model of DNA. In order to obtain some exact soliton solutions of equation (3.70), we use the Jacobian elliptic function approach. First, we make the transformations

$$\psi_n = e^{i\theta_n}\varphi_n(\xi_n); \quad \theta_n = pn + qt + \zeta; \quad \xi_n = kn + ct + \chi \tag{3.169}$$

replacing ψ_n in equation 3.72, and separating the real from the imaginary part we get the following set of equations:

$$\begin{aligned} &- q\varphi_n + (\varphi_{n+1} + \varphi_{n-1})cos(p)(P_1 + 3Q_3\varphi_n^2) + Q_1\varphi_n^3 \\ &+ Q_2\varphi_n(\varphi_{n+1}^2 + \varphi_{n-1}^2)(2 + cos(2p)) + Q_3(\varphi_{n+1}^3 + \varphi_{n-1}^3)cos(p) = 0, \end{aligned} \tag{3.170}$$

$$\begin{aligned} &+ c\dot{\varphi}_n + (\varphi_{n+1} - \varphi_{n-1})sin(p)(P_1 + 3Q_3\varphi_n^2) + Q_1\varphi_n^3 \\ &+ Q_2\varphi_n(\varphi_{n+1}^2 - \varphi_{n-1}^2)sin(2p) + Q_3(\varphi_{n+1}^3 - \varphi_{n-1}^3)sin(p) = 0. \end{aligned} \tag{3.171}$$

With the properties of the Jacobian elliptic function . We use the following series expansion as a solution of equations (3.170) and (3.171), i.e.

$$\begin{aligned} \varphi_n(\xi_n) =& a_0 + a_1 sn(\xi_n), \\ \varphi_{n+1}(\xi_n) =& a_0 + a_1\frac{sn(\xi_n)cn(k)dn(k) + sn(k)cn(\xi_n)dn(\xi_n)}{1 - m^2sn^2(\xi_n)sn^2(k)}, \\ \varphi_{n-1}(\xi_n) =& a_0 + a_1\frac{sn(\xi_n)cn(k)dn(k) - sn(k)cn(\xi_n)dn(\xi_n)}{1 - m^2sn^2(\xi_n)sn^2(k)}, \end{aligned} \tag{3.172}$$

Now, we substitute the above equations into equations (3.170) and (3.171), a_0, a_1, c and q are determined. We then find after some calculations the following solutions of equation (3.72):

$$
\begin{aligned}
a_0 &= 0, \\
a_1 &= \pm m[\frac{2P_1 cn(k)cos(p)dn(k)}{Q_1 + 6Q_3 cos(p)cn(k)dn(k)}]^{1/2} sn(k), \\
c &= -2P_1 sn(k)sin(p), \\
q &= 2P_1 cn(k)dn(k)cos(p),
\end{aligned}
\tag{3.173}
$$

and hence the function

$$
\begin{aligned}
\varphi_n &= \pm m[\frac{2P_1 cn(k)cos(p)dn(k)}{Q_1 + 6Q_3 cos(p)cn(k)dn(k)}]^{1/2} sn(k)\ sn(k\ n - (2P_1 sn(k)sin(p))t + \varsigma) \\
\psi_n &= \pm m[\frac{2P_1}{Q_1 + 6Q_3 cos(p)cn(k)dn(k)} cn(k)cos(p)dn(k)]^{1/2} sn(k)\ sn(k\ n - (2P_1 sn(k)sin(p))t + \varsigma) \\
&\quad \times exp\ (i(p\ n + (2P_1 cn(k)dn(k)cos(p))t + \zeta))
\end{aligned}
\tag{3.174}
$$

$\mathbf{a_n^{(1)}}$ can then be written, taking the + sign:

$$
\begin{aligned}
a_n^{(1)}(t) &= m[\frac{4\omega_b P_1 cn(k)cos(p)dn(k)}{(Q_1 + 6Q_3 cos(p)cn(k)dn(k))(3K_5 + 6S_3)}]^{1/2} sn(k) \\
&\quad \times sn(k\ n - (2P_1 sn(k)sin(p))t + \varsigma), \\
&\quad \times exp\ (i(p\ n + [\frac{\omega_g^2 - \omega_b^2 + 2K_1}{2\omega_b} + 2P_1 cn(k)dn(k)cos(p)]t + \zeta)).
\end{aligned}
\tag{3.175}
$$

The general solution of Eq.(3.69), giving the displacement of the base pairs, i.e $\mathbf{u_n}$, take the form:

$$
\begin{aligned}
u_n(t) &= m[\frac{4\omega_b P_1 cn(k)cos(p)dn(k)}{(Q_1 + 6Q_3 cos(p)cn(k)dn(k))(3K_5 + 6S_3)}]^{1/2} sn(k) \\
&\quad \times sn(k\ n - (2P_1 sn(k)sin(p))t + \varsigma) \\
&\quad \times exp\ (i(p\ n + [\frac{\omega_g^2 + \omega_b^2 + 2K_1}{2\omega_b} + 2P_1 cn(k)dn(k)cos(p)]t + \zeta))
\end{aligned}
\tag{3.176}
$$

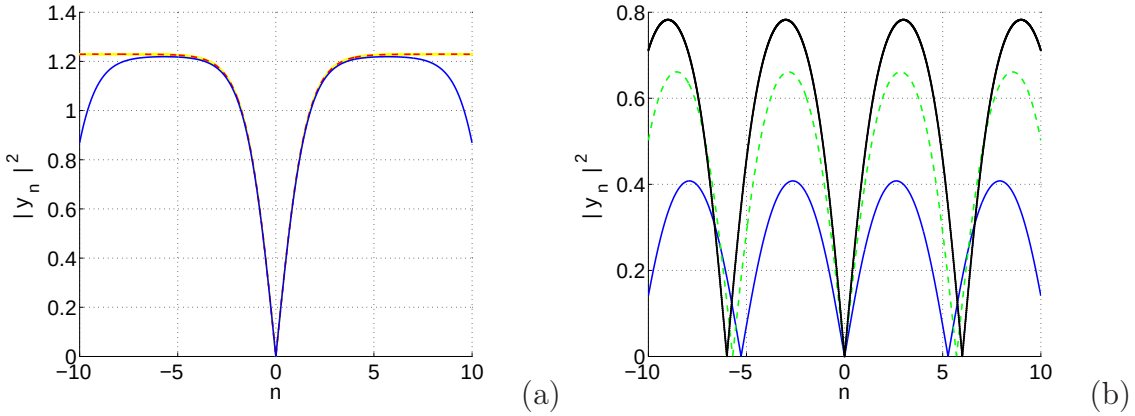

Figure 54: Profile of the solution: (a) the asymptotic evolution of the solutions according to the values of m,m = 0.3 (blue), 0.5 (green) and 0.6 (black); (b) the asymptotic evolution of the solution towards the bubble soliton, m = 0.99 (blue), 0.9998 (red) and 1 (yellow) and for $\theta = 0.25\pi$ $\omega_b = 1$, $\rho = 2$ D = 0.04 eV , $\alpha = 0.35$Å, K=60mev.Å^{-2}, $f_s = 0.3$, and $l_s = 3$Å.

The figure 54 present the profile of the above solution of base pairs for different values of the modulus m of Jacobian elliptic functions. One can see that on figure 54a as the modulus m of the Jacobian elliptic function increases, the magnitude of the base pairs through the DNA. If the modulus of the Jacobian elliptic function approaches the value 1, one can see from figure 54(b)that the solutions of the base pairs are described by the bubble soliton solution. This soliton solution translate the bubbles of transcription observed during the denaturation of the DNA as described in Davydov's theory. The figure 55 present the profile of the solution en function of twisted angle and for different values of the modulus m of Jacobian elliptic functions, through these figure, we observe the same comportment that the figure 54; what shows us that the twisted angle is important in the process of denaturation of the DNA.

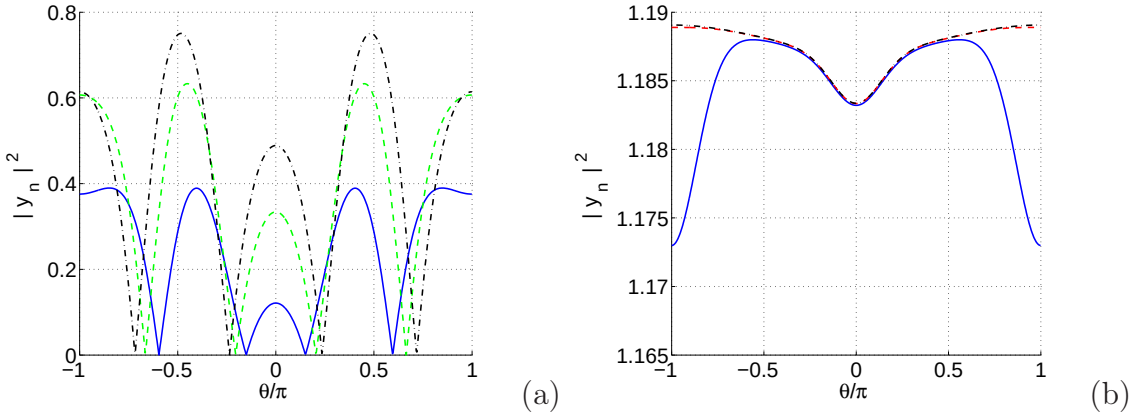

Figure 55: Profile of the solution according to the values of θ: (a) the asymptotic evolution of the solutions according to the values of m,m = 0.3 (blue), 0.5 (green) and 0.6 (black); (b) the asymptotic evolution of the solution towards the bubble soliton, m = 0.9998 (blue), 0.99999 (red) and 1 (black), and for $\omega_b = 1$, $\rho = 2$ D = 0.04 eV , $\alpha = 0.35$Å, K=60mev.Å^{-2}, $f_s = 0.3$, and $l_s = 3$Å.

Several authors already studied the static dark solitons of the NLS equation. these solution can be classified into two broad classes. Bubbles are 1D, 2D, and 3D nontopological solitons arising typically in models with competing interactions [150, 151]. The second class includes topological solitons of the Gross-Pitayevski equation and their 1D counterparts, kinks. The static bubbles are always unstable [150, 152], and this property endows them with a transparent physical interpretation as nuclei of the first order transition [153]. The numerical solitonic solution obtained by Cadoni et al [128] has the shape of the kink soliton of the sine- Gordon equation. Tabi et al. [133] obtains obtained two types of solutions o the MDNLS equation: the Jacobi periodic solution (small value of m) and the bubble soliton (when m is around the value 1) depending of the modulus of the Jacobian elliptic function. in addition of results obtained by Tabi, we observe that the bubble soliton depend to the twisted angle θ

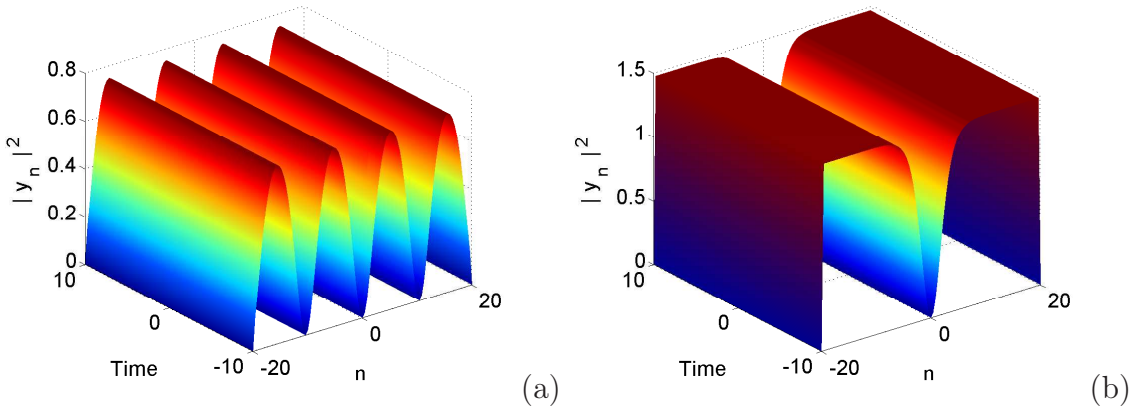

Figure 56: Propagation of solutions through the DNA molecule: (a) Jacobi periodic solution for m = 0.6; (b) bubble soliton for m = 1.for $\theta = 0.25\pi$, $\omega_b = 1$, $\rho = 2$ D = 0.04 eV , $\alpha = 0.35$Å, K=60mev.Å^{-2}, $f_s = 0.3$, and $l_s = 3$Å.

Figure 56 presents the propagation of the Jacobi solution (figure 56(a)) and the bubble soliton (figure 56(b)) through the DNA molecule. One can remark that as the waves move along the molecule, their magnitude increases.

3.10.1 Stability analysis of the solution

In this section, we investigate the stability of the above solution. In doing so, we introduce the following expansion:

$$\psi_n = [\phi_n + \gamma_n(t)]e^{i\omega t}, \tag{3.177}$$

Substituting equation (3.83) into the MDNLS equation, we find that the linearized equation satisfied by $\gamma_n(t)$ is given by

$$\begin{aligned}
&i\dot{\gamma}_n - \omega\gamma_n + P(\gamma_{n+1} + \gamma_{n-1}) + Q_1(2|\phi_n|^2\gamma_n + \phi_n^2\gamma_n^*) \\
&+ Q_2[2\gamma_n(|\phi_{n+1}|^2 + |\phi_{n-1}|^2) + 2\phi_n(\gamma_{n+1}\phi_{n+1}^* + \gamma_{n-1}\phi_{n-1}^*) + 2\phi_n(\phi_{n+1}\gamma_{n+1}^* + \phi_{n-1}\gamma_{n-1}^*)] \\
&+ Q_2[2\phi_n^*(\gamma_{n+1}\phi_{n+1} + \gamma_{n-1}\phi_{n-1}) + \gamma_n^*(\phi_{n+1}^2 + \phi_{n-1}^2)] \\
&+ Q_3(2|\phi_{n+1}|^2\gamma_{n+1} + \gamma_{n+1}^*\phi_{n+1}^2 + 2|\phi_{n-1}|^2\gamma_{n-1} + \gamma_{n-1}^*\phi_{n-1}^2) \\
&+ Q_3[\phi_n^2(\gamma_{n+1}^* + \gamma_{n-1}^*) + 2\gamma_n\phi_n(\phi_{n+1}^* + \phi_{n-1}^*) + 2|\phi_n|^2(\gamma_{n+1} + \gamma_{n-1}) + 2(\phi_{n+1} + \phi_{n-1})(\phi_n\gamma_n^* + \gamma_n\phi_n^*))] = 0.
\end{aligned} \tag{3.178}$$

Expanding $\gamma_n(t)$ in real and imaginary parts: $\gamma_n(t) = u_n(t) + iv_n(t)$ the linearized equations can be written as:

$$\begin{pmatrix} \{\dot{u}_n\} \\ \\ \{\dot{v}_n\} \end{pmatrix} = \begin{pmatrix} A_1 & A_2 \\ \\ -A_3 & A_4 \end{pmatrix} \begin{pmatrix} \{u_n\} \\ \\ \{v_n\} \end{pmatrix} \equiv \hat{A} \begin{pmatrix} \{u_n\} \\ \\ \{v_n\} \end{pmatrix}, \tag{3.179}$$

with:

$$
\begin{aligned}
&(A_1)_{nm} = 0,\\
&(A_2)_{nm} = P(\delta_{n,m+1} + \delta_{n,m-1}) + \{\ Q_1(2|\phi_n|^2 + \phi_n^2) + 2Q_2(|\phi_{n+1}|^2 + |\phi_{n-1}|^2 + \phi_{n+1}^2 + \phi_{n-1}^2)\\
&+Q_3(2\phi_n(\phi_{n+1}^* + \phi_{n-1}^*) + (\phi_{n+1} + \phi_{n-1})(\phi_n + \phi_n^*)) - \omega\}\ \delta_{n,m} + \{\ Q_2(2\phi_n\phi_{n+1}^* + 2\phi_n\phi_{n+1} + 2\phi_{n+1}\phi_n^*) +\\
&Q_3(2|\phi_{n+1}|^2 + 2|\phi_n|^2 + \phi_n^2 + \phi_{n+1}^2)\}\ \delta_{n,m+1} + \{\ Q_2(2\phi_n\phi_{n-1}^* + 2\phi_n\phi_{n-1} + 2\phi_{n-1}\phi_n^*) +\\
&Q_3(2|\phi_{n-1}|^2 + 2|\phi_n|^2 + \phi_n^2 + \phi_{n-1}^2)\}\ \delta_{n,m-1},\\
&(A_3)_{nm} = P(\delta_{n,m+1} + \delta_{n,m-1}) + \{\ Q_1(2|\phi_n|^2 + \phi_n^2) + Q_2(2|\phi_{n+1}|^2 + 2|\phi_{n-1}|^2 - \phi_{n+1}^2 - \phi_{n-1}^2)\\
&+Q_3(2\phi_n(\phi_{n+1}^* + \phi_{n-1}^*) + (\phi_{n+1} + \phi_{n-1})(-\phi_n + \phi_n^*)) + \omega\}\ \delta_{n,m} + \{\ Q_2(-2\phi_n\phi_{n+1}^* + 2\phi_n\phi_{n+1} + 2\phi_{n+1}\phi_n^*) +\\
&Q_3(2|\phi_{n+1}|^2 + 2|\phi_n|^2 - \phi_n^2 - \phi_{n+1}^2)\}\ \delta_{n,m+1} + \{\ Q_2(-2\phi_n\phi_{n-1}^* + 2\phi_n\phi_{n-1} + 2\phi_{n-1}\phi_n^*) +\\
&Q_3(2|\phi_{n-1}|^2 + 2|\phi_n|^2 - \phi_n^2 - \phi_{n-1}^2)\}\ \delta_{n,m-1},\\
&(A_4)_{nm} = 0,
\end{aligned}
\tag{3.180}
$$

by using the periodic boundary conditions, we study the stability of exact solution Jacobi and bubble soliton (see figure 57 and 58)through the eigenvalue spectrum of the matrix $\hat{A}$. The stationary soliton solution is linearly stable if and only if the matrix has all its eigenvalues on the imaginary axis ($\lambda = \lambda_r + i\lambda_i$).

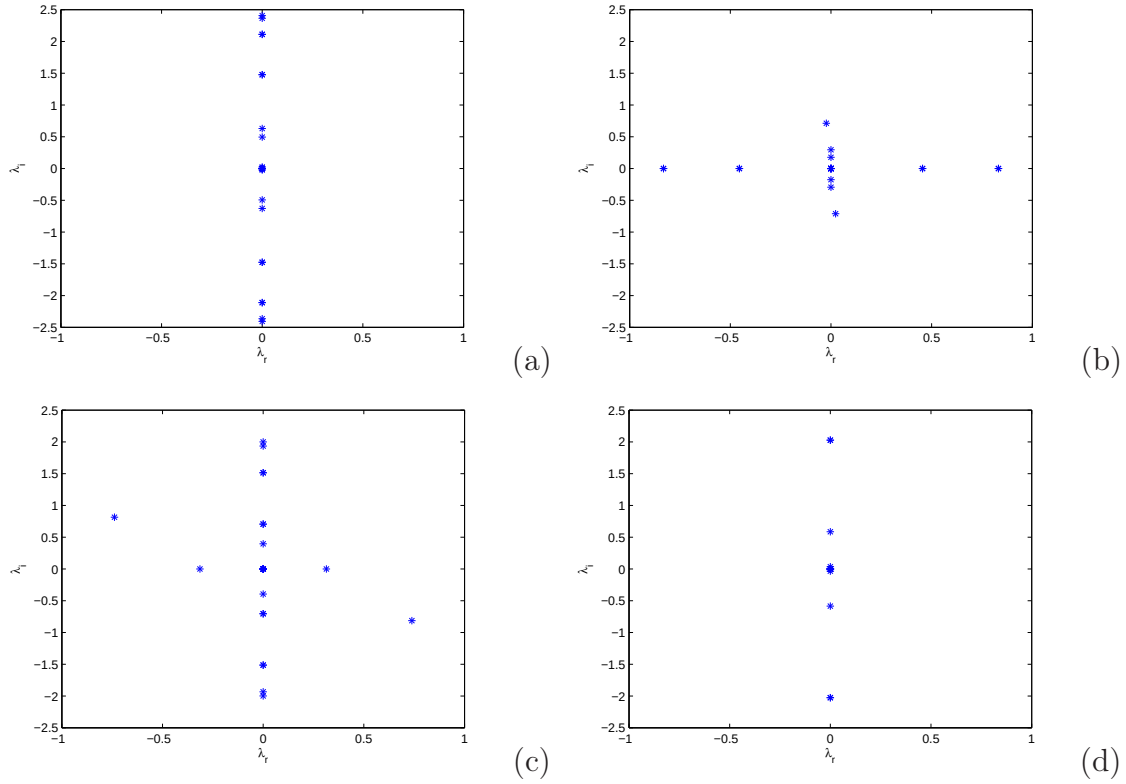

Figure 57: Instability diagrams: eigenvalue spectrum of the bubble soliton for m = 1 and (a) $\theta = 0$; (b)$\theta = 0.35\pi$; (c) $\theta = 0.55\pi$; (d) $\theta = 0.75\pi$

We observe through the figure 57 that for certain value of θ solutions are steady. for the value of m = 0.7, and $\theta = 0$, or $\theta = 0.75\pi$, we see that the spectra plane (λ_i, λ_r) of the Jacobi solutions shows all the eigenvalues to be in the imaginary axis, so one can say that the Jacobi solutions are stable.

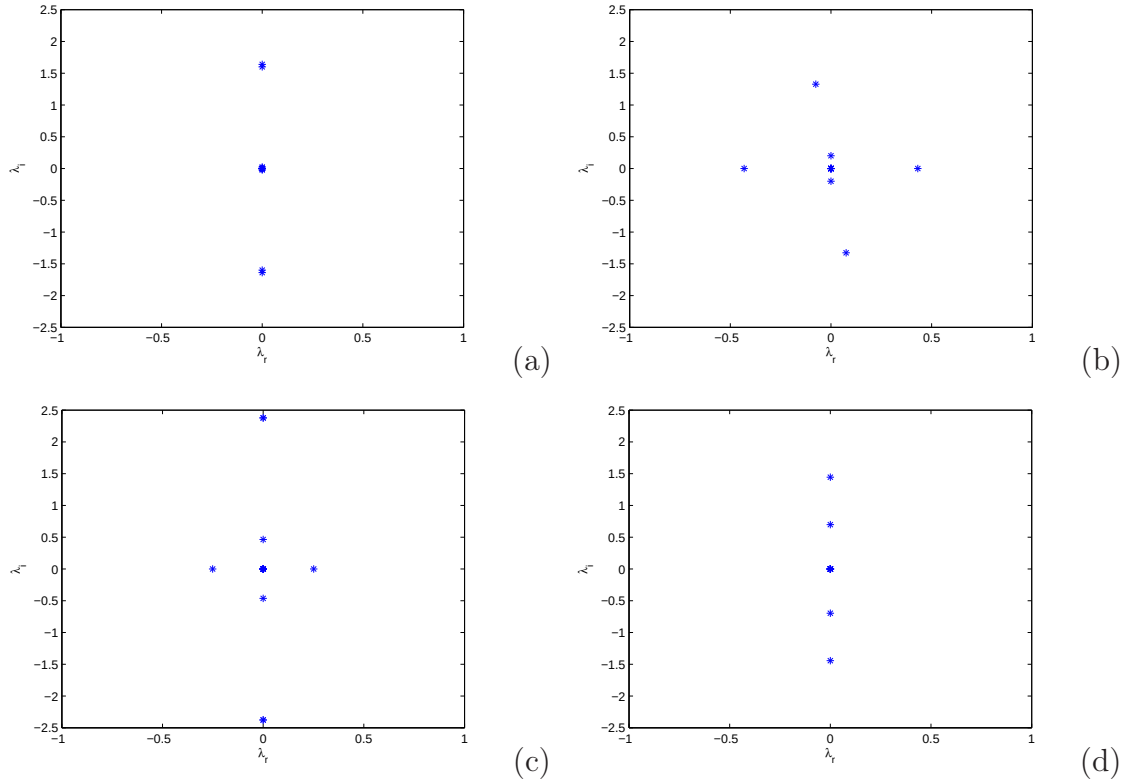

Figure 58: Instability diagrams: eigenvalue spectrum of the Jacobi periodic solution for m = 0.7 and (a) $\theta = 0$; (b)$\theta = 0.35\pi$; (c) $\theta = 0.55\pi$; (d) $\theta = 0.75\pi$

On the other hand, we see in figure 58 that the eigenvalues leave the imaginary axis for certain values of θ ($\theta = 0.35\pi$ and $\theta = 0.55\pi$); Thus, the bubble soliton here is unstable for the parameters used. In fact, Barashenkov et al [153] have already pointed out the fact that bubbles and dark solitons are always unstable, whereas pulse and discrete breather are always stable. Tabi et al [133] arrived to the same conclusion that Barashenkov et al. But recently, Tiofack et al [147] have shown that bubble solitons of the discrete cubic-quintic NLS equation are stable due to the presence of the quintic nonlinearity.In this work, we show through the figure 58a and 58c that for a certain values of twisted angle (θ=0 and $\theta \geq 0.56\pi$), the bubble soliton become stable. If one introduces a stochastic white noise in the system, we find that the Jacobi solution is modified during its propagation through the molecule as depicted in figure 58. The noise effect destroys the coherence of the initial solution.

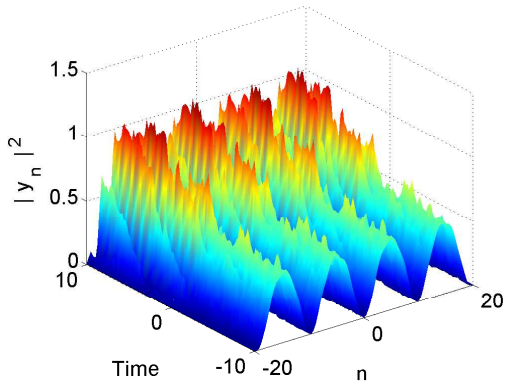

Figure 59: Propagation of the Jacobi solution in the presence of noise effects for m = 1 and $\theta = 0.75\pi$

We have considered the twisted DNA with solvent, looking for solitary wave excitations. while using the model of twisted PBD,our study in this model permitted us to find the MDNLS, with the parameters P, Q_1, Q_2 and Q_3 dependent to θ (fig.23). In the purpose to find the exact solution, we have derived the MDNLS equation using the Jacobi method and the solution is represented in the figure 54,55 and 56. All these solutions include the Jacobi periodic solution as well as the bubble soliton depending on the value of the modulus of the Jacobi function. Through the figure 54, we show that these solutions depend on the twisted angle θ in a periodic manner. Also, we have studied the stability of stationary solutions under small perturbations. We have found that Jacobi solutions are stable for certain value of twisted angle (θ=0 and $\theta \geq 0.6\pi$), and the bubble solitons are also stable for θ=0 and $\theta \geq 0.56\pi$.

General Conclusion

Summary and Contributions

In this thesis, we have considered some mathematical models of DNA molecule. We have investigated different aspects of MI and energy localization of the nonlinear dynamics of DNA molecule as well as soliton-like structures.

To achieve our goals, the thesis has been divided into three chapters. Chapter 1 was devoted to the historical overview of the DNA molecule. In this chapter, we introduced DNA as a biological entity on one hand and as a dynamical entity on the other hand. Then, we focused much more on the dynamic aspect of the molecule. We have introduced model like the PB model, the PBD model and its extensions, the Yakushevich model and BSJ model.

Chapter 2 was devoted to the description of analytical and numerical methods used through the thesis. In this chapter, we presented several methods, such as perturbation method that led to the CQNLS equation and the CNLS equation from the helical PB model, and NLS equation from the PBJ model. We also presented the multiple scales method that leads to DCNLS equation from the Yakushevich model. Another method which have been presented is the Fourier expansion method that has led us to obtain the DNLS equation from the PBD model with the effect of the twist angle and the solvent interaction. We also presented some method to derive excat soliton solutions.

Chapter 3 is subjected to our results and discussions. We have investigated the MI in the PB model. For this purpose, the nonlinear dispersion relation have been derived from the cubic-quintic NLS equation using two different approaches, namely, the standard linear stability analysis and the variational approach. It is found that the quintic term can be used to reduce the magnitude of waves and hence to stabilize the propagation of waves in the system. The theoretical findings have been numerically tested through direct simulations of the behavior of the system predicted by analytical results. Next, we studied the MI of two-component Peyrard-Bishop-Dauxois Model. We show using the reductive perturbation method that the dynamics of the system can be described by a set of coupled NLS equations. The relevant MI scenarios are explored and we note that the system is stable under the modulation for certains parameters value of the Peyrad-Bishop-Dauxois model. We have investigated the occurrence of MI in a pair of coupled waves, co-propagating in the PBD model of DNA. This two-component

model of DNA can be used to investigate the idea that a breather mechanism could ensure signal propagation in a chain of biological macromolecule supported by the mechanism of two-component breathers within the nonlinear PBD model of DNA. Excellent agreement has been obtained between analytical predictions and numerical experiments.

In the literature, anharmonicity and twist-opening coupling have been shown to produce very sharp transition. Within the study of MI, this has been confirmed in chapter 3, where the twist-opening models have been considered. The amplitude of the waves train mainly with helical coefficient describes the action of RNA polymerase, which breaks progressively the hydrogen bonds for the messenger RNA to come and copy the genetic code. Decreasing the amplitude of the pairing coefficient reflects the interaction of the wave with many loads (phonon) within the molecule. We believe that the existence and the formation of solitons in the DNA molecule could be a proper candidate to explain how data are exchanged during basic biological phenomena such as transcription and replication. As it is well known, for the hydrogen bonds to be broken, there should be a concentration of the enzyme and of the energy brought through the hydrolysis of adenosine triphosphate (ATP) [155].

The study of soliton solutions and nonlinear excitations in DNA has been performed. We analyze the possibility of coherent modes for DNA dynamics in a general model recently proposed by Joyeux and Florescu [129]. We show that the value they used for their results are not suitable to describe wave propagation in DNA. We therefore investigate parameter values in order to obtain coherent solitary waves with characteristics that are know experimentally. We study the propagation of localized excitations in a DNA molecule which takes into account helicity and solvent interaction. The small amplitude dynamics of the model is described by envelope solutions made of breathers. Our solutions drastically depends on the twist angle and solvent interaction. It is found that increasing the twist angle decreases the width of the pulse which can be used for the transportation of energy. Increase the solvent interaction term, increases the width of the pulses while the number of waves train decreases with time. The stability of the solutions has been checked through numerical simulations.

The study of solitary wave solutions is of prime significance for nonlinear physical systems. The Peyrard-Bishop model for DNA dynamics is generalized specifically to include the difference among bases pairs. The small amplitude dynamics of the model is studied analytically and reduced to the CQNLS equation and the exact bright and dark soliton solutions is obtained. These amplitude solutions are made of bubble solitons. The impact of elasticity on DNA dynamic is also presented. The profile of solitary wave structures is displayed for some fixed parameters. We have checked solutions for the MDNLS equation. First we have found, using the Jacobi elliptic function method, a bubble soliton. Using that solution as the initial condition, the bubble in the lattice transformed into pulse and train of pulses. Furthermore, the strong coupling between the upper and lower cut-off optical modes gave rise to a new type of excitation, the "kink-breather" soliton, which could have interesting biological meanings and

enrich the family of solitons describing the oscillations of the hydrogen bonds connecting the pairs.

Open problems and future directions

Many interesting results have thus been obtained in the present thesis. However numerous points remain unsolved, and then may be subject to future investigations.

♣ One of the most ambitious goals of the modeling process is the genetic description of the processes of replication and transcription taking proper account of actual interaction between the intrinsic dynamics of DNA and the molecular motors. In fact, a molecular motor must exclude the double strand to move forward and, in most prior studies, this dynamic is described by a kinetic model incorporated into the protein which broadcasts on a discrete space effective energy is ie from one site to another (see eg [154, 155]). A first concern is to use these in discrete energy models realistic temperature dependent, ie, the spectra obtained by calculating the energy required to exclude one or more base pairs for a particular sequence and a given temperature. The next step is obviously to provide a Hamiltonian describing, based on continuous variables, the dynamics of coupled, for example, our DNA model proteins.

♣ From a theoretical point of view, it is known that the stability and lifetime of localized solutions are very sensitive to such properties of the thermal fluctuations as viscosity and temperature. The DNA is in contact with a thermal bath in the cell. Therefore, the friction and thermal forces play an important role in its internal dynamics. So, it necessary to explore the role of the thermal noise in the formation of localized structures in the models studied in this thesis.

♣ The base functional process of DNA such as replication and transcription are controlled through the action of proteins that are only internal interactions. Therefore, to understand the workings of DNA, it is not enough to take into account internal interactions. It is necessary to study the interaction between the internal movement as inertial oscillations in DNA and proteins involved in its dynamics.

♣ It should also be interesting to study of nonlinear dynamics of microtubules.

Related works of the thesis

1. **D. Toko**, A. Mohamadou, C. B. Tabi and T. C. Kofane, "*Modulational Instability of Two-Component Peyrard-Bishop-Dauxois Model*" J. Comput. Theor. Nano. Sc. **8**, 1776 (2011).

2. **D. Toko**, A. Mohamadou, C. B. Tabi and T. C. Kofane, "*Coherent Modes and Parameter Selection in DNA Models with Finite Stacking Enthalpy*" J. Comput. Theor. Nano. Sc. **9**, 1-5 (2012).

3. **Toko D**, Woulache RL, Tabi CB, Kavitha L, Mohamadou A, et al. (2013) "*Breather-Like Solutions of the Twisted DNA with Solvent Interaction*". J Phys Chem Biophys 3: 112. doi:10.4172/2161-0398.1000112

4. A. Mohamadou, **D. Toko**, Alim, C. B. Tabi, and T. C. Kofane "*Modulational instability and energy localization of twisted DNA with solvent interaction* ". Int. J. Mod. Phys B 0217-9792 (2015) 1793-6578.

Bibliography

[1] Watson, J., Crick, F. Nature **171**, 737 (1953).

[2] R.Thomas, Bull. Sté. Chim. Biol., 7, 609 (1953)

[3] J.Marmur, R. Rownd et C. L. Schildkraut, Prog. Nucleic Acid Res. 1, 231 (1963)

[4] Sahin BUYUKDAGLI, Etude de la dynamique et de la physique statistique de modèles d'ADN non-linéaires à la dénaturation thermique, Ph.D Thesis,L'UNIVERSITÉ JOSEPH FOURIER GRENOBLE I (2007).

[5] D. Poland et H. A. Scheraga, J. Chem. Phys. 45, 1456 (1966) ; 45, 1464 (1966).

[6] Y. Gao et E. W. Prohofsky, J. Chem. Phys, 80,2242 (1984)

[7] T. Dauxois, M. Peyrard et A. R. Bishop, Phys. Rev. E 47, R44 (1993).

[8] S. Cocco, M. Barbi, et M. Peyrard, Phys. Lett. A, 253, 161 (1999).

[9] T. Dauxois et M. Peyrard. Physics of Solitons, Nonlinear Science and Fluid Dynamics, Cambridge, 2006.

[10] S. Komineas, G. Kalosakas et A. R. Bishop, Phys. Rev. E, 65, 061905 (2002)

[11] G. Kalosakas, K. Rasmussen et A. R. Bishop, J. Chem. Phys, 118, 3731 (2003)

[12] S. Ares, N. K. Voulgarakis, K. Rasmussen et A. R. Bishop, Phys. Rev. Lett. **94**, 035504 (2005)

[13] Y.L. Zhang, W.M. Zheng, J.X. Liu and Y. Z. Chen, Phys. Rev. E **56**, 7100 (2003).

[14] T. Michoel et Y. Van de Peer, Phys. Rev. E 73, 011908 (2006)

[15] M. Joyeux et S. Buyukdagli, Phys. Rev. E 72, 051902 (2005).

[16] T. Shimomura, K. Denda, A. Kitamura, T. Kawaguchi, M. Kito, J. Kondo, S. Kagaya, L. Qin, H. Takata, K. Miyazawa et N. Kitamura, J. Biol. Chem.272, 6370 (1997).

[17] A. Brünger, C. B. Brooks et M. Karplus, Chem. Phys. Lett. 105, 495 (1984).

[18] E. Carlon, M. L. Malki et R. Blossey, Phys. Rev. Lett. 94, 178101 (2005).

[19] A. Campa et A. Giansanti, Phys. Rev. E 58, 3585 (1998).

[20] M. Peyrard, Nonlinearity 17, R1 (2004).

[21] Alberts, B., Bray, D., Lewis, J., Raff, M., Roberts, K., Watson, J.D. Biologie Moléculaire de la Cellule. Flammarion.

[22] M. Laurent NONY, Analyse de la microscopie de force dynamique : Application à l'étude de l'A.D.N., Ph.D Thesis, L'UNIVERSITÉ BORDEAUX I, ÉCOLE DOCTORALE DES SCIENCES PHYSIQUES ET DE L'INGÉNIEUR (2000).

[23] Mika Gustafsson, Coherent waves in DNA within the Peyrard-Bishop model,Master thesis, Reg No. LiU-IFM-EX-1084

[24] Emmanuel GIUDICE, ÉTUDE PAR DYNAMIQUE MOLÉCULAIRE DES ASPECTS ÉNERGÉTIQUES ET CONFORMATIONNELS DES DÉFORMATIONS DE LA DOUBLE HÉLICE D.ADN EN FONCTION DE SA SÉQUENCE DE BASES, Ph.D Thesis, UNIVERSITE PARIS 6 PIERRE ET MARIE CURIE (2003)

[25] www.micro.magnet.fsu.edu/cells/ ; www.wikipedia.org.

[26] Boccara, M., Verdière-Sahuqué, M. Les Acides Nucléiques. Pavages. Diderot Editeur, Arts et Sciences, (1998).

[27] Michel Peyrard et Thierry Dauxois, physique des solitons, 2004, EDP Sciences, **17**, avenue du Hoggar, BP 112, Parc d'activités de Courtaboeuf, 91944 Les Ulis Cedex A et CNRS ÉDITIONS 15 ,rue Malebranche, 75005 Paris.

[28] Integrated Dynamics Engineering GmbH, Karl Liebknecht-Str. 30 D-65479 Raunheim.

[29] BOLTONP .H., JAMETS. L., " Fast and slow conformational fluctuations of RNA and DNA-sub-nanosecond internal motion correlation times determined by P-31-NMR" , Journal of the American Chemical Society **102**, 25-31 (1980).

[30] HOGANM .E., JARDETZOK.Y, « Internal motions in desoxyriboriiicleic-Acid II D , Biochemistry **19**, 3460-3468 (1980)

[31] MILLARD .P. , ROBBINSR . J . , ZEWAIL A.H., <(Direct observation of the torsional dynamics of DNA and RNA by picosecond spectroscopy >), Proceedings of the National Academy of Sciences (USA) **77**, 5593-5597 (1980).

[32] PAINTEPR. C., MOSHERL ., RHOADSC ., « Low frequency modes in the Raman spectrum of DNA », Biopolymers **20**, 243-247 (1981).

[33] URABEH ., TOMINAYG.,A « Low-lying collective modes of DNA double helix by raman-spectroscopy » B, iopolymers **21**, 2477-2481(1982).

[34] PROHOFSEK.YW ., LLJK .C., VANZ ANDTL .L., PUTNABL. F., «Breathing modes and induced resonant melting of the double helix D, Physics Letters A **70**, 492-494 (1979).

[35] PUTNABM. F.,V ANZ ANDTL .L., PROHOFSKEY.W ., LU K.C. , MEI W.N., "Resonant and localized breathing niodes in terminal regions of the DNA double helix", Biophysical Joiirnal **35**, 271-287(1981).

[36] Giuseppe Gaeta, simple model of DNA dynamic, centre de physique théorique, Ecole polytechnique, F-91128 Palaiseau (france)

[37] W. Saenger, " Principles of Nucleic Acid Structure ", Springer, New York, 1984 ; second corrected printing 1988

[38] S. Yomosa, Phys. Rev. A **27** (1983), 2120; Phys. Rev. A 30 (1984), 474

[39] M. Ya. Azbel, J. Phys. A **12** (1979), L29

[40] M. Peyrard and A.R. Bischop, Phys. Rev. Lett. **62** (1989), 2755

[41] L. V. Yakushevich, Phys. Lett. A **136** (1989), 413

[42] L. V. Yakushevich, A. V. Savin and L. I. Manevitch, Phys. Rev. E **66** (2002) 016614.

[43] G. Gaeta, Phys. Lett. A **143** (1990) 227.

[44] T. Dauxois, Phys. Lett. A **159** (1991) 390.

[45] Dauxois T, Peyrard M and Bishop A.R. 1993 Entropy-driven DNA denaturation Phys. Rev. E **47** R44-7

[46] Dauxois T and PeyrardM 1995 Entropy-driven transition in a one-dimensional system Phys. Rev. E **51** 4027-40

[47] Gerald Weber, Niall Haslam, JonathanW Essex and Cameron Neylon, J. Phys.: Condens. Matter **21** (2009) 034106 (11pp)

[48] Weber G, Haslam N, Whiteford N, Prügel-Bennett A, Essex J W and Neylon C 2006 Thermal equivalence of DNA duplexes without melting temperature calculation Nat. Phys. 2 55-9

[49] Weber G 2006 Sharp DNA denaturation due to solvent interaction Europhys. Lett. **73** 806-11

[50] Barbi M, Lepri S, PeyrardM and Theodorakopoulos N 2003 Thermal denaturation of a helicoidal DNA model Phys. Rev. E **68** 061909

[51] Drukker K, Wu G and Schatz G C 2001 Model simulations of DNA denaturation dynamics J. Chem. Phys. **114** 579-90

[52] Dauxois T, Peyrard M and Bishop A R 1993 Entropy-driven DNA denaturation Phys. Rev. E **47** R44-7

[53] Dauxois T and PeyrardM 1995 Entropy-driven transition in a one-dimensional system Phys. Rev. E **51** 4027-40

[54] Peyrard M. and Bishop A.R. 1989 Statistical mechanics of a nonlinear model for DNA denaturation Phys. Rev. Lett. **62** 2755-7

[55] Joyeux M and Buyukdagli S 2005 Dynamical model based on finite stacking enthalpies for homogeneous and inhomogeneous DNA thermal denaturation Phys. Rev. E **72** 051902

[56] Saccomandi G and Sgura I 2006 The relevance of nonlinear stacking interactions in simple models of double-stranded DNA J. R. Soc. Interface **3** 655-67

[57] Weber G 2006 Sharp DNA denaturation due to solvent interaction Europhys. Lett. **73** 806-11

[58] S. Buyukdagli, M. Sanrey et M. Joyeux, Chem. Phys. Lett. **419**, 434 (2006)

[59] EDLERJ. , HAMMP ., "Self-trapping of the amide I band in a peptide model crystal", Journal of Chemical Physics **117**, 2415-2424 (2002).

[60] PEYRARD M., Nondinear Excitations in Biomolecules, Les Éditions de Physique, Les Ulis (1995).

[61] M. Barbi, S. Cocco, and M. Peyrard, Phys. Lett. A **253**, 358 (1999); C. B. Tabi, A. Mohamadou, and T. C. Kofane, ibid. **373**, 2476 (2009).

[62] C. B. Tabi, A. Mohamadou, and T. C. Kofane, J. Phys.: Condens. Matter **20**, 415104 (2008).

[63] Y. S. Kivshar and M. Peyrard, Phys. Rev. A **46**, 3198 (1992).

[64] C. B. Tabi, A. Mohamadou, and T. C. Kofane, Eur. Phys. J. D **50**, 307 (2008).

[65] M. Remoissenet, Phys. Rev. B **33**, 2386 (1986).

[66] C. B. Tabi, A. Mohamadou, and T. C. Kofané, J. Bionanosci. **3,** 110 (2009).

[67] Remoissenet M (1986) Low-amplitude breather and envelope solitons in quasi-one-dimensional physical models. Phys Rev B **33**: 2386.

[68] Zdravkovic S, Tuszynski JA, Sataric MV (2005) Peyrard-Bishop-Dauxois Model of DNA Dynamics and Impact of Viscosity. J Comput Theor Nanosci 2: 1-9.

[69] Dauxois T (1991) Dynamics of breather modes in a nonlinear "*helicoidal*" model of DNA. Phys Lett A **159**: 390.

[70] Tabi C. B, Mohamadou A, Kofane TC (2008) Soliton excitation in the DNA double helix. Phys Lett A **77**: 045002.

[71] M. Remoissenet, Waves Called Solitons, 3rd ed. (Springer, Berlin, 1999).

[72] T. Taniuti and N. Yajima, J. Math. Phys. **10**, 1369 (1969); **14**, 1389 (1973).

[73] F. B. Pelap, T. C. Kofane, N. Flytzanis, and M. Remoissenet, J. Phys. Soc. Jpn. **70**, 2568 (2001).

[74] Y. Kivshar, G. P. Agrawal, Optical Solitons, Form Fibers to Photonic Crystals, Academic, New York (2003).

[75] B. A. Malomed, Soliton Management in Periodic Systems, Springer, New York (2006).

[76] T. Ueda and W. L. Kath, Phys. Rev. A 42, 563 (1990); J. Yang, Phys. Rev. E **59**, 2393 (1999).

[77] I. Kourakis and P. K. Shukla, Eur. Phys. J. B **50**, 321 (2006).

[78] J. Leon and M. Manna, J. Phys. A **32**, 2845 (1999).

[79] J. Leon and M. Manna, Phys. Rev. Lett. **83**, 2324 (1999).

[80] C. B. Tabi, A. Mohamadou, and T. C. Kofane, Phys. Scr. **77**, 045002 (2008).

[81] I. Kourakis and P.K. Shukla. Modulational instability in asymmetric coupled wave functions 21 November 2005

[82] M. Bondeson, M. Lisak, and D. Anderson, Phys. Scripta **20**, 479 (1979).

[83] D. Anderson, Phys. Rev. A **27**, 3135 (1983).

[84] B. A. Malomed, Prog. Opt. **43**, 71 (2002).

[85] B. Crosignani, P. Di Port, and A. Treppiedi, Quantum Semiclassic. Opt. **7**, 73 (1995).

[86] Z. Rapti, P. G. Kevrekidis, A. Smerzi, and A. R. Bishop, Phys. Rev. E **69**, 017601 (2004).

[87] S. Trillo and S. Wabnitz, Opt. Lett. **16**, 986 (1991); G. Cappellini and S. Trillo, J. Opt. Soc. Am. B **8**, 824 (1991); S. Trillo and S. Wabnitz, Opt. Lett. **16**, 1566 (1991).

[88] C.J. Chen, P.K.A. Wai, C.R. Menyuk, Opt. Lett. **20** (1995) 350.

[89] J.M. Soto-Crespo, L. Pesquera, Phys. Rev. E **56** (1997) 7288.

[90] T. Jinping et al., Phys. Scripta **67** (2003) 325.

[91] B. A. Malomed, Soliton Management in Periodic Systems, Springer, New York (2006).

[92] Li Zhonghao, Li Lu, T. Huiping, Z. Guosheng, Phys. Rev. Lett. **84** (2000) 4096. [14] B.A. Malomed, Prog

[93] B. Crosignani, P. Di Port, A. Treppiedi, Quant. Semiclassic. Opt. **7** (1995) 73.

[94] K. Aikawa, A. Frisch, M. Mark, S. Baier, A. Rietzler, R. Grimm, and F. Ferlaino, Phys. Rev. Lett. **108**, 210401 (2012).

[95] F.Kh. Abdullaev, A.A. Abdumalikov, R.M. and Galimzyanov, Phys. Lett. A **367**, 149 (2007).

[96] F.Kh. Abdullaev and M. Salerno, Phys. Rev. A **72**, 033617 (2005).

[97] T. Dauxois, Phys. Lett. A 159, 390 (1991).

[98] S. Zdravkovic and J. A. Tuzinsky, J. Comput. Theor. Nanosci. 2, **263** (2005).

[99] Zdravkovi'c S., in Finely Dispersed Particles: Micro, Nano, and Atto-Engineering, 130 Surfactant Science Series, edited by Spasic A. M. and Hsu J. P. (Dekker/CRC Press/Taylor Francis Group, Boca Raton, Fla) 2005.

[100] Zdravkovi'c S., Tuszi'nsky J. A. and Satari'c M. V., J. Comput. Theor. Nanosci., **2** (2005) 263. ¯bers to Photonic Crystals, (Academic Press, San Diego).

[101] A. Tsurui, Prog. Theor. Phys. **48**, 1196 (1972).

[102] T. Kawahara, J. Phys. Soc. Jpn. **35**, 1537 (1973).

[103] L. V. Yakushevich, Nonlinear Physics of DNA, Wiley Series in Nonlinear Science, John Wiley, Chichester (1998).

[104] S. W. Englander, N. R. Kalenbach, A. J. Heeger, J. A. Krumhansl, and S. Litwin, Proc. Natl. Acad. Sci. USA 77, 7222 (1980).

[105] K. Kasamatsu and M. Tsubota, Phys. Rev. Lett **93**, 100402 (2004).

[106] Peyrard M. and Bishop A. R., Phys. Rev. Lett., 62 (1989) 2755.

[107] Drukker K., Wu G. and Schatz G. C., J. Chem. Phys. **114, 579** (2001).

[108] J. Palmeri, M. Manghi and N. Destainville, Phys. Rev. Lett. **99**, 088103 (2007).

[109] M. Peyrard and A. R. Bishop, Phys. Rev. Lett. **62**, 2755 (1989).

[110] C. B. Tabi A. Mohamadou, and T. C. Kofane, Eur. Phys. J. D 50, 307 (2008).

[111] C. B. Tabi, A. Mohamadou, and T. C. Kofane, Journal of Bionanoscience Vol. **3**, 18,2009

[112] Marco Zoli, J. Chem. Phys. **135**, 115101 (2011); doi: 10.1063/1.3631564.

[113] S. Buyukdagli and M. Joyeux, Phys. Rev. E 77, 032903 (2008); M. Joyeux and A.-M. Florescu, J. Phys.:Condens. Matter 21, 034101 (2009).

[114] S. Aubry, Physica D 103, 201 (1997); R. MacKay, Physica A, 288, 175 (2000).

[115] S. Flach, C. R. Willis, Phys. Resp. **295,** 181 (1998).

[116] D. Chen, S. Aubry, G. P. Tsironis, Phys. Rev. Lett. **77**, 4776 (1996).

[117] R. M. Haas, Phys. Rev. D **57**, 7422 (1998); J. J.-L. Ting and M. Peyrard, Phys. Rev. E 53, 1011 (1996).

[118] E. Zamora-Sillero, A. V. Shapovalov, and F. J. Esteban, Phys. Rev. E **76**, 066603 (2007).

[119] M. Wadati, T. Lizuka, and T. Yajima, Physica (Amsterdam) 51D, **388** (1991).

[120] C. B. Tabi, A. Mohamadou.CHAOS **19**, 043101 (2009)

[121] M. Daniel and V. Vasumathi, Physica D **231**, 10 (2007).

[122] M. Salerno and Y. S. Kivshar, Phys. Lett. A 193, 263 (1994).

[123] M. Salerno, Phys. Rev. A **46**, 6856 (1992).

[124] G. Gaeta, Phys. Rev. E **74**, 021921 (2006).

[125] I. Daumont, T. Dauxois, and M. Peyrard, Nonlinearity **10**, 617 (1997).

[126] Y. S. Kivshar and M. Peyrard, Phys. Rev. A **46**, 3198 (1992).

[127] T. Dauxois, M. Peyrard, A.R. Bishop, Phys. Rev. E **47** (1993) R44.

[128] Cadoni M, De Leo R and Gaeta G 2007 Phys. Rev. E **75** 021919

[129] M.Joyeux and A.-M. Florescu, J. Phys.: Condens. Matter. **21**,034101 (2009).

[130] M. Joyeux and S. Buyukdagli, Phys. Rev. E **72**, 051902 (2005).

[131] S. Buyukdagli and M. Joyeux, Phys. Rev. E **77**, 032903 (2008).

[132] S. Zdravkovic and M. V. Sataric, Phys. Lett. A **373**, 126 (2008).

[133] Conrad B Tabi, Alidou Mohamadou, and Timol¶eon C Kofanae Phys. Scr. **77** (2008) 045002

[134] S. Zdravkovic and C. B. Tabi, J. Comput. Theor. Nanosci. **7**, 1418 (2010).

[135] Remoissenet M 1986 Phys. Rev. B **33**, 2386 (1986).

[136] Zdravkovic S, Tuszynski J A and Sataric M V 2005 J. Comput. Theor. Nanosci **2**, 1.

[137] Dauxois T 1991 Phys. Lett. A **159** 390.

[138] Tabi C B, Mohamadou A and Kofane T C 2008 Phys. Lett. A **77** 045002; Zdravkovic S and Sataric M V 2008 Phys. Lett. A **373** 126.

[139] Flach S, Willis C R 1998 Phys. Rep. **295** 181.

[140] Aubry S 1997 Physica D **103** 201.

[141] Chen D, Aubry S, Tsironis G P 1996 Phys. Rev. Lett. **77** 4776.

[142] Polozov R V and Yakushevich L V 1998 J. Theor. Biol **130** 423.

[143] T. Dauxois, M. Peyrard, C.R. Willis, Physica D **57** (1992)267.

[144] Zoli M 2011 J. Chem. Phys. **135** 115101.

[145] Wahlquist H D and Estabrook F B 1971 Phys. Lett. **31** 1386

[146] Pickerng A 1993 J. Phys. A: Math. Gen. **26** 4395

[147] Tiofack G C L, Mohamadou A and Kofane T C 2007 J. Phys. A: Math. Theor. **40** 6133

[148] Tang X Y, Lou S Y and Zhang Y 2002 Phys. Rev. E **66** 046601

[149] Wang M L 1995 Phys. Lett. A **199** 169

[150] Barashenkov I V and Makhankov V G 1988 Phys. Lett. A **128** 52

[151] Barashenkov I V, Gocheva A D, Makhankov V G and Puzynin IV 1988 Physica D **34** 240

[152] Barashenkov I V and Woodford S R 2005 Phys. Rev. E **71** 026613 [47] De Bouard A 1995 SIAM J. Math. Anal. 26

[153] Barashenkov I V and Panova Y E 1993 Physica D 69 114

[154] F. Julicher et J. Prost, Phys. Rev. Lett, **75**, 4510 (1997)

[155] Y. Kafri, D. Lubensky et D. Nelson, Biophysical Journal, **86**, 3373 (2004)

interaction de solvant. Nous présentons une expression analytique du gain de modulation et nous montrons les effets de l'angle de torsion sur celui-ci ainsi que sur le diagramme de la stabilité. Des simulations numériques sont effectuées pour montrer la validité de l'approche analytique. L'impact de l'angle de torsion est étudié et l'on obtient que l'angle de torsion affecte la dynamique des modes stables générés par la molécule. La localisation de l'énergie dans le cadre du modèle de torsion de l'ADN avec interaction de solvant est également étudiée. Les degrés de liberté de la séquence d'ADN de rotation et de torsion sont considérés comme jouant un rôle important pour la transcription de l'ADN en tant que témoins du modèle rotationnel de Yakushevich. En utilisant la méthode de perturbation, nous tirons de ce modèle l'équation de Schrödinger non linéaire discrète et couplée qui nous a permis d'étudier l'instabilité de modulation (IM) grâce à une simple mode d'excitation d'une part et une double mode d'excitation d'autre part. Nous avons porté notre attention sur l'effet des paramètres de couplage, y compris les coefficients de torsion. Des simulations numériques de l'équation de Schrödinger non linéaire discrète ont été effectuées afin de vérifier la validité de nos résultats analytiques. Nous avons également été intéressés à chercher des solutions analytiques exactes des modèles de PB et de PBD. En ce qui concerne le modèle de PB, l'effet de couplage harmonique est mis en évidence, alors que dans le modèle de PBD, nous avons jeté notre dévolu sur l'impact de l'angle de torsion et le coefficient solvant. La stabilité de ces solutions a été également étudiée.

Mots clés

ADN, ARN, enzymes, réplication, transcription, transport de charges, instabilité modulationnelle, localisation de l'énergie, solitons, excitations non linéaires, Schrödinger, angle de torsion.

Abstract

Applied mathematics is one of the research fields that developed over the last few thousand years and still continues to develop. Mathematical models allow researchers to analyze a simplified structure of a biological system and predict its behavior. In fact, interdisciplinary research can offer answers to several unexplained phenomena and mathematical biology, in particular, allows the analysis of living organisms. Such analysis might involve the appearance, the development or even the death of the organisms, or simply explain the causes and the conditions in which a process takes place. Deoxyribonucleic acid (DNA) is one of a major focus for mathematical biologists, biophysicists, chemists as well as biologists. DNA is a long polymer consisting of two chains of bases, in which the genetic information is stored. A base from one chain has a corresponding base on the other chain which together forms a so-called base-pair. Our starting is focused on the nonlinear dynamics of the DNA molecule, particularly the study of its denaturation. We revisit one of the first nonlinear models of denaturation process of DNA, which neglects the inhomogeneities due to the base sequence and the asymmetry of the two strands: the Peyrard Bishop (PB) model. Using the semi-discrete method, we derive a nonlinear Schrödinger equation with higher-order term. Thereafter, the modulational instability (MI) is investigated through the linear stability analysis as well as the variational approach. The effect of the coupling between the base pairs is examined. Knowing that the PB model does not take into account the helical nature of the DNA molecule, we consider the Peyrard Bishop Dauxois model, which takes into account the double helix of DNA. We show using the reductive perturbation method that the dynamics of the system can be described by a set of coupled nonlinear Schrödinger equations. The relevant MI scenarios are explored and we note that the system is stable under the modulation for certain parameter values of the PBD model. We also point out the impact of the group velocity on the stability of the system understudy. The PBD model does not take into account the angle of torsion between pairs of adjacent bases and the effect of solvent. So, we reconsidered the PBD model improved by Marco Zoli. The generalized discrete nonlinear Schrödinger equation is then derived for the twisted DNA with solvent interaction. We present an analytical expression for the MI gain and show the effects of twist angle on MI gain spectra as well as on stability diagram. Numerical simulations are carried out to show the validity of the analytical approach. The impact of the twist angle is investigated and we obtain that the twist angle affects the dynamics of stable patterns gener-

ated through the molecule. Energy localization in the framework of twisted DNA with solvent interaction is also studied. The rotational and torsional degrees of freedom of the DNA sequence are considered to play an important role for DNA transcription as witnesses rotational model of Yakushevich. Using the perturbation method, we derive from this model a discrete coupled nonlinear Schrödinger equation that allowed us to study the MI through a simple mode excitation as well as through a double mode excitation. We have focused our attention on the effect of the coupling parameters, including the torsion coefficients. Direct numerical simulations of the nonlinear Schrödinger equation have been carried out in order to verify the validity of our analytical results. We have also been interested to look for exact analytical solutions of the PB and PBD models. As regards the model of PB, the effect of harmonic coupling is highlighted, while in the PBD model, we threw our sights on the impact of the angle of torsion and the solvent coefficient. The stability of these solitons has been also investigated.

Keywords: DNA, RNA, enzymes, replication, transcription, carrying loads, modulational instability, localization of the energy, solitons, nonlinear excitations, Schrödinger, torsion angle.